THE STABILITY AND DYNAMICS OF SPIKE-TYPE SOLUTIONS TO THE GIERER-MEINHARDT MODEL

by

DAVID IRON

B.A.Sc. The University of Toronto, 1988
M.Sc. The University of British Columbia, 1997

A THESIS SUBMITTED IN PARTIAL FULFILLMENT OF

THE REQUIREMENTS FOR THE DEGREE OF

DOCTOR OF PHILOSOPHY

in

THE FACULTY OF GRADUATE STUDIES

Department of Mathematics
Institute of Applied Mathematics

We accept this thesis as conforming
to the required standard

THE UNIVERSITY OF BRITISH COLUMBIA

April 2001

In presenting this thesis in partial fulfillment of the requirements for an advanced degree at the University of British Columbia, I agree that the Library shall make it freely available for reference and study. I further agree that permission for extensive copying of this thesis for scholarly purposes may be granted by the head of my department or by his or her representatives. It is understood that copying or publication of this thesis for financial gain shall not be allowed without my written permission.

Department of Mathematics
The University of British Columbia
Vancouver, Canada

Date April 27/2001

Abstract

A well-known system of partial differential equations, known as the Gierer-Meinhardt system, has been used to model cellular differentiation and morphogenesis. The system is of reaction-diffusion type and involves the determination of an activator and an inhibitor concentration field. It is believed that long-lived isolated spike solutions for the activator model the localized concentration profile that is responsible for cellular differentiation. In a biological context, the Gierer-Meinhardt system has been used to model such events as head determination in the hydra and heart formation in axolotl.

This thesis involves a careful numerical and asymptotic analysis of the Gierer-Meinhardt system in one dimension and a limited analysis of this system in a multi-dimensional setting. We begin by studying a reduced model, referred to as the shadow system, which results from simplifying the Gierer-Meinhardt model in the limit of inhibitor diffusivity tending to infinity. This reduced model is studied in both one and in several spatial dimensions. In §2 we study the stability and dynamics of interior spike profiles for this reduced model. We find that any n-spike profile, with $n > 1$, is unstable on a fast time scale. Profiles with a single interior spike are also unstable but on an exponentially slow time scale. In this case the spike tends towards the closest point on the boundary. In §3 we examine the behaviour of a spike profile in which the spike is confined to the boundary. This scenario is studied in the case of a two and a three dimensional domain. It is found that the spike moves in the direction of increasing boundary curvature and increasing boundary mean curvature in two and three dimensions, respectively. Stable spike equilbria correspond to local maxima of these curvatures. We then study the case of a spike confined to a flat portion of the boundary in two dimensions. In this case it is found that the spike moves on an exponentially slow time scale.

The remainder of this thesis examines the full Gierer-Meinhardt system in a one-dimensional spatial domain. In §4 we study the stability properties of n-spike equilibrium solutions to the full system. A necessary and sufficient condition is found for the linear stability of an n-spike solution. In §5 we study the dynamics of spike profiles. We derive a system of ordinary differential equations which govern the motions of the spikes in one spatial dimension. Numerical computations of this asymptotic system are compared with numerical computations of the full system. In §6 we study the effects of precursor gradients. The mathematical result of these spatial inhomogeneities in the chemical reaction is that some of the coefficients in the equations are no longer constant in space. We study the effects of spatially varying activator and inhibitor decay rates as well as a spatially inhomogeneous activator diffusivity. It is found that these spatial inhomogeneities can affect both the dynamics and equilibrium position of the spikes.

Table of Contents

List of Tables

List of Figures

Chapter 1
Introduction

Developmental biology is the study of the mechanisms by which a single cell develops into a complex organism with many different cell types. This process is extremely complex and involves both mechanical and biochemical processes. We will be focusing on the biochemical processes related to organ formation, or organogenesis, here. In this process, the initial cell divides into a large number of identical cells. Then a variety of mechanical and biochemical events occur. One such event is the formation of locally elevated levels of a substance, which we refer to as an activator, which cause the cells in a neighborhood of the elevated levels to differentiate from the surrounding cells. Thus a particular organ, such as a heart, is formed. In this thesis, we will analyze a mathematical model, known as the Gierer-Meinhardt model, of a proposed mechanism that may be responsible for the localization of the activator. This model uses the combination of a catalytic reaction with diffusion to produce an equilibrium in which the concentrations form a spatial pattern. The possible existence of such systems was first proposed by Turing in 1952 (see [46]).

An outline of this chapter is as follows. In §1.1 we present an overview of the initial work done by Turing. We will then present some explicit models of processes that are known to yield equilibrium solutions with spatial patterns. Specifically, in §1.2.1, §1.2.2, §1.2.3 and §1.2.4 we present models using long range inhibition, depletion of substrates, a model of microwave heating and a model of combustion occurring on a slowly diffusing fuel source, respectively. A full discussion of the first two of these models, as well as some striking numerical simulations, may be found in [32] and [33]. The remainder of this thesis will then focus on the long range

inhibition model, which is commonly referred to as the Gierer-Meinhardt equations (see [12]). In §1.3 we begin the mathematical analysis of the Gierer-Meinhart equations, by finding a suitable scaling as well as deriving a simplified model commonly referred to as the shadow system [35]. In §1.4 we overview some of the history of the mathematical analysis of the Gierer-Meinhartd equations. Finally, we discuss the goals of the thesis and give an outline of the remaining chapters.

1.1 The Turing Instability

Turing examined systems of the form,

$$A_t = D_A \Delta A + F(A,H)\,, \text{ in } \Omega\,, \tag{1.1a}$$

$$H_t = D_H \Delta H + G(A,H)\,, \text{ in } \Omega\,, \tag{1.1b}$$

with Neumann boundary conditions on $\partial\Omega$. Here A represents the activator concentration, H represents the inhibitor concentration, D_A is the activator diffusivity, D_H is the inhibitor diffusivity and F and G are nonlinear reaction terms. For simplicity we will consider Ω to be the one dimensional domain $[0,1]$. To determine if stable spatial patterns are possible, we examine the stability of the spatially homogeneous solution. We let A_E, H_E be such a solution (so that $F(A_E,H_E)=0$ and $G(A_E,H_E)=0$), and we consider a sinusoidal perturbation from this state. We let,

$$A = A_E + a\cos(\omega_i x)e^{\lambda t}\,, \tag{1.2a}$$

$$H = H_E + h\cos(\omega_i x)e^{\lambda t}\,. \tag{1.2b}$$

Here $\omega_i = \pi i$ in order to satisfy the boundary conditions. We substitute (1.2) into (1.1) and expand F and G in a Taylor series about A_E and H_E. This results in the eigenvalue problem,

$$\lambda a = -\omega_i^2 D_A a + K_1 a + K_2 h\,, \tag{1.3a}$$

$$\lambda h = -\omega_i^2 D_H h + K_3 a + K_4 h\,, \tag{1.3b}$$

where,

$$K_1 = \frac{\partial F}{\partial A}(A_E, H_E), \quad K_2 = \frac{\partial F}{\partial I}(A_E, H_E)\,, \tag{1.4a}$$

$$K_3 = \frac{\partial G}{\partial A}(A_E, H_E), \quad K_4 = \frac{\partial G}{\partial I}(A_E, H_E)\,. \tag{1.4b}$$

We must assume that the spatially homogeneous solution (A_E, H_E) is always stable in the absence of diffusion. This assumption results in several restrictions on the values of K_i. If this previous assumption is true, and the following condition is met,

$$(K_1 D_H + K_4 D_A)^2 - 4 D_A D_H (K_1 K_4 - K_2 K_3) > 0, \tag{1.5}$$

then the eigenvalue problem (1.3) will have eigenvalues with $\mathrm{Re}(\lambda_i) > 0$ when,

$$4((K_1 - \omega_i^2 D_A)(K_4 - \omega_i^2 D_H - K_2 K_3) < (K_1 + K_4 - \omega_i^2 (D_A + D_H))^2\,. \tag{1.6}$$

Thus, for a certain range of ω_i values, sinusoidal perturbations may grow. The end result is that only certain modes become unstable. Through numerical simulations, such as those in [12] and [16], these instabilities have been shown to yield spike-type solutions when D_A is small. The non-linear effects will then cause the spikes to stabilize. For an in-depth analysis of the parameter regime for spike growth see [28]. Numerical methods have now made it possible to simulate such systems thus verifying the existence of spike-type solutions.

1.2 Examples of Reaction-Diffusion Models

We now present some mathematical models of reaction-diffusion systems that are known to produce solutions with spatial patterns. Each system has different properties making them suitable for modeling different phenomena. For example, the depletion of substrate system seems to produce periodic patterns and thus may be of use in the modeling of structures with a periodic nature such as the spinal cord. The long range inhibition model tends to produce isolated structures and thus may be more appropriate for the modeling of isolated structures such as the heart. The microwave heating equation models the formation of hot-spots that can occur during sintering. The Grey-Scott model of combustion on a slowly diffusing fuel field produces pulses of locally elevated temperature that can split into traveling pulses which may again divide. We now present some details of the models.

1.2.1 Long Range Inhibition

In this two component reaction-diffusion system, the activator is a slowly diffusing substance which promotes its own formation with autocatalysis. The inhibitor is a rapidly diffusing substance which uses the activator as a catalyst in its formation and itself as an inhibitor of both its own formation and that of the activator. The formation of an isolated peak happens as follows. If the system is at a spatially homogeneous equilibrium, small perturbations in the concentration of the activator will grow due to the autocatalysis. These elevated levels of activator will promote a localized increase in the concentration of inhibitor. The elevated levels of inhibitor then diffuse rapidly preventing the formation of spikes in the activator concentration elsewhere. We now present a mathematical model of this system in a one-dimensional domain and in dimensionless form. This model, known as the Gierer-Meinhardt model, is

$$A_t = \epsilon^2 A_{xx} - A + \frac{A^p}{H^q}, \qquad -1 < x < 1, \quad t > 0, \tag{1.7a}$$

$$\tau H_t = D H_{xx} - \mu H + \frac{A^r}{H^s}, \qquad -1 < x < 1, \quad t > 0, \tag{1.7b}$$

$$A_x(\pm 1, t) = H_x(\pm 1, t) = 0, \tag{1.7c}$$

where the exponents (p, q, r, s) are assumed to satisfy the relations,

$$p > 1, \qquad q > 0, \qquad r > 0, \qquad s \geq 0, \qquad 0 < \frac{p-1}{q} < \frac{r}{s+1}. \tag{1.8}$$

Here D and ϵ^2 are the diffusivities of the inhibitor and activator, respectively. This model is a scaled and slightly simplified version of that presented in [12]. Simulations of this system show that it supports extremely robust isolated spike solutions. This is the model that is studied in this thesis.

1.2.2 Depletion of Substrate

In this model, the activator is autocatalytic but instead of an inhibitor, a rapidly diffusing substrate is required and used by the catalytic reaction. Thus, a localized slight increase of the concentration of the activator will grow due to autocatalysis. The autocatalytic reaction will use up the substrate required for the growth of the activator and thus regulate the size of the

spike. The details of the mathematical model of this reactions are as follows.

$$A_t = D_a A_{xx} - \mu A + cA^2 S\,, \tag{1.9a}$$

$$S_t = D_s S_{xx} - \nu S + c_0 - cA^2 S\,. \tag{1.9b}$$

This model is commonly referred to as the Brusselator (see [40]). As previously mentioned, this model has a tendency to produce periodic patterns.

1.2.3 Microwave Heating of Ceramic Fibers

We now give a partial differential equation modeling the microwave heating of thin ceramic cylinders in single-mode highly resonant cavity. An analysis of the equations in the limit of small Biot number results in the following non-local reaction diffusion equation (see [4]),

$$U_t = DU_{xx} - 2(U + \beta[(U+1)^4 - 1]) + P\frac{f(U)}{1 + \chi^2(\int_0^1 f(U)\,dy)^2}\,, \quad 0 < x < 1\,, \tag{1.10a}$$

$$U_x(0) = U_x(1) = 0\,, \tag{1.10b}$$

where U is the scaled temperature of the ceramic cylinder, D is the thermal diffusivity, χ and β are dimensionless physical parameters, P is dimensionless power parameter and $f(U)$ is the effective electrical conductivity. In [4] it shown that (1.10) supports highly localized hot-spot solutions. The forms of (1.10) and an asymptotic reduction of (1.17) known as the shadow system, given below in (1.18), are very similar. Thus, the analysis for the shadow system given in §2 should be useful for analyzing (1.10).

1.2.4 Combustion on a Slowly Diffusing Fuel Field - The Grey-Scot Model

This model is used for the simulation of brush fires or small forest fires. One of the most interesting features of this model is that it has spike solutions that may split into two spikes which then travel in opposite directions. This splitting process may then continue. In one spatial dimension, the model in non-dimensional form is (see [9]),

$$U_t = U_{xx} - UV^2 + \delta a(1-U)\,, \quad -1 < x < 1 \tag{1.11a}$$

$$V_t = \delta^2 V_{xx} + UV^2 - \delta^\beta bV \quad -1 < x < 1\,, \tag{1.11b}$$

$$U_x(\pm 1) = V_x(\pm 1) = 0\,. \tag{1.11c}$$

Here U is a scaled temperature field and V is a fuel concentration field. The model is studied in [9] in the limit of small δ, for various ranges of the positive parameters a, b and β.

1.3 Scaling of Gierer-Meinhardt Equations for Spike Solutions

Before we begin the scaling of (1.7), we make the simplification of setting $\tau = 0$, as finite values of τ can lead to complicated oscillatory behaviour which is beyond the scope of this thesis (see [34]). From numerical computations, it is evident that for sufficiently small values of τ, this simplification will cause no difficulties. Thus, for simplicity we $\tau = 0$ in (1.7).

The amplitude of a spike solution to (1.7) will tend to infinity as $\epsilon \to 0$. Therefore, we introduce new variables for which the spike solution has an $O(1)$ amplitude as $\epsilon \to 0$. To this end, we introduce a and h by

$$A = \epsilon^{-\nu_a} a\,, \qquad H = \epsilon^{-\nu_h} h, \tag{1.12}$$

where ν_a and ν_h are to be found. To balance the terms in (1.7a), we require,

$$-\nu_a = -\nu_a p + q\nu_h. \tag{1.13}$$

We will construct a solution in which the spike has its support in an $O(\epsilon)$ region near some point in Ω. Therefore, to obtain an additional equation relating ν_a and ν_h we consider an average balancing of (1.7b). Specifically, we integrate (1.7b) over the domain to get,

$$-\mu \int_{-1}^{1} H\, dx + \int_{-1}^{1} \frac{A^r}{H^s}\, dx = 0\,. \tag{1.14}$$

Since A will be localized to an $O(\epsilon)$ region about the spike center x_0, we scale x in the last term by $y = \epsilon^{-1}(x - x_0)$. Balancing the terms in this equation we get

$$-\nu_h = -\nu_a r + \nu_h s + 1\,. \tag{1.15}$$

The solution of (1.13) and (1.15) yields,

$$\nu_a = \frac{q}{(1-p)(1+s) + rq}, \qquad \nu_h = \frac{(p-1)}{(1-p)(1+s) + rq}. \tag{1.16}$$

In terms of these new variables (1.7) becomes

$$a_t = \epsilon^2 a_{xx} - a + \frac{a^p}{h^q}, \qquad -1 < x < 1, \quad t > 0, \tag{1.17a}$$

$$0 = D h_{xx} - \mu h + \epsilon^{-1} \frac{a^r}{h^s}, \qquad -1 < x < 1, \quad t > 0, \tag{1.17b}$$

$$a_x(\pm 1, t) = h_x(\pm 1, t) = 0. \tag{1.17c}$$

1.3.1 The Simplified Gierer-Meinhardt Equations – The Shadow System

In §1.2.1 it was stated that the inhibitor must be a rapidly diffusing substance. Thus, it seems logical to study this system in the limit $D \to \infty$. In this limit, h is a constant in space which may be determined from a solvability condition. In this limit, (1.17) reduces to the following nonlocal ordinary differential equation,

$$a_t = \epsilon^2 a_{xx} - a + \frac{a^p}{h^q}, \qquad -1 < x < 1, \quad t > 0, \tag{1.18a}$$

$$h = \left(\frac{\epsilon^{-1}}{2\mu} \int_{-1}^{1} a^r \, dx \right)^{\frac{1}{s+1}}, \tag{1.18b}$$

$$a_x(\pm 1, t) = 0. \tag{1.18c}$$

All of the analysis above can also be carried out in $\mathbb{R}^N$. We omit the details as the analysis is almost identical to that given above except for some minor changes in the scaling. As the analysis of the full system in $\mathbb{R}^N$ is beyond the scope of this thesis, we only present the N-dimensional version of the shadow system. It is given by,

$$a_t = \epsilon^2 \Delta a - a + \frac{a^p}{h^q}, \quad \text{in} \quad \Omega, \quad t > 0, \tag{1.19a}$$

$$h = \left(\frac{\epsilon^{-N}}{\mu |\Omega|} \int_{\Omega} a^r \, d\mathbf{x} \right)^{\frac{1}{s+1}}, \tag{1.19b}$$

$$\partial_n a = 0 \quad \text{on} \quad \partial\Omega, \tag{1.19c}$$

where Ω is a bounded subset of $\mathbb{R}^N$ and ∂_n refers to the normal derivative.

1.4 A Brief History of the Analysis of the Gierer-Meinhardt Equations

There are very few results for (1.17). Those that we have found will be discussed in the main body of the thesis at the appropriate times. Here we will restrict ourselves to results found previously for (1.19). The first results are for equilibrium solutions to (1.19). If we set $a_t = 0$ and $a = h^{\frac{q}{p-1}}u$ in (1.19), then (1.19) reduces to,

$$\epsilon^2 \Delta u - u + u^p = 0\,, \text{ in } \Omega\,, \tag{1.20a}$$

$$\partial_n u = 0\,, \text{ on } \partial\Omega\,. \tag{1.20b}$$

A spike solution for (1.20) in the limit $\epsilon \to 0$ is a solution of the form, $u(x) \sim u_c[\epsilon^{-1}|\boldsymbol{x} - \boldsymbol{x_0}|]$ where $\boldsymbol{x_0}$ is a point in Ω or on $\partial\Omega$ to be determined, and $u_c(\rho)$ is the unique positive radially symmetric solution to,

$$u_c'' + \frac{N-1}{\rho}u_c' - u_c + u_c^p = 0\,, \quad 0 < \rho < \infty\,, \tag{1.21a}$$

$$u_c \to \alpha e^{-\rho} \quad \text{as} \quad \rho \to \infty\,, \tag{1.21b}$$

for some $\alpha > 0$. An n-spike solution is defined as,

$$u \sim \sum_{i=1}^{n} u_c[\epsilon^{-1}|\boldsymbol{x} - \boldsymbol{x_i}|]\,, \tag{1.22}$$

where u_c is defined in (1.21) and the spikes are centered at points $\boldsymbol{x_i}$, $i = 1, \ldots, n$, to be determined. In [35] the existence of a single spike solution centered on the boundary at the global maximum point of the boundaries mean curvature is proven using variational methods, in particular the Mountain Pass Lemma. In axially symmetric domains, multiple peak solutions, with the peaks all resting on the boundary at local critical points of the boundaries mean curvature are constructed in [36]. In [13] multiple peak boundary spike solutions are found in a general domain with a smooth boundary. In [14] solutions with multiple interior peaks are constructed where the locations of the peaks coincide, in the limit $\epsilon \to 0$, with centers of spheres that solve a ball packing problem in the domain. In [15] solutions with spikes resting in the interior as well as on the boundary are found.

There are some key results in [48], which we will examine in more detail, as many of the ideas in this paper are important to an understanding of the analysis in this thesis. The result which concerns us states that all of the solutions found for equation (1.20) are dynamically unstable when the nonlocal effects from (1.18) are ignored. We briefly explain how this result is obtained. If we consider Ω in (1.20) to be all of $\mathbb{R}^N$, then $u_c\left(\frac{|\boldsymbol{x}-\boldsymbol{x_0}|}{\epsilon}\right)$ from (1.21) will satisfy (1.20) for any choice of $\boldsymbol{x_0}$. If we consider now a finite domain, u_c will still satisfy (1.20a) and will fail to satisfy the boundary conditions by exponentially small amounts for any choice of $\boldsymbol{x_0}$ in the interior of Ω. Next, we linearize about this approximate solution and obtain the following eigenvalue problem,

$$L_\epsilon\phi = \epsilon^2\Delta\phi + (-1 + pu_c^{p-1})\phi = \lambda\phi\,, \tag{1.23a}$$

$$\partial_n\phi = 0 \quad \text{on} \quad \partial\Omega\,. \tag{1.23b}$$

We note that the function $\phi_i = \frac{\partial u_c}{\partial x_i}$, for $i = 1, \ldots, N$ satisfies $L_\epsilon\phi_i = 0$ and fails to satisfy the boundary conditions by only exponentially small amounts. This suggests that in the limit $\epsilon \to 0$, (1.23a) has N exponentially small eigenvalues. We note that the eigenfunctions associated with these eigenvalues each have exactly one nodal line. Thus, these are not the principal eigenfunctions. Therefore, (1.23a) must have a proper positive eigenvalue. Since, by a rescaling of the spatial variables, we may eliminate the ϵ from (1.23a), this eigenvalue must be $O(1)$. Thus, the linearization about a spike solution has a positive $O(1)$ eigenvalue and therefore, these spike solutions are not stable. These large and small eigenvalues will reappear many times in the course of this thesis. One of the main tasks in this thesis is to show what conditions are necessary to move the positive $O(1)$ eigenvalue into the left half of the complex plane.

We now present the main goals of this thesis and an overview of the remainder of the chapters. Turing did his initial work in 1952 using the techniques of linear analysis. The only questions that this form of analysis has been able to answer are what are some of the necessary conditions for spikes to form from spatially homogeneous initial data. The conditions arriving from this analysis are far from sufficient. Once the initial Turing instability is triggered it is assumed that the nonlinear effects will stabilize the spike profile. This linear analysis can say nothing about the fully formed spike profile, which is far from the linear regime. Until recently, the only

way to verify that the fully formed spike profiles are stable is to use numerical analysis. One of the main goals of this thesis is to use modern analytical techniques to find explicit criteria, both necessary and sufficient, determining the stability of a particular spike profile. There are many other questions that this thesis will address. We will consider the behavior of spikes after they are fully formed. We will also address such questions as how do the spikes move and how do they interact dynamically. We will also examine the differences in the behaviour of the full system (1.17) with the shadow system (1.18) and determine under what circumstances it is appropriate to use the reduced model (1.18).

The remainder of the thesis proceeds as follows. In §2 we consider equilibrium and quasi-equilibrium solutions to (1.18) and (1.19). In §2.1 we construct a canonical spike solution to (1.18). A linearization about this solution leads to a non-local eigenvalue problem. The principal eigenvalue of this spectrum is shown to be exponentially small. A projection method is then used to derive a solvability condition resulting from the exponentially small eigenvalue. This leads to an ordinary differential equation governing the exponentially slow motion of one spike. These results are then favorably compared to numerical simulations of (1.18). We now present the main result from this chapter. For $\epsilon \to 0$, metastable spike solution for (1.18), is represented by $a(x,t) = a_E(x; x_0(t))$, where a_E is defined below in (2.1) and $x_0(t)$ satisfies,

$$\frac{dx_0}{dt} \sim \frac{2a^2\epsilon}{\hat{\beta}} \left[e^{-2(1-x_0)/\epsilon} - e^{-2(1+x_0)/\epsilon} \right]. \tag{1.24}$$

Here a and $\hat{\beta}$ are positive constants defined below in (2.5) and (2.20), respectively. In §2.2 we demonstrate than an n-spike solution, with $n > 1$, to (1.18) is always unstable with an $O(1)$ positive eigenvalue. In §2.3 we repeat the analysis of §2.1 in an N-dimensional setting. The differential equation governing the motion of the spike shows that the spike will drift exponentially slowly towards the closest point on the boundary.

In §3 we examine the dynamics of the spike once it has merged with the boundary. This is carried out in two and three dimensions in §3.1 and §3.2 respectively. In both cases it is found that the spike moves in the direction of increasing curvature (mean curvature in the case of three dimensions) until reaching a stable equilibrium at a local maximum of the (mean) curvature of

the boundary. We now provide the main results of this chapter. For $\epsilon \to 0$, the motion of a spike confined to the smooth boundary of a two-dimensional domain follows the trajectory

$$s_0'(t) \sim \frac{4b}{3\pi}\epsilon^3 \kappa'(s_0)\,, \tag{1.25}$$

where $\gamma = q/(p-1)$ and $b > 0$ defined below in (3.20c). Here s is the arclength along the boundary and $\kappa(s) > 0$ is the curvature of the boundary. This differential equation has stable equilibrium when we are at a local maximum of $\kappa(s)$. Correspondingly in three dimensions, for $\epsilon \to 0$ the motion of a spike confined to a smooth boundary is described by

$$\boldsymbol{\xi}'(t) \sim \frac{3}{4} b\epsilon^3 \nabla H(\boldsymbol{\xi})\,. \tag{1.26}$$

Here $\boldsymbol{\xi} = (\xi_1, \xi_2)$, $\gamma = q/(p-1)$, $b > 0$ is defined in (3.37b) and H is the mean curvature of $\partial\Omega$, with $H > 0$ for a sphere. Stable equilibria are at local maxima of H.

In §4 we examine the stability of n-spike solutions to (1.17). We find explicit conditions, both necessary and sufficient, to determine the stability of an n-spike solution. This is accomplished by linearizing about an n-spike solution and finding criteria that guarantee that both the large and small eigenvalues discussed previously lie in the left half of the complex plane. The main result of this chapter is a stability result which we now provide. An n-spike equilibrium solution to (1.17) is stable when $D < D_n^*$ where, as $\epsilon \to 0$,

$$D_n^* \sim \frac{\mu}{\left[n \ln(\sqrt{\beta} + \sqrt{\beta+1})\right]^2}\,, \qquad \beta \equiv \left[\frac{qr}{p-1} - (1+s)\right]^{-1}\,. \tag{1.27}$$

An n-spike solution is unstable when $D > D_n^*$.

In §4.4 these results are used to construct an ordinary differential equation governing the motion of a single spike profile. These results are compared with full numerical simulations of (1.17). These results predict $D_1^* = \infty$. A more refined analysis shows that a one-spike solution is stable only when $D < O(e^{C/\epsilon})$. Thus the shadow system (1.18) and the the full system (1.17) give similar stability conclusions for a one spike solution only when $D > O(e^{C/\epsilon})$.

In §5 we examine the dynamic properties to n-spike profiles under (1.17). A solvability conditions resulting from the small eigenvalues results in a differential algebraic system governing

the motion of the spikes. However, the validity of this system will depend on the location of the large eigenvalues in the complex plane. Thus, a criterion is developed to ensure the validity of the derived system at any given time. We now provide some of the details of this result. For $\epsilon \ll 1$, the quasi-equilibrium solution for a and h is given by

$$a(x,t) \sim a_c \equiv \sum_{j=1}^{n} h_j^{\gamma} u_c \left[\epsilon^{-1}(x - x_j)\right] , \tag{1.28a}$$

$$h(x,t) \sim h_c \equiv b_r \sum_{j=1}^{n} h_j^{\gamma r - s} G(x; x_j) , \tag{1.28b}$$

where $h_i = h_i(\tau)$ and $x_i = x_i(\tau)$ satisfy the differential-algebraic system for $i = 1, .., n$

$$h_i = b_r \sum_{j=1}^{n} h_j^{\gamma r - s} G(x_i; x_j) , \tag{1.29a}$$

$$\frac{dx_i}{d\tau} \sim -\frac{2qb_r}{p-1} h_i^{-1} \left(h_i^{\gamma r - s} \langle G_x \rangle_i + \sum_{\substack{j=1 \\ j \neq i}}^{n} h_j^{\gamma r - s} G_x(x_i; x_j) \right) . \tag{1.29b}$$

Here u_c satisfies (5.5), b_m is defined in (5.11a), $\tau = \epsilon^2 t$, and $\langle G_x \rangle_i \equiv \left[G_x(x_{i+}; x_i) + G_x(x_{i-}; x_i)\right]/2$. Here G is the Green's functions satisfying,

$$DG_{xx} - \mu G = -\delta(x - x_k) , \qquad -1 < x < 1 , \tag{1.30a}$$

$$G_x(\pm 1; x_k) = 0 . \tag{1.30b}$$

In §6 we examine the effects of precursor gradients on the equilibrium position of a single spike. A precursor gradient is a pre-existing spatially inhomogeneity which is imposed on the model. It could come into existence from the inherent polarity of the developing cells or due to localized sources of a precursor which diffuse through the group of cells. The mathematical consequence of a precursor gradient is that the coefficients in the model will now depend on space. This can have a variety of effects depending on the nature of the inhomogeneity. Several different scenarios will be explored.

Chapter 2
The Shadow System

We begin by considering the shadow system (1.18) which is a simplified model of the Gierer-Meinhardt system. In [35] it was shown that for sufficiently large values of D the solutions to the shadow system and that of the full system will coincide. However, we will show in §4.4.2 that D will have to be asymptotically exponentially large as $\epsilon \to 0$ for this to be the case and thus outside the range of any physical model. The shadow system still warrants investigation as techniques used in its investigation will be useful in the investigation of the full system. In addition, the shadow system provides an interesting example of a non-local differential equation and a novel application of the projection method.

The outline of this chapter is as follows. In §2.1 we consider the one-spike quasi-equilibrium solution to the one-dimensional problem (1.18). We examine the stability and dynamics of this solution by analyzing the spectrum of the linear operator resulting from a linearization of (1.18) about this non-constant solution. This eigenvalue problem is a non-local Sturm-Liouville problem of the type considered in [11]. A combination of analytical and numerical techniques will be used to demonstrate that the principle eigenvalue of this operator is exponentially small. The non-local term in the Sturm-Liouville operator is essential for this conclusion. The exponentially small eigenvalue will be estimated asymptotically. A differential equation characterizing the motion of the center of the spike will be derived in the limit $\epsilon \to 0$ by using a limiting solvability condition, which requires that the solution to the quasi-steady linearized problem has no component in the eigenspace associated with the exponentially small eigenvalue. This procedure is known as the projection method and has been used in other contexts (see

[48], [49]). The resulting ODE for the motion of the center of the spike shows that the spike drifts exponentially slowly towards the point on the boundary closest to the initial location of the spike. This metastable behavior is verified by calculating full numerical solutions to (1.17) in §2.2. Solutions with n-spikes, where $n > 1$, will be shown to be unstable. In §2.3 we give a similar analysis of metastable spike-layer motion for the multi-dimensional problem (1.19).

2.1 A Spike in a One-Dimensional Domain

We first construct a one-spike quasi-equilibrium solution a_E for (1.18) in the form

$$a = a_E(x; x_0) \equiv h^\gamma u_c[\epsilon^{-1}(x - x_0)], \qquad \gamma = q/(p-1). \tag{2.1}$$

Here x_0, with $|x_0| < 1$, is the center of the spike. The function $u_c(y)$, called the canonical spike solution, is the unique positive solution satisfying,

$$u_c'' - u_c + u_c^p = 0, \qquad 0 < y < \infty, \tag{2.2a}$$

$$u_c'(0) = 0; \qquad u_c(y) \sim a e^{-y}, \qquad \text{as} \quad y \to \infty, \tag{2.2b}$$

with $a > 0$. The existence and uniqueness of the solution to (2.2a) is proven in [45]. In terms of this solution, $h = h_E$, where

$$h_E = \left(\frac{1}{2\epsilon\mu} \int_{-1}^{1} u_c^r \, dx \right)^{\frac{p-1}{(s+1)(p-1)-qr}}. \tag{2.3}$$

Since u_c is localized near x_0, we estimate as $\epsilon \to 0$, that

$$h_E \sim \left(\frac{\beta}{\mu} \right)^{\frac{p-1}{(s+1)(p-1)-qr}}, \qquad \beta \equiv \int_0^\infty [u_c(y)]^r \, dy. \tag{2.4}$$

To determine numerical values for certain asymptotic quantities below we must compute $u_c(y)$, β, and a numerically. The constant a is obtained by integrating (2.2)

$$\log(a) = \frac{\log\left(\frac{p+1}{2}\right)}{p-1} + \int_0^{\left(\frac{p+1}{2}\right)^{\frac{1}{p-1}}} \left[\frac{-1}{\sqrt{\eta^2 - \frac{2}{p+1}\eta^{p+1}}} - \frac{1}{\eta} \right] d\eta. \tag{2.5}$$

To compute u_c numerically, we use the asymptotic boundary condition $u_c' + u_c = 0$ at $y = y_L$, where y_L is a large positive constant. To compute solutions for various values of p, we use a

continuation procedure starting from the special analytical solution,

$$u_c(y) = \frac{3}{2}\text{sech}^2\left(\frac{y}{2}\right), \tag{2.6}$$

which holds when $p = 2$. The boundary value problem solver COLNEW (see [3]) is then used to solve the resulting boundary value problem. In Fig. 2.1, we plot the numerically computed $u_c(y)$ when $p = 2, 3, 4$.

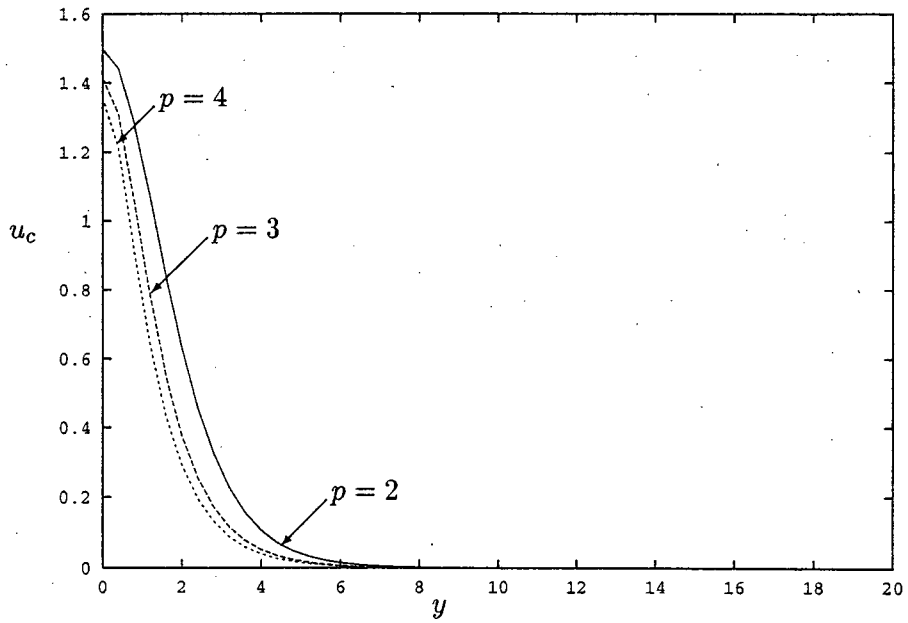

Figure 2.1: Numerical solution for $u_c(y)$ when $p = 2, 3, 4$.

We note that, for any x_0 with $|x_0| < 1$, the solution $a_E(x; x_0)$ will satisfy the steady-state problem corresponding to (1.18a), (1.18b), but will fail to satisfy the boundary conditions in (1.18c) by only exponentially small terms as $\epsilon \to 0$. Thus, we expect that the spectrum of the eigenvalue problem associated with the linearization about a_E will contain an exponentially small eigenvalue.

2.1.1 The Nonlocal Eigenvalue Problem

Let $x_0 \in (-1,1)$ be fixed and linearize (1.18) around a_E, h_E. We obtain the eigenvalue problem for the linearization by introducing ϕ and η by

$$a(x,t) = a_E(x;x_0) + e^{\lambda t}\phi \tag{2.7a}$$

$$h(t) = h_E + e^{\lambda t}\eta\,, \tag{2.7b}$$

where $\phi \ll 1$ and $\eta \ll 1$. Substituting (2.7) into (1.18) we obtain the following non-local eigenvalue problem of Sturm-Liouville type on $[-1,1]$:

$$L_\epsilon\phi \equiv \epsilon^2\phi_{xx} + (-1 + pu_c^{p-1})\phi - \frac{rq\epsilon^{-1}u_c^p}{2\beta(s+1)}\int_{-1}^{1} u_c^{r-1}\phi\,dx = \lambda\phi, \tag{2.8a}$$

$$\phi_x(\pm 1) = 0. \tag{2.8b}$$

The non-local integral term in (2.8) will drastically change the nature of the eigenvalue problem.

In (2.8), $u_c = u_c\left[\epsilon^{-1}(x-x_0)\right]$. Therefore, we will only seek eigenfunctions that are localized near $x = x_0$. These eigenfunctions are of the form

$$\tilde{\phi}(y) = \phi(x_0 + \epsilon y)\,, \qquad y = \epsilon^{-1}(x - x_0)\,. \tag{2.9}$$

Therefore, we can replace the finite interval by an infinite interval in the integral in (2.8) and impose a decay condition for $\tilde{\phi}(y)$ as $y \to \pm\infty$. This gives us the non-local eigenvalue problem for the infinite domain $-\infty < y < \infty$:

$$\tilde{L}_\epsilon\tilde{\phi} \equiv \tilde{\phi}_{yy} + (-1 + pu_c^{p-1})\tilde{\phi} - \frac{rqu_c^p}{2\beta(s+1)}\int_{-\infty}^{\infty} u_c^{r-1}\tilde{\phi}\,dy = \lambda\tilde{\phi}, \tag{2.10a}$$

$$\tilde{\phi} \to 0 \quad \text{as} \quad y \to \pm\infty\,. \tag{2.10b}$$

Now we examine the spectrum of the operator in (2.10). To demonstrate that this operator has no eigenvalues with positive real part, we apply a theorem from [52].

Theorem 2.1 (Wei [52]) *Consider the eigenvalue problem for* $\gamma_0 \geq 0$

$$\Phi'' - \Phi + p u_c^{p-1}\Phi - \gamma_0(p-1)u_c^p \left(\frac{\int_{-\infty}^{\infty} [u_c(y)]^{r-1}\,\Phi(y)\,dy}{\int_{-\infty}^{\infty} [u_c(y)]^r\,dy} \right) = \lambda\Phi\,, \qquad -\infty < y < \infty\,, \tag{2.11a}$$

$$\Phi \to 0 \quad as \quad |y| \to \infty\,, \tag{2.11b}$$

corresponding to eigenpairs for which $\lambda \neq 0$. *Here* u_c *satisfies (2.2). Let* $\lambda_0 \neq 0$ *be the eigenvalue of (2.11) with the largest real part. Then, if* $\gamma_0 < 1$, *we conclude that*

$$Re(\lambda_0) > 0\,. \tag{2.12}$$

Alternatively, if $\gamma_0 > 1$ *and if either of the following two conditions hold*

$$(i) \quad r = 2\,,\ 1 < p \leq 5\,, \qquad or \qquad (ii) \quad r = p+1\,,\ p > 1\,, \tag{2.13a}$$

then

$$Re(\lambda_0) < 0\,. \tag{2.13b}$$

Thus for all the parameter sets satisfying (2.13a) we have that the operator $\tilde{L}_\epsilon$ has no eigenvalues with positive real part. The non-constant coefficients of both the operators L_ϵ and $\tilde{L}_\epsilon$ are both localized to a small region about x_0, so we will only consider eigenfunctions which are also localized to an $O(\epsilon)$ region about x_0. Such eigenfunctions of the operator $\tilde{L}_\epsilon$ satisfy (2.8a), but fail to satisfy (2.8b) by exponentially small terms. Thus, we expect the eigenvalues of $\tilde{L}_\epsilon$ to differ from those of L_ϵ by exponentially small terms. The operator $\tilde{L}_\epsilon$ has one zero eigenvalue with eigenfunction u_c'. We will carefully examine below the effect of a finite domain on this eigenvalue for the operator L_ϵ. The important point is that Theorem 2.1 shows that the operator L_ϵ has no $O(1)$ eigenvalues with positive real part. The proof of this theorem is given in Appendix A.

It is instructive to see how the presence of non-local term in (2.8) effects the operators spectrum. We may use a numerical solution to see the precise effect the non-local term has on the spectrum

of L_ϵ. To treat the non-local eigenvalue problem numerically, we split the operator L_ϵ into two parts,

$$A\phi \equiv \epsilon^2\phi_{xx} + (-1 + pu_c^{p-1})\phi, \qquad B\phi \equiv \frac{rq\epsilon^{-1}u_c^p}{2\beta(s+1)}\int_{-1}^{1} u_c^{r-1}\phi\, dx\,. \tag{2.14}$$

We define a new operator L_δ by $L_\delta\phi \equiv A\phi - \delta B\phi$. where δ, with $0 \le \delta \le 1$, is a continuation parameter. When $\delta = 0$ we have a simple Sturm-Liouville problem. At $\delta = 1$ we have our full non-local eigenvalue problem (2.8). We define $\tilde{L}_\delta$, $\tilde{A}$ and $\tilde{B}$ in a similar fashion, but on the extended domain $-\infty < y < \infty$ with the appropriate decay boundary conditions at $\pm\infty$.

The zero eigenvalue of the operator $\tilde{L}_\epsilon$ corresponds to the eigenfunction u_c', which decays exponentially as $|y| \to \infty$. To see this, we differentiate (2.2a) with respect to y, to show that $\tilde{A}u_c' = 0$. This is translation invariance. In addition, due to the symmetry of $u_c(y)$, we also have $\tilde{B}u_c' = 0$. For the finite domain problem (2.8), the function $u_c'\left[\epsilon^{-1}(x - x_0)\right]$ fails to satisfy the equation and boundary conditions in (2.8) by only exponentially small terms as $\epsilon \to 0$. Therefore, as estimated carefully below, the presence of the finite domain will perturb the zero eigenvalue and the corresponding eigenfunction of the extended problem (2.10) by only an exponentially small amount. Thus, L_ϵ has an exponentially small eigenvalue.

The function $u_c(y)$ has a unique maximum at $y = 0$ and thus the eigenfunction $u_c'(y)$ has exactly one zero at $y = 0$. This implies that $u_c'(y)$ corresponds to the second eigenfunction of $\tilde{A}$. The principal eigenvalue of $\tilde{A}$ is simple, positive and independent of ϵ. The principal eigenvalue of A is exponentially close to the principal eigenvalue of $\tilde{A}$. Hence, in the absence of the non-local term, the operator L_ϵ has an $O(1)$ positive eigenvalue and no metastable spike motion can occur.

Since $\tilde{L}_\delta$ has a positive eigenvalue when $\delta = 0$, we must consider what happens to this eigenvalue as δ ranges from 0 to 1. If this eigenvalue remains positive then, since the eigenvalues of L_δ and $\tilde{L}_\delta$ will differ by only exponentially small amounts as $\epsilon \to 0$, we can conclude that the one-spike quasi-equilibrium solution is unstable. Alternatively, if this eigenvalue crosses through zero at some finite value of $\delta < 1$, then the principal eigenvalue of L_δ when $\delta = 1$ (which corresponds to our eigenvalue problem (2.8)) will be exponentially small. Hence, if this occurs, the one-

spike solution is anticipated to be metastable. Applying theorem 2.1 to the operator $\tilde{L}_\epsilon$, we conclude that for any parameter set satisfying (2.13a), the eigenvalue should cross through zero at $\delta = \frac{(p-1)(s+1)}{rq}$.

The calculation of the eigenvalues of $\tilde{L}_\delta$ will require some numerical analysis. Thus, we will work with specific parameter sets. We first consider the set $(p,q,r,s) = (2,1,2,0)$, which is commonly used in simulations and satisfies (2.13a). For this parameter set, we begin by reviewing some exact results for the spectrum of the local eigenvalue problem

$$\tilde{A}\tilde{\phi} \equiv \tilde{\phi}_{yy} + (-1 + pu_c^{p-1})\tilde{\phi} = \lambda\tilde{\phi} \qquad -\infty < y < \infty\,, \tag{2.15a}$$

$$\tilde{\phi} \to 0 \quad \text{as} \quad y \to \pm\infty\,. \tag{2.15b}$$

This problem has three isolated eigenvalues, and a continuous spectrum in the left half plane. When $p = 2$, these three isolated eigenpairs are (see [26]),

$$\lambda_0 = 5/4\,, \qquad \tilde{\phi}_0 = \mathrm{sech}^3(y/2)\,, \tag{2.16}$$

$$\lambda_1 = 0\,, \qquad \tilde{\phi}_1 = \tanh(y/2)\mathrm{sech}^2(y/2)\,, \tag{2.17}$$

$$\lambda_2 = -3/4\,, \qquad \tilde{\phi}_2 = 5\mathrm{sech}^3(y/2) - 4\mathrm{sech}(y/2)\,. \tag{2.18}$$

Since these eigenfunctions, written in terms of $y = \epsilon^{-1}(x - x_0)$, will fail to satisfy the boundary conditions in (2.8) by only exponentially small terms as $\epsilon \to 0$, we expect that the eigenvalues of A will be only slightly perturbed from those of $\tilde{A}$. As we have previously noted, the zero eigenvalue of (2.15) will persist for $\tilde{L}_\delta$ as δ ranges from zero to one. Hence, there is an eigenvalue of (2.8) that is exponentially small as $\epsilon \to 0$.

To numerically compute the eigenvalue branches $\lambda_0(\delta)$ and $\lambda_2(\delta)$ of $\tilde{L}_\delta$ for which $\lambda_0(\delta) \to 5/4$ and $\lambda_2(\delta) \to -3/4$, as $\delta \to 0$, we use the initial guesses provided above for $\delta = 0$ and a continuation procedure to compute these eigenvalues as δ increases. The computations are done using COLNEW. The analysis of [11] showed that these eigenvalue branches are smooth functions of δ, and they cannot terminate suddenly at some value of δ. Hence, δ is a natural homotopy parameter. In Fig. 2.2 we plot the numerically computed $\lambda_0(\delta)$ and $\lambda_2(\delta)$ versus δ. As can be seen from this graph, $\lambda_0 \approx 0$ for $\delta = 1/2$, agreeing with Theorem 2.1. As δ

increases past $1/2$, λ_0 becomes negative and then complex. At this point, COLNEW is no longer able to track the eigenvalue. As δ increases from 0 to 1, λ_0 decreases and λ_2 increases. At a value of $\delta \approx 0.65$ the two eigenvalues collide and split into complex conjugates eigenvalues with negative real parts. To track the eigenvalues beyond $\delta \approx 0.65$ one must employ a different numerical technique. We accomplish this by discretizing the finite domain problem (2.8), which has eigenvalues exponentially close to those of $\tilde{L}_\delta$. This is done using a centered difference approximation applied to the second derivative and Simpson's rule applied to the integral. Thus, the operator L_δ is approximated by a discrete linear operator $\mathcal{L}_\delta$. The eigenvalues of the continuous problem may then be approximated by the eigenvalues of this matrix. Numerical calculations of the eigenvalue λ_0 of $\mathcal{L}_\delta$ are shown in Table 2.1. As seen in Table 2.1, the real part of λ_0 remains negative as δ tends to one. Similar computations, with similar conclusions, can be performed for other values of p, q, r and s. In particular, λ_0 and λ_2 are shown in Fig. 2.3 for the parameter set $(p, q, r, s) = (3, 2, 2, 0)$.

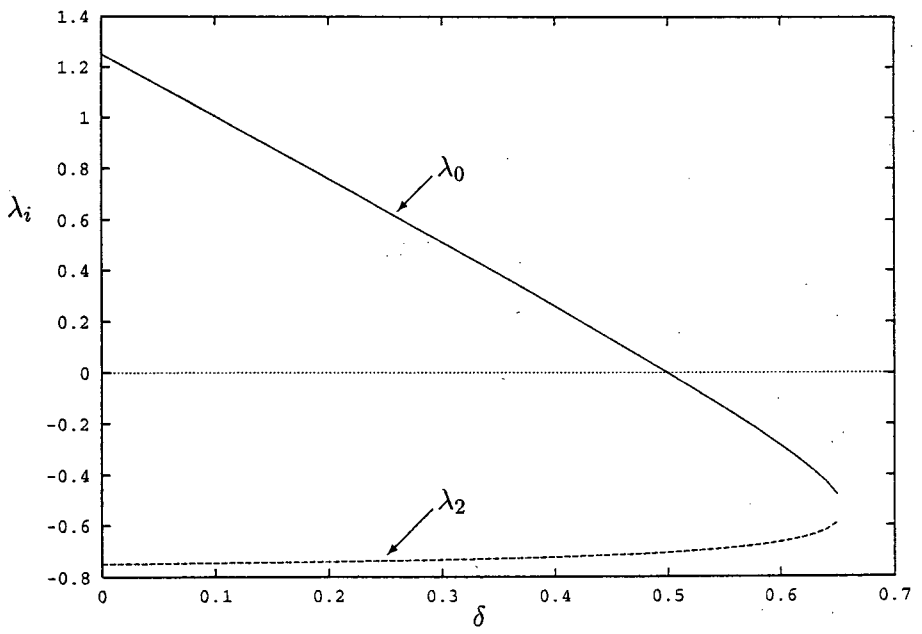

Figure 2.2: λ_0 and λ_2 versus δ for the parameter set $(p, q, r, s) = (2, 1, 2, 0)$.

δ	λ_0
0.0	1.2518
0.1	1.0073
0.2	0.76149
0.3	0.51345
0.4	0.26158
0.5	0.0052548
0.6	-0.28247
0.7	$-.59237 + 0.15315i$
0.8	$-.71522 + 0.23035i$
0.9	$-.84093 + 0.23008i$
1.0	$-.98551 + 0.14507i$

Table 2.1: δ and λ_0 for the case $(p, q, r, s) = (2, 1, 2, 0)$.

2.1.2 An Exponentially Small Eigenvalue

In the previous section, we explained qualitatively why the principal eigenvalue of L_ϵ is exponentially small. The non-local term in (2.8) was found to be essential to this conclusion. In this section we calculate the exponentially small eigenvalue precisely. We denote the eigenpair corresponding to the exponentially small eigenvalue by λ_1, ϕ_1. To predict the dynamics of the quasi-equilibrium solution, we must obtain a very accurate estimate of λ_1. We expect that $\phi_1 \sim C_1 u_c'\left(\epsilon^{-1}(x - x_0)\right)$ in the outer region away from $O(\epsilon)$ boundary layers near $x = \pm 1$. The behavior of ϕ_1 in these regions will be analyzed using a boundary layer analysis.

The eigenfunction ϕ_1 has the boundary layer form

$$\phi_1(x) = C_1\left(u_c'\left[\epsilon^{-1}(x - x_0)\right] + \phi_l\left[\epsilon^{-1}(x + 1)\right] + \phi_r\left[\epsilon^{-1}(1 - x)\right]\right). \tag{2.19}$$

Here $\phi_l(\eta)$ and $\phi_r(\eta)$ are boundary layer correction terms and C_1 is a normalization constant

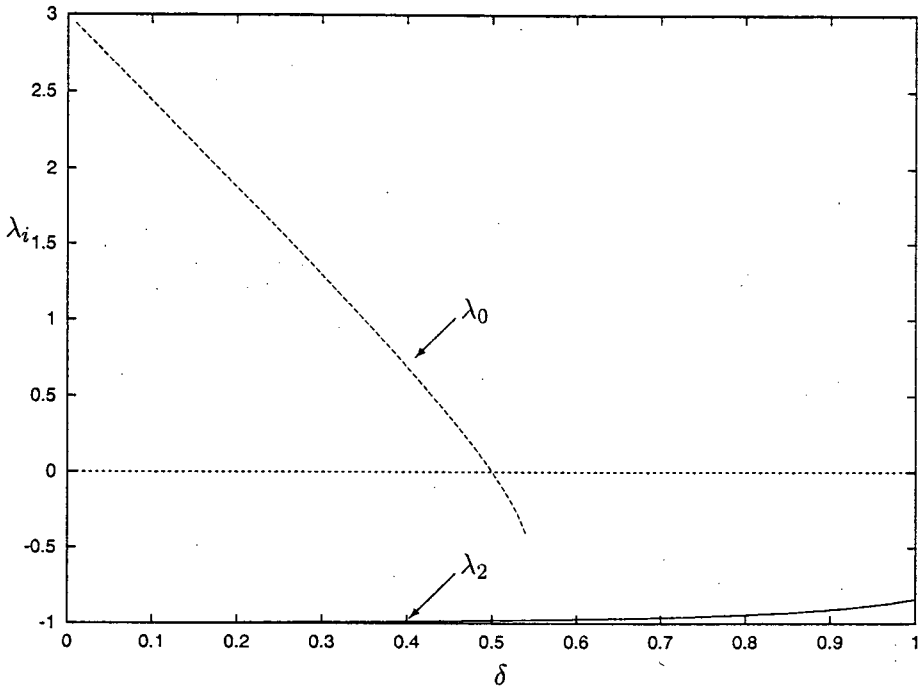

Figure 2.3: λ_0 and λ_2 versus δ for the parameter set $(p, q, r, s) = (3, 2, 2, 0)$.

given by

$$C_1 = \left(\epsilon\hat{\beta}\right)^{-1/2}, \qquad \text{where} \quad \hat{\beta} = \int_{-\infty}^{\infty} \left[u_c'(y)\right]^2 \, dy \,. \tag{2.20}$$

In the boundary layer region near $x = -1$, $u_c'\left[\epsilon^{-1}(x - x_0)\right]$ is exponentially small as $\epsilon \to 0$. Thus, as $\epsilon \to 0$, $\phi_l(\eta)$ satisfies

$$\phi_l'' - \phi_l = 0, \qquad 0 \le \eta < \infty \,, \tag{2.21a}$$

$$\phi_l'(0) \sim -ae^{-\epsilon^{-1}(1+x_0)} \,. \tag{2.21b}$$

Similarly, the boundary layer equation for $\phi_r(\eta)$ is

$$\phi_r'' - \phi_r = 0, \qquad 0 \le \eta < \infty \,, \tag{2.22a}$$

$$\phi_r'(0) \sim ae^{-\epsilon^{-1}(1-x_0)} \,. \tag{2.22b}$$

Here a is defined in (2.5). Solving the boundary layer equations we get

$$\phi_l(\eta) = ae^{-\epsilon^{-1}(1+x_0)}e^{-\eta}, \tag{2.23a}$$

$$\phi_r(\eta) = -ae^{-\epsilon^{-1}(1-x_0)}e^{-\eta}. \tag{2.23b}$$

To estimate λ_1 we first derive Lagrange's identity for $(u, L_\epsilon v)$, where $(u,v) \equiv \int_{-1}^{1} uv\,dx$. Using integration by parts we derive

$$(v, L_\epsilon u) = \epsilon^2 \left(u_x v - v_x u\right)|_{-1}^{1} + (u, L_\epsilon^* v), \tag{2.24}$$

where

$$L_\epsilon^* v \equiv \epsilon^2 v_{xx} + (-1 + pu_c^{p-1})v - \frac{rq\epsilon^{-1}u_c^{r-1}}{2\beta(s+1)} \int_{-1}^{1} u_c^p v\,dx\,. \tag{2.25}$$

We now apply this identity to the functions $u_c'[\epsilon^{-1}(x-x_0)]$ and $\phi_1(x)$ to get

$$\lambda_1(u_c', \phi_1) = -\epsilon\phi_1 u_c''|_{-1}^{1} + (\phi_1, L_\epsilon^* u_c')\,. \tag{2.26}$$

We examine each of the terms in (2.26). We begin with (u_c', ϕ_1). The dominant contribution to this integral arises from the region near $x = x_0$ where $\phi_1 \sim C_1 u_c'[\epsilon^{-1}(x-x_0)]$. Therefore, the inner product can be estimated as

$$(u_c', \phi_1) = C_1(u_c', u_c') \sim C_1\epsilon\hat{\beta}\,. \tag{2.27}$$

Next, to estimate $-\epsilon\phi_1 u_c''|_{-1}^{1}$, we use our asymptotic estimates of u_c and ϕ_1. Since $u_c(z) \sim ae^{-|z|}$ as $z \to \pm\infty$ we have that $u_c''\left[\epsilon^{-1}(\pm 1 - x_0)\right] \sim ae^{-\epsilon^{-1}(1\mp x_0)}$. In addition, using the previous boundary layer results for ϕ_1 we get the following estimate for $\phi_1(\pm 1)$:

$$\phi_1(\pm 1) \sim \mp 2C_1 a e^{-\epsilon^{-1}(1\mp x_0)}\,. \tag{2.28}$$

Using these results, we get

$$-\epsilon\phi_1 u_c''|_{-1}^{1} \sim 2\epsilon C_1 a^2 \left(e^{-2\epsilon^{-1}(1+x_0)} + e^{-2\epsilon^{-1}(1-x_0)}\right). \tag{2.29}$$

The only term left to examine is $(\phi_1, L_\epsilon^* u_c')$. Since u_c' is a solution to the local operator, we have

$$L_\epsilon^* u_c' = -\frac{rq\epsilon^{-1}u_c^{r-1}}{2\beta(s+1)} \int_{-1}^{1} u_c^p u_c' \, dx,$$
$$\sim -\frac{rq\epsilon^{-1}a^{p+1}u_c^{r-1}}{2\beta(s+1)(p+1)} \left(e_+^{p+1} - e_-^{p+1}\right), \tag{2.30}$$

where

$$e_\pm^p \equiv e^{-p\epsilon^{-1}(1\pm x_0)}. \tag{2.31}$$

In a similar way, the term $(\phi_1, L_\epsilon^* u_c')$ is approximated by

$$(\phi_1, L_\epsilon^* u_c') \sim -\frac{rq\epsilon^{-1}a^{p+1}C_1}{2\beta(s+1)(p+1)} \left(e_+^{p+1} - e_-^{p+1}\right) \int_{-1}^{1} u_c^{r-1} u_c' \, dx,$$
$$\sim -\frac{rq\epsilon^{-1}a^{p+r+1}C_1}{2\beta(s+1)(p+1)r} \left(e_+^{p+1} - e_-^{p+1}\right) \left(e_+^r - e_-^{-r}\right). \tag{2.32}$$

Since $p > 1$ and $r > 0$, upon comparing the terms in (2.32) and (2.29), it is clear that the second term on the right side of (2.26) is asymptotically negligible compared to the first term. Finally, substituting (2.27) and (2.29) into (2.26), we get the following asymptotic estimate for the exponentially small eigenvalue λ_1 as $\epsilon \to 0$:

$$\lambda_1 \sim 2a^2\hat{\beta}^{-1} \left(e^{-2\epsilon^{-1}(1+x_0)} + e^{-2\epsilon^{-1}(1-x_0)}\right). \tag{2.33}$$

In (2.33), a and $\hat{\beta}$ are defined in (2.5) and (2.20), respectively. The estimate (2.33) holds for p, q, r and s satisfying (1.8). Since $\lambda_1 > 0$, the quasi-equilibrium profile is unstable. However, since λ_1 is exponentially small, the instability is extremely weak and the quasi-equilibrium profile can persist for an exponentially long time interval.

To verify the estimate for λ_1, we also numerically estimate λ_1 by solving (2.8) using COLNEW. In Fig. 2.4, we compare the numerically computed values of λ_1 (the dots) with the asymptotic estimate (2.33) (dashed curve) for various values of ϵ for the parameter set $(p, q, r, s) = (2, 1, 2, 0)$. The asymptotic and numerical results are also shown in Table 2.2. Similar favorable comparisons can be made for other parameter sets.

ϵ	λ_1(full numerics)	λ_1(asymptotic)
.220000	$.12005\times10^{-1}$	$.135223\times10^{-1}$
.210000	$.80010\times10^{-2}$	$.877088\times10^{-2}$
.200000	$.50829\times10^{-2}$	$.544799\times10^{-2}$
.190000	$.30582\times10^{-2}$	$.321855\times10^{-2}$
.180000	$.17289\times10^{-2}$	$.179344\times10^{-2}$
.170000	$.90945\times10^{-3}$	$.932899\times10^{-3}$
.160000	$.43964\times10^{-3}$	$.447198\times10^{-3}$
.150000	$.19224\times10^{-3}$	$.194352\times10^{-3}$
.140000	$.74490\times10^{-4}$	$.74985\times10^{-4}$
.130000	$.24894\times10^{-4}$	$.249878\times10^{-4}$
.120000	$.69198\times10^{-5}$	$.69333\times10^{-5}$
.110000	$.15224\times10^{-5}$	$.152376\times10^{-5}$
.100000	$.24725\times10^{-6}$	$.247338\times10^{-6}$
$.90000\times10^{-1}$	$.26800\times10^{-7}$	$.268036\times10^{-7}$
$.80000\times10^{-1}$	$.16665\times10^{-8}$	$.166655\times10^{-8}$
$.70000\times10^{-1}$	$.46857\times10^{-10}$	$.468562\times10^{-10}$
$.60000\times10^{-1}$	$.40156\times10^{-12}$	$.400589\times10^{-12}$

Table 2.2: Comparison of asymptotic and fully numerical estimates of λ_1 for various values of ϵ with the parameter set $(p, q, r, s) = (2, 1, 2, 0)$.

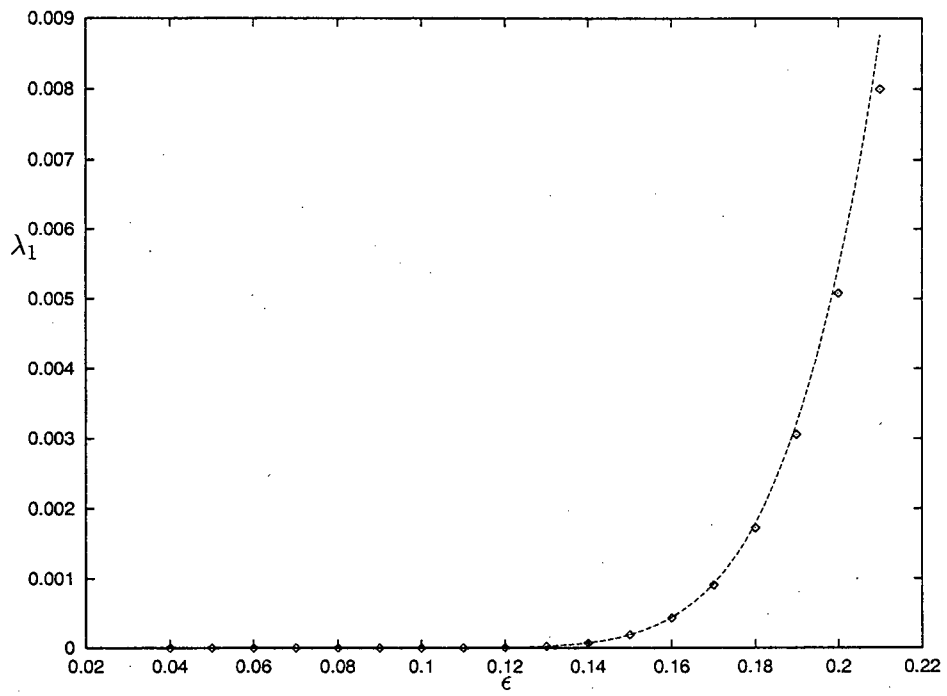

Figure 2.4: λ_1 versus ϵ for the parameter set $(p, q, r, s) = (2, 1, 2, 0)$.

We end this section with a few remarks. Firstly, we recall that λ_1 and $\phi_1 \sim C_1 u_c'\left(\epsilon^{-1}(x - x_0)\right)$ are an eigenpair of L_δ when $\delta = 0$. To within negligible exponentially small terms this eigenpair remains an eigenpair of L_δ as δ ranges from 0 to 1. To see this, we note that the only difference between the calculations of the eigenvalue for the local problem and for the non-local problem, is that the term $(L_\epsilon^* u_c', \phi_1)$ in (2.26) would be replaced by $(A\phi_1, \phi_1) = 0$, since A is self-adjoint. In the final calculation of λ_1 the term $(L_\epsilon^* u_c', \phi_1)$ was ignored since it is asymptotically exponentially smaller than the other terms in (2.26). Secondly, we note that λ_1, ϕ_1 is exponentially close to an eigenpair λ_1^*, ϕ_1^* of the adjoint operator, L_ϵ^*. For the same reasoning as above, ϕ_1^* would have the same interior behavior near $x = x_0$ as ϕ_1 and the same boundary layer correction terms near $x = \pm 1$. Repeating the calculation to find λ_1^*, we would arrive at the same estimate as in (2.33).

2.1.3 The Slow Motion of the Spike

The quasi-equilibrium solution fails to satisfy the steady-state problem corresponding to (1.18) by only exponentially small terms for any value of x_0 in $|x_0| < 1$. Moreover, the linearization about this solution admits a principal eigenvalue that is exponentially small. Therefore, we expect that the one-spike quasi-equilibrium profile evolves on an exponentially slow time-scale. We will now derive an equation of motion for the center of the spike corresponding to the quasi-equilibrium profile. To do so we first linearize (1.18) about $a(x,t) = h^\gamma u_c\left[\epsilon^{-1}(x - x_0(t))\right]$, where the spike location $x_0 = x_0(t)$ is to be determined. For a fixed x_0 we have shown that the linearization around this solution has an exponentially small principal eigenvalue as $\epsilon \to 0$. By eliminating the projection of the solution on the eigenfunction corresponding to this eigenvalue, we will derive an equation of motion for $x_0(t)$.

We begin by linearizing around a moving spike solution by writing,

$$a(x,t) = a_E(x; x_0(t)) + w(x,t), \tag{2.34}$$

where a_E is defined in (2.1) and $x_0(t)$ is the trajectory of the spike. Since (2.8) does not have an $O(1)$ positive eigenvalue, we may assume that $w \ll a_E$ and $w_t \ll \partial_t a_E$. Substituting (2.34) into (1.18), we get

$$L_\epsilon w = \partial_t a_E\,, \qquad -1 < x < 1\,, \quad t \geq 0 \tag{2.35a}$$

$$w_x(\pm 1, t) = -\partial_x a_E(\pm 1; x_0)\,. \tag{2.35b}$$

Next, we expand w in terms of the eigenfunctions ϕ_i of L_ϵ as

$$w = \sum_{i=0}^{\infty} E_i(t)\phi_i\,. \tag{2.36}$$

The solvability condition for w is that w is orthogonal to the eigenspace of L_ϵ^* associated with the exponentially small eigenvalue. Let ϕ_i^* be the i^{th} eigenfunction of L_ϵ^*. Then, since $(\phi_i, \phi_j^*) = \delta_{ij}$, we integrate by parts to show that

$$E_i(t) = (w, \phi_i^*) = \frac{1}{\lambda_i^*}\left[(L_\epsilon w, \phi_i^*) - \epsilon^2 w_x \phi_i^*|_{-1}^{1}\right]\,, \tag{2.37}$$

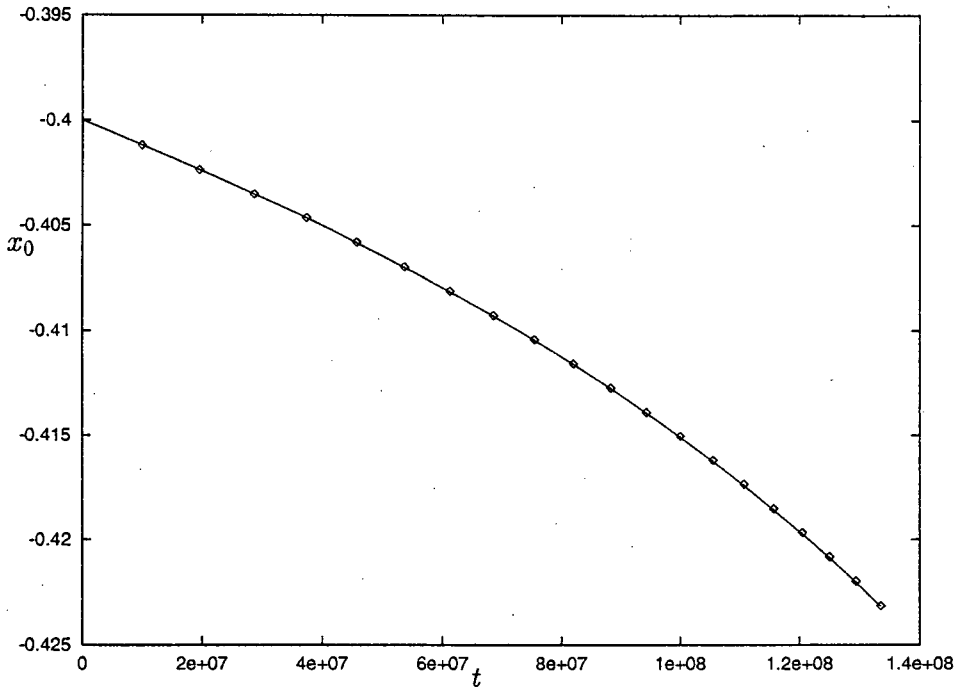

Figure 2.5: x_0 versus t for $\epsilon = .05$, $x_0(0) = -0.4$ and the parameter set $(p, q, r, s) = (2, 1, 2, 0)$.

where $L_\epsilon^* \phi_i^* = \lambda_i^* \phi_i^*$. Using (2.35), we have

$$E_i(t) = \frac{1}{\lambda_i^*} \left[(\partial_t a_E, \phi_i^*) + \epsilon^2 \phi_i^* \partial_x a_E |_{-1}^1 \right] . \tag{2.38}$$

As discussed previously, when $\epsilon \ll 1$, the nonlocal term in the eigenvalue problem (2.8) is insignificant in the asymptotic estimation of the eigenspace associated with the exponentially small eigenvalue of L_ϵ. Therefore, we can replace ϕ_1^* and λ_1^* by ϕ_1 and λ_1 in (2.38), where ϕ_1 and λ_1 are given in (2.19) and (2.33), respectively.

Since $\lambda_1 \to 0$ exponentially as $\epsilon \to 0$, we must impose the limiting solvability condition that $E_1 = 0$. This projection step yields the following implicit differential equation for $x_0(t)$:

$$(\partial_t a_E, \phi_1) = -\epsilon^2 \phi_1 \partial_x a_E |_{-1}^1 . \tag{2.39}$$

The dominant contribution to the left side of (2.39) arises from the region near x_0. For $\epsilon \to 0$,

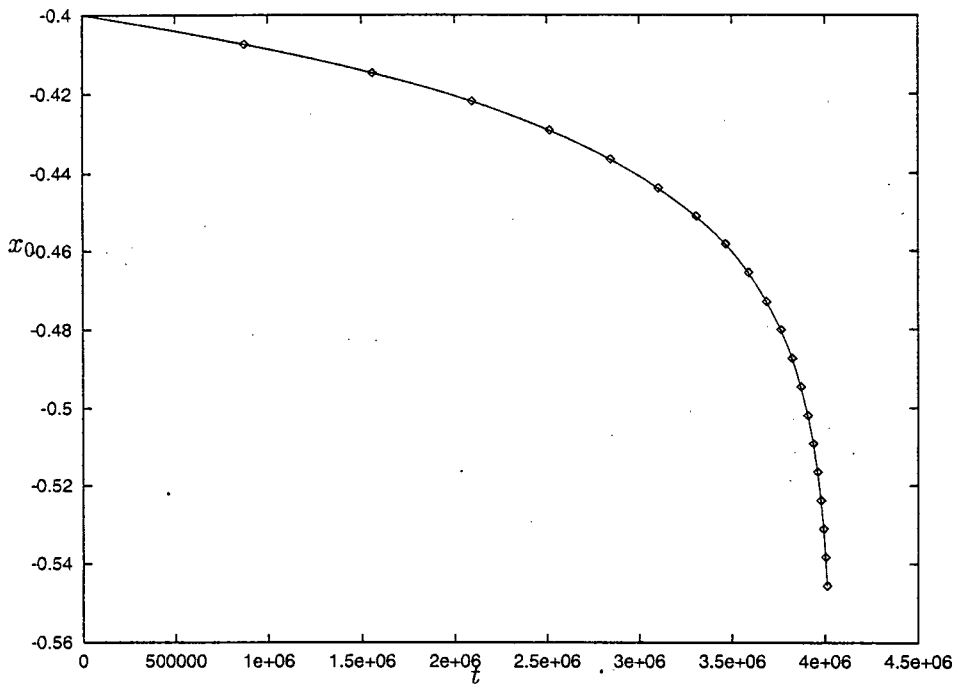

Figure 2.6: x_0 versus t for $\epsilon = .06$, $x_0(0) = -0.4$ and the parameter set $(p, q, r, s) = (2, 1, 2, 0)$

we calculate

$$(\partial_t a_E, \phi_1) \sim -C_1 h_E^{\gamma} \dot{x}_0 \hat{\beta} \epsilon^{-1}, \tag{2.40}$$

where $\dot{x}_0 \equiv dx_0/dt$. Finally, we can evaluate the right side of (2.39) using our estimates for $\phi_1(\pm 1)$ in (2.28) and for $u_c(z)$ as $z \to \infty$. This yields our main result of this section.

Proposition 2.1 (Metastability) *For $\epsilon \to 0$, metastable spike solution for (1.17), is represented by $a(x,t) = a_E(x; x_0(t))$, where a_E is defined in (2.1) and $x_0(t)$ satisfies,*

$$\dot{x}_0(t) \sim \frac{2a^2\epsilon}{\hat{\beta}} \left[e^{-2(1-x_0)/\epsilon} - e^{-2(1+x_0)/\epsilon} \right]. \tag{2.41}$$

Here a and $\hat{\beta}$ are defined in (2.5) and (2.20), respectively.

For a given initial condition $x_0(0) \in (-1, 1)$, this ODE shows that the spike drifts towards the endpoint that is closest to the initial location $x_0(0)$. As a consistency check on our solvability

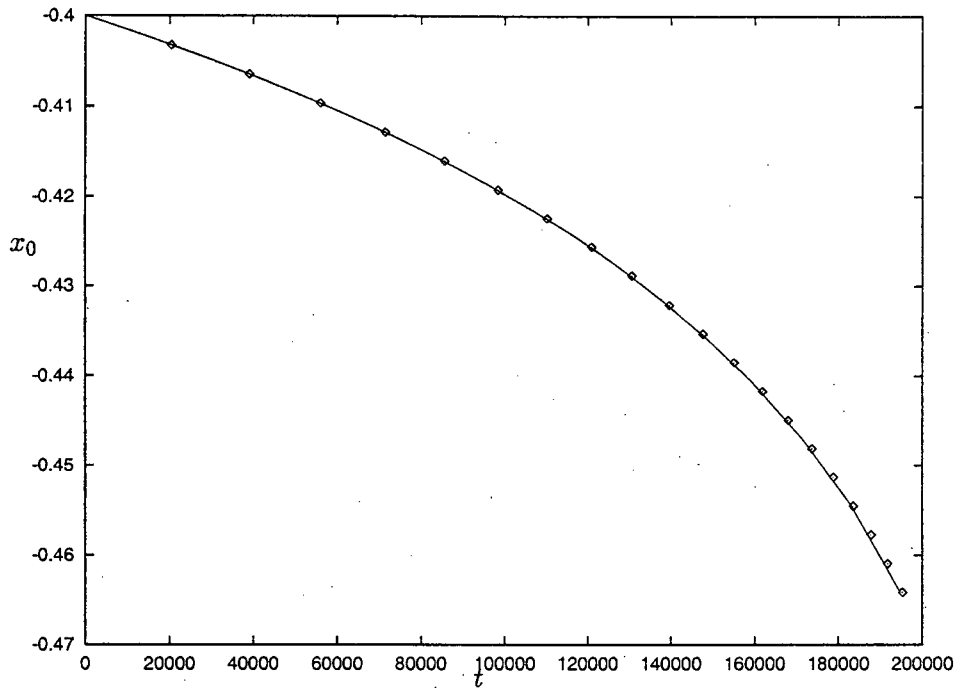

Figure 2.7: x_0 versus t for $\epsilon = .07$, $x_0(0) = -0.4$ and the parameter set $(p, q, r, s) = (2, 1, 2, 0)$.

condition $E_1 = 0$, we note from (2.20), (2.33), (2.40) and 2.41), that if the solvability condition were not imposed, then $E_1\phi_1 = O(\epsilon^{-1/2})$, which would violate our linearization assumption.

To verify the asymptotic result (2.41) we computed numerical solutions to (1.17) for various values of ϵ for the parameter set $(p, q, r, s) = (2, 1, 2, 0)$. The computations were done by using a variable coefficient variable time step backward-differentiation (BDF) scheme to integrate in time (see [44] where a similar scheme is used). The boundary value problem solver, COLNEW (see [3]), was then used to solve the resulting boundary value problem at each time step. At each time step the solution is calculated using a third and fourth order BDF scheme to estimate the error and determine the next maximum allowable time step. Comparisons of these results with a numerical integration of the asymptotic ODE (2.41) may be found in Fig. 2.5-2.7. In the figures the solid curves are the numerical solutions and the dots are obtained from the asymptotic ODE. In computing numerical solutions to (1.18) the initial condition $a_E(x; x_0(0))$

was used for certain values of $x_0(0)$ as can be seen from these figures.

2.2 An n-Spike Solution

We will now examine the properties of an n-spike quasi-equilibrium solution. The analysis will proceed in the same manner as for the case of the one-spike quasi-equilibrium solution. The stability of an n-spike quasi-equilibrium solution will be examined by linearizing about this solution and studying the resulting spectrum.

We begin by defining an n-spike quasi-equilibrium solution by

$$a_{n,E}(x) = h_{n,E}^{\gamma} \sum_{i=0}^{n-1} u_c \left[\epsilon^{-1}(x - x_i)\right] , \tag{2.42a}$$

$$h_{n,E} = \left(\epsilon^{-1} \frac{1}{2\mu} \int_{-1}^{1} a_{n,E}^{r} \, dx\right)^{\frac{1}{s+1}} , \tag{2.42b}$$

where $\gamma = q/(p-1)$. Substituting (2.42a) into (2.42b), we can determine $h_{n,E}$ as $\epsilon \to 0$ as,

$$h_{n,E} = \left(\frac{n\beta}{\mu}\right)^{\frac{p-1}{(s+1)(p-1)-qr}} , \tag{2.43}$$

where β was defined in (2.4). In (2.42a), the spike locations x_i for $i = 0, .., n-1$ satisfy $-1 < x_0 < x_1, .., < x_{n-1} < 1$. They correspond to local maxima of $a_{n,E}$.

We now linearize (1.18) about $a_{n,E}$ and $h_{n,E}$ by introducing ϕ and η defined by

$$a(x,t) = a_{n,E}(x) + e^{\lambda t}\phi(x), \tag{2.44a}$$

$$h(x,t) = h_{n,E} + e^{\lambda t}\eta(x) . \tag{2.44b}$$

Here $\phi \ll a_{n,E}$ and $\eta \ll h_{n,E}$. Substituting (2.44) into (1.18) we get the following eigenvalue problem,

$$\epsilon^2 \phi_{xx} - \phi + p\frac{a_{n,E}^{p-1}}{h_{n,E}^{q}}\phi - q\frac{a_{n,E}^{p}}{h_{n,E}^{q+1}}\eta = \lambda\phi, \tag{2.45a}$$

$$\eta = \frac{r h_{n,E}^{-s}}{s+1} \frac{\epsilon^{-1}}{2\mu} \int_{-1}^{1} a_{n,E}^{r-1}\phi \, dx . \tag{2.45b}$$

Since each spike of the quasi-equilibrium solution is localized to within an $O(\epsilon)$ region near $x = x_i$ for some i, we look for an eigenfunction $\phi(x)$ of the form

$$\phi(x) = \sum_{i=0}^{n-1} \tilde{\phi}_i \left[\epsilon^{-1}(x - x_i)\right] . \tag{2.46}$$

Therefore, we need to introduce local coordinates near each spike. In particular, the i^{th} set of inner variables are defined as

$$\tilde{\phi}_i(y_i) = \phi(x_i + \epsilon y_i), \qquad y_i = \epsilon^{-1}(x - x_i). \tag{2.47}$$

Substituting (2.43) and (2.45b) into (2.45a) and switching to the localized coordinate system (2.47), we get the following system of eigenvalue problems,

$$\tilde{\phi}_{i y_i y_i} - \tilde{\phi}_i + p \sum_{j=0}^{n-1} u_c^p \left[\epsilon^{-1}(x - x_j)\right] \tilde{\phi}_i$$

$$- \frac{r q \mu u_c^p}{2n\beta\mu(s+1)} \sum_{j=0}^{n-1} \int_{-\infty}^{\infty} u_c^{r-1}(y_j) \tilde{\phi}_j(y_j)\, dy_j = \lambda \tilde{\phi}_i\,, \quad |y_i| < \infty\,, \tag{2.48a}$$

$$\tilde{\phi}_i' \to 0 \quad \text{as} \quad y_i \to \pm\infty\,. \tag{2.48b}$$

Now we note that if each $\tilde{\phi}_i$ were independent of i (i. e. $\tilde{\phi}_i(y_i) = \Phi(y_i)$) for $i = 0, .., n-1$, then $\sum_{i=0}^{n-1} \int_{-\infty}^{\infty} u_c^{r-1}(y_i) \tilde{\phi}_i(y_i)\, dy_i = n \int_{-\infty}^{\infty} u_c^{r-1}(y) \Phi(y)\, dy$. The factor of n would cancel in (2.48) and we would be left with the same eigenvalue problem as (2.10). Thus, for the parameter set we have used previously, we would conclude that an n-spike solution has no $O(1)$ positive eigenvalue. However, we now show that this conclusion is erroneous. To see this we note that we can construct a global eigenfunction by taking $\tilde{\phi}_i(y_i) = b_i \Phi(y)$ for some constant b_i. The non-local term in (2.48) then becomes

$$\sum_{i=0}^{n-1} \int_{-\infty}^{\infty} u_c^{r-1}(y_i) \tilde{\phi}_i(y_i)\, dy_i = \int_{-\infty}^{\infty} u_c^{r-1}(y) \Phi(y)\, dy \left(\sum_{i=0}^{n-1} b_i \right) . \tag{2.49}$$

Then, if we impose the constraint that

$$\sum_{i=0}^{n-1} b_i = 0\,, \tag{2.50}$$

the non-local term vanishes. Hence, with this constraint, $\Phi(y)$ satisfies the local eigenvalue problem

$$\Phi'' - \Phi + pu_c^{p-1}\Phi = \bar{\lambda}_0\Phi. \tag{2.51}$$

This problem has exactly one positive eigenvalue $\bar{\lambda}_0$. When $p = 2$, we found that $\bar{\lambda}_0 = 5/4$ with corresponding eigenfunction $\Phi_0(y) = \mathrm{sech}^2(y/2)$. Hence, under the constraint (2.50), $\bar{\lambda}_0$ is also a positive eigenvalue of (2.48). This then leads to an instability.

In summary, when there is more than one spike we may always construct an eigenfunction of the form $\phi(x) = \sum_{i=0}^{n-1} b_i\Phi\left[\epsilon^{-1}(x - x_i)\right]$ where $\sum_{i=0}^{n-1} b_i = 0$. This eigenfunction has a positive eigenvalue. Therefore, it is impossible to find a stable multiple spike solution for the shadow problem.

We now illustrate this instability result numerically for a two-spike solution for the parameter set $(p, q, r, s) = (2, 1, 2, 0)$, $\mu = 1$, $\tau = 0.01$, $D = 40$, and $\epsilon = 0.05$. We took the quasi-equilibrium solution as our initial condition. The first spike (Spike 1) is centered at $x_0 = -0.5$ while the second spike (Spike 2) is centered at $x_1 = 0.5$. In Table 2.3 we tabulate the numerically computed amplitudes of the two spikes as a function of time. We now use this data to estimate the positive eigenvalue. We remark that the data in Table 2.3 is taken after the simulation has been run approximately $t = 20$ units to eliminate any transients and to ensure that the positive eigenvalue is dominant. After this time the solution at the spike locations $x = x_0$ and $x = x_1$ will be approximately given by,

$$a(x_i, t) \approx a_{2,E}(x_i) + e^{\lambda_0 t}\phi_0(x_i)\,, \qquad i = 0, 1\,. \tag{2.52}$$

This relation will only govern the linear instability of $a_{2,E}$. For the parameter set we have used $a_{2,E}(x_i) = 6.25$. Then, we can re-write (2.52) as,

$$\lambda_0 t + \log\left[\phi_0(x_i)\right] \approx \log(|a(x_i, t) - 6.25|)\,, \qquad i = 0, 1\,. \tag{2.53}$$

To estimate λ_0 from the data in Table 2.3, we take $x_1 = 0.5$ and evaluate (2.53) at two different values of time, labeled by t_1 and t_2. Using the numerically computed values for $a(0.5, t)$ at

$t = t_1$ and $t = t_2$ gives us two equations for the two unknowns $\phi_0(0.5)$ and λ_0. In this way, λ_0 can be estimated. In Table 2.4 we give the numerical results for λ_0 and $\phi_0(0.5)$ using various values of t_1 and t_2. For this parameter set, we would expect that the principal eigenvalue is 1.25. The interpolated values, obtained by our numerical procedure, are all close to 1.25 as expected.

2.3 A Spike in a Multi-Dimensional Domain

We now construct a quasi-equilibrium solution a_E for (1.19). This is done in a similar manner as in the one-dimensional case, except that here the quasi-equilibrium solution will be radially symmetric about the center of the spike. Thus, we look for a steady-state solution to (1.19) in all of $\mathbb{R}^N$ of the form

$$a = a_E(\mathbf{x}; \mathbf{x_0}) \equiv h^\gamma u_c(\epsilon^{-1}|\mathbf{x} - \mathbf{x}_0|)\,, \qquad \gamma = q/(p-1)\,, \tag{2.54}$$

where $\mathbf{x_0}$ is arbitrary. The function $u_c(\rho)$, called the canonical spike solution, is a non-negative radially symmetric function, which decays exponentially as $\rho \to \infty$. It satisfies

$$u_c'' + \frac{N-1}{\rho}u_c' - u_c + u_c^p = 0\,, \qquad \rho > 0\,, \tag{2.55a}$$

$$u_c'(0) = 0\,; \qquad u_c(\rho) \sim a\rho^{(1-N)/2}e^{-\rho}\,, \quad \text{as} \quad \rho \to \infty\,, \tag{2.55b}$$

where $a > 0$ is some constant. In dimension $N > 2$, we require that $p < p_c$, where p_c is the critical Sobolev exponent for dimension N. In terms of this solution, $h = h_E$, where

$$h_E = \left(\frac{\epsilon^{-N}}{\mu|\Omega|}\int_\Omega u_c^r\, d\mathbf{x}\right)^{\frac{p-1}{(s+1)(p-1)-qr}}\,. \tag{2.56}$$

Here $|\Omega|$ is the volume of Ω. Since u_c is localized near $\mathbf{x_0}$, as $\epsilon \to 0$ we get,

$$h_E \sim \left(\frac{\Omega_N}{\mu|\Omega|}\int_0^\infty u_c^r\, \rho^{N-1} d\rho\right)^{\frac{p-1}{(s+1)(p-1)-qr}}\,, \tag{2.57}$$

where Ω_N is the surface area of the unit N-dimensional sphere.

Recall that in the one-dimensional case and with $p = 2$ we have the exact solution $u_c(\rho) = \frac{3}{2}\mathrm{sech}^2(\frac{\rho}{2})$, and hence $a = 6$. To find numerical solutions for $u_c(\rho)$ and for a in other dimensions,

time	Spike 1 Height	Spike 2 Height
19.5	6.2738663390032	6.2635545772640
19.8	6.2761841264723	6.2612374542097
20.1	6.2795439171902	6.2578790593718
20.4	6.2844142872978	6.2530116219365
20.7	6.2914746492378	6.2459574213615
21.0	6.3017102226534	6.2357347923334
21.3	6.3165498360813	6.2209223724487
21.6	6.3380658088900	6.1994635220925
21.9	6.3692634678024	6.1683858288480
22.2	6.4144988374999	6.1234022942033
22.5	6.4800753144382	6.0583539884737
22.8	6.5750761790975	5.9644587136514
23.1	6.7124619645111	5.8293778760449
23.4	6.9103141671528	5.6362910167926
23.7	7.1926098041313	5.3636802602846
24.0	7.5876099073842	4.9877041819062
24.3	8.1196649411629	4.4906888214834
24.6	8.7900467006609	3.8780493118962
24.9	9.5540932480348	3.1943794842134
25.2	10.3232394145038	2.5150430348060
25.5	11.006159488840	1.9098035904776

Table 2.3: Height of spike 1 centered at $x_0 = -0.5$ and of spike 2 centered at $x_1 = 0.5$.

t_1	t_2	$a(.5,t_1)$	$a(.5,t_2)$	λ_0	$\phi_0(.5)$
22.8	23.4	5.9644587136514	5.6362910167926	1.275223721	$-e^{-30.32846949}$
23.1	23.7	5.8293778760449	5.3636802602846	1.242238171	$-e^{-29.56172215}$
22.5	23.7	6.0583539884737	5.3636802602846	1.276189822	$-e^{-30.36637629}$
22.2	23.4	6.1234022942033	5.6362910167926	1.315422050	$-e^{-31.26911038}$

Table 2.4: Logarithmic Interpolation of λ_0 and $\phi_0(.5)$.

we will treat N as a real parameter, and use N (and p for $p \neq 2$) as continuation parameters. We can use the far field asymptotic behavior (2.55b) to obtain the boundary condition $u_c' = \frac{(1-N)}{2\rho} u_c$, which we impose at some large value $\rho = \rho_L$ in our numerical computations of (2.55). The computations are done using COLNEW. In Fig. 2.8 we plot the numerically computed solutions $u_c(\rho)$ for $N = 1, 2, 3$ when $p = 2$.

For the finite domain problem we restrict $\mathbf{x}_0$ to be strictly contained in Ω so that $\text{dist}(\mathbf{x}_0, \partial\Omega) >> O(\epsilon)$. Then, under this restriction we note that, a_E will satisfy the steady-state problem for (1.19a), but will fail to satisfy the no flux boundary condition (1.19c) by only exponentially small terms for any value of $\mathbf{x}_0$ in the interior of Ω. Thus, we expect that the spectrum of the eigenvalue problem associated with the linearization about a_E contains exponentially small eigenvalues.

2.3.1 The Nonlocal Eigenvalue Problem

Let $\mathbf{x_0} \in \Omega$ be fixed, and linearize (1.19) about a_E, h_E. We obtain the eigenvalue problem for this linearization by introducing ϕ and η defined by

$$a(\mathbf{x}, t) = a_E(\mathbf{x}; \mathbf{x_0}) + e^{\lambda t}\phi(\mathbf{x}), \tag{2.58a}$$

$$h(t) = h_E + e^{\lambda t}\eta\,, \tag{2.58b}$$

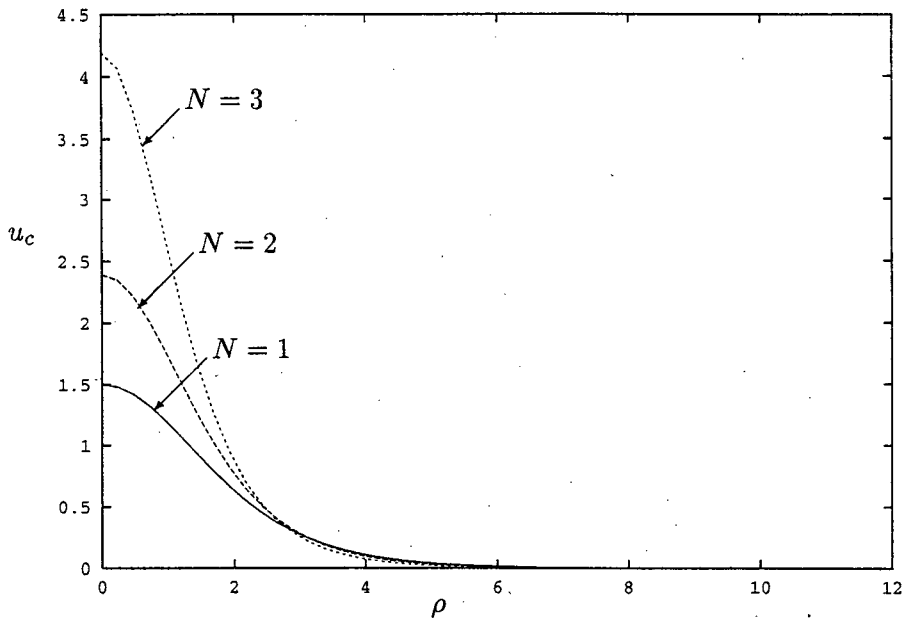

Figure 2.8: Numerical solution for $u_c(\rho)$ when $N = 1, 2, 3$ and $p = 2$.

where $\phi \ll a_E$ and $\eta \ll h$. Substituting (2.58) into (1.19) we obtain, after a lengthy calculation, the following non-local eigenvalue problem;

$$L_\epsilon \phi \equiv \epsilon^2 \Delta \phi + (-1 + p u_c^{p-1})\phi - \frac{r q \epsilon^{-N} u_c^p}{\beta_N \Omega_N (s+1)} \int_\Omega u_c^{r-1} \phi \, d\mathbf{x} = \lambda \phi, \quad \text{in} \quad \Omega, \tag{2.59a}$$

$$\phi_n = 0 \quad \text{on} \quad \partial\Omega \, . \tag{2.59b}$$

Here $u_c = u_c\left[\epsilon^{-1}|\mathbf{x} - \mathbf{x_0}|\right]$, and β_N is defined by

$$\beta_N = \int_0^\infty u_c^{r-1} \rho^{N-1} \, d\rho \, . \tag{2.60}$$

Since u_c is localized near $\mathbf{x}_0$, we will only seek eigenfunctions that are localized near $\mathbf{x} = \mathbf{x_0}$. These eigenfunctions are of the form

$$\tilde{\phi}(\mathbf{y}) = \phi(\mathbf{x_0} + \epsilon \mathbf{y}) \, , \qquad \mathbf{y} = \epsilon^{-1}(\mathbf{x} - \mathbf{x_0}) \, . \tag{2.61}$$

Therefore, we can replace Ω by $\mathbb{R}^n$ in (2.59a) and impose a decay condition for $\tilde{\phi}$ as $|\mathbf{y}| \to \infty$. This gives us the non-local eigenvalue problem for the infinite domain

$$\hat{L}_\epsilon \tilde{\phi} \equiv \Delta_y \tilde{\phi} + (-1 + p u_c^{p-1})\tilde{\phi} - \frac{r q u_c^p}{\beta_N \Omega_N (s+1)} \int_{\mathbb{R}^N} u_c^{r-1} \tilde{\phi}\, d\mathbf{y} = \tilde{\lambda}\tilde{\phi}, \quad \text{in} \quad \mathbb{R}^N, \tag{2.62a}$$

$$\tilde{\phi} \to 0 \qquad \text{as} \quad |\mathbf{y}| \to \infty\,. \tag{2.62b}$$

In this problem $u_c = u_c(|\mathbf{y}|)$. If, in addition, we consider an eigenfunction that is radially symmetric (i. e. $\tilde{\phi} = \tilde{\phi}(\rho)$, where $\rho = |\mathbf{y}|$), then (2.62) reduces to

$$\tilde{L}_\epsilon \tilde{\phi} \equiv \Delta_\rho \tilde{\phi} + (-1 + p u_c^{p-1})\tilde{\phi} - \frac{r q u_c^p}{\beta_N (s+1)} \int_0^\infty u_c^{r-1} \tilde{\phi} \rho^{N-1}\, d\rho = \tilde{\lambda}\tilde{\phi}, \quad \rho > 0, \tag{2.63a}$$

$$\tilde{\phi} \to 0 \quad \text{as} \quad \rho \to \infty\,, \tag{2.63b}$$

where $\Delta_\rho \tilde{\phi} \equiv \tilde{\phi}'' + (N-1)\rho^{-1}\tilde{\phi}'$.

We now analyze the spectra of these eigenvalue problems. We first note that, for each $i = 1, .., N$, the function $\tilde{\phi}_i = \partial_{y_i} u_c(|\mathbf{y}|)$ satisfies (2.62) with $\lambda = 0$. Here y_i is the i^{th} coordinate of $\mathbf{y}$. This follows from the combined effects of translation invariance and the vanishing of the integral in (2.62) by symmetry considerations. Thus, (2.62) has a zero eigenvalue of multiplicity N with corresponding eigenfunctions $\tilde{\phi}_i = \partial_{y_i} u_c(|\mathbf{y}|)$ for $i = 1, .., N$. Each of these eigenfunctions has one nodal line. These eigenpairs will be perturbed by only exponentially small terms as a result of the finite domain. Hence, there are N eigenvalues of (2.59) that are exponentially small, and they are estimated below. The goal is to determine whether these are the principal eigenvalues of (2.59).

We claim that these are not the principal eigenvalues for (2.59) when the non-local term in (2.59) is absent. To see this, suppose that the non-local term in (2.59), (2.62) and (2.63) is absent. The corresponding eigenvalue problems are then local and self-adjoint, and several key properties follow. In particular, since $\tilde{\phi}_i = \partial_{y_i} u_c(|\mathbf{y}|)$ is an eigenfunction of (2.62) with a zero eigenvalue and has one nodal line, the local eigenvalue problem must have a simple, positive eigenvalue, which is independent of ϵ. The corresponding positive, radially symmetric, eigenfunction satisfies the local version of (2.63). The effect of the finite domain in (2.59) is to

perturb this eigenvalue by only exponentially small terms. Thus, when the non-local term is absent no metastable behavior can occur.

The effect of the non-local term will be to ensure that the exponentially small eigenvalues are the principal eigenvalues for the non-local eigenvalue problem (2.59). Thus, the quasi-equilibrium solution will be metastable if we can show that the principal eigenvalue of (2.63) has a negative real part. We may apply a multi-dimensional version of Theorem 2.1 to show that (2.63) has no eigenvalues with positive real part.

Theorem 2.2 (Wei[52]; Multi-Dimensional) *Consider the eigenvalue problem for* $\gamma_0 \geq 0$,

$$\Delta\phi - \phi + pu_c^{p-1}\phi - \gamma_0(p-1)u_c^p \left(\frac{\int_{\mathbb{R}^n} u_c(y)^{r-1}\phi(y)\,dy}{\int_{\mathbb{R}^n} u_c(y)^r\,dy} \right) = \lambda\phi, \tag{2.64}$$

$$\phi \to 0 \quad as \quad |y| \to \infty. \tag{2.65}$$

corresponding to eigenpairs for which $\lambda \neq 0$. *Here* u_c *satisfies (2.55). Let* $\lambda_0 \neq 0$ *be the eigenvalue of (2.64) with the largest real part. Then if* $\gamma_0 < 1$,

$$Re(\lambda_0) > 0\,. \tag{2.66}$$

Alternatively, if $\gamma_0 > 1$ *and if either of the following two conditions hold,*

$$r = 2, \quad 1 < p \leq 5, \quad or \quad r = p+1, p > 1. \tag{2.67}$$

Then,

$$Re(\lambda_0) < 0\,. \tag{2.68}$$

As in the case for one-dimension, for any parameter set satisfying (2.67), the operator L_ϵ will have no $O(1)$ eigenvalues with positive real part.

Again it is instructive to consider how the non-local terms in (2.63) effect the spectrum. To do so, we compute the eigenvalues and eigenfunctions of the radially symmetric problem (2.63),

where a continuation parameter δ, with $0 \leq \delta \leq 1$, multiplies the nonlocal term

$$L_\delta \tilde{\phi} \equiv \Delta_\rho \tilde{\phi} + (-1 + p u_c^{p-1})\tilde{\phi} - \delta \frac{r q u_c^p}{\beta_N (s+1)} \int_0^\infty u_c^{r-1} \tilde{\phi} \rho^{N-1} \, d\rho = \lambda \tilde{\phi}, \quad \rho > 0, \tag{2.69a}$$

$$\tilde{\phi} \to 0 \quad \text{as} \quad \rho \to \infty \, . \tag{2.69b}$$

We compute the eigenvalues of this problem as a function of δ, and in particular track the first eigenvalue $\lambda_0(\delta)$. We will show that the positive principal eigenvalue $\lambda_0(0)$, which occurs when the non-local term is absent, will cross through zero into the left half plane as δ increases. Thus, we must show that the first eigenvalue $\lambda_0(\delta)$ has a negative real part when $\delta = 1$.

For the parameter set $(p, q, r, s) = (2, 1, 2, 0)$, in Fig. 2.9 and Fig. 2.10 we plot the first two eigenvalues $\lambda_0(\delta)$ and $\lambda_{N+1}(\delta)$ of (2.69) as a function of δ for $N = 2$ and $N = 3$, respectively. Here λ_{N+1} is the first eigenvalue in the sequence for (2.62) following the zero λ_i, $i = 1, .., N$. These computations were done using COLNEW. These plots clearly indicate that $\lambda_0(\delta)$ crosses through 0 before $\delta = 1$. At some value of δ, λ_0 and λ_{N+1} collide and become complex. To track the eigenvalues past the point where they become complex, we use the same technique as in the one-dimensional case. The differential operator is approximated by a matrix and the eigenvalues of the matrix are then approximations of the eigenvalues of the differential operator. Using this numerical procedure, we give numerical values for the real and imaginary part of $\lambda_0(\delta)$ in Table 2.5. This table shows that the real part of λ_0 is negative when $\delta = 1$. Similar computations, with similar conclusions, can be performed for other values of p, q, r and s.

2.3.2 An Exponentially Small Eigenvalue

We will now use a boundary layer analysis to construct a composite approximation to the eigenfunctions corresponding to the exponentially small eigenvalues of (2.59). The corresponding eigenfunctions are well approximated by $\partial_{x_i} u_c$, for $i = 1, .., N$ in the interior of the domain and each of these eigenfunctions has a boundary layer correction term near $\partial\Omega$ in order to satisfy the no-flux boundary condition on $\partial\Omega$. In order to resolve the boundary layer we must define a local coordinate system. Let $\hat{\eta}$ represent the distance from a point in Ω to $\partial\Omega$, where $\hat{\eta} < 0$ corresponds to the interior of Ω. Let ζ correspond to the other $N - 1$ orthogonal coordinates.

δ	λ_0 in $\mathbb{R}^2$	λ_0 in $\mathbb{R}^3$
0.00000	1.6388	2.3703
0.05000	1.4814	2.1588
0.10000	1.3231	1.9456
0.15000	1.1638	1.7304
0.20000	1.0030	1.5125
0.25000	0.84032	1.2910
0.30000	0.67516	1.0646
0.35000	0.50641	0.83098
0.40000	0.33218	0.58554
0.45000	0.14857	0.31741
0.50000	-.055026	-.019898
0.55000	-.37526	$-.33843 + 0.29744i$
0.60000	$-.48239 + 0.24569i$	$-.44368 + 0.45028i$
0.65000	$-.56115 + 0.33165i$	$-.54978 + 0.54508i$
0.70000	$-.64059 + 0.38475i$	$-.65696 + 0.60964i$
0.75000	$-.72097 + 0.41770i$	$-.76550 + 0.65310i$
0.80000	$-.80268 + 0.43510i$	$-.87584 + 0.67970i$
0.85000	$-.88640 + 0.43886i$	$-.98857 + 0.69170i$
0.90000	$-.97333 + 0.42959i$	$-1.1045 + 0.69037i$
0.95000	$-.10657 + 0.40726i$	$-1.2249 + 0.67652i$
0.10000	$-.11678 + 0.37248i$	$-1.3513 + 0.65089i$

Table 2.5: δ and λ_0 in $\mathbb{R}^2$ and $\mathbb{R}^3$ for the case of $(p, q, r, s) = (2, 1, 2, 0)$.

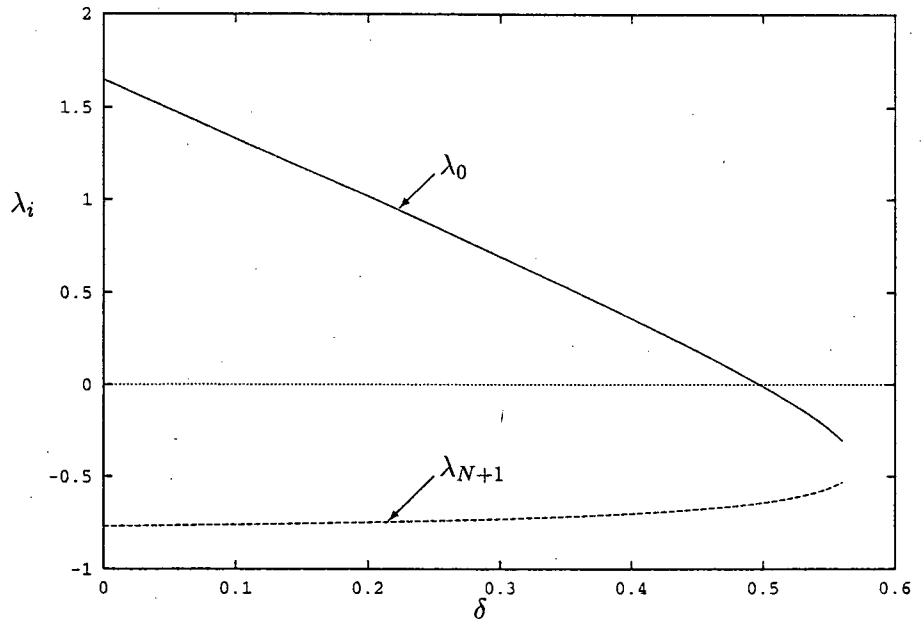

Figure 2.9: $\lambda_0(\delta)$ and $\lambda_{N+1}(\delta)$ versus δ in $\mathbb{R}^2$ for the parameter set $(p,q,r,s) = (2,1,2,0)$.

To localize the region near $\partial\Omega$, we let $\eta = \epsilon^{-1}\hat{\eta}$. The eigenfunction on the finite domain can then be approximated by,

$$\phi_i = C_i \left(\partial_{x_i} u_c \left(\epsilon^{-1} |\mathbf{x} - \mathbf{x}_0| \right) + \hat{\phi}_i \right) , \tag{2.70}$$

where C_i is a normalization constant and $\hat{\phi}_i$ is a boundary layer correction term. Using the fact that u_c is exponentially small near $\partial\Omega$, we get the following boundary layer problem

$$\partial_{\eta\eta}\hat{\phi}_i - \hat{\phi}_i = 0, \quad \eta < 0, \tag{2.71}$$

$$\partial_{\eta}\hat{\phi}_i = \underbrace{-\epsilon \partial_{\hat{\eta}} (\partial_{x_i} u_c)|_{\eta=0}}_{\text{a function of } \zeta}, \quad \text{on} \quad \eta = 0, \tag{2.72}$$

$$\hat{\phi}_i \to 0 \quad \text{as} \quad \eta \to -\infty . \tag{2.73}$$

We require that $\hat{\phi}_i \to 0$ as $\eta \to -\infty$ to match to the outer solution. Then, the solution for $\hat{\phi}_i$ is

$$\hat{\phi}_i = \epsilon g_i(\zeta) e^{\eta}, \quad \text{where} \quad g_i(\zeta) \equiv -\partial_{\hat{\eta}} (\partial_{x_i} u_c)|_{\eta=0}. \tag{2.74}$$

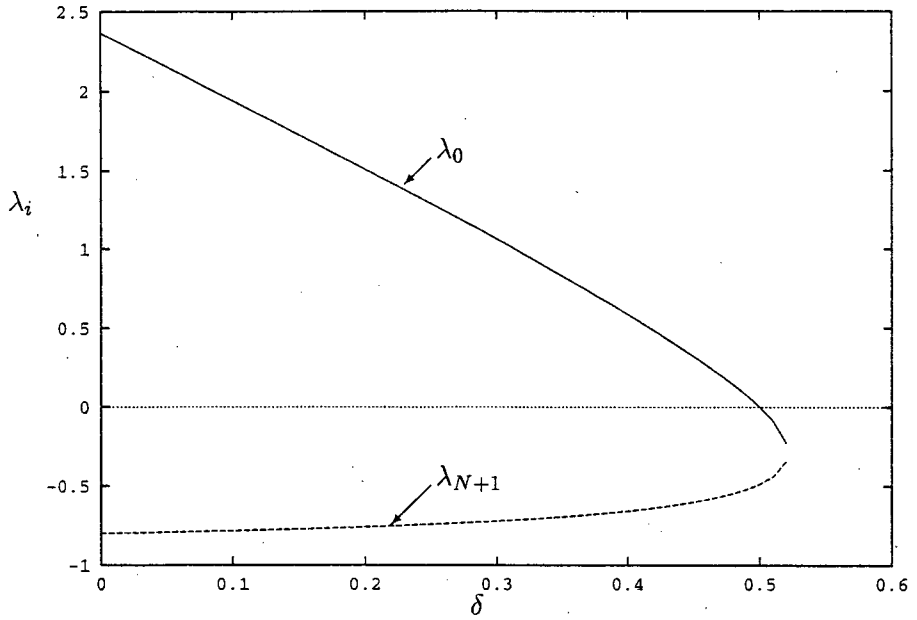

Figure 2.10: $\lambda_0(\delta)$ and $\lambda_{N+1}(\delta)$ versus δ in $\mathbb{R}^3$ for the parameter set $(p,q,r,s) = (2,1,2,0)$.

Thus, the composite asymptotic solution for the eigenfunction is

$$\phi_i = C_i \left[\partial_{x_i} u_c + \epsilon g_i(\zeta) e^{\hat{\eta}/\epsilon} \right], \quad i = 1 \ldots, N. \tag{2.75}$$

Below we need an estimate for ϕ_i on $\partial\Omega$. To do so we need to calculate g_i. Let x_{0i} represent the i^{th} coordinate of $\mathbf{x}_0$. So, setting $r = |\mathbf{x} - \mathbf{x_0}|$, we apply the chain rule, which gives

$$g_i \sim -\frac{(x_i - x_{0i})}{\epsilon^2 r} \left[u_c''(r/\epsilon)\mathbf{r} \cdot \mathbf{n} \right], \tag{2.76}$$

where $\mathbf{n}$ is the outward unit normal to Ω. Since $u_c(\rho) \sim a\rho^{(1-N)/2} e^{-\rho}$ as $\rho \to \infty$ we get that,

$$g_i \sim -a\epsilon^{(N-5)/2}(x_i - x_{0i}) r^{-(1+N)/2} e^{-r/\epsilon} \mathbf{r} \cdot \mathbf{n}, \quad \text{on} \quad \partial\Omega\,. \tag{2.77}$$

Combining (2.75) with (2.77), we get an asymptotic approximation for ϕ_i on $\partial\Omega$,

$$\phi_i \sim -C_i a\epsilon^{(N-3)/2} a(x_i - x_{0i}) r^{-(1+N)/2} e^{-r/\epsilon}(1 + \mathbf{r} \cdot \mathbf{n}), \quad \text{on} \quad \partial\Omega\,. \tag{2.78}$$

In order to complete our asymptotic estimate of the exponentially small eigenvalues, we apply Green's identity to ϕ_i and $\partial_{x_i} u_c$ to get the following relationship:

$$\lambda_i(\partial_{x_i} u_c, \phi_i) = -\epsilon^2 \int_{\partial\Omega} \phi_i \partial_n(\partial_{x_i} u_c) dS + \left(L_\epsilon^* \left[\partial_{x_i} u_c\right], \phi_i\right). \tag{2.79}$$

Here L_ϵ^* is the adjoint of L_ϵ,

$$L_\epsilon^* v \equiv \epsilon^2 \Delta v - v + u_c^{p-1} v - \frac{rq\epsilon^{-N} u_c^{r-1}}{\beta_N \Omega_N (s+1)} \int_\Omega u_c^p v \, d\mathbf{x}. \tag{2.80}$$

We will now estimate each term in (2.79). Since $\partial_{x_i} u_c$ is an exact solution to the local problem, we have that,

$$L_\epsilon^* \left(\partial_{x_i} u_c\right) = -\frac{rq\epsilon^{-N} u_c^{r-1}}{\beta_N \Omega_N (s+1)} \int_\Omega u_c^p \partial_{x_i} u_c \, d\mathbf{x}. \tag{2.81}$$

Next, since u_c is radially symmetric and localized to a small region in the interior of Ω, it is clear that $\int_\Omega u_c^p \partial_{x_i} u_c \, d\mathbf{x} \sim \int_\Omega u_c^p \partial_{x_j} u_c \, d\mathbf{x}$, as $\epsilon \to 0 \ \forall i, j = 1 \ldots N$. Thus, we may write the expression above as,

$$L_\epsilon^* \left(\partial_{x_i} u_c\right) \sim -\frac{rq\epsilon^{-N} u_c^{r-1}}{N\beta_N \Omega_N (s+1)} \int_\Omega \sum_{i=1}^{N} u_c^p \partial_{x_i} u_c \, d\mathbf{x}. \tag{2.82}$$

An application of the Divergence Theorem results in,

$$L_\epsilon^* \left(\partial_{x_i} u_c\right) \sim -\frac{rq\epsilon^{-N} u_c^{r-1}}{N\beta_N \Omega_N (s+1)} \int_{\partial\Omega} \left(\frac{u_c^{p+1}}{p+1}\right) dS. \tag{2.83}$$

On the boundary of Ω, $u_c \left[\epsilon^{-1}|\mathbf{x} - \mathbf{x_0}|\right] \sim a\epsilon^{(N-1)/2} r^{(1-N)/2} e^{-\epsilon^{-1}|\mathbf{x}-\mathbf{x_0}|}$. Therefore, the integral in (2.83) will be exponentially small. We then estimate the integral in (2.83) to get the following bound:

$$|L_\epsilon^* \left(\partial_{x_i} u_c\right)| < F\epsilon^{-N} |\partial\Omega| u_c^{r-1} \epsilon^{(N-1)(p+1)/2} \rho_0^{(1-N)(p+1)/2} e^{-\epsilon^{-1}(p+1)\rho_0}, \tag{2.84}$$

where

$$F = \frac{rqa^{p+1}}{N\beta_N \Omega_N (s+1)(p+1)}. \tag{2.85}$$

Here $\rho_0 = \text{dist}(\mathbf{x_0}, \partial\Omega)$. Therefore, with $\phi_i \sim C_i \partial_{x_i} u_c$, we have

$$|\left(L_\epsilon^* \left(\partial_{x_i} u_c\right), \phi_i\right)| < FC_i \epsilon^{-N} |\partial\Omega| \epsilon^{(N-1)(p+1)/2} \times \rho_0^{(1-N)(p+1)/2} e^{-\epsilon^{-1}(p+1)\rho_0} \int_\Omega u_c^{r-1} \partial_{x_i} u_c \, d\mathbf{x}. \tag{2.86}$$

Estimating the integral term in (2.86) by a similar procedure, (2.86) reduces to the following,

$$|(L_\epsilon^* \partial_{x_i} u_c, \phi_i)| < \frac{a^r |\partial\Omega|^2 F C_i \epsilon^{-N}}{rN} \epsilon^{(N-1)(p+r+1)/2} \rho_0^{-(N-1)(p+r+1)/2} e^{-\epsilon^{-1}\rho_0(p+r+1)}. \tag{2.87}$$

Therefore, we conclude that

$$|(L_\epsilon^* \partial_{x_i} u_c, \phi_i)| = 0\left(\epsilon^b e^{-\epsilon^{-1}\rho_0(p+r+1)}\right), \tag{2.88}$$

for some b. We will show that this term is exponentially smaller than the first term on the right side of (2.79), and therefore, we can ignore it.

Now we estimate the left hand side of (2.79). Since ϕ_i and $\partial_{x_i} u_c$ are exponentially small outside of a neighborhood of $\mathbf{x} = \mathbf{x}_0$, this inner product is dominated by the contribution from the region near $\mathbf{x} = \mathbf{x_0}$. Using a Laplace-type approximation, we can approximate the inner product to get

$$(\partial_{x_i} u_c, \phi_i) \sim \frac{C_i}{\epsilon^2} \int_\Omega \left[u_c'(r/\epsilon)\right]^2 \left(\frac{x_i - x_{0i}}{r}\right)^2 d\mathbf{x} \sim \frac{C_i \epsilon^{N-2}}{N} \int_{\mathbb{R}^N} \left[u_c'(\rho)\right]^2 \rho^{N-1}\, d\rho\, d\theta\,, \tag{2.89}$$

where θ represents the $N-1$ angular co-ordinates. Since the integrand is independent of θ,

$$(\partial_{x_i} u_c, \phi_i) \sim C_i \epsilon^{N-2} \Omega_N \hat{\beta}_N / N, \quad \text{where} \quad \hat{\beta}_N \equiv \int_0^\infty \left[u_c'(\rho)\right]^2 \rho^{N-1}\, d\rho\,. \tag{2.90}$$

Here Ω_N is the surface area of the N-dimensional unit sphere. Then we determine C_i by using the normalization relation $\int_\Omega \phi_i^2\, d\mathbf{x} = 1$ to obtain,

$$C_i = \left(\frac{N}{\hat{\beta}_N \Omega_N}\right)^{1/2} \epsilon^{(2-N)/2}. \tag{2.91}$$

Finally, we get our asymptotic estimate of λ_i by substituting (2.90) and (2.78) into (2.79), and using the estimate $\partial_n(\partial_{x_i} u_c) \sim a\epsilon^{(N-5)/2} r^{-(N+1)/2} e^{-r/\epsilon}$, on $\partial\Omega$. In this way, we get

$$\lambda_i \sim \frac{a^2 N}{\hat{\beta}_N \Omega_n} \int_{\partial\Omega} (x_i - x_{0i})^2 r^{-(1+N)} e^{-2r/\epsilon} (\mathbf{r}\cdot\mathbf{n})(1 + \mathbf{r}\cdot\mathbf{n})\, dS\,, \tag{2.92}$$

where $\mathbf{r} = (\mathbf{x} - \mathbf{x_0})/r$ and $r = |\mathbf{x} - \mathbf{x_0}|$, with $\mathbf{x} \in \partial\Omega$. As a consistency check we use (2.88) to observe, by comparing the asymptotic orders of the two terms on the right side of (2.79), that the second term is asymptotically negligible compared to the first term, since the exponents satisfy $p + m + 1 > 1$.

The surface integral in (2.92) can be evaluated asymptotically by using a multi-dimensional Laplace technique. Assume that there exists a unique point $\mathbf{x_m} \in \partial\Omega$ where $r_m = \text{dist}(\mathbf{x}_0, \partial\Omega)$ is minimized. If we parameterize the boundary near ζ_m (where $\mathbf{x}(\zeta_m) = \mathbf{x}_m$) such that each ζ_i corresponds to arclength along one of the principal directions through ζ_m, then for any smooth $F(r)$, we have (see [48]),

$$\int_{\partial\Omega} r^{1-N} F(r) e^{-2r/\epsilon}\, dS = \left(\frac{\pi\epsilon}{r_m}\right)^{(N-1)/2} F(r_m) H(r_m) e^{-2r_m/\epsilon}\,, \tag{2.93}$$

where

$$H(r_m) \equiv (1 - r_m/R_1)^{-1/2}(1 - r_m/R_2)^{-1/2} \cdots (1 - r_m/R_{N-1})^{-1/2}\,. \tag{2.94}$$

Here $R_j > 0$, for $j = 1, .., N-1$ are the principal radii of curvature of $\partial\Omega$ at $\mathbf{x_m}$. This result assumes that the non-degeneracy condition $R_j > r_m$, $j = 1, \ldots, N-1$ holds. In this way, we obtain the following explicit asymptotic estimate for the exponentially small eigenvalue,

$$\lambda_i \sim \frac{2a^2 N}{\hat{\beta}_N \Omega_N} \left(\frac{\pi\epsilon}{r_m}\right)^{(N-1)/2} \left(\frac{\mathbf{r_m}\cdot\mathbf{e}_i}{r_m}\right)^2 H(r_m) e^{-2r_m/\epsilon}\,, \tag{2.95}$$

where $\mathbf{e}_i$ is the standard unit basis vector in the i^{th} direction and $\mathbf{r_m} \equiv (x_m - x_0)/r_m$.

2.3.3 The Slow Motion of the Spike

Now we derive an ODE characterizing the metastable spike dynamics. We first linearize (1.19) about a moving spike by writing,

$$a(\mathbf{x}, t) = a_E(\mathbf{x}; \mathbf{x}_0(t)) + w(x, t)\,, \tag{2.96}$$

where $a_E(\mathbf{x}; \mathbf{x}_0)$ is defined in (2.54). Since, (2.59) does not have an $O(1)$ positive eigenvalue, we may assume that $w \ll a_E$, $w_t \ll \partial_t a_E$ uniformly in time. Substituting (2.96) into (1.19), we obtain

$$L_\epsilon w = \partial_t a_E, \quad \text{in} \quad \Omega\,, \tag{2.97a}$$

$$\partial_n w = -\partial_n a_E, \quad \text{on} \quad \partial\Omega\,. \tag{2.97b}$$

Next, we expand w in terms of the eigenfunctions ϕ_i of L_ϵ as

$$w = \sum_{i=0}^{\infty} E_i(t)\phi_i \,. \tag{2.98}$$

We assume that the eigenfunctions form a complete set. However, this is not required for the construction of the solvability condition as the key requirement is that w is orthogonal to the eigenspace of L_ϵ^* associated with the exponentially small eigenvalues. Let ϕ_i^* be the i^{th} eigenfunction of L_ϵ^*. Then, since $(\phi_i, \phi_j^*) = \delta_{ij}$, we integrate by parts to show that

$$E_i(t) = (w, \phi_i^*) = \frac{1}{\lambda_i^*}\left[(L_\epsilon w, \phi_i^*) - \epsilon^2 \int_{\partial\Omega} w_n \phi_i^* \, dS\right] , \tag{2.99}$$

where $L_\epsilon^*\phi_i^* = \lambda_i^*\phi_i^*$. Using (2.97), we have

$$E_i(t) = \frac{1}{\lambda_i^*}\left[(\partial_t a_E, \phi_i^*) + \epsilon^2 \int_{\partial\Omega} \partial_n a_E \phi_i^* \, dS\right] . \tag{2.100}$$

As seen in (2.79)-(2.88), the nonlocal term in the eigenvalue problem $L_\epsilon\phi = \lambda\phi$ is insignificant when $\epsilon \ll 1$ in the asymptotic estimation of the eigenspace associated with the exponentially small eigenvalues of L_ϵ. Therefore, for $i = 1, .., N$ and $\epsilon \to 0$, we can replace ϕ_i^* and λ_i^* by ϕ_i and λ_i in (2.100), where ϕ_i and λ_i are given in (2.75) and (2.95), respectively.

Since $\lambda_i \to 0$ exponentially as $\epsilon \to 0$, for $i = 1, .., N$, we must impose the limiting solvability conditions that $E_i = 0$, for $i = 1, .., N$. This projection step yields the following implicit differential equation for $\mathbf{x_0}(t)$:

$$(\partial_t a_E, \phi_i) = -\epsilon^2 \int_{\partial\Omega} \partial_n a_E \phi_i \, dS \,. \tag{2.101}$$

The dominant contribution to the left side of (2.101) arises from the region near $\mathbf{x_0}$, and we calculate

$$(\partial_t a_E, \phi_i) \sim -\frac{C_i h_E^\gamma}{N} \dot{x}_{0i} \Omega_N \hat{\beta}_N \epsilon^{N-2} \,. \tag{2.102}$$

Finally, we can evaluate the right side of (2.101) using our estimates for ϕ_i on $\partial\Omega$ in (2.78) and for $u_c(\rho)$ as $\rho \to \infty$. This yields the main result of this section.

Proposition 2.2 (Metastability) *For $\epsilon \to 0$, a metastable spike solution for (1.19), is represented by $a(\mathbf{x},t) = a_E(\mathbf{x};\mathbf{x}_0(t))$, where a_E is defined in (2.54) and $\mathbf{x}_0(t)$ satisfies,*

$$\dot{\mathbf{x}}_0 \sim \frac{\epsilon N a^2}{\hat{\beta}_N \Omega_N} \int_{\partial\Omega} \hat{\mathbf{r}}\, r^{1-N} e^{-2r/\epsilon}(1+\hat{\mathbf{r}}\cdot\mathbf{n})\hat{\mathbf{r}}\cdot\mathbf{n}\, d\mathbf{S}\,. \tag{2.103}$$

Here $\hat{\mathbf{r}} = (\mathbf{x}-\mathbf{x}_0)r^{-1}$, $r = |\mathbf{x}-\mathbf{x}_0|$, $\mathbf{x}\in\partial\Omega$, and $\mathbf{n}$ is the unit outward normal to $\partial\Omega$. In addition, a and $\hat{\beta}_N$ are defined in (2.55b) and (2.90), respectively.

There are a few corollaries that follow from this result.

Corollary 2.1 (Equilibrium) *For $\epsilon \to 0$, an equilibrium solution for (1.19), is represented by $a(\mathbf{x},t) = a_E(\mathbf{x};\mathbf{x}_{0e})$, where $\mathbf{x}_{0e}$ is a root of $I(\mathbf{x}_0)$, where*

$$I(\mathbf{x}_0) \equiv \int_{\partial\Omega} \hat{\mathbf{r}}\, r^{1-N} e^{-2r/\epsilon}(1+\hat{\mathbf{r}}\cdot\mathbf{n})\hat{\mathbf{r}}\cdot\mathbf{n}\, d\mathbf{S} \tag{2.104}$$

It was shown in [48] that for a strictly convex domain $\mathbf{x}_{0e}$ is unique and is centered at an $O(\epsilon)$ distance from the center of the uniquely determined largest inscribed sphere for Ω. This equilibrium solution is unstable.

Assuming that there is a unique point $\mathbf{x}_m \in \partial\Omega$ closest to the initial center $\mathbf{x}_0(0)$ of the spike, we can evaluate the surface integral in (2.103) using Laplace's method to get the following explicit result:

Corollary 2.2 (Explicit Motion) *Let $\mathbf{x}_m$ be the point on $\partial\Omega$ closest to $\mathbf{x}_0(0)$. Then, for $t>0$, and $\epsilon\to 0$, the spike moves in the direction of $\mathbf{x}_m$ and the distance $r_m(t) = |\mathbf{x}_m - \mathbf{x}_0(t)|$, satisfies the first order nonlinear differential equation*

$$\dot{r}_m = -\xi r_m \left(\frac{\epsilon}{r_m}\right)^{(N+1)/2} H(r_m) e^{-2r_m/\epsilon}\,, \tag{2.105}$$

where

$$\xi \equiv \frac{2Na^2}{\Omega_N \hat{\beta}_N}\pi^{(N-1)/2}\,. \tag{2.106}$$

Here $\hat{\beta}_N$ is defined in (2.90) and $H(r_m)$ is determined in the terms of the principal radii of curvature of $\partial\Omega$ at $\mathbf{x}_m$ given in (2.94).

This result is valid up until the spike approaches to within an $O(\epsilon)$ distance of $\mathbf{x}_m$. If the initial condition for (2.105) is $r_m(0) = r_0$, then the time T needed for $r_m(T) = 0$, is readily found for $\epsilon \to 0$ to be,

$$T \sim \frac{\epsilon^{(1-N)/2} r_0^{(N-1)/2}}{2H(r_0)\xi} e^{2r_0/\epsilon}. \tag{2.107}$$

Once the spike reaches the boundary, it moves in the direction of increasing mean curvature until it reaches an equilibrium point where the mean curvature of the boundary has a local maximum (see [20]). The existence of such equilibrium solutions, where the spike is located at these special points on the boundary, is demonstrated rigorously in [13], [35].

Chapter 3
Spike Motion on the Boundary

When the spike approaches to within an $O(\epsilon)$ distance from the boundary, the analysis leading to Proposition 2.1 is no longer valid, and the spike presumably begins to merge with the boundary. This process is difficult to study in the multi-dimensional case without a full-scale numerical analysis. In Fig. 3.1 we show this merging process in the simpler case of one dimension by solving (1.18) numerically with $p = 2$ and $\epsilon = .07$ using the method described in §2.1.3. Results concerning the stability of an equilibrium boundary spike in one dimension for (1.18) are given in [54]. The merging process of a spike with the boundary should probably be similar in higher dimensions. For the equilibrium problem, the existence of boundary spike solutions to the multi-dimensional problem (1.19) has been proved in [13] and [35]. In particular, the result of [13] proved that there exists a solution to (1.19) where the spike is centered at a local maximum of the mean curvature of the boundary of a three-dimensional domain.

The goal of this chapter is to analyze the motion of a spike solution for the non-local shadow problem (1.19) when the spike is confined to the smooth boundary of a two or three-dimensional domain. Since all spikes that are initially located in the interior will tend towards the boundary of the domain (cf. Proposition 2.1), it is natural to study the motion of a spike on the boundary as it tries to reach an equilibrium where its associated energy can be minimized. We assume that the merging process of an interior spike with the boundary has taken place and thus our initial condition is a spike located at an arbitrary point on the boundary. From using a formal asymptotic analysis combined with imposing appropriate solvability conditions on the linearized problem, we derive differential equations characterizing the motion of a boundary spike. This

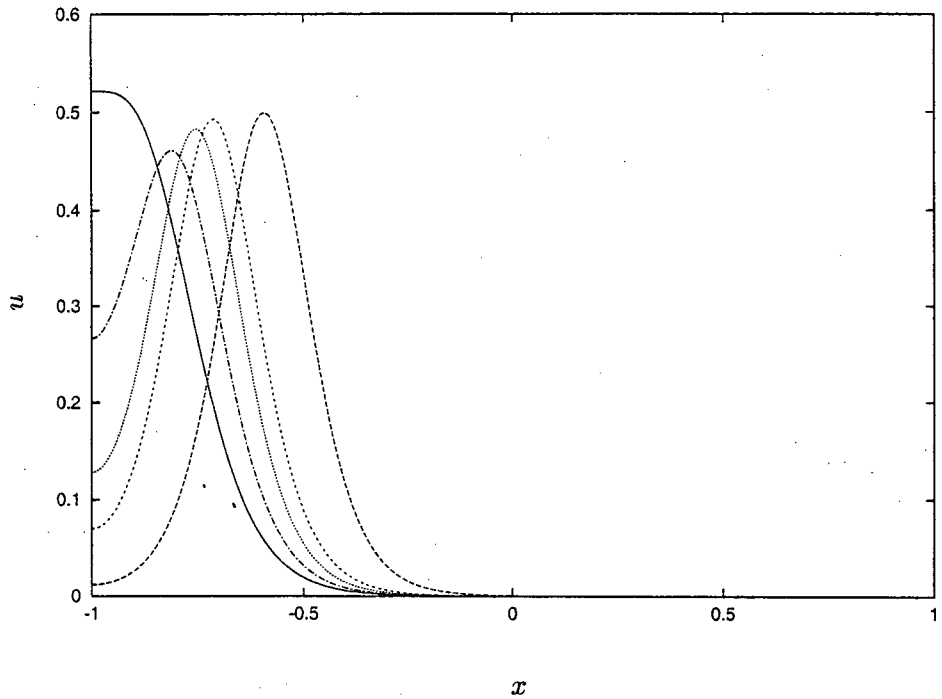

Figure 3.1: A plot of u versus x at different times showing a spike merging with the boundary in one dimension. Times from the simulation are $t = 389, 1354, 1375, 1383, 1386$ from right to left.

motion generically occurs on a slow time scale of $O(\epsilon^3)$. From this differential equation for the spike motion, we show that the spike drifts towards a local maximum of the curvature in two dimensions and a local maximum of the mean curvature in three dimensions. Again the non-local term in (1.19) is essential for ensuring the existence of this slow motion. In the derivation we assume the boundary is sufficiently smooth so that the derivatives of the curvatures exists. The differential equations mentioned above predict no motion when a spike is on a segment of the boundary having constant curvature. To illustrate the spike motion in this case, we analyze the motion of a spike on a flat boundary segment of a two-dimensional domain (see Fig. 3.6 below for the geometrical configuration). For this case, we show that the motion is metastable and depends critically on the local behavior of the boundary near the corner points at the two ends of the flat segment. A similar analysis for the constrained Allen-Cahn equation of material

science has been studied in [43] (see also the references therein).

The remainder of this chapter proceeds as follows. In §3.1 and §3.2 we analyze the motion of boundary spikes for (1.19) in two and three dimensions, respectively. In §3.3, we examine the stability properties of the equilibrium boundary spike solutions found in §3.2 and §3.2 by using the results of [52] and [53]. Finally, in §3.4 we analyze the metastable behavior of a boundary spike in two dimensions that lies on a flat segment of the boundary.

In this chapter we will be using r as a radial variable for polar and spherical co-ordinates. In order to avoid confusion with the parameter r in the equation (1.19), for this chapter only we write the equations as,

$$a_t = \epsilon^2 \Delta a - a + \frac{a^p}{h^q}, \quad \text{in} \quad \Omega, \quad t > 0, \tag{3.1a}$$

$$h = \left(\frac{\epsilon^{-N}}{\mu |\Omega|} \int_\Omega a^m \, d\mathbf{x} \right)^{\frac{1}{s+1}}, \tag{3.1b}$$

$$\partial_n a = 0 \quad \text{on} \quad \partial\Omega. \tag{3.1c}$$

The only difference between (1.19) and (3.1) is the substitution of m for r.

3.1 Spike Motion on the Boundary in Two Dimensions

We now derive an asymptotic differential equation for the motion of a spike confined to the boundary of a two-dimensional domain. The boundary of the domain is assumed to be sufficiently smooth so that the curvature and its derivatives are differentiable functions. To derive this differential equation we first transform (3.1) to a localized boundary layer coordinate system centered near the spike. The solution is then expanded in powers of ϵ. A nontrivial solvability condition for the $O(\epsilon^2)$ equation in this expansion is obtained when we choose the time scale of the spike motion to be $O(\epsilon^3)$. The differential equation for the motion of the spike is obtained from this solvability condition.

We now give the details of the analysis. We first introduce a boundary layer coordinate system, where $\eta > 0$ denotes the distance from $\boldsymbol{x} \in \Omega$ to $\partial\Omega$ and where s is arclength along $\partial\Omega$. In

terms of these coordinates, (3.1a) transforms to

$$a_t = \epsilon^2 \left(a_{\eta\eta} - \frac{\kappa}{1-\kappa\eta} a_\eta + \frac{1}{1-\kappa\eta} \partial_s \left(\frac{1}{1-\kappa\eta} a_s \right) \right) - a + a^p/h^q \,, \tag{3.2a}$$

$$a_\eta = 0 \,, \qquad \text{on} \quad \eta = 0 \,. \tag{3.2b}$$

Here $\kappa = \kappa(s)$ is the curvature of the boundary and $h = h(t)$ is given in (3.1b). Next, we introduce $u(\eta, s, t)$ by

$$a = h^\gamma u \,, \qquad \gamma = q/(p-1) \,. \tag{3.3}$$

Substituting (3.3) into (3.2) we obtain

$$\frac{\gamma u h_t}{h} + u_t = \epsilon^2 \left(u_{\eta\eta} - \frac{\kappa}{1-\kappa\eta} u_\eta + \frac{1}{1-\kappa\eta} \partial_s \left(\frac{1}{1-\kappa\eta} u_s \right) \right) - u + u^p \,, \tag{3.4a}$$

$$u_\eta = 0 \,, \qquad \text{on} \quad \eta = 0 \,. \tag{3.4b}$$

Suppose that the spike is initially located on the boundary of the domain. Then, its subsequent location is given by $s = s_0(t)$ and $\eta = 0$, where $s_0(t)$ is to be determined. Since the spike has a support of order $O(\epsilon)$ near $s_0(t)$, we introduce local variables v, $\tilde{s}$ and $\tilde{\eta}$ by

$$\tilde{s} = \epsilon^{-1} \left[s - s_0(t) \right] \,, \qquad \tilde{\eta} = \epsilon^{-1} \eta \,, \qquad v(\tilde{\eta}, \tilde{s}) = u(\epsilon\tilde{\eta}, s_0 + \epsilon\tilde{s}, t) \,. \tag{3.5}$$

Then, (3.4) transforms to

$$\frac{\gamma v h_t}{h} - \epsilon^{-1} s_0' v_{\tilde{s}} = v_{\tilde{\eta}\tilde{\eta}} - \frac{\epsilon\kappa}{1-\epsilon\kappa\tilde{\eta}} v_{\tilde{\eta}} + \frac{1}{1-\epsilon\kappa\tilde{\eta}} \partial_{\tilde{s}} \left(\frac{1}{1-\epsilon\kappa\tilde{\eta}} v_{\tilde{s}} \right) - v + v^p \,, \tag{3.6a}$$

$$v_{\tilde{\eta}} = 0 \,, \qquad \text{on} \quad \tilde{\eta} = 0 \,, \tag{3.6b}$$

where $s_0' \equiv ds_0/dt$ and $\kappa = \kappa(s_0 + \epsilon\tilde{s})$. Since the boundary was assumed to have a well-defined tangent plane at each point, the domain of definition for (3.6) is

$$\tilde{\Omega} = \{ (\tilde{\eta}, \tilde{s}) \,|\, -\infty < \tilde{s} < \infty \,, \tilde{\eta} > 0 \} \,. \tag{3.6c}$$

From differentiating the integral in (3.1b) with respect to t, it follows that

$$h_t = O\left(\epsilon^{-1} s_0' \right) \,. \tag{3.7}$$

Thus, the two terms on the left hand side of (3.6a) are of the same order in ϵ. However, as we show below, only one of these terms will contribute a nonzero term to a solvability condition.

The solution to (3.6a), (3.6b) is expanded as

$$v = v_0 + \epsilon v_1 + \epsilon^2 v_2 + \cdots , \tag{3.8}$$

and the curvature is expanded as

$$\kappa(s_0 + \epsilon\tilde{s}) = \kappa_0 + \epsilon\tilde{s}\kappa_0^{'} + O(\epsilon^2) . \tag{3.9}$$

Here we have defined $\kappa_0 \equiv \kappa(s_0)$ and $\kappa_0^{'} \equiv \kappa^{'}(s_0)$. Since a nontrivial solvability condition arises at order $O(\epsilon^2)$, we must choose a slow time scale τ by

$$\tau = \epsilon^3 t . \tag{3.10}$$

Substituting (3.8)–(3.10) into (3.6), and collecting powers of ϵ, we obtain the following sequence of problems that are to be solved on the half-plane Ω:

$$v_{0\tilde{\eta}\tilde{\eta}} + v_{0\tilde{s}\tilde{s}} + Q(v_0) = 0 , \tag{3.11a}$$

$$\mathcal{L}v_1 \equiv v_{1\tilde{\eta}\tilde{\eta}} + v_{1\tilde{s}\tilde{s}} + Q^{'}(v_0)v_1 = \kappa_0 v_{0\tilde{\eta}} - 2\tilde{\eta}\kappa_0 v_{0\tilde{s}\tilde{s}} , \tag{3.11b}$$

$$\mathcal{L}v_2 \equiv v_{2\tilde{\eta}\tilde{\eta}} + v_{2\tilde{s}\tilde{s}} + Q^{'}(v_0)v_2 = -\dot{s}_0 v_{0\tilde{s}} + \frac{\epsilon\gamma v_0 \dot{h}}{h} + F_e + F_o . \tag{3.11c}$$

Here $\dot{s}_0 \equiv ds_0/d\tau$. The boundary conditions for (3.11a)–(3.11c) are

$$v_{0\tilde{\eta}} = v_{1\tilde{\eta}} = v_{2\tilde{\eta}} = 0 , \qquad \text{on} \quad \tilde{\eta} = 0 . \tag{3.11d}$$

In (3.11) we have defined $Q(v_0)$ and its derivatives by

$$Q(v_0) = -v_0 + v_0^p , \qquad Q^{'}(v_0) = -1 + pv_0^{p-1} , \qquad Q^{''}(v_0) = p(p-1)v_0^{p-2} . \tag{3.12}$$

The terms F_e and F_o in (3.11c) are defined by

$$F_e = \kappa_0 v_{1\tilde{\eta}} + \tilde{\eta}\kappa_0^2 v_{0\tilde{\eta}} - 2\tilde{\eta}\kappa_0 v_{1\tilde{s}\tilde{s}} - \frac{Q^{''}(v_0)}{2} v_1^2 - 3\kappa_0^2\tilde{\eta}^2 v_{0\tilde{s}\tilde{s}} , \tag{3.13a}$$

$$F_o = \tilde{s}\kappa_0^{'} v_{0\tilde{\eta}} - \tilde{\eta}\kappa_0^{'} v_{0\tilde{s}} - 2\tilde{\eta}\tilde{s}\kappa_0^{'} v_{0\tilde{s}\tilde{s}} . \tag{3.13b}$$

The leading-order problem (3.11a) has a unique positive radially symmetric solution $u_c(\rho)$ that satisfies (see [35])

$$u_c'' + \frac{1}{\rho}u_c' + Q(u_c) = 0\,, \qquad 0 < \rho < \infty\,, \tag{3.14a}$$

$$u_c'(0) = 0\,; \qquad u_c(\rho) \sim a_c \rho^{-1/2} e^{-\rho}\,, \qquad \text{as} \quad \rho \to \infty\,. \tag{3.14b}$$

Here a_c is some positive constant and $\rho \equiv \left(\tilde{\eta}^2 + \tilde{s}^2\right)^{1/2}$. Thus, we take

$$v_0(\tilde{\eta}, \tilde{s}) = u_c\left[(\tilde{\eta}^2 + \tilde{s}^2)^{1/2}\right]\,, \tag{3.15}$$

which also satisfies the boundary condition in (3.11d). To obtain our solvability condition, we notice that the tangential derivative $v_{0\tilde{s}}$ satisfies $\mathcal{L}v_{0\tilde{s}} = 0$ and the boundary condition (3.11d). Hence, upon defining the inner product $(f, g) \equiv \int_{\tilde{\Omega}} fg\, d\mathbf{x}$, we must have that the right-hand sides of (3.11b) and (3.11c) are orthogonal to $v_{0\tilde{s}}$ with respect to this inner product. An important observation is that $v_{0\tilde{s}}$ is an odd function of $\tilde{s}$.

This solvability condition for (3.11b) yields,

$$\kappa_0\left(v_{0\tilde{\eta}}, v_{0\tilde{s}}\right) - 2\kappa_0\left(\tilde{\eta} v_{0\tilde{s}\tilde{s}}, v_{0\tilde{s}}\right) = 0\,. \tag{3.16}$$

Since $v_{0\tilde{\eta}}$ and $v_{0\tilde{s}\tilde{s}}$ are even functions of $\tilde{s}$, the integrands associated with the inner products in (3.16) are odd, and hence the left hand side of (3.16) vanishes identically. Then, we can solve (3.11b) for v_1 and obtain that v_1 is even in $\tilde{s}$. Next, upon applying the solvability condition to (3.11c), we obtain

$$\dot{s}_0\left(v_{0\tilde{s}}, v_{0\tilde{s}}\right) = \left(F_o, v_{0\tilde{s}}\right) + \left(F_e, v_{0\tilde{s}}\right) + \frac{\epsilon\gamma\dot{h}}{h}\left(v_0, v_{0\tilde{s}}\right)\,. \tag{3.17}$$

The significance of the decomposition in (3.11c) is that F_e is even in $\tilde{s}$, whereas F_o is odd in $\tilde{s}$. Hence, the last two terms on the right-hand side of (3.17) are zero. Next, substituting (3.13b) into (3.17), we get

$$\dot{s}_0\left(v_{0\tilde{s}}, v_{0\tilde{s}}\right) = \kappa_0'\left(\tilde{s} v_{0\tilde{\eta}}, v_{0\tilde{s}}\right) - \kappa_0'\left(\tilde{\eta} v_{0\tilde{s}}, v_{0\tilde{s}}\right) - 2\kappa_0'\left(\tilde{\eta}\tilde{s} v_{0\tilde{s}\tilde{s}}, v_{0\tilde{s}}\right)\,. \tag{3.18}$$

Finally, the inner products in (3.18) are evaluated exactly using polar coordinates to get

$$(\tilde{s}v_{0\tilde{\eta}}, v_{0\tilde{s}}) = (\tilde{\eta}v_{0\tilde{s}}, v_{0\tilde{s}}) = \frac{2}{3}\int_0^\infty \rho^2 \left[u_c'(\rho)\right]^2 d\rho\,, \tag{3.19a}$$

$$(v_{0\tilde{s}}, v_{0\tilde{s}}) = \frac{\pi}{2}\int_0^\infty \rho \left[u_c'(\rho)\right]^2 d\rho\,, \tag{3.19b}$$

$$2\,(\tilde{\eta}\tilde{s}v_{0\tilde{s}\tilde{s}}, v_{0\tilde{s}}) = -\frac{2}{3}\int_0^\infty \rho^2 \left[u_c'(\rho)\right]^2 d\rho\,. \tag{3.19c}$$

Substituting (3.19) into (3.18) we obtain the following main result:

Proposition 3.1 (Boundary Motion in 2 Dimensions) *For $\epsilon \to 0$, the motion of a spike confined to the smooth boundary of a two-dimensional domain is described by*

$$a \sim h^\gamma u_c\left(\epsilon^{-1}\left[(s - s_0(t))^2 + \eta^2\right]^{1/2}\right) + O(\epsilon)\,, \tag{3.20a}$$

$$s_0'(t) \sim \frac{4b}{3\pi}\epsilon^3 \kappa'(s_0)\,, \tag{3.20b}$$

where $\gamma = q/(p-1)$ and $b > 0$ is defined by

$$b \equiv \frac{\int_0^\infty \rho^2 \left[u_c'(\rho)\right]^2 d\rho}{\int_0^\infty \rho \left[u_c'(\rho)\right]^2 d\rho}\,. \tag{3.20c}$$

Here $u_c(\rho)$ is the positive solution to (3.14) and κ is the curvature of the boundary, with $\kappa > 0$ for a circle.

From (3.20b), we observe that the spike will move on the boundary in the direction of increasing curvature until a local maximum of the curvature is reached. The stable steady-states of (3.20b) are at the local maxima of the curvature. A similar differential equation has been derived in [1] for small bubble solutions of the constrained Allen-Cahn equation.

3.1.1 A Few Explicit Examples

We now illustrate (3.20b) in a convex domain. Let the origin be contained in Ω and let (x_1, x_2) be a point on $\partial\Omega$. Let ζ denote the perpendicular distance from the origin to the tangent line to $\partial\Omega$ that passes through (x_1, x_2). Let θ denote the angle between this perpendicular line and

the positive x_1 axis. Then, when θ ranges over $0 \leq \theta \leq 2\pi$, we sweep out a closed domain Ω whose boundary is given parametrically by (see [17])

$$x_1(\theta) = \zeta(\theta)\cos(\theta) - \zeta'(\theta)\sin(\theta)\,, \qquad x_2(\theta) = \zeta(\theta)\sin(\theta) + \zeta'(\theta)\cos(\theta)\,. \tag{3.21}$$

Here $\zeta(\theta)$ is 2π periodic.

Next, we transform the ODE (3.20b), written in terms of arclength, to one involving θ. Let $s = f(\theta)$ be the mapping between θ and the arclength s. Then, $f'(\theta)$ and the curvature of the boundary $\kappa(\theta)$ are given by

$$f'(\theta) = \zeta(\theta) + \zeta''(\theta)\,, \qquad \kappa(\theta) = \left[\zeta(\theta) + \zeta''(\theta)\right]^{-1}\,. \tag{3.22}$$

Hence, (3.20b) transforms to

$$\theta_0'(\tau) \sim -\frac{4b}{3\pi}\frac{\left[\zeta'(\theta_0) + \zeta'''(\theta_0)\right]}{\left[\zeta(\theta_0) + \zeta''(\theta_0)\right]^4}\,. \tag{3.23}$$

Here $\theta_0(\tau)$ is the value of θ at the center of the spike, and $\tau = \epsilon^3 t$ is the slow time variable.

Using the boundary value problem solver COLSYS [3] we can solve (3.14) numerically to determine the constant b in (3.20b). In the examples below we took $p = 2$. For this value, we compute that

$$\int_0^\infty \rho^2 \left[u_c'(\rho)\right]^2 d\rho = 4.23\,, \qquad \int_0^\infty \rho \left[u_c'(\rho)\right]^2 d\rho = 2.47\,. \tag{3.24}$$

Hence, when $p = 2$, we get $b = 1.71$. In the examples below, solutions to (3.23) were computed using the Sandia ODE solver [42].

Example 1: Let $\zeta(\theta) = 3 + 1.2\sin^3(\theta)$, and take the initial condition for (3.23) as $\theta_0(0) = -1.5$, for which $x_1 = 0.339$ and $x_2 = -1.790$ at $\tau = 0$. The curvature has three local maxima for this domain. In Fig. 3.2 we plot the domain bounded by $\zeta(\theta)$ and show snapshots of the motion of the center of the spike (labeled by the starred points) towards the nearby local maximum of the curvature. In Fig. 3.3 we plot the numerical solution to (3.23) with $\theta_0(0) = -1.5$. For this initial value and with $\epsilon = 0.1$, this figure shows that it takes a time $t = \tau/\epsilon^3 \approx 77500.0$ to reach the steady-state value.

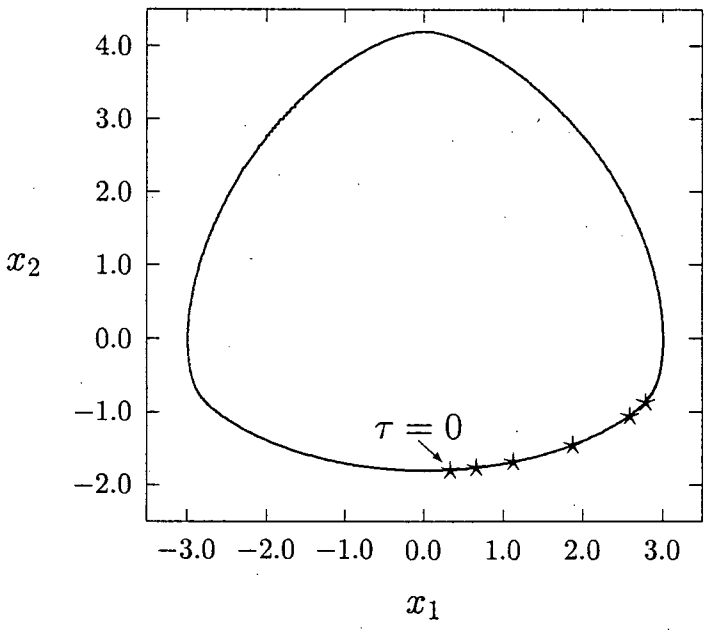

Figure 3.2: For Example 1 we plot the motion of the center of the spike on the boundary at different times as it tends to its steady-state limit. The initial point is labeled and the times corresponding to the other points (in counterclockwise order) are $\tau = 34.49$, $\tau = 58.71$, $\tau = 74.01$, $\tau = 76.98$ and $\tau = 77.50$.

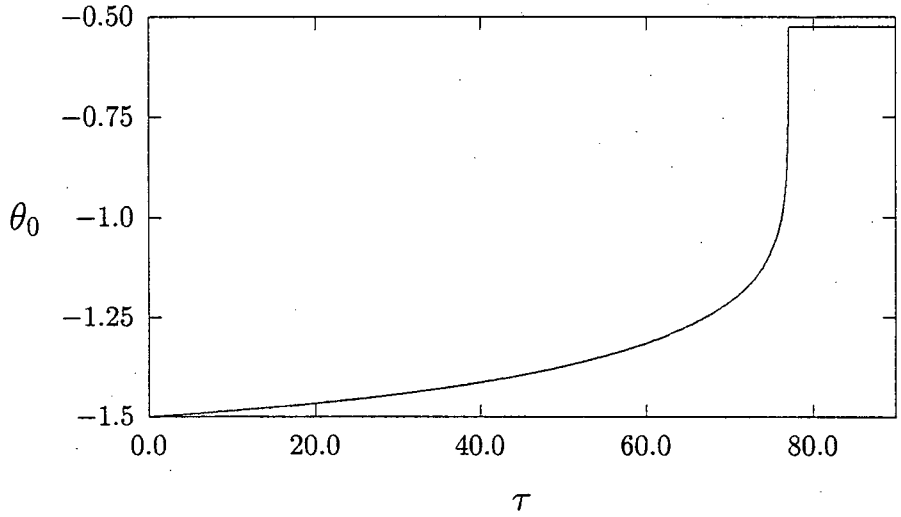

Figure 3.3: For Example 1 we plot the solution θ_0 versus τ to (3.23) showing the behavior towards a local maximum of the curvature.

Example 2: Let $\zeta(\theta) = 3 + \cos(5\theta)/10$, and take $\theta_0(0) = 0.6$, for which $x_1 = 2.430$ and $x_2 = 1.567$ at $\tau = 0$. For this case, the ODE (3.23) becomes

$$\theta_0' = -\frac{4b}{3\pi}\left(\frac{12\sin(5\theta_0)}{[3 - 2.4\cos(5\theta_0)]^4}\right). \tag{3.25}$$

Hence there are five local maxima of the curvature. In Fig. 3.4 we plot the domain bounded by $\zeta(\theta)$ and show snapshots of the spike motion towards the nearby local maximum of the curvature at $\theta_0 = 0$. In Fig. 3.5 we plot the numerical solution to (3.25) with $\theta_0(0) = 0.6$. The apparent nonsmoothness of the graph of θ_0 versus τ near the equilibrium point results from the fact that the linearization of (3.25) near $\theta_0 = 0$ has the form $\theta' \approx -c\theta$, where $c > 0$ is a large constant. A similar explanation hold for the apparent nonsmoothness in Fig. 3.3.

3.2 Spike Motion on the Boundary in Three Dimensions

We now derive an asymptotic differential equation for the motion of a spike confined to the boundary of a three-dimensional domain. The boundary of the domain is assumed to be sufficiently smooth so that the principal curvatures and their partial derivatives are differentiable

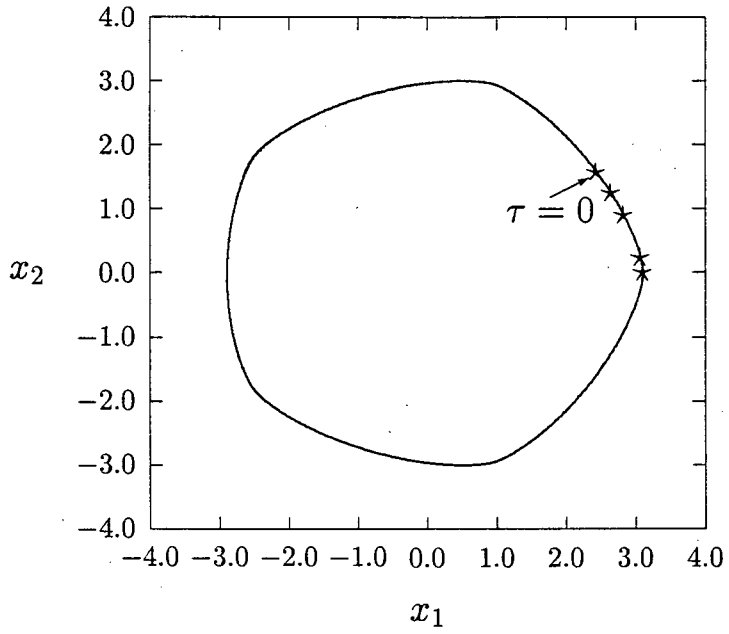

Figure 3.4: For Example 2 we plot the motion of the center of the spike on the boundary at different times as it tends to its steady-state limit. The initial point is labeled and the times corresponding to the other points (in clockwise order) are $\tau = 23.40$, $\tau = 31.41$, $\tau = 35.38$, and $\tau = 35.5$.

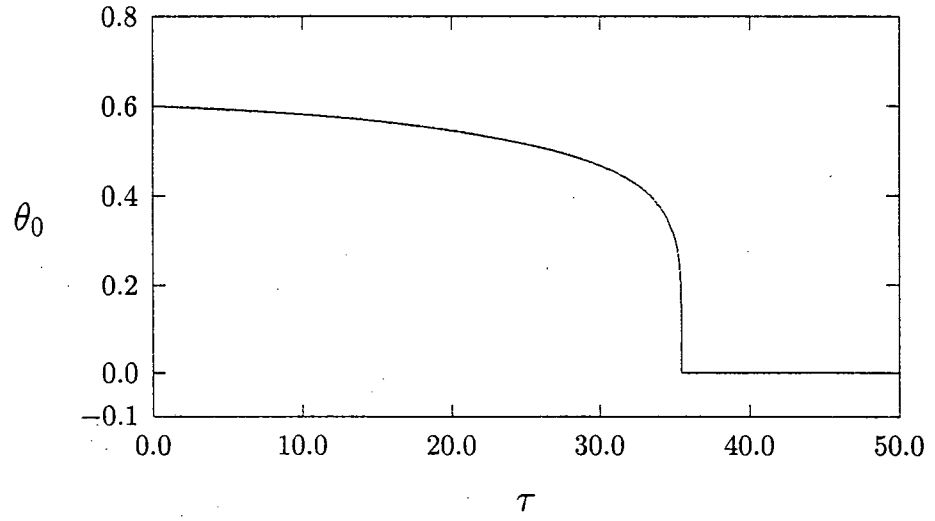

Figure 3.5: For Example 2 we plot the solution θ_0 versus τ to (3.25) showing the behavior towards a local maximum of the curvature. The initial condition was $\theta_0(0) = 0.6$.

functions. In order to evaluate the Laplacian on the boundary we will use boundary layer coordinates. Lines of curvature form a local orthonormal basis for a coordinate system restricted to the boundary. We may then extend this system locally using the normal to the boundary as our third coordinate. The formulation of the Laplacian operator using these coordinates is not as simple as for the two-dimensional case. However, since the spike is localized on the boundary, we do not need an exact expression for the Laplacian in terms of these coordinates as only the first few terms in the local expansion will suffice for the analysis.

We introduce a boundary layer coordinate system (s_1, s_2, η), where $\eta > 0$ is the distance from $\boldsymbol{x} \in \Omega$ to $\partial\Omega$ and where s_1 and s_2 correspond to coordinates through the two principal directions at the center of the spike. The boundary spike is assumed to be located at $s_1 = \xi_1(t)$

and $s_2 = \xi_2(t)$ with $\eta = 0$. Using Appendix B, we obtain that (3.1a) transforms to

$$a_t = \epsilon^2 a_{\eta\eta} - \epsilon^2 \left(\frac{\kappa_1}{1-\eta\kappa_1} + \frac{\kappa_2}{1-\eta\kappa_2} \right) a_\eta + \frac{\epsilon^2}{(1-\eta\kappa_1)(1-\eta\kappa_2)} \partial_{s_1} \left(\frac{1-\eta\kappa_2}{1-\eta\kappa_1} a_{s_1} \right) + \frac{\epsilon^2}{(1-\eta\kappa_1)(1-\eta\kappa_2)} \partial_{s_2} \left(\frac{1-\eta\kappa_1}{1-\eta\kappa_2} a_{s_2} \right) - a + a^p/h^q \,, \tag{3.26a}$$

$$a_\eta = 0 \,, \qquad \text{on} \quad \eta = 0 \,. \tag{3.26b}$$

Here $\kappa_1 = \kappa_1(s_1, s_2)$ and $\kappa_2(s_1, s_2)$ are the two principal curvatures at each point on the boundary.

As in (3.3) we set $a = h^\gamma u$, where $u = u(\eta, s_1, s_2, t)$. Then, we introduce local coordinates v, $\tilde{s}_1$, $\tilde{s}_2$ and $\tilde{\eta}$ by

$$\tilde{s}_1 = \epsilon^{-1} [s_1 - \xi_1(t)] \,, \qquad \tilde{s}_2 = \epsilon^{-1} [s_2 - \xi_2(t)] \,, \qquad \tilde{\eta} = \epsilon^{-1} \eta \,,$$
$$v(\tilde{\eta}, \tilde{s}_1, \tilde{s}_2, t) = u(\epsilon\tilde{\eta}, \xi_1 + \epsilon\tilde{s}_1, \xi_2 + \epsilon\tilde{s}_2, t) \,. \tag{3.27}$$

The estimate (3.7) and the time scale (3.10) still apply in the three-dimensional case. Next, we expand v as in (3.8). The principal curvatures are also expanded in the Taylor series

$$\kappa_1(\xi_1 + \epsilon\tilde{s}_1, \xi_2 + \epsilon\tilde{s}_2) = \kappa_1 + \epsilon\tilde{s}_1\kappa_{11} + \epsilon\tilde{s}_2\kappa_{12} + O(\epsilon^2) \,, \tag{3.28a}$$

$$\kappa_2(\xi_1 + \epsilon\tilde{s}_1, \xi_2 + \epsilon\tilde{s}_2) = \kappa_2 + \epsilon\tilde{s}_1\kappa_{21} + \epsilon\tilde{s}_2\kappa_{22} + O(\epsilon^2) \,. \tag{3.28b}$$

Here on the right-hand side of (3.28a) and (3.28b) we have defined $\kappa_1 \equiv \kappa_1(\xi_1, \xi_2)$, $\kappa_2 \equiv \kappa_2(\xi_1, \xi_2)$, and $\kappa_{ij} \equiv \partial_{s_j} \kappa_i(s_1, s_2)$ evaluated at $(s_1, s_2) = (\xi_1, \xi_2)$.

Substituting (3.7), (3.8), (3.10), (3.27) and (3.28) into (3.26), we obtain the following sequence of problems upon collecting powers of ϵ:

$$v_{0\tilde{\eta}\tilde{\eta}} + v_{0\tilde{s}_1\tilde{s}_1} + v_{0\tilde{s}_2\tilde{s}_2} + Q(v_0) = 0 \,, \tag{3.29a}$$

$$\mathcal{L}v_1 \equiv v_{1\tilde{\eta}\tilde{\eta}} + v_{1\tilde{s}_1\tilde{s}_1} + v_{1\tilde{s}_2\tilde{s}_2} + Q'(v_0)v_1 = (\kappa_1 + \kappa_2)v_{0\tilde{\eta}} - 2\tilde{\eta}\kappa_1 v_{0\tilde{s}_1\tilde{s}_1} - 2\tilde{\eta}\kappa_2 v_{0\tilde{s}_2\tilde{s}_2} \,, \tag{3.29b}$$

$$\mathcal{L}v_2 \equiv v_{2\tilde{\eta}\tilde{\eta}} + v_{2\tilde{s}_1\tilde{s}_1} + v_{2\tilde{s}_2\tilde{s}_2} + Q'(v_0)v_2 = F_{ee} + F_{eo} + F_{oe} \,. \tag{3.29c}$$

The boundary conditions for (3.29) are

$$v_{0\tilde{\eta}} = v_{1\tilde{\eta}} = v_{2\tilde{\eta}} = 0 \,, \qquad \text{on} \quad \tilde{\eta} = 0 \,. \tag{3.29d}$$

In (3.11), $Q(v_0)$ is defined in (3.12). The terms F_{ee}, F_{eo} and F_{oe} in (3.29c) are defined by

$$F_{ee} = -\frac{1}{2}Q''(v_0)v_1^2 + (\kappa_1+\kappa_2)v_{1\tilde{\eta}} + \tilde{\eta}(\kappa_1^2+\kappa_2^2)v_{0\tilde{\eta}} + \frac{\epsilon v_0 \gamma \dot{h}}{h}$$
$$- 2\tilde{\eta}\kappa_1 v_{1\tilde{s}_1\tilde{s}_1} - 2\tilde{\eta}\kappa_2 v_{1\tilde{s}_2\tilde{s}_2} - 3\kappa_1^2\tilde{\eta}^2 v_{0\tilde{s}_1\tilde{s}_1} - 3\kappa_2^2\tilde{\eta}^2 v_{0\tilde{s}_2\tilde{s}_2}\,, \tag{3.30a}$$

$$F_{eo} = (\kappa_{12}+\kappa_{22})\tilde{s}_2 v_{0\tilde{\eta}} - 2\tilde{\eta}\kappa_{12}\tilde{s}_2 v_{0\tilde{s}_1\tilde{s}_1} - 2\tilde{\eta}\kappa_{22}\tilde{s}_2 v_{0\tilde{s}_2\tilde{s}_2}$$
$$- \tilde{\eta}(\kappa_{22}-\kappa_{12})v_{0\tilde{s}_2} - \dot{\xi}_1 v_{0\tilde{s}_2}\,, \tag{3.30b}$$

$$F_{oe} = (\kappa_{21}+\kappa_{11})\tilde{s}_1 v_{0\tilde{\eta}} - 2\tilde{\eta}\kappa_{11}\tilde{s}_1 v_{0\tilde{s}_1\tilde{s}_1} - 2\tilde{\eta}\kappa_{21}\tilde{s}_1 v_{0\tilde{s}_2\tilde{s}_2}$$
$$- \tilde{\eta}(\kappa_{11}-\kappa_{21})v_{0\tilde{s}_1} - \dot{\xi}_2 v_{0\tilde{s}_1}\,. \tag{3.30c}$$

Here $\dot{\xi}_j \equiv d\xi_j/d\tau$ for $j = 1, 2$. The problems in (3.29) are to be solved in the half-space $\tilde{\Omega}$ defined by

$$\tilde{\Omega} = \{(\tilde{\eta}, \tilde{s}_1, \tilde{s}_2) \,|\, -\infty < \tilde{s}_1 < \infty\,, -\infty < \tilde{s}_2 < \infty\,, \tilde{\eta} > 0\}\,. \tag{3.31}$$

When p is less than the critical Sobolev exponent $p_c = 5$, there is a unique positive radially symmetric solution $u_c(\rho)$ to (3.30a) that satisfies (see [35])

$$u_c'' + \frac{2}{\rho}u_c' + Q(u_c) = 0\,, \qquad 0 < \rho < \infty\,, \tag{3.32a}$$

$$u_c'(0) = 0\,; \qquad u_c(\rho) \sim a_c \rho^{-1} e^{-\rho}\,, \qquad \text{as} \quad \rho \to \infty\,, \tag{3.32b}$$

for some $a_c > 0$ where $\rho \equiv \left(\tilde{\eta}^2 + \tilde{s}_1^2 + \tilde{s}_2^2\right)^{1/2}$. Therefore, our leading-order spike solution is given by

$$v_0(\tilde{\eta}, \tilde{s}_1, \tilde{s}_2) = u_c\left[(\tilde{\eta}^2 + \tilde{s}_1^2 + \tilde{s}_2^2)^{1/2}\right]\,. \tag{3.33}$$

To obtain our solvability condition, we first define the inner product (f, g) by $(f, g) \equiv \int_{\tilde{\Omega}} fg\, d\mathbf{x}$ where $\tilde{\Omega}$ is the half-space defined in (3.31). Then, we note that $\mathcal{L}v_{0\tilde{s}_1} = 0$ and $\mathcal{L}v_{0\tilde{s}_2} = 0$, where $\mathcal{L}$ is the operator defined in (3.29b), and that $v_{0\tilde{s}_1}$ and $v_{0\tilde{s}_2}$ satisfy the boundary condition in (3.29d). Therefore, the solvability condition is that the right hand sides of (3.29b) and (3.29c) must be orthogonal to both $v_{0\tilde{s}_1}$ and $v_{0\tilde{s}_2}$ with respect to this inner product.

In imposing the solvability condition on (3.29b), we note that the right-hand side of (3.29b) is even in both $\tilde{s}_1$ and $\tilde{s}_2$, whereas $v_{0\tilde{s}_1}$ is odd in $\tilde{s}_1$ and even in $\tilde{s}_2$, while $v_{0\tilde{s}_2}$ is even in $\tilde{s}_1$ and

odd in $\tilde{s}_2$. Hence, the solvability condition for (3.29b) is automatically satisfied. Then, from (3.29b) together with (3.29d) we can calculate a function v_1, which is even in both $\tilde{s}_1$ and $\tilde{s}_2$. Next, the solvability condition for (3.29c) yields the two equations

$$(F_{ee}, v_{0\tilde{s}_1}) + (F_{eo}, v_{0\tilde{s}_1}) + (F_{oe}, v_{0\tilde{s}_1}) = 0\,, \qquad (F_{ee}, v_{0\tilde{s}_2}) + (F_{eo}, v_{0\tilde{s}_2}) + (F_{oe}, v_{0\tilde{s}_2}) = 0\,. \quad (3.34)$$

The significance of the decomposition in (3.29c) is that F_{ee} is even in both $\tilde{s}_1$ and $\tilde{s}_2$, F_{eo} is even in $\tilde{s}_1$ and odd in $\tilde{s}_2$, and F_{oe} is odd in $\tilde{s}_1$ and even in $\tilde{s}_2$. Therefore, the inner products involving F_{ee} vanish, and also $(F_{eo}, v_{0\tilde{s}_1}) = (F_{oe}, v_{0\tilde{s}_2}) = 0$. Using these results, and substituting (3.30b) and (3.30c) into (3.34) we obtain

$$\begin{aligned}\dot{\xi}_1\,(v_{0\tilde{s}_1}, v_{0\tilde{s}_1}) &= (\kappa_{21}+\kappa_{11})\,(\tilde{s}_1 v_{0\tilde{\eta}}, v_{0\tilde{s}_1}) - 2\kappa_{11}\,(\tilde{\eta}\tilde{s}_1 v_{0\tilde{s}_1\tilde{s}_1}, v_{0\tilde{s}_1}) \\ &\quad - 2\kappa_{21}\,(\tilde{\eta}\tilde{s}_1 v_{0\tilde{s}_2\tilde{s}_2}, v_{0\tilde{s}_1}) - (\kappa_{11}-\kappa_{21})\,(\tilde{\eta} v_{0\tilde{s}_1}, v_{0\tilde{s}_1})\,, \qquad (3.35a)\\ \dot{\xi}_2\,(v_{0\tilde{s}_2}, v_{0\tilde{s}_2}) &= (\kappa_{12}+\kappa_{22})\,(\tilde{s}_2 v_{0\tilde{\eta}}, v_{0\tilde{s}_2}) - 2\kappa_{12}\,(\tilde{\eta}\tilde{s}_2 v_{0\tilde{s}_1\tilde{s}_1}, v_{0\tilde{s}_2}) \\ &\quad - 2\kappa_{22}\,(\tilde{\eta}\tilde{s}_2 v_{0\tilde{s}_2\tilde{s}_2}, v_{0\tilde{s}_2}) - (\kappa_{22}-\kappa_{12})\,(\tilde{\eta} v_{0\tilde{s}_2}, v_{0\tilde{s}_2})\,. \qquad (3.35b)\end{aligned}$$

We now evaluate the inner products in (3.35). We first integrate by parts to get

$$2\,(\tilde{\eta}\tilde{s}_j v_{0\tilde{s}_j\tilde{s}_j}, v_{0\tilde{s}_j}) = -\,(\tilde{\eta}, [v_{0\tilde{s}_j}]^2)\,, \qquad j=1,2\,. \quad (3.36a)$$

Next, we use spherical coordinates to obtain

$$(\tilde{\eta} v_{0\tilde{s}_j}, v_{0\tilde{s}_j}) = \frac{\pi}{4}\int_0^\infty \rho^3 \left[u_c'(\rho)\right]^2 d\rho\,, \qquad j=1,2\,, \quad (3.36b)$$

$$(v_{0\tilde{s}_j}, v_{0\tilde{s}_j}) = \frac{2\pi}{3}\int_0^\infty \rho^2 \left[u_c'(\rho)\right]^2 d\rho\,, \qquad j=1,2\,, \quad (3.36c)$$

$$(\tilde{s}_j v_{0\tilde{\eta}}, v_{0\tilde{s}_j}) = \frac{\pi}{4}\int_0^\infty \rho^3 \left[u_c'(\rho)\right]^2 d\rho\,, \qquad j=1,2\,, \quad (3.36d)$$

$$(\tilde{\eta}\tilde{s}_2 v_{0\tilde{s}_1\tilde{s}_1}, v_{0\tilde{s}_2}) = (\tilde{\eta}\tilde{s}_1 v_{0\tilde{s}_2\tilde{s}_2}, v_{0\tilde{s}_1}) = \frac{\pi}{8}\int_0^\infty \rho^3 \left[u_c'(\rho)\right]^2 d\rho\,. \quad (3.36e)$$

Then, substituting (3.36) into (3.35) we obtain,

$$\dot{\xi}_1 = \frac{3b}{8}(\kappa_{21}+\kappa_{11})\,, \qquad \dot{\xi}_2 = \frac{3b}{8}(\kappa_{22}+\kappa_{12})\,, \quad (3.37a)$$

where $b>0$ is defined by

$$b = \frac{\int_0^\infty \rho^3 \left[u_c'(\rho)\right]^2 d\rho}{\int_0^\infty \rho^2 \left[u_c'(\rho)\right]^2 d\rho}\,. \quad (3.37b)$$

Finally, upon introducing the mean curvature $H(\xi_1, \xi_2)$ defined by $H = (\kappa_1 + \kappa_2)/2$, we obtain the main result.

Proposition 3.2 (Boundary Motion in 3 Dimensions) *For $\epsilon \to 0$, the motion of a spike confined to the smooth boundary of a three-dimensional domain is described by*

$$a \sim h^{\gamma} u_c \left(\epsilon^{-1} \left[(s_1 - \xi_1(t))^2 + (s_2 - \xi_2(t))^2 + \eta^2 \right]^{1/2} \right) + O(\epsilon)\,, \tag{3.38a}$$

$$\boldsymbol{\xi}'(t) \sim \frac{3}{4} b \epsilon^3 \nabla H(\boldsymbol{\xi})\,. \tag{3.38b}$$

Here $\boldsymbol{\xi} = (\xi_1, \xi_2)$, $\gamma = q/(p-1)$, $b > 0$ is defined in (3.37b), $u_c(\rho)$ is the positive solution to (3.32), and H is the mean curvature of $\partial\Omega$, with $H > 0$ for a sphere.

Notice that the stable equilibrium points of (3.38b) are at local maxima of the mean curvature.

Using the boundary value problem solver COLSYS [3] we can solve (3.32) numerically to determine the constant b in (3.38b). In particular, when $p = 2$ we compute that

$$\int_0^{\infty} \rho^3 \left[u_c'(\rho) \right]^2 d\rho = 17.36\,, \qquad \int_0^{\infty} \rho^2 \left[u_c'(\rho) \right]^2 d\rho = 10.42\,. \tag{3.39}$$

Hence, when $p = 2$, we get $b = 1.67$.

3.3 Qualitative Properties of the Associated Eigenvalue Problem

In this section we qualitatively explain why the non-local term in (3.1) is essential for ensuring the existence of slow boundary spike motion.

We first consider the *local* problem corresponding to (3.1) in which we delete (3.1b) and fix $h > 0$. Let us suppose for the moment that the boundary is flat and is given by the coordinate line $x_N = 0$. Hence we take $\Omega = \{\mathbf{x} = (x_1, \ldots, x_N) \,|\, x_N \geq 0\}$. Setting $a = h^{q/(p-1)} u$, we then get

$$u_t = \epsilon^2 \triangle u - u + u^p\,, \qquad x_N \geq 0\,; \qquad \partial_{x_N} u = 0\,, \qquad \text{on} \quad x_N = 0\,. \tag{3.40}$$

Let $u = u_c\left(\epsilon^{-1}|\mathbf{x}|\right)$, where u_c is the canonical spike solution defined in (3.14) and (3.32) for $N = 2$ and $N = 3$, respectively. We linearize (3.40) around u_c by writing $u = u_c\left(\epsilon^{-1}|\mathbf{x}|\right) + \psi\left(\epsilon^{-1}|\mathbf{x}|\right) e^{\mu t}$. This leads to the local eigenvalue problem for $\psi(\mathbf{y})$ and μ on a flat boundary

$$\triangle' \psi + \left(-1 + p u_c^{p-1}\right) \psi = \mu \psi, \qquad y_N \geq 0, \tag{3.41a}$$

$$\partial_{y_N} \psi = 0, \qquad \text{on} \quad y_N = 0. \tag{3.41b}$$

Here $\mathbf{y} = \epsilon^{-1}\mathbf{x}$, $u_c = u_c(|\mathbf{y}|)$ and $\triangle'$ denotes the Laplacian in the $\mathbf{y}$ variable. The eigenvalues μ_j of (3.41) satisfy

$$\mu_1 > 0, \ \mu_2 = \ldots = \mu_N = 0, \ \mu_{N+1} < 0. \tag{3.42}$$

The positivity of μ_1 was shown in [27] and [48]. The eigenfunctions ψ_1 and ψ_{N+1} are radially symmetric (i. e. $\psi_1 = \psi_1(|\mathbf{y}|)$). A numerical procedure to calculate μ_1 was given in [48] and the results are shown in Table 1. The translation eigenfunctions corresponding to the zero eigenvalues are given by $\psi_j = \partial_{y_{j-1}} u_c(|\mathbf{y}|)$ for $j = 2, \ldots, N$.

p	$\mu_1(N=2)$	$\mu_1(N=3)$
2	1.65	2.36
3	5.41	15.29
4	13.23	144.18

Table 3.1: Numerical results for the principal eigenvalue μ_1 of the local problem on a flat boundary (3.41).

The *local* eigenvalue problem on a *curved* boundary has the form

$$\mathcal{A}_\epsilon \psi^\epsilon + \left(-1 + p u_c^{p-1}\right) \psi^\epsilon = \mu^\epsilon \psi^\epsilon, \qquad \tilde{\eta} \geq 0, \tag{3.43a}$$

$$\partial_{\tilde{\eta}} \psi^\epsilon = 0, \qquad \text{on} \quad \tilde{\eta} = 0. \tag{3.43b}$$

Here $\mathcal{A}_\epsilon$ is the operator that results from converting the Laplacian into local boundary coordinates as explained in §2 and §3. Clearly, $\mathcal{A}_\epsilon \to \triangle'$ as $\epsilon \to 0$. Hence, we would expect that the eigenvalues of (3.41) and (3.43) are close as $\epsilon \to 0$. In fact, it was proved in [53] that, for

$\epsilon \ll 1$, the eigenvalues μ_j^ϵ of (3.43) satisfy

$$\mu_j^\epsilon = \mu_j + o(1)\,, \qquad j = 1, \ldots, N+1, \ldots\,. \tag{3.44}$$

Hence, $\mu_1^\epsilon > 0$ for ϵ sufficiently small. This shows that a boundary spike solution for the local problem corresponding to (3.1) will not drift slowly along the boundary of the domain. The eigenvalues $\mu_2^\epsilon, \ldots, \mu_N^\epsilon$ corresponding to the near translation modes were calculated for $\epsilon \ll 1$ in [53].

Next, we linearize the *non-local problem* (3.1) around a spike solution centered on a flat boundary. In place of (3.41), we obtain the non-local eigenvalue problem for λ and ϕ given by

$$\triangle' \phi + \left(-1 + p u_c^{p-1}\right)\phi + I(\phi) = \lambda\phi\,, \qquad y_N \geq 0\,, \tag{3.45a}$$

$$\partial_{y_N}\phi = 0\,, \qquad \text{on} \quad y_N = 0\,, \tag{3.45b}$$

where $I(\phi)$ is defined by

$$I(\phi) \equiv -\frac{2mqu_c^p}{\Omega_N \beta(s+1)} \int_D u_c^{m-1}\phi\, d\mathbf{y}\,, \qquad \beta \equiv \int_0^\infty [u_c(\rho)]^m \rho^{N-1}\, d\rho\,. \tag{3.45c}$$

Here Ω is the half-space $y_N \geq 0$, Ω_N is the surface area of the unit N-dimensional sphere, and $u_c = u_c(|\mathbf{y}|)$.

As is similar to (3.44), the eigenvalues of the non-local problem defined on a curved boundary should be asymptotically close to within $o(1)$ terms to the eigenvalues of (3.45). Hence, to ensure the existence of slow boundary spike motion for (3.1) we need only show that all of the eigenvalues of (3.45) satisfy $\mathrm{Re}(\lambda) \leq 0$.

To accomplish this, we will apply Theorem 2.2. Before we may apply this theorem, we note that the boundary conditions, (3.45b) and (2.65) don't match. However, the eigenfunctions we are concerned with are radially symmetric and thus will satisfy (3.45b) automatically. Thus, for any parameter set satisfying (2.67), we may conclude that the real part of all of the eigenvalues satisfy $\mathrm{Re}(\lambda) \leq 0$. For any parameter set not satisfying (2.67), we must apply numerical techniques, as in §2.1.1, to determine if the spectrum of (3.45) contains an eigenvalue with positive real part.

Finally, we note that the problem (3.45) preserves the translation eigenvalues associated with the local problem (3.41), since by symmetry the non-local term $I(\phi)$ satisfies $I\left(\partial_{y_{j-1}} u_c\right) = 0$ for $j = 2, \ldots, N$. As is similar to (3.44), these translation eigenvalues are perturbed by $o(1)$ as $\epsilon \to 0$ when the non-local eigenvalue problem is defined on a curved boundary. The resulting small eigenvalues are responsible for the slow boundary spike motion derived in §3.2 and §3.3.

3.4 A Spike on a Flat Boundary in Two Dimensions

In §3.2 we showed that the motion of a spike centered on the boundary of a two-dimensional domain is in the direction of increasing curvature. This leads us to the problem of determining the motion of a spike when the curvature is constant. In particular, we will analyze the motion of a spike on a flat boundary where the curvature vanishes. Our analysis below shows that this motion is metastable. To obtain this result, in §3.5.1 we show that the principal eigenvalue associated with the linearization of a spike solution centered on a flat boundary is exponentially small. This establishes the metastability. Then, in §3.5.2 we derive an asymptotic differential equation for the metastable spike motion on the flat boundary by imposing a limiting solvability condition on the solution to the linearized problem. This condition ensures that this linearized solution is orthogonal to the eigenfunction associated with the exponentially small eigenvalue.

For the analysis we let $\mathbf{x} = (x, y)$ and we suppose that the spike is located on the straight-line boundary segment joining the points $(x_L, 0)$ and $(x_R, 0)$ as shown in Fig. 3.6. The flat portion of $\partial\Omega$ is taken to be the straight-line segment between $(x_L, 0)$ and $(x_R, 0)$. The spike is centered at $\mathbf{x}_0 = (\xi, 0)$ where $x_L < \xi < x_R$. We decompose $\partial\Omega$ as $\partial\Omega = \partial\Omega_c \cup \partial\Omega_s$ where $\partial\Omega_s$ refers to the straight-line segment of the boundary and $\partial\Omega_c$ denotes the remaining curved part of $\partial\Omega$. The distance between the spike and $\partial\Omega_c$ is assumed to be a minimum at either of the two corners $(x_L, 0)$ or $(x_R, 0)$.

The local behavior of the boundary near the corner points is critical to our analysis. Near the

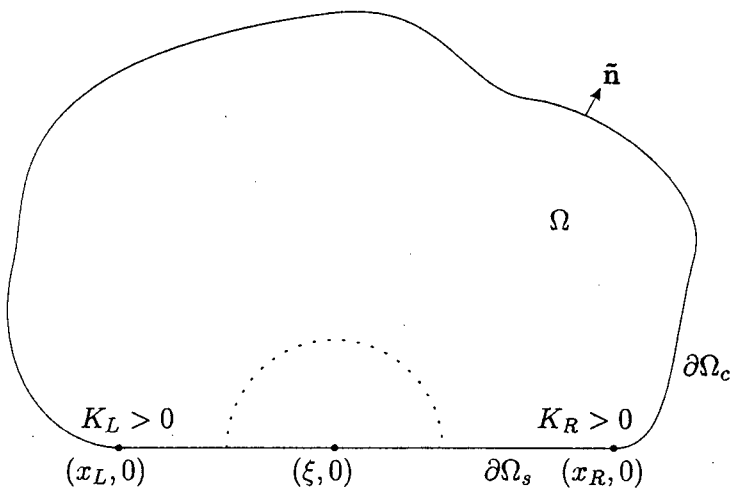

Figure 3.6: Plot of a two-dimensional domain Ω with a flat boundary segment. The spike is centered at $x = \xi$ on the flat segment. The dotted line indicates an approximate equipotential for u.

corner points, $\partial\Omega_c$ is assumed to have the local behavior

$$\text{near } (x_L, 0)\,; \quad y = \psi_L(x), \qquad \psi_L'(x) \sim -K_L(x_L - x)^{\alpha_L}\,, \quad \text{as } x \to x_L^-, \tag{3.46a}$$

$$\text{near } (x_R, 0)\,; \quad y = \psi_R(x), \qquad \psi_R'(x) \sim K_R(x - x_R)^{\alpha_R}\,, \quad \text{as } x \to x_R^+, \tag{3.46b}$$

where $\alpha_L > 0$ and $\alpha_R > 0$. When $\alpha_L = \alpha_R = 1$, K_L and K_R are proportional to the curvature of $\partial\Omega_c$ at the left and right corners, respectively.

The spike solution to (3.1) is given asymptotically by

$$a(\mathbf{x}, t) \sim a_e \equiv h_e^{q/(p-1)} u_c\left(\epsilon^{-1}|\mathbf{x} - \mathbf{x}_0(t)|\right)\,, \tag{3.47a}$$

$$h \sim h_e \equiv \left(\frac{\pi}{\mu|\Omega|}\int_0^\infty [u_c(\rho)]^m\,\rho\,d\rho\right)^{\frac{p-1}{(s+1)(p-1)-qm}}\,, \tag{3.47b}$$

where $\mathbf{x}_0(t) = (\xi(t), 0)$ is to be determined. Here $u_c(\rho)$ is the radially symmetric solution defined in (3.14), and $|\Omega|$ denotes the area of Ω.

We first linearize (3.1) around a_e by writing $a = a_e + v$, where $v \ll a_e$. We get that v satisfies,

$$\mathcal{L}_\epsilon v \equiv \epsilon^2\Delta v + (-1 + p u_c^{p-1})v - \frac{mq\epsilon^{-2}u_c^p}{\pi\beta(s+1)}\int_\Omega u_c^{m-1} v\,d\mathbf{x} = v_t + \partial_t a_e\,, \quad \text{in} \quad \Omega\,, \tag{3.48a}$$

$$\partial_n v = -\partial_n a_e \quad \text{on} \quad \partial\Omega\,. \tag{3.48b}$$

Here β is defined by

$$\beta = \int_0^\infty [u_c(\rho)]^m \, \rho \, d\rho \,. \tag{3.49}$$

Now we let $v = e^{\lambda t}\phi$ to get the eigenvalue problem,

$$\mathcal{L}_\epsilon \phi = \lambda \phi, \quad \text{in} \quad \Omega; \qquad \partial_n \phi = 0 \quad \text{on} \quad \partial\Omega \,. \tag{3.50}$$

3.4.1 The Translation Eigenvalue

Suppose for the moment that Ω is the half-space $y \geq 0$ so that $\partial\Omega_s$ is the entire x-axis. Then, the function $\tilde{\phi} \equiv \partial_x u_c$ satisfies $\mathcal{L}_\epsilon \tilde{\phi} = 0$ and the normal derivative boundary condition $\partial_n \tilde{\phi} = 0$. Hence, for this case, $\tilde{\phi}$ is an eigenfunction of $\mathcal{L}$ with a zero eigenvalue. This corresponds to translation invariance in the x direction. For our geometry, $\tilde{\phi}$ is localized near $(\xi, 0)$ on the flat segment $\partial\Omega_s$ and $\tilde{\phi}$ decays exponentially away from this point. The interaction of the exponentially small far-field behavior of $\tilde{\phi}$ with the corner regions, where $\partial\Omega_s$ and $\partial\Omega_c$ meet, perturbs the zero eigenvalue by exponentially small terms. This shift in the zero eigenvalue is calculated below. The non-local term in the operator $\mathcal{L}_\epsilon$ is asymptotically negligible in the calculation of this shift. However, as shown in §3.4, the non-local term is essential for ensuring that the translation eigenvalue is the principal eigenvalue of the linearization.

Now we calculate λ_1 and ϕ_1. Since $\tilde{\phi}$ fails to satisfy the boundary condition on $\partial\Omega_c$, the principal eigenfunction ϕ_1 has the form

$$\phi_1 \sim C_1 \left(\partial_x u_c + \phi_L\right) . \tag{3.51}$$

Here C_1 is a normalization constant and ϕ_L is a boundary layer correction term localized near $\partial\Omega_c$. Let $\eta < 0$ be the distance between $\boldsymbol{x} \in \Omega$ and $\partial\Omega$ and let $\tilde{\eta} = \epsilon^{-1}\eta$ be the localized coordinate. Then, from (3.50), we get that ϕ_L satisfies

$$\phi_{L\tilde{\eta}\tilde{\eta}} - \phi_L = 0, \qquad \tilde{\eta} < 0 \,, \tag{3.52a}$$

$$\partial_{\tilde{\eta}} \phi_L = -\epsilon \partial_{\tilde{\eta}} [\partial_x u_c]|_{\tilde{\eta}=0} \,, \quad \text{on} \quad \tilde{\eta} = 0; \qquad \phi_L \to 0 \,, \quad \text{as} \quad \tilde{\eta} \to -\infty \,. \tag{3.52b}$$

The solution to (3.52) is

$$\phi_L = -\epsilon \left(\partial_{\tilde{\eta}} [\partial_x u_c]|_{\tilde{\eta}=0}\right) e^{\eta/\epsilon} \,. \tag{3.53}$$

Since u_c is localized near $x = \xi \in \partial\Omega_s$, we can calculate ϕ_1 and ϕ_L on $\partial\Omega_c$ by using the far-field behavior of u_c given in (3.14b). In this way, we get an estimate for ϕ_1 on $\partial\Omega_c$ from (3.51) and (3.53)

$$\phi_1 \sim -C_1 a_c \epsilon^{-1/2} r^{-3/2} (x-\xi) e^{-r/\epsilon} \left(1 + \tilde{\mathbf{r}} \cdot \tilde{\mathbf{n}}\right), \quad \text{on} \quad \partial\Omega_c. \tag{3.54}$$

Here a_c is defined in (3.14b), $r = |\boldsymbol{x} - \mathbf{x}_0|$, $\mathbf{r} = (\boldsymbol{x} - \mathbf{x}_0)/r$, and $\mathbf{n}$ is the unit outward normal to $\partial\Omega_c$.

Applying Green's identity to ϕ_1 and $\partial_x u_c$, and using the facts that $\partial_n \phi_1 = 0$ on $\partial\Omega$ and $\partial_n[\partial_x u_c] = 0$ on $\partial\Omega_s$, we obtain

$$\lambda_1 \left(\partial_x u_c, \phi_1\right) = -\epsilon^2 \int_{\partial\Omega_c} \phi_1 \partial_n [\partial_x u_c] \, dS + \left(\mathcal{L}_\epsilon^* [\partial_x u_c], \phi_1\right). \tag{3.55}$$

Here $(f, g) \equiv \int_\Omega fg \, d\mathbf{x}$ and $\mathcal{L}_\epsilon^*$ is the adjoint operator defined by

$$\mathcal{L}_\epsilon^* \phi \equiv \epsilon^2 \Delta\phi - \phi + u_c^{p-1}\phi - \frac{mq\epsilon^{-2} u_c^{m-1}}{\beta\pi(s+1)} \int_\Omega u_c^p \phi \, d\mathbf{x}. \tag{3.56}$$

We now estimate each term in (3.55). Using polar coordinates, we calculate

$$\left(\phi_1, \partial_x u_c\right) \sim \frac{\pi C_1 \gamma}{2}, \qquad \text{where} \quad \gamma \equiv \int_0^\infty \rho \left[u_c'(\rho)\right]^2 d\rho. \tag{3.57}$$

Next, we use (3.54) and the far-field form of u_c in (3.14b) to get

$$\phi_1 \partial_n \left[\partial_x u_c\right] \sim -\frac{C_1 a_c^2 \epsilon^{-2}}{r} \left(\frac{x-\xi}{r}\right)^2 e^{-2r/\epsilon} \tilde{\mathbf{r}} \cdot \tilde{\mathbf{n}} \left(1 + \tilde{\mathbf{r}} \cdot \tilde{\mathbf{n}}\right), \qquad \text{on} \quad \partial\Omega_c. \tag{3.58}$$

Substituting (3.58) into the boundary integral in (3.55), we observe that the dominant contribution to this integral arises from the corner regions of $\partial\Omega_c$, where r is the smallest. Near the corner regions we use the local behavior (3.46) to calculate

$$\tilde{\mathbf{r}} \cdot \tilde{\mathbf{n}} \sim \begin{cases} K_L (x_L - x)^{\alpha_L}, & \text{as} \quad x \to x_L^- \\ K_R (x - x_R)^{\alpha_R}, & \text{as} \quad x \to x_R^+. \end{cases} \tag{3.59}$$

Substituting (3.58) and (3.59) into the boundary integral in (3.55), and using Laplace's method, we get

$$\begin{aligned} B \equiv -\epsilon^2 \int_{\partial\Omega_c} \phi_1 \partial_n [\partial_x u_c] \, dS \sim C_1 a_c^2 \int_{-\infty}^{x_L} \frac{K_L (x_L - x)^{\alpha_L}}{\xi - x_L} e^{-2(\xi - x)/\epsilon} \, dx, \\ + C_1 a_c^2 \int_{x_R}^{\infty} \frac{K_R (x - x_R)^{\alpha_R}}{x_R - \xi} e^{-2(x-\xi)/\epsilon} \, dx. \end{aligned} \tag{3.60}$$

The integrals in (3.60) are evaluated explicitly by using

$$\int_0^\infty z^\alpha e^{-2z/\epsilon}\,dz = \left(\frac{\epsilon}{2}\right)^{\alpha+1}\Gamma(\alpha+1)\,, \tag{3.61}$$

where $\Gamma(z)$ is the Gamma function. In this way, (3.60) becomes

$$B \sim C_1 a_c^2 \left\{ \frac{K_R}{x_R-\xi}\left(\frac{\epsilon}{2}\right)^{\alpha_R+1}\Gamma(\alpha_R+1)\,e^{-2(x_R-\xi)/\epsilon} \right. \\ \left. + \frac{K_L}{\xi-x_L}\left(\frac{\epsilon}{2}\right)^{\alpha_L+1}\Gamma(\alpha_L+1)\,e^{-2(\xi-x_L)/\epsilon}\right\}. \tag{3.62}$$

Finally, in Appendix B.1 we give asymptotic estimates to show that $(\mathcal{L}_\epsilon^*[\partial_x u_c], \phi_1) = o(B)$, as $\epsilon \to 0$. Hence, we can neglect the last term on the right side of (3.55). Substituting (3.57) and (3.62) into (3.55), we get the following key asymptotic formula for the principal eigenvalue of (3.50):

Proposition 3.3 (Eigenvalue) *Assume that the distance between ξ and ∂D_c is a minimum at either of the two corners $(x_L, 0)$ or $(x_R, 0)$. Then, for $\epsilon \to 0$, the principal eigenvalue λ_1 of (3.50) has the asymptotic estimate*

$$\lambda_1 \sim \frac{2a_c^2}{\pi\gamma}\left\{ \frac{K_R}{x_R-\xi}\left(\frac{\epsilon}{2}\right)^{\alpha_R+1}\Gamma(\alpha_R+1)\,e^{-2(x_R-\xi)/\epsilon} \right. \\ \left. + \frac{K_L}{\xi-x_L}\left(\frac{\epsilon}{2}\right)^{\alpha_L+1}\Gamma(\alpha_L+1)\,e^{-2(\xi-x_L)/\epsilon}\right\}. \tag{3.63}$$

Here a_c is given in (3.14b), γ is defined in (3.57), and K_L, K_R, α_L and α_R are defined in (3.46) in terms of the local behavior of $\partial\Omega_c$ near the corners.

3.4.2 The Slow Spike Motion

We now derive a differential equation for $\xi(t)$ for the time-dependent problem. We assume that the spike is initially on $\partial\Omega_s$. Then, since the spike motion is metastable we have $v_t \ll \partial_t a_e$ in (3.48a). Multiplying (3.48a) by ϕ_1, and using $\partial_n\phi_1 = 0$ on $\partial\Omega$, we obtain upon integration by parts that

$$(\mathcal{L}_\epsilon v, \phi_1) \sim \epsilon^2 \int_{\partial\Omega} \phi_1 \partial_n v\,dS + (\mathcal{L}_\epsilon^*\phi_1, v)\,. \tag{3.64}$$

From (3.48) we have $\mathcal{L}_\epsilon v \sim \partial_t a_e$ in Ω, and $\partial_n v = -\partial_n a_e$ on $\partial\Omega$, where $\partial_n a_e = 0$ on $\partial\Omega_s$. Thus, (3.64) reduces to

$$(\partial_t u_c, \phi_1) \sim -\epsilon^2 \int_{\partial\Omega_c} \phi_1 \partial_n u_c \, dS + h_e^{-q/(p-1)} \left(\mathcal{L}_\epsilon^* \phi_1, v\right) . \tag{3.65}$$

Similar estimates to those given in Appendix B.1, which we omit, shows that the last term on the right-hand side of (3.65) is negligible as compared to the boundary integral term. Hence,

$$(\partial_t u_c, \phi_1) \sim -\epsilon^2 \int_{\partial\Omega_c} \phi_1 \partial_n u_c \, dS \,, \tag{3.66}$$

where $u_c = u_c\left[\epsilon^{-1}|\boldsymbol{x} - \mathbf{x}_0|\right]$ and $\mathbf{x}_0(t) = (\xi(t), 0)$.

The remaining part of the analysis is very similar to the derivation of the eigenvalue estimate for λ_1, and hence we omit many of the details. For $\epsilon \ll 1$, we calculate using (3.51) that

$$(\partial_t u_c, \phi_1) \sim -\frac{\pi C_1 \xi' \gamma}{2} , \tag{3.67}$$

where γ was defined in (3.57). Next, using the far-field behavior of u_c given in (3.14b), the estimate for ϕ_1 on $\partial\Omega_c$ given in (3.54), and Laplace's method, the boundary integral in (3.66) can be evaluated asymptotically as in (3.58)–(3.62). The following main result is obtained from this calculation:

Proposition 3.4 (Spike Motion) *Assume that the distance between ξ and $\partial\Omega_c$ is a minimum at either of the two corners $(x_L, 0)$ or $(x_R, 0)$. Then, for $\epsilon \to 0$, the x-coordinate of the center of the spike along the flat segment $\partial\Omega_s$, denoted by $\xi(t)$, satisfies the asymptotic differential equation,*

$$\xi'(t) \sim \frac{2\epsilon a_c^2}{\pi\gamma} \left\{ \frac{K_R}{x_R - \xi} \left(\frac{\epsilon}{2}\right)^{\alpha_R+1} \Gamma(\alpha_R + 1)\, e^{-2(x_R-\xi)/\epsilon} \right.$$
$$\left. - \frac{K_L}{\xi - x_L} \left(\frac{\epsilon}{2}\right)^{\alpha_L+1} \Gamma(\alpha_L + 1)\, e^{-2(\xi-x_L)/\epsilon} \right\} . \tag{3.68}$$

Here a_c is given in (3.14b), γ is defined in (3.57), and K_L, K_R, α_L and α_R are defined in (3.46) in terms of the local behavior of $\partial\Omega_c$ near the corners.

A similar differential equation for the motion of a straight-line interface in a constant width neck region of a dumbbell-shaped domain has been derived in [25] for the Allen-Cahn equation. Using

the boundary value problem solver COLSYS [3] we can solve (3.14) numerically to determine the constants a_c and γ in (3.63) and (3.68). In this way, when $p = 2$ we compute that $a_c = 10.80$ and $\gamma = 2.47$.

The result (3.68) shows that the motion of the spike along the straight-line boundary segment between $(x_L, 0)$ and $(x_R, 0)$ is determined by the shape of the boundary at $(x_L, 0)$ and $(x_R, 0)$ and by the distance between the spike and the corner regions. The spike will move according to (3.68) until a stable steady state is reached or until the spike touches $(x_L, 0)$ or $(x_R, 0)$. Once the spike reaches the curved part of the boundary $\partial\Omega_c$, it will subsequently evolve according to (3.20b).

From (3.68), the steady-state spike-layer location ξ_e on $\partial\Omega_s$ satisfies

$$\frac{\xi_e - x_L}{x_R - \xi_e} e^{4\xi_e/\epsilon} = \frac{K_L \Gamma(\alpha_L + 1)}{K_R \Gamma(\alpha_R + 1)} \left(\frac{\epsilon}{2}\right)^{\alpha_L - \alpha_R} e^{2(x_R + x_L)/\epsilon}. \tag{3.69}$$

Since the left hand side of (3.69) increases from 0 to ∞ as ξ_e ranges from x_L to x_R, a unique steady-state solution to (3.69) exists on $x_L < \xi < x_R$ whenever K_L and K_R have the same sign. This solution is stable when $K_L < 0$ and $K_R < 0$, and is unstable when $K_L > 0$ and $K_R > 0$. In particular, this implies that if Ω is convex near $(x_L, 0)$ and $(x_R, 0)$, then there is no stable equilibrium spike location on $\partial\Omega_s$. A simple calculation using (3.69) shows that the equilibrium spike-layer location ξ_e, when it exists, has the expansion

$$\xi_e \sim \frac{x_L + x_R}{2} + \frac{\epsilon}{4} \log\left[\frac{K_L \Gamma(\alpha_L + 1)}{K_R \Gamma(\alpha_R + 1)} \left(\frac{\epsilon}{2}\right)^{\alpha_L - \alpha_R}\right] + \cdots. \tag{3.70}$$

Thus, the equilibrium location, ξ_e is located at an $O(\epsilon)$ distance from the midpoint of the straight-line boundary segment.

The following dynamical behavior can be deduced from (3.68) and (3.70) when the initial condition is $\xi(0) = \xi_0$. When $K_L > 0$ and $K_R > 0$, $\xi(t)$ will move monotonically towards x_L if $\xi_0 < \xi_e$, or monotonically towards x_R if $\xi_0 > \xi_e$ (see Fig. 3.7). When $K_L < 0$ and $K_R < 0$, $\xi(t)$ will approach the stable steady-state at ξ_e (see Fig. 3.8). If $K_L < 0$ and $K_R > 0$, then $\xi(t)$ will move towards x_R (see Fig. 3.9). Similarly, $\xi(t)$ will move towards x_L if $K_L > 0$ and $K_R < 0$. When the spike touches $(x_L, 0)$ or $(x_R, 0)$, its subsequent evolution is determined by (3.20b).

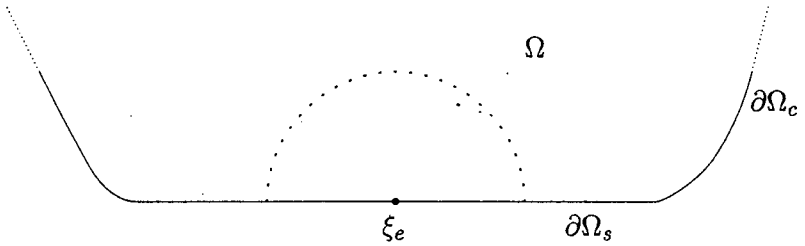

Figure 3.7: Plot of part of a domain boundary, $\partial\Omega$, upon which the center of the spike is at an unstable steady state. $K_L > 0$, $K_R > 0$ for this domain.

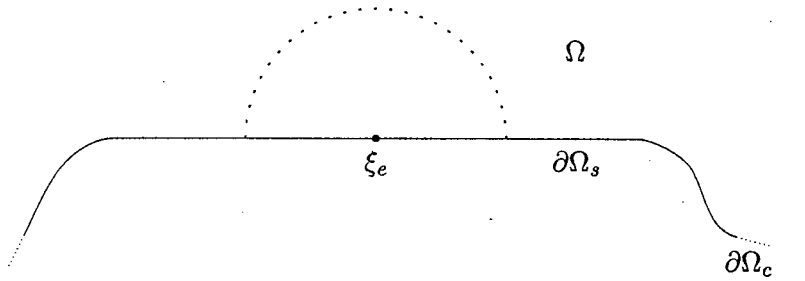

Figure 3.8: Plot of part of a domain boundary, $\partial\Omega$, upon which the center of the spike is at a stable steady state. $K_L < 0$, $K_R < 0$ for this domain.

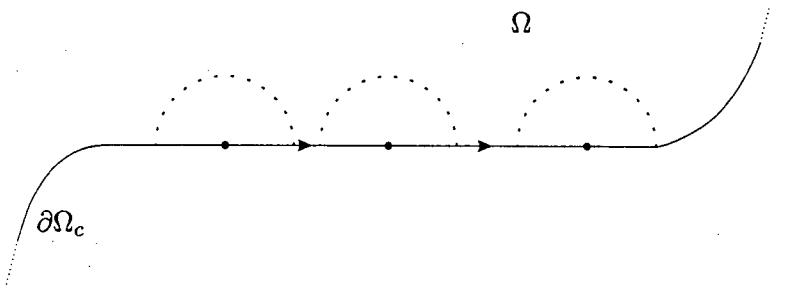

Figure 3.9: Plot of part of a domain boundary, $\partial\Omega$, upon which the center of the spike moves towards the right. $K_L < 0$ and $K_R > 0$ for this domain.

Chapter 4

Stability of n-spike equilibrium solutions to (1.19)

In this chapter, we study the stability of n-spike equilibrium solutions to (1.17). As will be demonstrated below, the analysis of (1.17) is considerably more involved than the previous analysis of (1.18). The motivation for carrying out this difficult procedure are certain discrepancies between the behaviour of (1.18) found in §2 and numerical simulations of the full system (1.17) which (1.18) is supposed to mimic. In §2.2 we found that n-spike solutions to (1.18), where $n > 1$ and the spikes are all strictly within the interior of the domain, are unstable with an $O(1)$ positive eigenvalue. Solutions with one interior spike are also unstable but with an exponentially small principle eigenvalue as $\epsilon \to 0$. However, numerical computations, such at those in [16], [32] and [33] suggest that equilibrium solutions with $n > 1$ stable interior spike solutions to (1.19) may be possible. We conjecture that for sufficiently small values of D, solutions to (1.19) with $n \geq 1$ interior spikes may be stable. The goal of this chapter is to investigate this conjecture analytically in the simple case of a one-dimensional spatial domain for equilibrium solutions with spikes of equal height. Equilibrium solutions with asymmetric equilibrium spike solutions are studied in [50] and the case of spikes in a two dimensional domain are studied in [30]. It is important to mention that our stability analysis is very different from the classical Turing-type stability analysis that is based on linearizing a reaction-diffusion system around a spatially homogeneous steady-state equilibrium solution. Our analysis is based on the study of the linearization of (1.17) around an n-spike equilibrium solution, which has a very high degree of spatial inhomogeneity. A similar analysis for the Fitzhugh-Nagumo model has been carried out in [38]. Some stability results for the case of one spike with $\tau \neq 0$ is given in [37].

We now give an outline of the chapter and summarize some of the key results obtained. In §4.1 we use the method of matched asymptotic expansions to construct equilibrium solutions to (1.17) in the limit $\epsilon \to 0$ that have $n \geq 1$ spikes of equal amplitude in the activator concentration. In §4.2 and §4.3 we study the spectrum of the eigenvalue problem associated with linearizing (1.17) around the equilibrium solution constructed in §4.1. In §4.2 we study the large eigenvalues of order $\lambda = O(1)$ in the spectrum, while in §4.3 we study the small eigenvalues of order $\lambda = O(\epsilon^2)$. The n-spike solution is stable when both sets of eigenvalues lie in the left half-plane. For $n \geq 2$ and $\epsilon \to 0$, in §4.2 we obtain an explicit critical value D_n such that the large $O(1)$ eigenvalues are in the left half-plane only when $D < D_n$. When this condition on D is satisfied, we say that the equilibrium solution is stable with respect to the $O(1)$ eigenvalues. In §4.3, for $n \geq 2$ and $\epsilon \to 0$, we show that the small eigenvalues are always real and that they are negative only when $D < D_n^*$. An explicit formula for D_n^* is derived and it is found that $D_n^* < D_n$. Thus, for $n \geq 2$ and $\epsilon \to 0$, an n-spike symmetric equilibrium spike pattern is stable when $D < D_n^*$ and is unstable otherwise. The results for D_n and D_n^* are given below in Propositions 4.7 and 4.11, respectively. The main stability results, summarized in propositions 4.5, 4.7, 4.8, 4.10, and 4.11, are obtained from a careful but formal asymptotic analysis. It would be of interest to establish these results rigorously.

Finally, in §4.4 we study the stability and dynamics of a solution to (1.17) with exactly one spike. For a certain range of exponents (p, q, r, s), we show that a one-spike equilibrium solution to (1.17) will be stable when $D < D_1(\epsilon)$, where $D_1(\epsilon)$ is exponentially large as $\epsilon \to 0$. It is unstable when $D > D_1(\epsilon)$. An asymptotic formula for $D_1(\epsilon)$ is given in Proposition 4.13 of §4.4.2. This result is consistent with the result of [18] for the shadow problem (1.18) for which $D = \infty$, where it was shown that a one-spike equilibrium solution is unstable, but with an asymptotically exponentially small positive eigenvalue. In §4.4.1, we study the dynamics of a one-spike solution to (1.17) for finite D by deriving an asymptotic differential equation for the trajectory of the center of the spike using the method of matched asymptotic expansions. The asymptotic differential equation is given in Proposition 4.12 of §4.4.1 and is favorably compared in §4.4.1 with results from full numerical computations.

4.1 An Asymptotic Analysis of the Equilibrium Solution

For $\epsilon \to 0$, we construct an n-spike equilibrium solution to (1.17) with equal amplitude using the method of matched asymptotic expansions. A solution with three spikes is shown in Fig. 4.1. The locations x_j, for $j = 0, \ldots, n-1$, of the spikes for an n-spike solution, which follows from symmetry considerations under the Neumann conditions (1.17c), satisfy

$$x_j = -1 + \frac{1+2j}{n}, \qquad j = 0, 1, \ldots, n-1. \tag{4.1}$$

At these points the equilibrium solution satisfies $a'(x_j) = 0$ and $h(x_j) = H$, where H is independent of j. For an n-peak equilibrium solution to (1.17), the activator concentration is localized in the inner regions defined near each x_j, and is exponentially small in the outer regions defined away from the spike locations.

In the inner region near the j^{th} spike we introduce new variables by

$$y_j = \epsilon^{-1}(x - x_j), \qquad \tilde{h}(y_j) = h(x_j + \epsilon y), \qquad \tilde{a}(y_j) = a(x_j + \epsilon y), \tag{4.2a}$$

and we expand

$$\tilde{h}(y_j) = \tilde{h}_0(y_j) + \epsilon \tilde{h}_1(y_j) + \cdots, \qquad \tilde{a}(y_j) = \tilde{a}_0(y_j) + O(\epsilon). \tag{4.2b}$$

Substituting (4.2) into the equilibrium problem for (1.17), and collecting powers of ϵ, we get

$$\tilde{a}_0'' - \tilde{a}_0 + \tilde{a}_0^p/\tilde{h}_0^q = 0, \qquad -\infty < y_j < \infty, \tag{4.3a}$$

$$\tilde{h}_0'' = 0, \tag{4.3b}$$

$$D\tilde{h}_1'' = -\tilde{a}_0^r/\tilde{h}_0^s. \tag{4.3c}$$

The conditions at $y_j = 0$ are that $\tilde{a}_0'(0) = 0$, $\tilde{h}_0(0) = H$, and $\tilde{h}_1(0) = 0$. The conditions needed to match to the outer solution are that $\tilde{h}_0$ is bounded as $|y_j| \to \infty$ and $\tilde{a}_0 \to 0$ as $|y_j| \to \infty$. Thus, the solution to (4.3b) is $\tilde{h}_0 = H$. Next, we introduce u_c by

$$\tilde{a}_0 = H^\gamma u_c, \qquad \text{where} \qquad \gamma \equiv q/(p-1). \tag{4.4}$$

Then, (4.3a) and (4.3c) become

$$u_c'' - u_c + u_c^p = 0\,, \qquad -\infty < y_j < \infty\,, \tag{4.5a}$$

$$u_c \to 0 \quad \text{as} \quad |y_j| \to \infty\,; \qquad u_c'(0) = 0\,, \tag{4.5b}$$

$$D\tilde{h}_1'' = -u_c^r H^{\gamma r - s}\,. \tag{4.5c}$$

From phase-plane considerations, there is a unique positive solution to (4.5). In particular, when $p = 2$ we have

$$u_c(y) = \frac{3}{2}\mathrm{sech}^2\left(\frac{y}{2}\right)\,. \tag{4.6}$$

Upon integrating (4.5c) from $y_j = -\infty$ to $y_j = \infty$ we obtain

$$\lim_{y_j \to +\infty} \tilde{h}_1' - \lim_{y_j \to -\infty} \tilde{h}_1' = -\frac{1}{D} H^{\gamma r - s} b_r\,, \qquad \text{where} \qquad b_r \equiv \int_{-\infty}^{\infty} [u_c(y)]^r\, dy\,. \tag{4.7}$$

This equation yields a jump condition for the outer solution.

In the outer region, defined away from $O(\epsilon)$ regions near each x_j, a is exponentially small and h is expanded as

$$h(x) = h_0(x) + o(\epsilon)\,. \tag{4.8}$$

Here h_0 satisfies $Dh_0'' - \mu h_0 = 0$ on the interval $[-1, 1]$ with suitable jump conditions imposed across the x_j. Upon matching to the inner solution constructed above, we obtain that h_0 is continuous across each x_j and that the jump in h_0' is given by the right-hand side of (4.7). Therefore, h_0 satisfies

$$Dh_0'' - \mu h_0 = -H^{\gamma r - s} b_r \sum_{k=0}^{n-1} \delta(x - x_k)\,, \qquad -1 < x < 1\,, \tag{4.9a}$$

$$h_0'(\pm 1) = 0\,, \tag{4.9b}$$

where $\delta(y)$ is the Dirac delta function. To solve (4.9) we introduce the Green's function $G(x; x_k)$ satisfying

$$DG_{xx} - \mu G = -\delta(x - x_k)\,, \qquad -1 < x < 1\,, \tag{4.10a}$$

$$G_x(\pm 1; x_k) = 0\,. \tag{4.10b}$$

A simple calculation gives,

$$G(x;x_k) = \begin{cases} A_k \cosh\left[\theta(1+x)\right] / \cosh\left[\theta(1+x_k)\right], & -1 < x < x_k\,, \\ A_k \cosh\left[\theta(1-x)\right] / \cosh\left[\theta(1-x_k)\right], & x_k < x < 1\,. \end{cases} \tag{4.11a}$$

Here

$$A_k = \frac{1}{\sqrt{\mu D}} \left(\tanh\left[\theta(1-x_k)\right] + \tanh\left[\theta(1+x_k)\right]\right)^{-1}\,, \qquad \theta \equiv (\mu/D)^{1/2}\,. \tag{4.11b}$$

In terms of $G(x;x_k)$, the solution to (4.9) is

$$h_0(x) = H^{\gamma r - s} b_r \sum_{k=0}^{n-1} G(x;x_k)\,. \tag{4.12}$$

Finally, to determine H we set $h_0(x_j) = H$ and use the fact that $\sum_{k=0}^{n-1} G(x_j;x_k)$ is independent of j when the locations satisfy (4.1). This can be shown directly either by using (4.11) and summing certain geometric series, or by using the matrix analysis given following Proposition 4 below. In either way, we get

$$H^{\gamma r - (s+1)} = \frac{1}{b_r a_g}\,, \qquad \text{where} \qquad a_g \equiv \sum_{k=0}^{n-1} G(x_j;x_k)\,. \tag{4.13}$$

This leads to the following equilibrium result:

Proposition 4.1 *For $\epsilon \to 0$, an n-spike equilibrium solution to (1.17), which we label by $a_e(x)$ and $h_e(x)$, is given asymptotically by*

$$a_e(x) \sim H^{\gamma} \sum_{k=0}^{n-1} u_c\left[\epsilon^{-1}(x-x_k)\right]\,, \tag{4.14a}$$

$$h_e(x) \sim \frac{H}{a_g} \sum_{k=0}^{n-1} G(x;x_k)\,. \tag{4.14b}$$

Here $u_c(y)$ is the positive solution to (4.5), H and a_g are defined in (4.13), G is given in (4.11), and x_k satisfies (4.1).

The three-spike equilibrium solution plotted in Fig. 4.1 is obtained from (4.14).

To determine the stability properties of the equilibrium solution we introduce the perturbation

$$a(x,t) = a_e(x) + e^{\lambda t}\phi(x)\,, \qquad h(x,t) = h_e(x) + e^{\lambda t}\eta(x)\,, \tag{4.15}$$

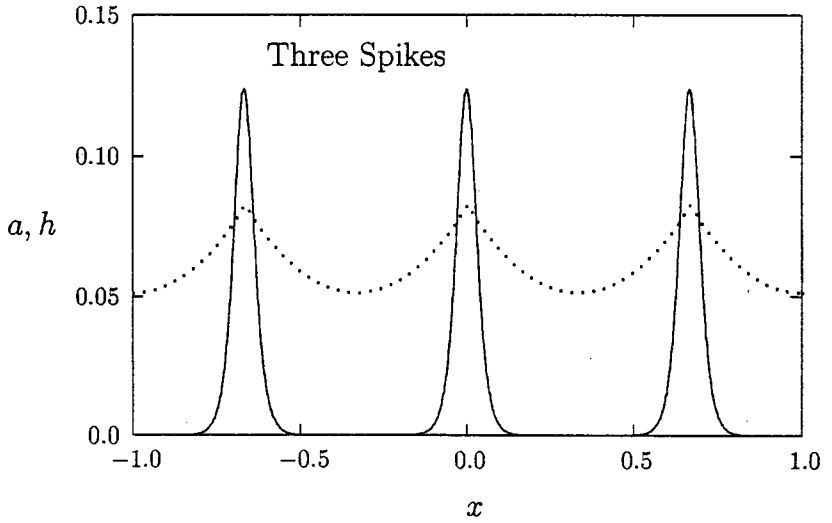

Figure 4.1: Plot of the activator and inhibitor concentration for a three-spike asymptotic symmetric equilibrium solution with $\epsilon = .02$, $D = .10$, $\mu = 1$, and $(p, q, r, s) = (2, 1, 2, 0)$. The solid curve is the activator concentration and the dotted curve is the inhibitor concentration.

where $\eta \ll 1$ and $\phi \ll 1$. Substituting (4.15) into (1.17) and linearizing, we obtain the eigenvalue problem

$$\epsilon^2 \phi_{xx} - \phi + \frac{p a_e^{p-1}}{h_e^q}\phi - \frac{q a_e^p}{h_e^{q+1}}\eta = \lambda\phi\,, \qquad -1 < x < 1\,, \tag{4.16a}$$

$$D\eta_{xx} - \mu\eta = -\epsilon^{-1} r \frac{a_e^{r-1}}{h_e^s}\phi + \epsilon^{-1} s \frac{a_e^r}{h_e^{s+1}}\eta\,, \qquad -1 < x < 1\,, \tag{4.16b}$$

$$\phi_x(\pm 1) = \eta_x(\pm 1) = 0\,. \tag{4.16c}$$

In §3 we analyze the spectrum of (4.16) corresponding to those eigenvalues that are bounded away from zero as $\epsilon \to 0$. These eigenvalues are referred to as the large eigenvalues. In §4 we analyze the spectrum of (4.16) corresponding to those eigenvalues that approach zero as $\epsilon \to 0$. These eigenvalues, referred to as the small eigenvalues, are shown to be $O(\epsilon^2)$ as $\epsilon \to 0$. The goal is to determine the range of D as a function of n for which the large and the small eigenvalues both have negative real parts.

Qualitatively, the small eigenvalues arise from the near translation invariance property of the system. When $D = \infty$, then h_e and η are constants in (4.16a). In this special case, the resulting

eigenvalue problem has n exponentially small eigenvalues. These exponentially small eigenvalues arise as a consequence of the near translation invariance property and an exponentially weak interaction between adjacent spikes (mediated by their tail behavior) and between the spikes and the boundary. The corresponding eigenfunction is, to within exponentially small terms, a linear combination of the first spatial derivative of $u_c\left[\epsilon^{-1}(x-x_j)\right]$. However, when D is finite so that η is a slowly varying function of x near each spike, then these exponentially small eigenvalues are dominated by an algebraically small spike interaction mediated by the function $\eta(x)$. The leading term in the eigenfunction is still a linear combination of the first spatial derivative of u_c, but the expansion of the eigenfunction proceeds in powers of ϵ. When $D=\infty$ and $\eta=0$, the operator in (4.16) has exactly one positive eigenvalue in the vicinity of each spike, and this eigenfunction is of one sign. Hence, when $D=\infty$ and $\eta=0$, an n-spike solution is unstable on an $O(1)$ time scale. However, when D is decreased from infinity, the $O(1)$ positive eigenvalue near each spike can be pushed into the left-half plane owing to the dependence of η on D. This is the origin of the large $O(1)$ eigenvalues.

4.2 Analysis of the Large Eigenvalues

In this section we analyze the eigenvalues of (4.16) that do not approach zero as $\epsilon\to 0$. In §4.2.1 we consider the case where $s=0$ and in §4.2.2 we extend the analysis to treat $s>0$. For ease of notation, the subscripts such as η_x shall indicate derivatives with respect to x, whereas the primes will generally refer to differentiation with respect to the stretched variable y.

4.2.1 Analysis for $s=0$

To study the eigenvalue problem (4.16) it is convenient to introduce scaled variables defined by

$$a_e = H^{\gamma}u\,, \qquad h_e = Hv\,, \qquad \phi = H^{\gamma}\bar{\phi}\,, \qquad \eta = H\bar{\eta}\,, \tag{4.17}$$

where $\gamma\equiv q/(p-1)$. From (4.14a), we conclude that $u\sim\sum_{k=0}^{n-1}u_c\left[\epsilon^{-1}(x-x_k)\right]$. Substituting (4.17) into (4.16) with $s=0$, using (4.13) for $H^{\gamma r-1}$, and dropping the overbar notation, we

get

$$\epsilon^2\phi_{xx} - \phi + \frac{pu^{p-1}}{v^q}\phi - \frac{qu^p}{v^{q+1}}\eta = \lambda\phi\,, \qquad -1 < x < 1\,, \tag{4.18a}$$

$$D\eta_{xx} - \mu\eta = -\frac{ru^{r-1}}{\epsilon b_r a_g}\phi\,, \qquad -1 < x < 1\,, \tag{4.18b}$$

$$\phi_x(\pm 1) = \eta_x(\pm 1) = 0\,. \tag{4.18c}$$

Using the symmetry of the equilibrium solution and the localization of the coefficients in (4.18), we look for an eigenfunction for (4.18) in the form

$$\phi(x) \sim \sum_{k=0}^{n-1} c_k \Phi\left[\epsilon^{-1}(x - x_k)\right]\,, \tag{4.19}$$

for some c_k, where $\Phi(y) \to 0$ as $|y| \to \infty$. The right-hand side of (4.18b) behaves like a sum of delta functions as $\epsilon \to 0$. Thus, for $\epsilon \to 0$, we calculate that η satisfies

$$D\eta_{xx} - \mu\eta = -\frac{r}{b_r a_g}\int_{-\infty}^{\infty} [u_c(y)]^{r-1}\,\Phi(y)\,dy \sum_{k=0}^{n-1} c_k \delta(x - x_k)\,, \qquad -1 < x < 1\,, \tag{4.20a}$$

$$\eta_x(\pm 1) = 0\,. \tag{4.20b}$$

The solution to (4.20) is written in terms of the Green's function $G(x; x_k)$ defined in (4.11) as

$$\eta(x) = \frac{r}{a_g b_r}\int_{-\infty}^{\infty} [u_c(y)]^{r-1}\,\Phi(y)\,dy \sum_{k=0}^{n-1} G(x; x_k)c_k\,. \tag{4.21}$$

Then, we substitute (4.19) and (4.21) into (4.18a), and use the fact that $v = 1 + O(\epsilon)$ when $|x - x_j| = O(\epsilon)$. The resulting eigenvalue problem, when written in terms of the stretched variable $y = \epsilon^{-1}(x - x_j)$, becomes for $j = 0, \ldots, n-1$,

$$c_j\left(\Phi'' - \Phi + pu_c^{p-1}\Phi\right) - \frac{qru_c^p}{a_g b_r}\int_{-\infty}^{\infty} [u_c(y)]^{r-1}\,\Phi(y)\,dy \sum_{k=0}^{n-1} G(x_j; x_k)c_k = c_j\lambda\Phi\,, \qquad -\infty < y < \infty\,, \tag{4.22}$$

with $\Phi \to 0$ as $|y| \to \infty$. This eigenvalue problem is the same for each j when $c_0, \ldots, c_{n-1}$ are the components of the eigenvector for the matrix problem

$$\mathcal{G}\mathbf{c} = \alpha\mathbf{c}\,, \qquad \mathbf{c} \equiv \begin{pmatrix} c_0 \\ \vdots \\ c_{n-1} \end{pmatrix}\,. \tag{4.23}$$

Here $\mathcal{G}$ is the $n \times n$ symmetric matrix whose entries are the coefficients $G(x_j; x_k)$. The eigenvalues of $\mathcal{G}$ are real. Then, using (4.7) for b_r, we get that (4.22) becomes the nonlocal eigenvalue problem

$$\Phi'' - \Phi + p u_c^{p-1} \Phi - \frac{\alpha q r u_c^p}{a_g} \left(\frac{\int_{-\infty}^{\infty} [u_c(y)]^{r-1} \Phi(y)\, dy}{\int_{-\infty}^{\infty} [u_c(y)]^r\, dy} \right) = \lambda \Phi\,, \qquad -\infty < y < \infty\,, \tag{4.24a}$$

$$\Phi \to 0 \quad \text{as} \quad |y| \to \infty\,. \tag{4.24b}$$

The goal is to determine conditions on D, μ and n for which the eigenvalue $\lambda_0 \neq 0$ of (4.24) with the largest real part satisfies $\mathrm{Re}(\lambda_0) > 0$ for any eigenvalue α of the matrix problem (4.23).

The outline of the rest of the analysis is as follows. First, we obtain explicit formulae for the eigenvalues α_j and the eigenvectors $\boldsymbol{c}_j$ of $\mathcal{G}$. These eigenpairs depend on the values of D, μ and n. The next step is to use a key result of [52], which we restate below, that proves that the principal eigenvalue of (4.24), in the restricted subset for which $\lambda \neq 0$, has a positive real part when $\alpha < \alpha_c$ and a negative real part when $\alpha > \alpha_c$. Here $\alpha_c > 0$ is some specific threshold value. Hence, we conclude that there is no eigenvalue of (4.24) with a positive real part when the minimum eigenvalue α_1 of the matrix problem (4.23) satisfies $\alpha_1 > \alpha_c$. We show explicitly the range of parameter values D, μ and n for which this relation holds. We now carry out the details of this analysis.

We first calculate the eigenvalues of the full symmetric matrix $\mathcal{G}$. This is readily done since $\mathcal{G}^{-1}$ is a symmetric tridiagonal matrix. To see this, in Appendix C we solve (4.18b) on each subinterval $[x_{j-1}, x_j]$ and impose the following jump conditions across each $x = x_j$ that are associated with (4.18*b*):

$$[\eta]_j = 0\,, \qquad [D\eta_x]_j = -\omega_j\,, \qquad \omega_j = \frac{r c_j}{a_g b_r} \int_{-\infty}^{\infty} [u_c(y)]^{r-1} \Phi(y)\, dy\,. \tag{4.25}$$

Here $[a]_j \equiv a(x_{j+}) - a(x_{j-})$. This procedure then leads to a linear system for $\eta(x_j), j = 0, \ldots, n-1$ of the form

$$\mathcal{B}\boldsymbol{\eta} = (\mu D)^{-1/2}\, \boldsymbol{\omega}\,, \tag{4.26a}$$

where the $n \times n$ tridiagonal matrix $\mathcal{B}$ and the n-vectors $\boldsymbol{\eta}$ and $\boldsymbol{\omega}$ are defined by

$$\mathcal{B} \equiv \begin{pmatrix} d & f & 0 & \cdots & 0 & 0 & 0 \\ f & e & f & \cdots & 0 & 0 & 0 \\ 0 & f & e & \ddots & 0 & 0 & 0 \\ \vdots & \vdots & \ddots & \ddots & \ddots & \vdots & \vdots \\ 0 & 0 & 0 & \ddots & e & f & 0 \\ 0 & 0 & 0 & \cdots & f & e & f \\ 0 & 0 & 0 & \cdots & 0 & f & d \end{pmatrix}, \qquad \boldsymbol{\eta} \equiv \begin{pmatrix} \eta(x_0) \\ \vdots \\ \eta(x_{n-1}) \end{pmatrix}, \qquad \boldsymbol{\omega} \equiv \begin{pmatrix} \omega_0 \\ \vdots \\ \omega_{n-1} \end{pmatrix}. \tag{4.26b}$$

Here d, e and f are defined by

$$d \equiv \coth(2\theta/n) + \tanh(\theta/n), \qquad e \equiv 2\coth(2\theta/n), \qquad f \equiv -\operatorname{csch}(2\theta/n), \tag{4.26c}$$

where $\theta = (\mu/D)^{1/2}$. Note that $d = e + f$. Thus, $\boldsymbol{\eta}$ is given by $\boldsymbol{\eta} = \mathcal{B}^{-1}\boldsymbol{\omega}\,(\mu D)^{-1/2}$. Another way to determine $\boldsymbol{\eta}$ is to evaluate (4.21) at $x = x_j$, for $j = 0, \ldots, n-1$. The equivalence of these two representations of $\boldsymbol{\eta}$ yields

$$\mathcal{G} = \frac{\mathcal{B}^{-1}}{\sqrt{\mu D}}. \tag{4.27}$$

In Appendix C.1 we show the explicit calculation that yields the following result for the eigenvalues κ_j and the eigenvectors $\boldsymbol{q}_j$ of $\mathcal{B}$:

Proposition 4.2 *The eigenvalues κ_j, ordered as $0 < \kappa_1 < \ldots < \kappa_n$, and the normalized eigenvectors $\boldsymbol{q}_j$ of $\mathcal{B}$ are*

$$\kappa_1 = e + 2f\,; \qquad \kappa_j = e + 2f\cos\left(\frac{\pi(j-1)}{n}\right), \quad j = 2, \ldots, n, \tag{4.28a}$$

$$\boldsymbol{q}_1^t = \frac{1}{\sqrt{n}}(1, \ldots, 1)\,; \quad q_{l,j} = \sqrt{\frac{2}{n}}\cos\left(\frac{\pi(j-1)}{n}(l - 1/2)\right), \quad j = 2, \ldots, n. \tag{4.28b}$$

Here $\boldsymbol{q}^t$ denotes transpose and $\boldsymbol{q}_j^t = (q_{1,j}, \ldots, q_{n,j})$.

Therefore, from (4.27) and since $e > 0$ and $f < 0$, the smallest eigenvalue of $\mathcal{G}$ is proportional to κ_n^{-1} and the corresponding eigenvector is proportional to $\boldsymbol{q}_n$. Relabeling this eigenpair we obtain:

Proposition 4.3 *The smallest eigenvalue α_1 of $\mathcal{G}$ and the corresponding (unnormalized) eigenvector $\boldsymbol{q}_1$ are*

$$\alpha_1 = \frac{(\mu D)^{-1/2}}{e - 2f\cos(\pi/n)}, \tag{4.29a}$$

$$q_{1,l} = \sin\left(\frac{\pi(n-1)}{2n}\right)\cos\left(\frac{\pi(n-1)(l-1/2)}{n}\right). \tag{4.29b}$$

Here e and f are defined in (4.26c) and $\boldsymbol{q}_1^t = (q_{1,1}, \ldots, q_{1,n})$.

We now apply Theorem 2.1 to find a criterion to ensure that the $O(1)$ eigenvalue has negative real part. Comparing (4.24) with (2.11), the theorem above yields the following key result on the spectrum associated with (4.24):

Proposition 4.4 *Let $\lambda_0 \neq 0$ be the eigenvalue of (4.24) with the largest real part and assume condition (2.13a) holds. Then, $Re(\lambda_0) > 0$ when*

$$\alpha_1 < \alpha_c \qquad \textit{where} \qquad \alpha_c = \frac{(p-1)a_g}{qr}. \tag{4.30}$$

Also $Re(\lambda_0) < 0$ when $\alpha_1 > \alpha_c$. Here α_1 is the minimum eigenvalue of $\mathcal{G}$ given in (4.29a) and a_g is the constant row sum of $\mathcal{G}$ defined in (4.13).

To get an explicit stability criterion we must calculate a_g. Since $\boldsymbol{q}_1^t = (1, \ldots, 1)$ is an eigenvector of $\mathcal{B}$ with eigenvalue $\kappa_1 = e + 2f$ we can multiply both sides of (4.27) by $\boldsymbol{q}_1$ to get

$$\mathcal{G}\boldsymbol{q}_1 = a_g(1, \ldots, 1)^t = \frac{1}{\sqrt{\mu D}}\mathcal{B}^{-1}\mathbf{q}_1 = \frac{1}{\kappa_1\sqrt{\mu D}}(1, \ldots, 1)^t. \tag{4.31}$$

Hence,

$$a_g = \frac{1}{\sqrt{\mu D}}(e + 2f)^{-1} = \frac{1}{2\sqrt{\mu D}}\frac{1}{\coth(2\theta/n) - \operatorname{csch}(2\theta/n)}. \tag{4.32}$$

Substituting (4.29a) and (4.32) into (4.30) we obtain that $\mathrm{Re}(\lambda_0) = 0$ when

$$\frac{e + 2f}{e - 2f\cos(\pi/n)} = \frac{p-1}{qr}. \tag{4.33}$$

Using the definition (4.26c) for e and f, we calculate $e/(2f) = -\cosh(2\theta/n)$. Substituting this expression into (4.33) and solving for the critical value of θ we get the following main result:

Proposition 4.5 *Let $\lambda_0 \neq 0$ be the eigenvalue of (4.24) with the largest real part and assume condition (2.13a) holds. Then, $Re(\lambda_0) < 0$ when*

$$D < D_n \equiv \frac{\mu}{\theta_n^2}, \quad n = 1, 2, \ldots, \tag{4.34a}$$

$$\theta_n \equiv \frac{n}{2} \ln\left[a + \sqrt{a^2 - 1}\right], \qquad a \equiv 1 + \left[1 + \cos\left(\frac{\pi}{n}\right)\right]\left(\frac{qr}{p-1} - 1\right)^{-1}. \tag{4.34b}$$

Alternatively, when $D > D_n$ then $Re(\lambda_0) > 0$.

This result gives the stability criterion for the large eigenvalues of (4.16) when $s = 0$. For example, from this result we can conclude that a three-spike equilibrium solution is stable with respect to the large $O(1)$ eigenvalues only when when $D < D_3$. To stabilize one additional spike we need to decrease D below D_4.

We now examine (4.34) for the GM parameter set $(p, q, r, s) = (2, 1, 2, 0)$ for which

$$\theta_n = \frac{n}{2} \ln\left[2 + \cos\left(\frac{\pi}{n}\right) + \sqrt{\left(2 + \cos\left(\frac{\pi}{n}\right)\right)^2 - 1}\right]. \tag{4.35}$$

We then calculate the following sequence of critical values of D_n:

$$D_1 = \mu/\theta_1^2 = \infty, \qquad \theta_1 = 0, \tag{4.36a}$$

$$D_2 = \mu/\theta_2^2 = 0.5766\mu, \qquad \theta_2 = \ln\left(2 + \sqrt{3}\right), \tag{4.36b}$$

$$D_3 = \mu/\theta_3^2 = 0.1810\mu, \qquad \theta_3 = \frac{3}{2}\ln\left(\frac{5}{2} + \frac{\sqrt{21}}{2}\right), \tag{4.36c}$$

$$D_4 = \mu/\theta_4^2 = 0.0915\mu, \qquad \theta_4 = 2\ln\left(2 + \frac{\sqrt{2}}{2} + \sqrt{\frac{7}{2} + 2\sqrt{2}}\right). \tag{4.36d}$$

In the limit $n \gg 1$, we get

$$D_n \sim 4\mu n^{-2}\left(\ln[3 + \sqrt{8}]\right)^{-2} + O\left(n^{-4}\right). \tag{4.37}$$

For the analysis leading to (4.34) to be valid we require that $D/\epsilon^2 \gg 1$ in order to ensure that h is slowly varying in the inner regions near each spike. Hence it follows that we require $n \ll 1/\epsilon$, which limits the range of validity of (4.37).

For the other common parameter set $(p,q,r,s)=(4,2,2,0)$ we get the critical values

$$D_1=\mu/\theta_1^2=\infty\,,\qquad \theta_1=0\,, \tag{4.38a}$$

$$D_2=\mu/\theta_2^2=0.2349\mu\,,\qquad \theta_2=\ln\left(4+\sqrt{15}\right), \tag{4.38b}$$

$$D_3=\mu/\theta_3^2=0.0778\mu\,,\qquad \theta_3=\frac{3}{2}\ln\left(\frac{11}{2}+\frac{\sqrt{117}}{2}\right), \tag{4.38c}$$

$$D_4=\mu/\theta_4^2=0.0401\mu\,,\qquad \theta_4=2\ln\left(4+\frac{3\sqrt{2}}{2}+\sqrt{\frac{39}{2}+12\sqrt{2}}\right). \tag{4.38d}$$

The results in (4.36a) and (4.38a) suggest that the principle eigenvalue of (4.24) for a one-spike equilibrium solution will always have a negative real part for any value of D. This conclusion is true when D is independent of ϵ, but needs to be modified if we allow D to depend on ϵ. More specifically, we show in §5 that a one-spike equilibrium solution is stable only when $D<D_1(\epsilon)$, where $D_1(\epsilon)$ is exponentially large as $\epsilon\to 0$ and satisfies $D_1(\epsilon)=O\left(\epsilon^2e^{2/\epsilon}\right)$ for $\epsilon\ll 1$.

4.2.2 Analysis for $s>0$

For $s>0$ we again introduce the new variables (4.17) into (4.16) and use $H^{\gamma r-(s+1)}=1/(b_ra_g)$ from (4.13), with the result

$$\epsilon^2\phi_{xx}-\phi+\frac{pu^{p-1}}{v^q}\phi-\frac{qu^p}{v^{q+1}}\eta=\lambda\phi\,,\qquad -1<x<1\,, \tag{4.39a}$$

$$D\eta_{xx}-\mu\eta-\frac{su^r}{\epsilon b_ra_gv^{s+1}}\eta=-\frac{ru^{r-1}}{\epsilon b_ra_gv^s}\phi\,,\qquad -1<x<1\,, \tag{4.39b}$$

$$\phi_x(\pm1)=\eta_x(\pm1)=0\,. \tag{4.39c}$$

Here $u\sim\sum_{k=0}^{n-1}u_c\left[\epsilon^{-1}(x-x_k)\right]$. Substitute the form for ϕ given in (4.19) into (4.39b) and use the facts that u is localized and that $v=1+O(\epsilon)$ near each x_k. Then, in place of (4.20), (4.39b) and (4.39c) become

$$fD\eta_{xx}-\left[\mu+\frac{s}{a_g}\sum_{k=0}^{n-1}\delta(x-x_k)\right]\eta=-\frac{r}{a_gb_r}\int_{-\infty}^{\infty}\left[u_c(y)\right]^{r-1}\Phi(y)dy\sum_{k=0}^{n-1}c_k\delta(x-x_k),\quad |x|<1, \tag{4.40a}$$

$$\eta_x(\pm1)=0\,. \tag{4.40b}$$

Thus the term proportional to s in (4.40a) acts as a psuedo-potential and hence will modify the jump condition for η_x across each x_j. Since u is localized near each x_j, and $\eta(x)$ is slowly varying with respect to ϵ near each x_j, we need only calculate $\eta(x_j)$ and substitute into (4.39a) to obtain the eigenvalue problem.

To calculate $\eta(x_j)$ we proceed as follows. We introduce $\boldsymbol{\eta}$ and $\boldsymbol{\omega}$ as defined in (4.25) and (4.26). We then solve (4.40a) analytically on each subinterval in terms of hyperbolic functions and then patch the subinterval solutions together using the appropriate jump conditions

$$[\eta]_j = 0\,, \qquad [D\eta_x]_j = -\omega_j + \frac{s}{a_g}\eta(x_j)\,, \tag{4.41}$$

where ω_j was defined in (4.25). This calculation, which we omit, shows that the solution for $\boldsymbol{\eta}$ can be written in the form

$$\mathcal{B}_s\boldsymbol{\eta} = (\mu D)^{-1/2}\,\boldsymbol{\omega}\,, \tag{4.42}$$

where the matrix $\mathcal{B}_s$ is given by

$$\mathcal{B}_s = \mathcal{B} + \frac{s}{a_g\sqrt{\mu D}}I\,. \tag{4.43}$$

Here I is the $n\times n$ identity matrix and $\mathcal{B}$ is the matrix defined in (4.26b) and (4.26c). Therefore, using (4.25) and (4.26b), we obtain

$$\boldsymbol{\eta} = \frac{r}{a_g b_r\sqrt{\mu D}}\int_{-\infty}^{\infty}[u_c(y)]^{r-1}\,\Phi(y)\,dy\;\mathcal{B}_s^{-1}\boldsymbol{c}\,, \tag{4.44}$$

where $\boldsymbol{c}$ is defined in (4.23). In place of (4.22) we get, for $j = 0,\ldots,n-1$, that

$$c_j\left(\Phi'' - \Phi + pu_c^{p-1}\Phi\right) - \frac{qru_c^p}{a_g b_r\sqrt{\mu D}}\int_{-\infty}^{\infty}[u_c(y)]^{r-1}\,\Phi(y)\,dy\;\left(\mathcal{B}_s^{-1}\boldsymbol{c}\right)_{j+1} = c_j\lambda\Phi\,, \qquad -\infty < y < \infty\,, \tag{4.45}$$

with $\Phi\to 0$ as $|y|\to\infty$. Here $\left(\mathcal{B}_s^{-1}\boldsymbol{c}\right)_j$ denotes the j^{th} component of the vector $\mathcal{B}_s^{-1}\boldsymbol{c}$.

Now let $\boldsymbol{c}$ be an eigenvector of the matrix eigenvalue problem

$$\mathcal{B}_s\boldsymbol{q} = \kappa\boldsymbol{q}\,. \tag{4.46}$$

Then, using (4.7) for b_r, (4.45) becomes

$$\Phi'' - \Phi + pu_c^{p-1}\Phi - \frac{qru_c^p}{a_g\kappa\sqrt{\mu D}}\left(\frac{\int_{-\infty}^{\infty}[u_c(y)]^{r-1}\,\Phi(y)\,dy}{\int_{-\infty}^{\infty}[u_c(y)]^r\,dy}\right) = \lambda\Phi\,, \qquad -\infty < y < \infty\,, \quad (4.47a)$$

$$\Phi \to 0 \quad \text{as} \quad |y| \to \infty\,. \quad (4.47b)$$

Let $\lambda_0 \neq 0$ be the eigenvalue of (4.47) with the largest real part. Then, from comparing (2.11) and (4.47), we conclude from the theorem of [52] stated above that $\mathrm{Re}(\lambda_0) < 0$ only when

$$\frac{1}{\kappa a_g\sqrt{\mu D}} > \frac{(p-1)}{qr}\,. \quad (4.48)$$

To obtain a condition in terms of the minimum eigenvalue of $\mathcal{G}$, we use (4.27) to get that $\mathcal{G}\boldsymbol{q} = \alpha\boldsymbol{q}$, where $\kappa a_g\sqrt{\mu D} = s + a_g/\alpha$. Substituting this relation between κ and α into (4.48), we obtain the following result in terms of the smallest eigenvalue α_1 of $\mathcal{G}$:

Proposition 4.6 *Let $\lambda_0 \neq 0$ be the eigenvalue of (4.24) with the largest real part and assume condition (2.13a) holds. Then, $Re(\lambda_0) > 0$ when*

$$\frac{\alpha_1}{a_g} < \left(\frac{qr}{p-1} - s\right)^{-1}\,. \quad (4.49)$$

Also $Re(\lambda_0) < 0$ when the inequality in (4.49) is reversed.

The right-hand side of (4.49) is always positive by the assumption (1.8) on the exponents. Setting $\alpha_1/a_g = [qr/(p-1) - s]^{-1}$, and using (4.29) and (4.32) for α_1 and a_g, respectively, we get the following main result for the stability of the equilibrium solution with regards to the large $O(1)$ eigenvalues:

Proposition 4.7 *Let $\lambda_0 \neq 0$ be the eigenvalue of (4.47) with the largest real part and assume condition (2.13a) holds. Then, $Re(\lambda_0) < 0$ when*

$$D < D_n \equiv \frac{\mu}{\theta_n^2}\,, \quad n = 1, 2, \ldots\,, \quad (4.50a)$$

$$\theta_n \equiv \frac{n}{2}\ln\left[a + \sqrt{a^2-1}\right]\,, \qquad a \equiv 1 + \left[1 + \cos\left(\frac{\pi}{n}\right)\right]\left(\frac{qr}{p-1} - (s+1)\right)^{-1}\,. \quad (4.50b)$$

Alternatively, when $D > D_n$ then $Re(\lambda_0) > 0$.

From (1.8) we get that $a > 1$ since $qr/(p-1) > (s+1)$. In addition, D_n decreases as s increases, and so for each fixed n it follows that D must be made smaller as s increases in order to stabilize an n-spike equilibrium solution.

4.3 Analysis of the Small Eigenvalues

The results in §4.2 establish conditions for which the equilibrium solution is stable on an $O(1)$ time scale. Now, we examine the more difficult problem of determining conditions guaranteeing that the small eigenvalues with $\lambda = O(\epsilon^2)$ lie in the left half-plane. The first step, done in §4.3.1, is to reduce (4.16) to the study of a matrix eigenvalue problem. In §4.3.2 we analyze this matrix eigenvalue problem to determine the small eigenvalues and their signs explicitly.

4.3.1 Deriving the Matrix Eigenvalue Problem

We begin by writing (4.16) in the form

$$L_\epsilon \phi - \frac{q a_e^p}{h_e^{q+1}} \eta = \lambda \phi \,, \qquad -1 < x < 1 \,, \tag{4.51a}$$

$$D\eta_{xx} - \mu \eta = -\epsilon^{-1} r \frac{a_e^{r-1}}{h_e^s} \phi + \epsilon^{-1} s \frac{a_e^r}{h_e^{s+1}} \eta \,, \qquad -1 < x < 1 \,, \tag{4.51b}$$

$$\phi_x(\pm 1) = \eta_x(\pm 1) = 0 \,, \tag{4.51c}$$

where

$$L_\epsilon \phi \equiv \epsilon^2 \phi_{xx} - \phi + \frac{p a_e^{p-1}}{h_e^q} \phi \,. \tag{4.51d}$$

Here a_e and h_e are given by

$$a_e \sim \sum_{k=0}^{n-1} H^\gamma u_k \,; \qquad h_e \sim \frac{H}{a_g} \sum_{k=0}^{n-1} G(x; x_k) \,; \qquad H^{\gamma r - (1+s)} = \frac{1}{b_r a_g} \,. \tag{4.52}$$

We have defined $u_k(y) \equiv u_c\left[\epsilon^{-1}(x - x_k)\right]$, where $u_c(y)$ satisfies (4.5). The equilibrium positions for x_j are such that

$$\langle h_{ex} \rangle_j = 0 \,, \qquad j = 0, .., n-1 \,. \tag{4.53}$$

Here and below we have defined $\langle \zeta \rangle_j \equiv (\zeta(x_{j+}) + \zeta(x_{j-}))/2$ and $[\zeta]_j \equiv \zeta(x_{j+}) - \zeta(x_{j-})$, where $\zeta(x_{j\pm})$ are the one-sided limits of $\zeta(x)$ as $x \to x_{j\pm}$.

If the inhibitor diffusivity was infinite and there only one spike, then by translation invariance we would obtain $L_\epsilon a_{ex} = 0$. Here we expect that $L_\epsilon a_{ex}$ is still small. To show this, we differentiate the equilibrium problem for (1.17a) with respect to x to get

$$L_\epsilon a_{ex} = \frac{q a_e^p}{h_e^{q+1}} h_{ex} \,. \tag{4.54}$$

Thus, for x near x_j we get

$$L_\epsilon u_j' \sim \frac{\epsilon q H^q u_j^p}{h_e^{q+1}} h_{ex} \,. \tag{4.55}$$

This fact suggests that we expand

$$\phi = \phi_0 + \epsilon\phi_1 + \cdots \,, \qquad \eta(x) = \epsilon\eta_0(x) + \cdots \,, \tag{4.56a}$$

where

$$\phi_0 \equiv \sum_{j=0}^{n-1} c_j u_j' \left[\epsilon^{-1}(x - x_j)\right] \,, \qquad \phi_1 \equiv \sum_{j=0}^{n-1} c_j \phi_{1j} \left[\epsilon^{-1}(x - x_j)\right] \,, \tag{4.56b}$$

and the c_j are arbitrary coefficients.

We substitute (4.56a) into (4.51a) and use (4.55) and $\lambda = O(\epsilon^2)$. For x near x_j, we get that $\phi_{1j}(y)$ satisfies

$$c_j L_\epsilon \phi_{1j} \sim -\frac{q u_j^p H^q}{h_e^{q+1}} \left[c_j h_{ex}(x_j + \epsilon y) - H^\gamma \eta_0(x_j + \epsilon y)\right] \,. \tag{4.57}$$

Before solving this equation for ϕ_{1j} we need to determine an important continuity property of the right-hand side of (4.57).

Substituting (4.56a) into (4.51b), we get that η_0 satisfies

$$D\eta_{0xx} - \mu\eta_0 = -\epsilon^{-2} r \frac{a_e^{r-1}}{h_e^s} (\phi_0 + \epsilon\phi_1) + \epsilon^{-1} s \frac{a_e^r}{h_e^{s+1}} \eta_0 \,, \qquad -1 < x < 1 \,. \tag{4.58}$$

Since ϕ_0 is a linear combination of u_j', it follows that the term multiplied by ϕ_0 on the right-hand side in (4.58) behaves like a dipole. Hence, for $\epsilon \ll 1$, this term is a linear combination of $\delta'(x - x_j)$ for $j = 0, .., n-1$, where $\delta(x)$ is the delta function. Thus, η_0 will be discontinuous across $x = x_j$. However, if we define the function $f(x)$ by

$$f(x) \equiv H^\gamma \eta_0(x) - c_j h_{ex}(x) \,, \tag{4.59}$$

then f is continuous across $x = x_j$. To see this, we differentiate (1.17b) for h_e with respect to x and subtract appropriate multiples of the resulting equation and (4.58) to find that the dipole term cancels exactly. Thus, f is continuous across $x = x_j$, and we have $\langle f \rangle_j = f(x_j)$. However, $\langle h_{ex} \rangle_j = 0$ from (4.53). Hence, $f(x_j) = H^\gamma \langle \eta_0 \rangle_j$. Therefore, for $\epsilon \ll 1$, we get from (4.57) that ϕ_{1j} satisfies

$$c_j L_\epsilon \phi_{1j} \sim q u_j^p H^{\gamma-1} \langle \eta_0 \rangle_j \,. \tag{4.60}$$

Since $L_\epsilon u_j = (p-1)u_j^p + O(\epsilon)$, (4.60) is easily solved to get

$$c_j \phi_{1j}(y) = \frac{q}{p-1} u_j(y) H^{\gamma-1} \langle \eta_0 \rangle_j + O(\epsilon) \,. \tag{4.61}$$

This condition shows that ϕ_{1j} is continuous across $x = x_j$ and has the form of a spike. This implies that the term in (4.58) proportional to ϕ_1 behaves like a linear combination of $\delta(x - x_j)$ when $\epsilon \ll 1$ and, most importantly, is *of the same order* in ϵ as the dipole term proportional to ϕ_0. This shows the fact that we need to determine the approximate eigenfunction for ϕ to both the $O(1)$ and $O(\epsilon)$ terms in order to calculate an eigenvalue of order $O(\epsilon^2)$.

Next, let $\epsilon \to 0$ and use (4.56b) and (4.13) for $H^{\gamma r-(s+1)}$ to calculate for x near x_j that

$$-\epsilon^{-2} r \frac{a_e^{r-1}}{h_e^s} \phi_0 \sim -\frac{H^{1-\gamma}}{a_g} c_j \delta'(x - x_j) \,, \tag{4.62a}$$

$$-\epsilon^{-1} r \frac{a_e^{r-1}}{h_e^s} \phi_{1j} \sim -\frac{r H^{1-\gamma} c_j}{a_g b_r} \int_{-\infty}^{\infty} u_c^{r-1} \phi_{1j} \, dy \, \delta(x - x_j) \,. \tag{4.62b}$$

Substituting (4.62) into (4.58), and using the formula (4.61) for ϕ_{1j}, we get

$$D\eta_{0xx} - \left[\mu + \frac{s}{a_g} \sum_{j=0}^{n-1} \delta(x - x_j) \right] \eta_0 = -\frac{H^{1-\gamma}}{a_g} \sum_{j=0}^{n-1} c_j \delta'(x - x_j) - \frac{qr}{(p-1)a_g} \sum_{j=0}^{n-1} \langle \eta_0 \rangle_j \delta(x - x_j) \,. \tag{4.63}$$

This problem is equivalent to

$$D\eta_{0xx} - \mu\eta_0 = 0 \,, \qquad -1 < x < 1 \,; \qquad \eta_{0x}(\pm 1) = 0 \,, \tag{4.64a}$$

$$[D\eta_0]_j = -\left(\frac{\epsilon c_j}{a_g} \right) H^{\gamma-1} \,; \qquad [D\eta_{0x}]_j = \frac{1}{a_g} \left(s - \frac{qr}{(p-1)} \right) \langle \eta_0 \rangle_j \,. \tag{4.64b}$$

For convenience we introduce $\tilde{\eta}_0$ defined by

$$\eta_0 = H^{1-\gamma}\tilde{\eta}_0\,. \tag{4.65}$$

Next, we estimate the small eigenvalue. Substitute (4.56) and (4.65) into (4.51a) and multiply both sides of (4.51a) by u_j'. Integrating the resulting equation across the domain, we get

$$\sum_{i=0}^{n-1}\left(u_j', c_i L_\epsilon u_i'\right) + \epsilon\sum_{i=0}^{n-1}\left(u_j', c_i L_\epsilon \phi_{1i}\right) - \epsilon q H^{1-\gamma}\left(u_j', \frac{a_e^p\tilde{\eta}_0}{h_e^{q+1}}\right) \sim \lambda\sum_{i=0}^{n-1}\left(c_i u_i', u_j'\right)\,. \tag{4.66}$$

Here we have defined $(f,g) \equiv \int_{-1}^{1} f(x)g(x)\,dx$. To within negligible exponentially small terms, the dominant contribution in the sum comes from $i=j$ since u_j' is exponentially localized near $x = x_j$. Thus, (4.66) becomes

$$c_j\left(u_j', L_\epsilon u_j'\right) + \epsilon c_j\left(u_j', L_\epsilon\phi_{1j}\right) - \epsilon q H^{1+q}\left(u_j', \frac{u_j^p\tilde{\eta}_0}{h_e^{q+1}}\right) \sim \lambda c_j\left(u_j', u_j'\right)\,. \tag{4.67}$$

Since L_ϵ is self-adjoint, we integrate by parts on the second term on the left-hand side of (4.67) and use (4.55) for $L_\epsilon u_j'$. The integrands are localized near $x = x_j$. Thus, writing the resulting integrals in terms of the stretched variable $y = \epsilon^{-1}(x - x_j)$, we get

$$\epsilon^2 q c_j H^q \int_{-\infty}^{\infty} \frac{u_j^p u_j'}{h_e^{q+1}} h_{ex}\,dy - \epsilon^2 q H^{1+q}\int_{-\infty}^{\infty}\frac{u_j^p u_j'}{h_e^{q+1}}\tilde{\eta}_0\,dy$$
$$+ \epsilon^3 q c_j H^q \int_{-\infty}^{\infty}\frac{u_j^p\phi_{1j}}{h_e^{q+1}}h_{ex}\,dy \sim \epsilon\lambda c_j\int_{-\infty}^{\infty}\left(u_c'\right)^2 dy\,. \tag{4.68}$$

In this expression $\tilde{\eta}_0 = \tilde{\eta}_0(x_j + \epsilon y)$, $h_e = h_e(x_j+\epsilon y)$, and $h_{ex} = h_{ex}(x_j+\epsilon y)$.

We now estimate each of the terms in (4.68). Since $[\phi_{1j}]_j = 0$, $\langle h_{ex}\rangle_j = 0$, and u_j' is odd, it follows that

$$\int_{-\infty}^{\infty}\frac{u_j^p\phi_{1j}}{h_e^{q+1}}h_{ex}\,dy = o(1) \qquad \text{as} \quad \epsilon\to 0\,. \tag{4.69}$$

Hence, the third integral on the left-hand side of (4.68) will be $o(\epsilon^3)$ and can be neglected. Next, we combine the first two terms on the left-hand side of (4.68) to get

$$\epsilon^2 q c_j H^q\int_{-\infty}^{\infty}\frac{u_j^p u_j'}{h_e^{q+1}}h_{ex}\,dy - \epsilon^2 q H^{1+q}\int_{-\infty}^{\infty}\frac{u_j^p u_j'}{h_e^{q+1}}\tilde{\eta}_0\,dy = -\epsilon^2 q H^q\int_{-\infty}^{\infty}\frac{u_j' u_j^p}{h_e^{q+1}}f(x_j+\epsilon y)\,dy\,. \tag{4.70}$$

Here $f(x)$, defined in (4.59), is given in terms of $\tilde{\eta}_0$ by $f(x) = H\tilde{\eta}_0(x) - c_j h_{ex}(x)$. The function f is continuous across $x = x_j$ but its derivative is not. For $\epsilon \ll 1$, we calculate

$$-\epsilon^2 q H^q \int_{-\infty}^{\infty} \frac{u_j' u_j^p}{h_e^{q+1}} f(x_j + \epsilon y)\, dy \sim \epsilon^3 q \frac{c_j h_{exx}(x_j)}{H} \int_{-\infty}^{\infty} y u_j' u_j^p\, dy - \epsilon^3 q \langle \tilde{\eta}_{0x} \rangle_j \int_{-\infty}^{\infty} y u_j' u_j^p\, dy\,. \tag{4.71}$$

Upon integrating by parts in (4.71), and using $h_{exx}(x_j) = \mu H/D$, we get

$$\epsilon^2 q H^{1+q} \int_{-\infty}^{\infty} \frac{u_j' u_j^p}{h_e^{q+1}} \left(\frac{c_j h_{ex}}{H} - \tilde{\eta}_0 \right) dy \sim \frac{\epsilon^3 q}{p+1} \left(\langle \tilde{\eta}_{0x} \rangle_j - \frac{c_j \mu}{D} \right) \int_{-\infty}^{\infty} [u_c(y)]^{p+1}\, dy\,. \tag{4.72}$$

Substituting (4.69) and (4.72) into (4.68), we obtain a formula for λ. We summarize the result (redefining η_0 for convenience) as follows:

Proposition 4.8 *The eigenvalues of order $O(\epsilon^2)$ for (4.16) satisfy*

$$\lambda c_j \int_{-\infty}^{\infty} \left[u_c'(y) \right]^2 dy \sim \frac{\epsilon^2 q}{p+1} \int_{-\infty}^{\infty} [u_c(y)]^{p+1}\, dy \left(\langle \eta_x \rangle_j - \frac{c_j \mu}{D} \right), \qquad j = 0, .., n-1\,. \tag{4.73}$$

Here $\langle \eta_x \rangle_j$ is obtained from the solution to the boundary value problem

$$D\eta_{xx} - \mu\eta = 0\,, \qquad -1 < x < 1\,; \qquad \eta_x(\pm 1) = 0\,, \tag{4.74a}$$

$$[D\eta]_j = -\frac{c_j}{a_g}\,; \qquad [D\eta_x]_j = \frac{1}{a_g} \tilde{s} \langle \eta \rangle_j\,, \qquad \tilde{s} \equiv s - \frac{qr}{(p-1)}\,. \tag{4.74b}$$

4.3.2 Analyzing the Matrix Eigenvalue Problem

The next step in the derivation is to calculate $\langle \eta_x \rangle_j$ from the solution to (4.74). The solution to (4.74) can be decomposed as

$$\eta(x) = \frac{1}{a_g} \left(\sum_{k=0}^{n-1} c_k g(x; x_k) + \sum_{k=0}^{n-1} m_k G(x; x_k) \right), \tag{4.75}$$

for some coefficients m_k, for $k = 0, \ldots, n-1$. Here G satisfies (4.10), and $g(x; x_k)$ is the dipole Green's function satisfying

$$Dg_{xx} - \mu g = -\delta'(x - x_k)\,, \qquad -1 < x < 1\,, \tag{4.76a}$$

$$g_x(\pm 1; x_k) = 0\,. \tag{4.76b}$$

Satisfying the jump conditions in (4.74b) we get the following matrix problem for the coefficients m_k:

$$\left(\frac{\tilde{s}}{a_g}\mathcal{G} + I\right)\boldsymbol{m} = -\frac{s}{a_g}\mathcal{P}_g\mathbf{c}\,. \tag{4.77}$$

Here $\mathcal{G}$ is the Green's function matrix defined in (4.23) with entries $G(x_j;x_k)$, and

$$\mathcal{P}_g \equiv \begin{pmatrix} \langle g(x_0;x_0)\rangle_0 & \cdots & g(x_0;x_{n-1}) \\ \vdots & \ddots & \vdots \\ g(x_{n-1};x_0) & \cdots & \langle g(x_{n-1};x_{n-1})\rangle_{n-1} \end{pmatrix}, \quad \boldsymbol{m} \equiv \begin{pmatrix} m_0 \\ \vdots \\ m_{n-1} \end{pmatrix}, \quad \mathbf{c} \equiv \begin{pmatrix} c_0 \\ \vdots \\ c_{n-1} \end{pmatrix}. \tag{4.78}$$

The problem (4.77) determines $\boldsymbol{m}$ in terms of $\mathbf{c}$. Then, using (4.75), we can calculate $\langle \eta_x\rangle_j$, for $j = 0,\ldots,n-1$, from the matrix problem

$$\langle \boldsymbol{\eta_x}\rangle = \frac{1}{a_g}\left(\mathcal{G}_g\mathbf{c} + \mathcal{P}\boldsymbol{m}\right), \tag{4.79}$$

where $\mathcal{G}_g$ is the Green's dipole matrix defined by

$$\mathcal{G}_g \equiv \begin{pmatrix} g_x(x_0;x_0) & \cdots & g_x(x_0;x_{n-1}) \\ \vdots & \ddots & \vdots \\ g_x(x_{n-1};x_0) & \cdots & g_x(x_{n-1};x_{n-1}) \end{pmatrix}, \tag{4.80}$$

and

$$\mathcal{P} \equiv \begin{pmatrix} \langle G_x(x_0;x_0)\rangle_0 & \cdots & G_x(x_0;x_{n-1}) \\ \vdots & \ddots & \vdots \\ G_x(x_{n-1};x_0) & \cdots & \langle G_x(x_{n-1};x_{n-1})\rangle_{n-1} \end{pmatrix}, \quad \langle \boldsymbol{\eta_x}\rangle \equiv \begin{pmatrix} \langle \eta_x\rangle_0 \\ \vdots \\ \langle \eta_x\rangle_{n-1} \end{pmatrix}. \tag{4.81}$$

Next, we define σ by

$$\lambda = \frac{\epsilon^2 q\sigma}{(p+1)a_g}\left(\frac{\int_{-\infty}^{\infty}[u_c(y)]^{p+1}\,dy}{\int_{-\infty}^{\infty}[u_c'(y)]^2\,dy}\right). \tag{4.82}$$

Substituting (4.79) and (4.82) into (4.73), we get a matrix eigenvalue problem for σ and $\mathbf{c}$

$$\mathcal{G}_g\mathbf{c} + \mathcal{P}\boldsymbol{m} = \left(\sigma + \frac{\mu a_g}{D}\right)\mathbf{c}\,. \tag{4.83}$$

Here m is determined in terms of c by (4.77).

The next step in the analysis is to reduce (4.77) and (4.83) to an equivalent generalized eigenvalue problem. This analysis involves matrices associated with G and g. To avoid confusion we have indicated with a subscript g those matrices associated with the dipole Green's function g.

In the analysis below we must find the eigenvalues of $\mathcal{G}_g$ explicitly. This is done as in §3 by showing that $\mathcal{G}_g^{-1}$ is a symmetric tridiagonal matrix. More specifically, in Appendix C.2 we show that

$$\mathcal{G}_g = \frac{\theta}{D}\mathcal{B}_g^{-1}, \tag{4.84}$$

where B_g is a tridiagonal matrix with exactly the same form as in (4.26b), except that here the definitions of d, e and f in (4.26c) are to replaced with

$$d \equiv \coth(2\theta/n) + \coth(\theta/n), \qquad e \equiv 2\coth(2\theta/n), \qquad f \equiv -\mathrm{csch}(2\theta/n), \tag{4.85}$$

where $d = e - f$. In Appendix C.3 we calculate the eigenvalues and eigenvectors of $\mathcal{B}_g$ analytically. The result is summarized as follows:

Proposition 4.9 *The eigenvalues ξ_j, ordered as $0 < \xi_1 < \ldots < \xi_n$, of $\mathcal{B}_g$ and the associated normalized eigenvectors $\boldsymbol{v}_j$ of $\mathcal{B}_g$ are*

$$\xi_j = 2\coth\left(\frac{2\theta}{n}\right) - 2csch\left(\frac{2\theta}{n}\right)\cos\left(\frac{\pi j}{n}\right) \qquad j = 1, \ldots, n, \tag{4.86a}$$

$$\boldsymbol{v}_n^t = \frac{1}{\sqrt{n}}\left(1, -1, 1, \ldots, (-1)^{n+1}\right); \quad \boldsymbol{v}_{l,j} = \sqrt{\frac{2}{n}}\sin\left(\frac{\pi j}{n}\left(l - 1/2\right)\right), \quad j = 1, \ldots, n-1. \tag{4.86b}$$

Here $\boldsymbol{v}^t$ denotes transpose and $\boldsymbol{v}_j^t = (v_{1,j}, \ldots, v_{n,j})$.

Other key relations that we need are derived in Appendices C and C.2, where we show that

$$\mathcal{P}_g = \frac{1}{2D}\mathrm{csch}\left(\frac{2\theta}{n}\right)\mathcal{C}\mathcal{B}_g^{-1}, \qquad \mathcal{P} = -\frac{1}{2D}\mathrm{csch}\left(\frac{2\theta}{n}\right)\mathcal{C}^t\mathcal{B}^{-1}. \tag{4.87a}$$

Here the matrix $\mathcal{C}$ is defined by

$$\mathcal{C} \equiv \begin{pmatrix} 1 & 1 & 0 & \cdots & 0 & 0 & 0 \\ -1 & 0 & 1 & \cdots & 0 & 0 & 0 \\ 0 & -1 & 0 & \ddots & 0 & 0 & 0 \\ \vdots & \vdots & \ddots & \ddots & \ddots & \vdots & \vdots \\ 0 & 0 & 0 & \ddots & 0 & 1 & 0 \\ 0 & 0 & 0 & \cdots & -1 & 0 & 1 \\ 0 & 0 & 0 & \cdots & 0 & -1 & -1 \end{pmatrix}. \tag{4.87b}$$

From (4.87a) we obtain the result that

$$\mathcal{P}\mathcal{B} = -\left(\mathcal{P}_g \mathcal{B}_g\right)^t . \tag{4.87c}$$

We begin by solving (4.77) for $\boldsymbol{m}$. The matrix in (4.77) is invertible if $\tilde{s}\,(\alpha_1/a_g) + 1 < 0$, where α_1 is the minimum eigenvalue of $\mathcal{G}$. From (4.49) and the definition of $\tilde{s}$ in (4.74b), we see that this condition is satisfied when the large $O(1)$ eigenvalues are in the left half-plane. We will assume that $D < D_n$ so that this condition holds. Let $\boldsymbol{q}_j$, κ_j be the normalized eigenpairs of $\mathcal{B}$ as given in Proposition 4.2 for $j = 1, \ldots, n$. Then,

$$\mathcal{B} = Q\mathcal{K}Q^t , \tag{4.88}$$

where Q is the orthogonal matrix whose columns are the normalized $\boldsymbol{q}_j$ and $\mathcal{K}$ is the diagonal matrix of the eigenvalues of $\mathcal{B}$. Since $\mathcal{G} = \mathcal{B}^{-1}/\sqrt{\mu D}$ from (4.27) and $Q^tQ = I$, we get

$$\left(\frac{\tilde{s}}{a_g}\mathcal{G} + I\right)^{-1} = Q\left(\frac{\tilde{s}}{a_g\sqrt{\mu D}}\mathcal{K}^{-1} + I\right)^{-1} Q^t . \tag{4.89}$$

Using $\theta = (\mu/D)^{1/2}$, we can solve for $\boldsymbol{m}$ in (4.77) in the form

$$\boldsymbol{m} = -\frac{\tilde{s}}{a_g} Q\left(\frac{\tilde{s}\theta}{a_g\mu}\mathcal{K}^{-1} + I\right)^{-1} Q^t\mathcal{P}_g\boldsymbol{c} . \tag{4.90}$$

We then substitute (4.90) and (4.84) into (4.83). This yields,

$$\mathcal{B}_g^{-1}\boldsymbol{c} - \tilde{s}D^2\left(\frac{\theta}{a_g\mu}\right)\mathcal{P}Q\left(\frac{\tilde{s}\theta}{a_g\mu}\mathcal{K}^{-1} + I\right)^{-1} Q^t\mathcal{P}_g\boldsymbol{c} = \left(\frac{D\sigma}{\theta} + \frac{\mu a_g}{\theta}\right)\boldsymbol{c} . \tag{4.91}$$

In (4.91) we use (4.87c) and (4.88) to replace $\mathcal{P}Q$ with

$$\mathcal{P}Q = \mathcal{P}\mathcal{B}\mathcal{B}^{-1}Q = -\left(\mathcal{P}_g\mathcal{B}_g\right)^t Q\mathcal{K}^{-1}. \tag{4.92}$$

We then introduce $\boldsymbol{u}$ and the diagonal matrix $\mathcal{D}$ defined by

$$\boldsymbol{u} \equiv \mathcal{B}_g^{-1}\boldsymbol{c}, \qquad \mathcal{D} \equiv \tilde{s}D^2\gamma\mathcal{K}^{-1}\left(\tilde{s}\gamma\mathcal{K}^{-1} + I\right)^{-1}. \tag{4.93}$$

Here we have defined γ by

$$\gamma \equiv \frac{\theta}{a_g\mu} = 2\left[\coth\left(\frac{2\theta}{n}\right) - \operatorname{csch}\left(\frac{2\theta}{n}\right)\right] = 2\tanh\left(\frac{\theta}{n}\right). \tag{4.94}$$

Equation (4.94) is obtained from using the expression for a_g in (4.32). Using Proposition 4.2 for the eigenvalues κ_j of $\mathcal{K}$ we then calculate $\mathcal{D}$ as

$$\mathcal{D} \equiv \begin{pmatrix} d_1 & 0 & \cdots & 0 \\ 0 & \ddots & \cdots & 0 \\ \vdots & \vdots & \ddots & \vdots \\ 0 & 0 & \cdots & d_n \end{pmatrix}, \qquad \text{where} \qquad d_j = \frac{\tilde{s}D^2\gamma}{\kappa_j + \tilde{s}\gamma}, \qquad j = 1, \ldots, n. \tag{4.95}$$

Substituting (4.92) and (4.93) into (4.91), we obtain the eigenvalue problem

$$\mathcal{B}_g\boldsymbol{u} = \omega\left(I + \mathcal{R}\right)\boldsymbol{u}. \tag{4.96a}$$

Here we have defined ω and $\mathcal{R}$ by

$$\omega \equiv \left(\frac{D\sigma}{\theta} + \frac{1}{\gamma}\right)^{-1}, \qquad \mathcal{R} \equiv \left(\mathcal{P}_g\mathcal{B}_g\right)^t Q\mathcal{D}Q^t\mathcal{P}_g\mathcal{B}_g. \tag{4.96b}$$

The assumption that the solution is stable with respect to the large $O(1)$ eigenvalues is equivalent to the condition that $\kappa_j + \tilde{s}\gamma < 0$ for $j = 1, .., n$. Under this condition, and since $\tilde{s} < -1$, we conclude that $\mathcal{D} > 0$. Hence, $I + \mathcal{R}$ is a positive-definite and symmetric matrix. This means that the eigenvalues ω_j, and consequently λ_j, for $j = 1, \ldots, n$ are real. The generalized eigenvalue problem (4.96) is equivalent to the combined problem (4.77) and (4.83).

The next step is to determine the spectrum of (4.96) analytically. To do so, we show that $\mathcal{R}$ has the same eigenvectors as $\mathcal{B}_g$. Hence, we claim that $\mathcal{R}$ can be written in terms of some positive

diagonal matrix Σ as

$$\mathcal{R} = Q_g \Sigma Q_g^t . \tag{4.97}$$

Here Q_g is the eigenvector matrix associated with $\mathcal{B}_g$. The j^{th} column of Q_g is the eigenvector v_j given in Proposition 4.9. Using the formula for $\mathcal{P}_g \mathcal{B}_g$ in (4.87a), we can write $\mathcal{R}$ in (4.96b) as

$$\mathcal{R} = \frac{1}{4D^2} \text{csch}^2 \left(\frac{2\theta}{n} \right) \mathcal{C}^t Q \mathcal{D} Q^t \mathcal{C} . \tag{4.98}$$

This is equivalent to

$$\mathcal{R} = \frac{1}{4D^2} \text{csch}^2 \left(\frac{2\theta}{n} \right) Q_g \mathcal{M} \mathcal{D} \mathcal{M}^t Q_g^t , \tag{4.99a}$$

where the matrix $\mathcal{M}$ is defined by

$$\mathcal{M} = Q_g^t \mathcal{C}^t Q . \tag{4.99b}$$

Comparing (4.99a) and (4.97), we then define Σ by

$$\Sigma \equiv \frac{1}{4D^2} \text{csch}^2 \left(\frac{2\theta}{n} \right) \mathcal{M} \mathcal{D} \mathcal{M}^t . \tag{4.100}$$

We now show that Σ defined in (4.100) is a diagonal matrix.

To show this, we first calculate the matrix $\mathcal{M}$ in (4.99b) using the explicit formulae for the eigenvectors of $\mathcal{B}$ and $\mathcal{B}_g$ given in Propositions 4.2 and 4.9. Let $m_{i,j}$ be the i,j^{th} entry of the matrix $\mathcal{M}$. Then, we calculate $m_{i,j}$ explicitly using (4.99b) and the definition of $\mathcal{C}$ in (4.87b), to get

$$m_{i,j} = \sum_{l=1}^{n} v_{l,i} \left(q_{l-1,j} - q_{l+1,j} \right) . \tag{4.101}$$

Here we have defined $q_{0,j} = q_{1,j}$ and $q_{n+1,j} = q_{n,j}$, where $q_{l,j}$ and $v_{l,j}$ are defined for $l = 1, \ldots, n$ and $j = 1, \ldots, n$ in (4.28b) and (4.86b), respectively. A tedious, but straightforward, calculation shows that $m_{i,j} = 0$ for $i \neq j - 1$. However, the entry $m_{j-1,j}$ is non-zero. We calculate, for $j = 2, \ldots, n$, that

$$m_{j-1,j} = v_{1,j-1} \left(q_{1,j} - q_{2,j} \right) + v_{n,j-1} \left(q_{n-1,j} - q_{n,j} \right) + \sum_{l=2}^{n-1} v_{l,j-1} \left(q_{l-1,j} - q_{l+1,j} \right) . \tag{4.102}$$

Using (4.28b) and (4.86b), and standard trigonometric identities, we can reduce (4.102) to

$$m_{j-1,j} = \frac{4}{n}\sin\left(\frac{\pi(j-1)}{n}\right)\sum_{l=1}^{n}\sin^2\left(\frac{\pi(j-1)(l-1/2)}{n}\right), \qquad j=2,\ldots,n. \tag{4.103}$$

Therefore, we get the key result that

$$m_{j-1,j} = 2\sin\left(\frac{\pi(j-1)}{n}\right) \qquad j=2,\ldots n; \qquad m_{i,j}=0 \quad \text{otherwise}. \tag{4.104}$$

Therefore, it is clear that the matrix product $\mathcal{M}\mathcal{D}\mathcal{M}^t$ in (4.100) is a diagonal matrix. This shows that $\mathcal{B}_g$ and $\mathcal{R}$ have the same eigenvectors. Then, by using (4.95) for the diagonal entries of $\mathcal{D}$, we calculate Σ in (4.100) explicitly as

$$\Sigma \equiv \begin{pmatrix} z_1 & 0 & \cdots & 0 \\ 0 & \ddots & \cdots & 0 \\ \vdots & \vdots & \ddots & \vdots \\ 0 & 0 & \cdots & z_n \end{pmatrix}, \tag{4.105a}$$

where

$$z_j = \frac{1}{4D^2}\mathrm{csch}^2\left(\frac{2\theta}{n}\right)(m_{j,j+1})^2\, d_{j+1}, \quad j=1,\ldots,n-1; \qquad z_n = 0. \tag{4.105b}$$

Finally, we use (4.104) for $m_{j,j+1}$, (4.95) for d_{j+1} and the result that $\kappa_{j+1} = \xi_j$ for $j = 1,\ldots,n-1$, as obtained by comparing (4.28a) and (4.86a). In this way, we find that $z_j = z_j(\tilde{s})$, where

$$z_j = \frac{\tilde{s}\gamma}{\xi_j + \tilde{s}\gamma}\mathrm{csch}^2\left(\frac{2\theta}{n}\right)\sin^2\left(\frac{\pi j}{n}\right), \qquad j=1,\ldots,n-1; \qquad z_n = 0. \tag{4.106}$$

Here γ was defined in (4.94). When $D < D_n$, so that the solution is stable with respect to the large $O(1)$ eigenvalues, then $\xi_j + \tilde{s}\gamma < 0$ for $j = 1,..,n-1$.

Since we have shown the crucial result that $\mathcal{B}_g$ and $\mathcal{R}$ have the same eigenvectors, it is easy to calculate the spectrum of (4.96). The eigenvalues ω_j of (4.96) are

$$\omega_j = \xi_j/(1+z_j), \qquad j=1,\ldots,n, \tag{4.107}$$

where ξ_j and z_j are given in (4.86a) and (4.106), respectively. Then, substituting (4.106) into the expression for σ in (4.96b), we get that $\sigma_j = \sigma_j(\tilde{s})$, where

$$\sigma_j = -\frac{\theta}{D\xi_j}\left(\frac{\xi_j}{\gamma} - 1 - z_j\right), \qquad j=1,\ldots,n. \tag{4.108}$$

Finally, we substitute (4.108) into (4.82) to obtain explicit formulae for the small eigenvalues $\lambda = O(\epsilon^2)$. The main result is summarized as follows:

Proposition 4.10 *For $\epsilon \ll 1$, consider the eigenvalues of (4.16) of order $\lambda = O(\epsilon^2)$. The corresponding eigenfunction has the form (4.56) where $\mathbf{c}_j = \boldsymbol{v}_j$, with $\boldsymbol{v}_j$ defined in (4.86b). The explicit formula for the small eigenvalues is*

$$\lambda_j \sim -\frac{\epsilon^2 q\mu}{D(p+1)} \left(\frac{\int_{-\infty}^{\infty} [u_c(y)]^{p+1}\, dy}{\int_{-\infty}^{\infty} [u_c'(y)]^2\, dy} \right) \left[\frac{1 - \cos(\pi j/n) - z_j(\cosh(2\theta/n) - 1)}{\cosh(2\theta/n) - \cos(\pi j/n)} \right], \qquad (4.109)$$

for $j = 1, \ldots, n$. Here $z_j = z_j(\tilde{s})$ is defined in (4.106).

The final step in the analysis is to determine the sign of σ_j with respect to the parameter D. The condition $\sigma_j < 0$ for $j = 1, .., n$ holds when

$$\frac{\xi_j}{\gamma} - 1 - z_j > 0\,, \qquad j = 1, .., n\,. \qquad (4.110)$$

Defining $w_j = \xi_j/\gamma$, we calculate from (4.86a) and (4.94), and from some standard trigonometric identities, that

$$w_j = 1 + \sin^2\left(\frac{\pi j}{2n}\right) \operatorname{csch}^2\left(\frac{\theta}{n}\right). \qquad (4.111)$$

Since $z_n = 0$ and $w_n > 1$, (4.110) holds when $j = n$. Substituting (4.106) and (4.111) into (4.110), we see that $\sigma_j < 0$ when

$$\sin^2\left(\frac{\pi j}{2n}\right) \operatorname{csch}^2\left(\frac{\theta}{n}\right)\left(\frac{w_j}{\tilde{s}} + 1\right) > \sin^2\left(\frac{\pi j}{n}\right) \operatorname{csch}^2\left(\frac{2\theta}{n}\right), \qquad \text{for} \quad j = 1, .., n-1\,. \quad (4.112)$$

Using (4.111) and some standard identities, (4.112) reduces to

$$\left(1 + \tilde{s} + \operatorname{csch}^2\left(\frac{\theta}{n}\right)\right)\left(1 - \cos^2\left(\frac{\pi j}{2n}\right) \operatorname{sech}^2\left(\frac{\theta}{n}\right)\right) < 0\,. \qquad (4.113)$$

The second bracketed term on the left-hand side of (4.113) is always positive for any $j = 1, .., n$. The first bracketed term is negative when D is very small since $\tilde{s} < -1$ and $\theta \gg 1$. However, this term will switch sign when D crosses through the critical value where

$$\operatorname{csch}^2\left(\frac{\theta}{n}\right) = -(1 + \tilde{s})\,. \qquad (4.114)$$

Hence, $n-1$ of the small eigenvalues switch sign at the *same* value of D. Let D_n^* be the value of D satisfying (4.114). By solving (4.114) we obtain the following main result for the stability of the solution with respect to the small eigenvalues:

Proposition 4.11 *For $\epsilon \ll 1$, consider the eigenvalues of (4.16) of order $\lambda = O(\epsilon^2)$. These eigenvalues are negative only when $D < D_n^*$, where*

$$D_n^* \equiv \frac{\mu}{\left[n \ln(\sqrt{\beta} + \sqrt{\beta+1})\right]^2}, \qquad \beta \equiv \left[\frac{qr}{p-1} - (1+s)\right]^{-1}. \tag{4.115}$$

There are $n-1$ small positive eigenvalues when $D > D_n^*$. When $D = D_n^*$, then $\lambda = 0$ is an eigenvalue of algebraic multiplicity $n-1$.

It is a simple exercise to show that, in general, these critical values are smaller than the critical values D_n given in Proposition 4.7 for the stability of the solution with respect to the large $O(1)$ eigenvalues. Thus, our final conclusion is that an n-spike equilibrium solution will be stable only when $D < D_n^*$. For the parameter sets $(p,q,r,s) = (2,1,2,0)$ we get $\beta = 1$, and for $(p,q,r,s) = (4,2,2,0)$ we get $\beta = 3$. From (4.115) we then calculate the critical values

$$n = 2 \quad \rightarrow \quad D_2 = 0.3218\mu \quad \beta = 1\,; \quad D_2 = 0.1441\mu \quad \beta = 3\,, \tag{4.116a}$$

$$n = 3 \quad \rightarrow \quad D_3 = 0.1430\mu \quad \beta = 1\,; \quad D_3 = 0.0641\mu \quad \beta = 3\,, \tag{4.116b}$$

$$n = 4 \quad \rightarrow \quad D_4 = 0.0805\mu \quad \beta = 1\,; \quad D_4 = 0.0361\mu \quad \beta = 3\,. \tag{4.116c}$$

The numerical computations of [19] of the time-dependent problem (1.17) with $(p,q,r,s) = (2,1,2,0)$, starting with initial conditions close to an asymptotic equilibrium solution, suggested that $D_2 \approx 0.33$ and $D_3 \approx 0.14$. The detailed analysis presented above gives the theoretical basis for these numerical predictions.

4.4 The Dynamics of a One-Spike Solution

In this section we analyze the dynamics of a one-spike solution to (1.17). For finite inhibitor diffusivity D, in §4.4.1 we derive a differential equation determining the location $x_0(t)$ of the maximum of the activator concentration for a one-spike solution to (1.17). By linearizing this

differential equation around the stable equilibrium location $x_0 = 0$, we show that the decay rate of infinitesimal perturbations coincides with the small eigenvalue result (4.109) when $n = 1$. Alternatively, when $D = \infty$, we know from [18] that the equilibrium solution $x_0 = 0$ for a one-spike solution is unstable. When $D = \infty$, the spike drifts exponentially slowly towards the closest endpoint of the domain (cf. [18]). To reconcile the finite D result with the infinite D analysis of [18], we show in §4.4.2 that the equilibrium location $x_0 = 0$ for a one-spike solution is stable when $D < D_1(\epsilon)$, where D_1 is exponentially large as $\epsilon \to 0$.

4.4.1 The Differential Equation for the Spike Location

In the inner region near the spike we introduce the new variables

$$y = \epsilon^{-1}\left[x - x_0(\tau)\right], \qquad \tilde{h}(y) = h(x_0 + \epsilon y), \qquad \tilde{a}(y) = a(x_0 + \epsilon y), \qquad \tau = \epsilon^2 t, \tag{4.117a}$$

and we expand

$$\tilde{h}(y) = \tilde{h}_0(y) + \epsilon\tilde{h}_1(y) + \cdots, \qquad \tilde{a}(y) = \tilde{a}_0(y) + \epsilon\tilde{a}_1(y) + \cdots. \tag{4.117b}$$

Substituting (4.117) into (1.17), we find from the leading terms that a_0 and h_0 satisfy (4.3a) and (4.3b), respectively. Hence,

$$\tilde{a}_0(y) = H^{\gamma}u_c(y), \qquad \tilde{h}_0(y) = H, \qquad \gamma = q/(p-1), \tag{4.118}$$

where $u_c(y)$ satisfies (4.5). Here $H = H(\tau)$ is a function to be determined. Setting $\tilde{a}_1 = H^{\gamma}u_1$, we get to next order that

$$u_1'' - u_1 + pu_c^{p-1}u_1 = \frac{qu_c^p\tilde{h}_1}{H} - x_0'u_c', \qquad -\infty < y < \infty, \tag{4.119a}$$

$$D\tilde{h}_1'' = -H^{\gamma r - s}u_c^r, \tag{4.119b}$$

with $u_1 \to 0$ exponentially as $|y| \to \infty$. The right-hand side of (4.119a) must be orthogonal to the homogeneous solution u_c' of (4.119a). From this solvability condition we obtain

$$x_0' = \frac{q}{H\int_{-\infty}^{\infty}\left[u_c'(y)\right]^2\,dy}\int_{-\infty}^{\infty}u_c^p u_c'\tilde{h}_1\,dy. \tag{4.120}$$

If we integrate (4.120) by parts twice, and use the facts that h_1'' and u_c are even functions, we get

$$x_0' = -\frac{q}{2H(p+1)}\left(\frac{\int_{-\infty}^{\infty}[u_c(y)]^{p+1}\,dy}{\int_{-\infty}^{\infty}[u_c'(y)]^2\,dy}\right)\left[\lim_{y\to+\infty}\tilde{h}_1' + \lim_{y\to-\infty}\tilde{h}_1'\right]. \tag{4.121}$$

In the outer region away from the spike, a is exponentially small and, similar to the analysis in §2, we expand $h = h_0 + \cdots$, where h_0 satisfies

$$Dh_0'' - \mu h_0 = -H^{\gamma r-s}b_r\delta(x-x_0)\,, \qquad -1<x<1\,, \tag{4.122a}$$

$$h_0'(\pm 1) = 0\,. \tag{4.122b}$$

Here b_r is defined in (4.7). To match with the inner solution we require that

$$h_0(x_0) = H\,, \qquad \lim_{y\to+\infty}\tilde{h}_1' + \lim_{y\to-\infty}\tilde{h}_1' = h_{0x}(x_{0+}) + h_{0x}(x_{0-})\,. \tag{4.123}$$

The solution to (4.122) is

$$h_0(x) = H^{\gamma r-s}b_r G(x;x_0)\,, \tag{4.124}$$

where the Green's function $G(x;x_0)$ satisfies (4.10). Substituting (4.124) into (4.123), and using (4.13) for $H^{\gamma r-s}$, we get

$$\lim_{y\to+\infty}\tilde{h}_1' + \lim_{y\to-\infty}\tilde{h}_1' = \frac{H}{G(x_0;x_0)}\left[G_x(x_{0+};x_0) + G_x(x_{0-};x_0)\right], \tag{4.125a}$$

$$H = \left[\frac{1}{b_r G(x_0;x_0)}\right]^{1/\gamma r-(s+1)}. \tag{4.125b}$$

The solution $G(x;x_0)$ was given in (4.11). Using this solution we can calculate the right-hand side of (4.125). Then, substituting the result into (4.121) and (4.124), we obtain

Proposition 4.12 *For $\epsilon \ll 1$, the dynamics of a one-spike solution to (1.17) is characterized by*

$$a(x,t) \sim H^{\gamma}u_c\left(\epsilon^{-1}[x-x_0(t)]\right), \tag{4.126a}$$

$$h(x,t) \sim HG\left[x;x_0(t)\right]/G\left[x_0(t);x_0(t)\right], \tag{4.126b}$$

where $H = H(t)$ is given in (4.125b). The spike location $x_0(t)$ satisfies the differential equation

$$\frac{dx_0}{dt} \equiv F(x_0) \sim -\epsilon^2 C \left[\tanh\left(\sqrt{\frac{\mu}{D}}(1+x_0)\right) - \tanh\left(\sqrt{\frac{\mu}{D}}(1-x_0)\right) \right], \tag{4.126c}$$

where C is defined by

$$C \equiv \frac{q}{2(p+1)}\sqrt{\frac{\mu}{D}} \left(\frac{\int_{-\infty}^{\infty} [u_c(y)]^{p+1}\, dy}{\int_{-\infty}^{\infty} [u_c'(y)]^2\, dy} \right). \tag{4.126d}$$

The equilibrium solution $x_0 = 0$ for this differential equation is stable for any D. The decay rate of infinitesimal perturbations around $x_0 = 0$ is

$$F'(0) \sim -\frac{\epsilon^2 q \mu}{D(p+1)} \left(\frac{\int_{-\infty}^{\infty} [u_c(y)]^{p+1}\, dy}{\int_{-\infty}^{\infty} [u_c'(y)]^2\, dy} \right) \operatorname{sech}^2\left(\sqrt{\frac{\mu}{D}}\right). \tag{4.127}$$

This result agrees precisely with the small eigenvalue result (4.109) when $n = j = 1$.

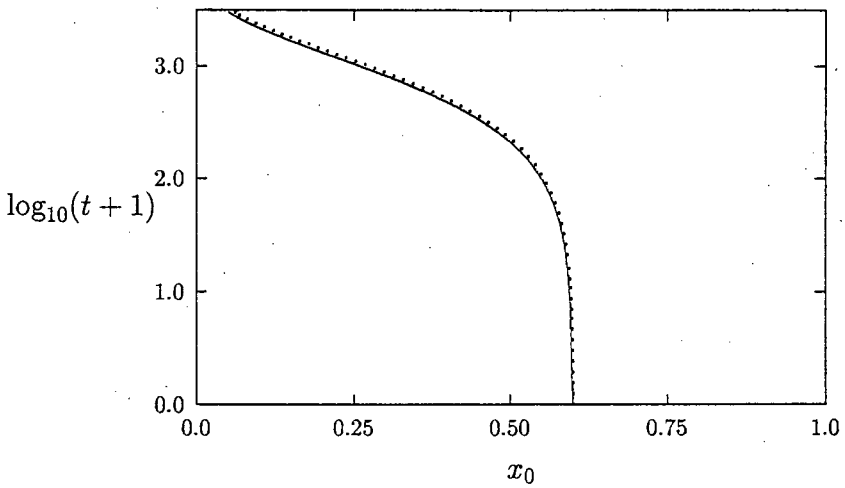

Figure 4.2: Plot of the trajectory $x_0(t)$ of the center of the spike for a one-spike solution with $\epsilon = .03$, $\mu = 1.0$, $D = 1.0$ and $(p, q, r, s) = (2, 1, 2, 0)$. The solid curve is the full numerical result and the dotted curve is the asymptotic result.

To verify (4.126c) for the parameter set $(p, q, r, s) = (2, 1, 2, 0)$ we compared the asymptotic result (4.126c) for $x_0(t)$ with the corresponding full numerical result computed from (1.17). The problem (1.17) was solved numerically using the routine D03PCF from the NAG library [39]. The initial condition was taken to be of the form (4.126a) and (4.126b) with $x_0(0) = 0.6$

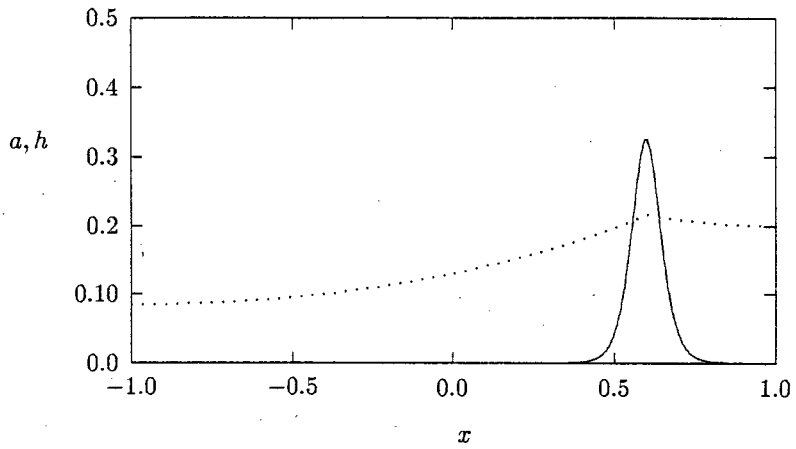

Figure 4.3: Plot of the initial condition for a one-spike solution corresponding to the parameter values shown in the caption of Fig. 4.2. The solid curve is the activator concentration and the dotted curve is the inhibitor concentration.

t	$\log_{10}(1+t)$	$x_0(t)$ (num.)	$x_0(t)$ (asy.)
12.0	1.114	0.5937	0.5942
96.0	1.987	0.5524	0.5552
204.0	2.312	0.5039	0.5091
486.0	2.688	0.3974	0.4073
864.0	2.937	0.2905	0.3035
1314.0	3.119	0.2008	0.2148
1884.0	3.275	0.1262	0.1392
2274.0	3.357	0.0919	0.1035

Table 4.1: A comparison of the asymptotic and numerical results for $x_0(t)$ corresponding to the parameter values shown in the caption of Fig. 4.2.

and $\epsilon = .03$, $\mu = 1.0$, and $D = 1.0$. An interpolation scheme was then used to locate the position of the maximum of a on the computational grid. In Fig. 4.2 and in Table 1 we compare this numerical result for x_0 with the corresponding asymptotic result obtained by solving the differential equation (4.126c) with the initial condition $x_0(0) = 0.6$. In solving the differential equation, the integrals in (4.126c) were evaluated using Romberg integration on a large but finite interval using the form for u_c given in (4.6). We find a close agreement between the asymptotic and numerical results for $x_0(t)$. In Fig. 4.3 we plot the initial condition used and then in Fig. 4.4(a) and Fig. 4.4(b) we plot the numerical solution to (1.17) at two different times showing the slow convergence to a one-spike equilibrium solution.

4.4.2 The Stability of a One-Spike Solution for $D \to \infty$

When $D = \infty$ it was shown in §2.1.3 that a one-spike solution is metastable and that the center $x_0(t)$ of the spike satisfies the asymptotic differential equation

$$\frac{dx_0}{dt} \equiv G(x_0) \sim \frac{2\alpha^2\epsilon}{\left(\int_{-\infty}^{\infty} [u_c'(y)]^2\, dy\right)} \left(e^{-2(1-x_0)/\epsilon} - e^{-2(1+x_0)/\epsilon}\right), \tag{4.128}$$

provided that x_0 is not within $O(\epsilon)$ of the endpoints, i. e. (4.128) is valid when $1 - x_0 \gg O(\epsilon)$ and $1 + x_0 \gg O(\epsilon)$. Here α is defined by the limiting behavior $u_c(y) \sim \alpha e^{-|y|}$ as $|y| \to \infty$. This result shows that $x_0 = 0$ is unstable and that there is a metastable drift of the spike towards the closest endpoint of the domain.

When D is asymptotically large we can superimpose the result (4.128) with (4.126c) to obtain

$$\frac{dx_0}{dt} \equiv G(x_0) + F(x_0)\,. \tag{4.129}$$

Here $F(x_0)$ and $G(x_0)$ are defined in (4.126c) and (4.128), respectively. This superposition is valid since the metastable interaction between the tails of the spike and the boundaries $x = \pm 1$ results in an additive term to the solvability condition that we impose on (4.119a). The stability property of the equilibrium solution for this differential equation is then given in the following result:

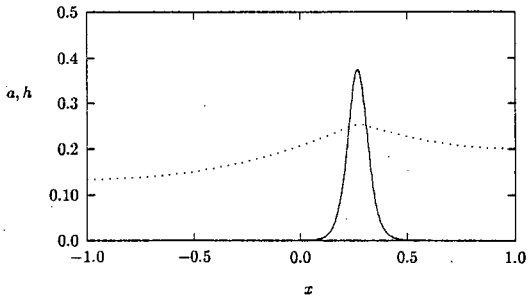

(a) $t = 960$

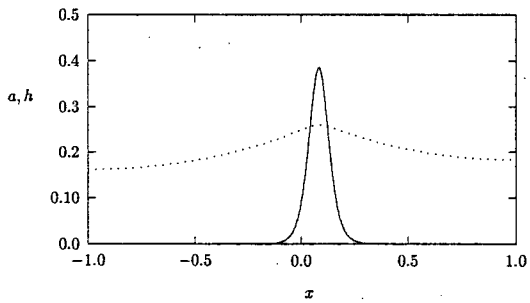

(b) $t = 2400$

Figure 4.4: Plot of a one-spike solution at two different times corresponding to the parameter values shown in the caption of Fig. 4.2. The solid curve is the activator concentration and the dotted curve is the inhibitor concentration.

Proposition 4.13 *For $\epsilon \ll 1$, a one-spike equilibrium solution to (1.17) is stable when $D < D_1(\epsilon)$ and is unstable when $D > D_1(\epsilon)$, where*

$$D_1(\epsilon) \sim \frac{q\mu\epsilon^2 e^{2/\epsilon}}{8(p+1)\alpha^2} \int_{-\infty}^{\infty} [u_c(y)]^{p+1}\, dy\,. \tag{4.130}$$

Here α is defined by the limiting behavior $u_c \sim \alpha e^{-|y|}$ as $|y| \to \infty$, where $u_c(y)$ satisfies (4.5).

For the special case with $\mu = 1$ and $(p, q, r, s) = (2, 1, 2, 0)$, where $u_c(y) = \frac{3}{2}\mathrm{sech}^2\,(y/2)$ and $\alpha = 6$, we can calculate analytically that $D_1(\epsilon) \sim \epsilon^2 e^{2\epsilon}/125.0$.

Chapter 5
Spike Dynamics

The goal of this chapter is to study the dynamics of multi-spike solutions to (1.17). In §4 we found criteria determining the stability of a multi-spike equilibrium solution to (1.17). These criteria were derived by ensuring that the spectrum of the operator associated with a linearization about an equilibrium multi-spike solution contains no eigenvalues with positive real part. In §4 we examine two different types of eigenvalues. The stability of the equilibrium solution on an $O(1)$ time scale was determined by the sign of the real part of the large eigenvalues, and the stability on an $O(\epsilon^{-2})$ time scale was determined by the sign of the $O(\epsilon^2)$ eigenvalues. The $O(\epsilon^2)$ eigenvalues were real. The stability of the equilibrium solution with respect to both sets of eigenvalues gave different ranges of D. Values of D that satisfy both ranges yield stable equilibrium spike solutions.

In this chapter we linearize (1.17) around a quasi-equilibrium solution consisting of a sequence of spikes of different heights. As with the one-spike case treated in §4, the motion of such a multi-spike quasi-equilibrium solution is on a slow $O(\epsilon^{-2})$ time scale. The quasi-equilibrium solution at a fixed time is stable on an $O(1)$ time scale when the large eigenvalues associated with the linearization are in the left-half plane.

The outline of this chapter is as follows. In §5.1 we linearize (1.17) about a quasi-equilibrium n-spike solution where the height and the spike centers are unknown functions of time. By imposing a solvability condition, we obtain a differential-algebraic system of ordinary differential equations governing the motion of the spikes. In §5.2 we discuss the equilibrium solutions to this system which yield both the symmetric solution discussed in §4 and new asymmetric solutions

found in [50]. In §5.3 the results of §4.2 are used to determine when a given spike profile is stable with respect to the large eigenvalues. In §5.4 numerical simulations of the full system are compared to numerical simulations of the system found in §5.1, and these results are compared with the stability results of §5.3 .

5.1 The Dynamics of Quasi-Equilibrium Solutions

We derive a system of ordinary differential equations describing the dynamics of the spike locations for an n-spike quasi-equilibrium solution to (1.17). The spike locations x_i are assumed to satisfy $-1 < x_i < x_{i+1} < 1$ for $i = 1, .., n-1$. In §4.4.1 a one-spike solution was analyzed in detail and it was found that the spike evolves on a long time-scale $t = O(\epsilon^{-2})$. Hence, we expect that $x_i = x_i(\tau)$, where $\tau = \epsilon^2 t$.

In the inner region near each x_i, we introduce the new variables

$$y_i = \epsilon^{-1}(x - x_i)\,, \quad h_i(y_i, \tau) = h(x_i + \epsilon y_i, \epsilon^{-2}\tau)\,, \quad a_i(y_i, \tau) = a(x_i + \epsilon y_i, \epsilon^{-2}\tau)\,, \quad \tau = \epsilon^2 t\,. \tag{5.1}$$

We then expand

$$h_i(y_i, \tau) = h_{i0}(y_i, \tau) + \epsilon h_{i1}(y_i, \tau) + \cdots\,, \qquad a_i(y_i, \tau) = a_{i0}(y_i) + \epsilon a_{i1}(y_i, \tau) + \cdots\,. \tag{5.2}$$

Substituting (5.2) into (1.17), we get to leading order that

$$a_{i0}'' - a_{i0} + a_{i0}^p / h_{i0}^q = 0\,, \qquad -\infty < y_i < \infty\,, \tag{5.3a}$$

$$h_{i0}'' = 0\,. \tag{5.3b}$$

Here the primes indicate derivatives with respect to y_i. In order to match to the outer solution below, we need that h_{i0} is bounded and that $a_{i0} \to 0$ as $|y_i| \to \infty$. Thus, from (5.3b), we get that

$$h_{i0} = H_i(\tau)\,, \tag{5.4a}$$

for some unknown H_i. The solution to (5.3a) is

$$a_{i0}(y_i) = H_i^{\gamma} u_c(y_i)\,, \qquad \text{where} \qquad \gamma = q/(p-1)\,, \tag{5.4b}$$

and $u_c(y)$ satisfies

$$u_c'' - u_c + u_c^p = 0\,, \qquad -\infty < y < \infty\,, \tag{5.5a}$$

$$u_c \to 0 \quad \text{as} \quad |y| \to \infty\,; \qquad u_c'(0) = 0\,, \qquad u_c(0) > 0\,. \tag{5.5b}$$

In particular, when $p = 2$, we have

$$u_c(y) = \frac{3}{2}\text{sech}^2\,(y/2)\,. \tag{5.5c}$$

The $O(\epsilon)$ problems, obtained from substituting (5.2) into (1.17), are

$$a_{i1}'' - a_{i1} + \frac{pa_{i0}^{p-1}}{h_{i0}^q}a_{i1} = \frac{qa_{i0}^p}{h_{i0}^{q+1}}h_{i1} - a_{i0}'\,\dot{x}_i\,, \tag{5.6a}$$

$$Dh_{i1}'' = -\frac{a_{i0}^r}{h_{i0}^s}\,. \tag{5.6b}$$

Here $\dot{x}_i \equiv dx_i/d\tau$. Substituting (5.4) into (5.6), we get

$$L(a_{i1}) \equiv a_{i1}'' - a_{i1} + pu_c^{p-1}a_{i1} = qH_i^{\gamma-1}u_c^p h_{i1} - H_i^{\gamma}u_c'\,\dot{x}_i\,, \tag{5.7a}$$

$$Dh_{i1}'' = -H_i^{\gamma r - s}u_c^r\,. \tag{5.7b}$$

Since $L(u_c') = 0$, and $u_c' \to 0$ exponentially as $|y| \to \infty$, the right-hand side of (5.7a) must satisfy the solvability condition that it be orthogonal to u_c'. In this way, we get

$$\dot{x}_i \int_{-\infty}^{\infty} \left[u_c'(y)\right]^2 dy \sim \frac{q}{H_i}\int_{-\infty}^{\infty} u_c^p u_c' h_{i1}\,dy_i\,. \tag{5.8}$$

Integrating (5.8) by parts twice, and using the facts that h_{i1} and u_c are even functions, we obtain

$$\dot{x}_i \int_{-\infty}^{\infty} \left[u_c'(y)\right]^2 dy \sim -\frac{q}{2H_i(p+1)}\left(\int_{-\infty}^{\infty}[u_c(y)]^{p+1}\,dy\right)\left(\lim_{y_i\to+\infty} h_{i1}' + \lim_{y_i\to-\infty} h_{i1}'\right)\,. \tag{5.9}$$

Now in the outer region, defined away from $O(\epsilon)$ regions near each x_i, a is exponentially small and we expand

$$h(x) = h_0(x) + o(\epsilon)\,. \tag{5.10}$$

Since $\epsilon \ll 1$, and a is localized, the term $\epsilon^{-1}a^m/h^s$ in the outer region behaves like a linear combination of delta functions. Substituting (5.4) and (5.10) into (1.17b), and letting $\epsilon \to 0$, we find that h_0 satisfies

$$Dh_{0xx} - \mu h_0 = -b_r \sum_{i=1}^{n} H_i^{\gamma r - s} \delta(x - x_i)\,, \qquad b_r \equiv \int_{-\infty}^{\infty} [u_c(y)]^r \, dy\,, \tag{5.11a}$$

$$h_{0x}(\pm 1) = 0\,. \tag{5.11b}$$

The solution to (5.11) is

$$h_0(x) = b_r \sum_{i=1}^{n} H_i^{\gamma r - s} G(x; x_i)\,, \tag{5.12}$$

where $G(x; x_i)$ satisfies

$$DG_{xx} - \mu G = -\delta(x - x_i)\,, \qquad -1 < x < 1\,, \tag{5.13a}$$

$$G_x(\pm 1; x_i) = 0\,. \tag{5.13b}$$

To match with the inner solutions near each x_i, we require for $i = 1, .., n$ that

$$h_0(x_i) = H_i\,, \tag{5.14a}$$

$$\lim_{y_i \to \infty} h_{i1}' + \lim_{y_i \to -\infty} h_{i1}' = h_{0x}(x_{i+}) + h_{0x}(x_{i-})\,. \tag{5.14b}$$

From (5.14a) and (5.12), we obtain a nonlinear algebraic system for H_i, $i = 1, .., n$.

The final step in the derivation is to calculate the integral f defined by

$$f \equiv \frac{\int_{-\infty}^{\infty} [u_c(y)]^{p+1} \, dy}{\int_{-\infty}^{\infty} [u_c'(y)]^2 \, dy}\,. \tag{5.15}$$

To do so, we first multiply (5.5a) by u_c. Upon integrating the resulting equation over the domain, we obtain

$$\int_{-\infty}^{\infty} u_c u_c'' \, dy - \int_{-\infty}^{\infty} u_c^2 \, dy + \int_{-\infty}^{\infty} u_c^{p+1} \, dy = 0\,. \tag{5.16}$$

Upon integrating the first term in this equation by parts, we get

$$-1 = e - f\,, \qquad \text{where} \qquad e \equiv \frac{\int_{-\infty}^{\infty} [u_c(y)]^2 \, dy}{\int_{-\infty}^{\infty} [u_c'(y)]^2 \, dy}\,. \tag{5.17}$$

To obtain an additional equation, we multiply (5.5a) by u_c' and integrate over the domain to fix the constant of integration. We then integrate the resulting expression again to get

$$1 = e - \frac{2f}{p+1}. \tag{5.18}$$

Solving (5.17) and (5.18), we obtain

$$f = \frac{2(p+1)}{p-1}. \tag{5.19}$$

The dynamics of the n-spike pattern is obtained by substituting (5.14) and (5.19) into (5.9) and (5.12). The main result is summarized as follows (relabeling H_i by h_i in the notation below):

Proposition 5.1 *For $\epsilon \ll 1$, the quasi-equilibrium solution for a and h is given by*

$$a(x,t) \sim a_c \equiv \sum_{j=1}^{n} h_j^{\gamma} u_c \left[\epsilon^{-1}(x - x_j)\right], \tag{5.20a}$$

$$h(x,t) \sim h_c \equiv b_r \sum_{j=1}^{n} h_j^{\gamma r - s} G(x; x_j), \tag{5.20b}$$

where $h_i = h_i(\tau)$ and $x_i = x_i(\tau)$ satisfy the differential-algebraic system for $i = 1, .., n$

$$h_i = b_r \sum_{j=1}^{n} h_j^{\gamma r - s} G(x_i; x_j), \tag{5.21a}$$

$$\frac{dx_i}{d\tau} \sim -\frac{2qb_r}{p-1} h_i^{-1} \left(h_i^{\gamma r - s} \langle G_x \rangle_i + \sum_{\substack{j=1 \\ j \neq i}}^{n} h_j^{\gamma r - s} G_x(x_i; x_j) \right). \tag{5.21b}$$

Here u_c satisfies (5.5), b_m is defined in (5.11a), $\tau = \epsilon^2 t$, and $\langle G_x \rangle_i \equiv \left[G_x(x_{i+}; x_i) + G_x(x_{i-}; x_i)\right]/2$.

The system (5.21) can also be written in matrix form as

$$\boldsymbol{h} = b_r \mathcal{G} \boldsymbol{h}^{\gamma r - s}, \qquad \frac{d\boldsymbol{x}}{d\tau} \sim -\frac{2qb_r}{p-1} \mathcal{H}^{-1} \mathcal{P} \boldsymbol{h}^{\gamma r - s}, \tag{5.22}$$

where $d\boldsymbol{x}/d\tau \equiv (\dot{x}_1, \ldots, \dot{x}_n)^t$. Here we have defined

$$\mathcal{G} \equiv \begin{pmatrix} G(x_1; x_1) & \cdots & G(x_1; x_n) \\ \vdots & \ddots & \vdots \\ G(x_n; x_1) & \cdots & G(x_n; x_n) \end{pmatrix}, \qquad \mathcal{H} \equiv \begin{pmatrix} h_1 & 0 & \cdots & 0 \\ 0 & \ddots & \cdots & 0 \\ \vdots & \vdots & \ddots & \vdots \\ 0 & 0 & \cdots & h_n \end{pmatrix}, \tag{5.23a}$$

and

$$\mathcal{P} \equiv \begin{pmatrix} \langle G_x(x_1;x_1)\rangle_0 & \cdots & G_x(x_1;x_n) \\ \vdots & \ddots & \vdots \\ G_x(x_n;x_1) & \cdots & \langle G_x(x_n;x_n)\rangle_n \end{pmatrix}, \qquad \boldsymbol{h} \equiv \begin{pmatrix} h_1 \\ \vdots \\ h_n \end{pmatrix}, \qquad \boldsymbol{h}^{\gamma r-s} \equiv \begin{pmatrix} h_1^{\gamma r-s} \\ \vdots \\ h_n^{\gamma r-s} \end{pmatrix}. \tag{5.23b}$$

Alternatively, we can write (5.22) in terms of certain tridiagonal matrices. In Appendix C, we show that

$$\mathcal{G} = \frac{\mathcal{B}^{-1}}{\sqrt{\mu D}}, \tag{5.24}$$

where $\mathcal{B}$ is the tridiagonal matrix

$$\mathcal{B} \equiv \begin{pmatrix} c_1 & d_1 & 0 & \cdots & 0 & 0 & 0 \\ d_1 & c_2 & \ddots & \ddots & \ddots & 0 & 0 \\ 0 & \ddots & \ddots & \ddots & \ddots & \ddots & 0 \\ \vdots & \ddots & \ddots & \ddots & \ddots & \ddots & \vdots \\ 0 & \ddots & \ddots & \ddots & \ddots & \ddots & 0 \\ 0 & 0 & \ddots & \ddots & \ddots & c_{n-1} & d_{n-1} \\ 0 & 0 & 0 & \cdots & 0 & d_{n-1} & c_n \end{pmatrix}, \tag{5.25a}$$

with matrix entries defined by

$$c_1 = \coth\left[\theta(x_2 - x_1)\right] + \tanh\left[\theta(1 + x_1)\right]\,; \quad c_n = \coth\left[\theta(x_n - x_{n-1})\right] + \tanh\left[\theta(1 - x_n)\right]\,, \tag{5.25b}$$

$$c_j = \coth\left[\theta(x_{j+1} - x_j)\right] + \coth\left[\theta(x_j - x_{j-1})\right]\,, \quad j = 2, .., n-1\,, \tag{5.25c}$$

$$d_j = -\mathrm{csch}\left[\theta(x_{j+1} - x_j)\right]\,, \quad j = 1, .., n-1\,. \tag{5.25d}$$

Here $\theta = \sqrt{\mu/D}$.

Next, we calculate the matrix product $\mathcal{P}\mathcal{B}$ using the procedure as outlined in Appendix A. We

find that $\mathcal{PB}$ is a tridiagonal matrix of the form

$$\mathcal{PB} \equiv \frac{1}{2D}\mathcal{P}_b\,, \qquad \text{where} \qquad \mathcal{P}_b \equiv \begin{pmatrix} e_1 & f_1 & 0 & \cdots & 0 & 0 & 0 \\ -f_1 & e_2 & \ddots & \ddots & \ddots & 0 & 0 \\ 0 & \ddots & \ddots & \ddots & \ddots & \ddots & 0 \\ \vdots & \ddots & \ddots & \ddots & \ddots & \ddots & \vdots \\ 0 & \ddots & \ddots & \ddots & \ddots & \ddots & 0 \\ 0 & 0 & \ddots & \ddots & \ddots & e_{n-1} & f_{n-1} \\ 0 & 0 & 0 & \cdots & 0 & -f_{n-1} & e_n \end{pmatrix}. \tag{5.26a}$$

The matrix entries are defined by

$$e_1 = \tanh\left[\theta(1+x_1)\right] - \coth\left[\theta(x_2-x_1)\right]\,; \quad e_n = \coth\left[\theta(x_n-x_{n-1})\right] - \tanh\left[\theta(1-x_n)\right]\,, \tag{5.26b}$$

$$e_j = \coth\left[\theta(x_j-x_{j-1})\right] - \coth\left[\theta(x_{j+1}-x_j)\right]\,, \quad j=2,..,n-1\,, \tag{5.26c}$$

$$f_j = \operatorname{csch}\left[\theta(x_{j+1}-x_j)\right]\,, \quad j=1,..,n-1\,. \tag{5.26d}$$

Substituting (5.24) into (5.22), we obtain the following result equivalent to (5.21):

Corollary 5.1 *The differential-algebraic system (5.21) is equivalent to the matrix system*

$$\frac{d\boldsymbol{x}}{d\tau} \sim -\frac{q}{p-1}\sqrt{\frac{\mu}{D}}\mathcal{H}^{-1}\mathcal{P}_b\boldsymbol{h}\,, \qquad \mathcal{B}\boldsymbol{h} = \frac{b_r}{\sqrt{\mu D}}\boldsymbol{h}^{\gamma r-s}\,. \tag{5.27}$$

Here $\mathcal{H}$, $\mathcal{B}$ and $\mathcal{P}_b$ are given in (5.23a), (5.25), and (5.26), respectively.

The advantage of this formulation over (5.21) is that (5.27) is expressed only in terms of tridiagonal matrices. Starting with certain initial data $\boldsymbol{x}(0)$, in §5.4 we give numerical examples showing the evolution of the quasi-equilibrium solution (5.20) and (5.27) towards a stable equilibrium solution. These asymptotic results are also compared with full numerical results computed from (1.17).

5.2 Symmetric and Asymmetric Equilibria

From (5.27), the equilibrium values of $\boldsymbol{h}$ and $\boldsymbol{x}$ satisfy

$$\mathcal{B}\boldsymbol{h} = \frac{b_r}{\sqrt{\mu D}}\boldsymbol{h}^{\gamma r - s}, \qquad \mathcal{P}_b\boldsymbol{h} = 0\,. \tag{5.28}$$

In this section we review some results obtained in §4 and in [50] for the existence and stability of symmetric and asymmetric spike patterns for (1.17) respectively.

As shown in §4, for the symmetric spike patterns where $h_j = H$ for $j = 1, .., n$, the x_j are located at the symmetry points

$$x_j = -1 + \frac{2j-1}{k}, \qquad j = 1, .., k\,. \tag{5.29}$$

In this case, it was shown in §4 that $2\tanh(\theta/n)$, with $\theta = \sqrt{\mu/D}$, is an eigenvalue of $\mathcal{B}$ with associated eigenvector $\boldsymbol{v} \equiv (1, 1, .., 1)^t$. In addition, $\mathcal{P}_b\boldsymbol{v} = 0$. Hence, from (5.28), the common spike value $h_j = H$ is

$$H^{\gamma r-(s+1)} = \frac{2\sqrt{\mu D}}{b_r}\tanh\left(\frac{\theta}{n}\right). \tag{5.30}$$

The symmetric n-spike solution is obtained by substituting (5.29) and $h_j = H$ into (5.20).

In [50], *asymmetric* n-spike equilibrium patterns were constructed asymptotically. The type of asymmetric patterns that were constructed consisted of $n_1 > 0$ small spikes of type A and $n_2 = n - n_1 > 0$ large spikes of type B arranged in any particular order from left to right across the interval $[-1, 1]$ as

$$\text{ABAAB....B}\,, \qquad n_1 - \text{A's}\,, \qquad n_2 - \text{B's}. \tag{5.31}$$

A plot of such a solution with five spikes in an ABBAB pattern is shown in Fig. 5.1. The following result for asymmetric equilibrium spike patterns was obtained in [50].

Proposition 5.2 (see [50]) *Let $\epsilon \to 0$ and $D < D_m$, where D_m is some critical value. Then, there exists an asymmetric n-spike equilibrium solution to (1.17) of the form (5.20), where h_j*

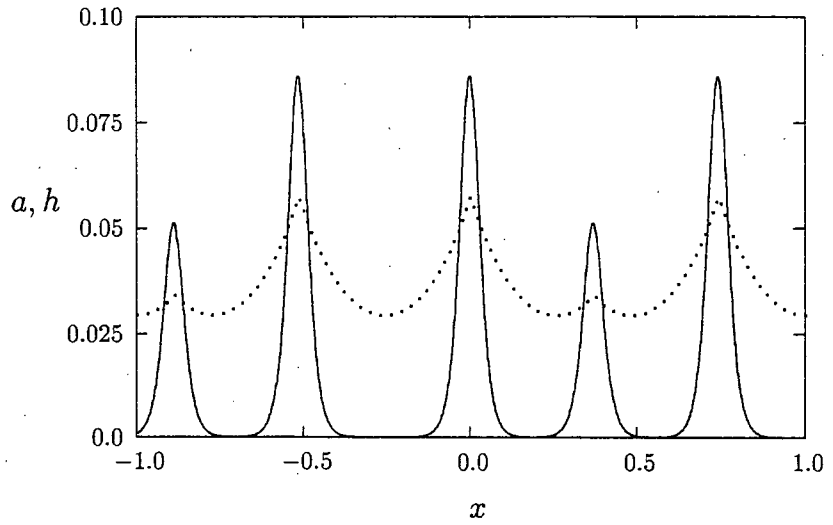

Figure 5.1: Plot of the activator and inhibitor concentration for a five-spike asymptotic asymmetric equilibrium solution with $\epsilon = .02$, $D = .04$, $\mu = 1$, and $(p, q, r, s) = (2, 1, 2, 0)$. The solid curve is the activator concentration and the dotted curve is the inhibitor concentration.

satisfies

$$h_j^{\gamma r-(s+1)} = \left(\frac{2\sqrt{\mu D}}{b_r}\right) \tanh\left(l_j\theta\right), \qquad \theta = \sqrt{\mu/D}\,. \tag{5.32}$$

Here for each j, $l_j = l$ *or* $l_j = \tilde{l}$, *where* l *and* $\tilde{l}$ *are determined in terms of* n_1, n_2 *and* $\sqrt{\mu/D}$ *by the nonlinear system*

$$n_1 l + n_2 \tilde{l} = 1\,, \qquad b\left[l\sqrt{\mu/D}\right] = b\left[\tilde{l}\sqrt{\mu/D}\right], \tag{5.33a}$$

where

$$b(z) \equiv \frac{\tanh^{\hat{r}} z}{\cosh z}, \qquad \hat{r} \equiv \frac{1}{\gamma r - (s+1)}\,. \tag{5.33b}$$

The value $l_j = l$ *must occur* $n_1 > 0$ *times, while* $l_j = \tilde{l}$ *must occur* $n_2 = n - n_1 > 0$ *times. The small and large spikes can be arranged in any sequence. Finally, the spike locations* x_j *are found from*

$$x_1 = l_1 - 1\,, \qquad x_k = 1 - l_k\,, \qquad x_{j+1} = x_j + l_{j+1} + l_j\,, \quad j = 1, .., k-2\,. \tag{5.34}$$

Detailed numerical computations for the critical value D_m and further more refined results were obtained in [50]. For our purposes, the key point concerns the relationship between the symmetric and the asymmetric spike patterns. Define an L_1-type norm of the equilibrium solution for a by

$$|a|_1 \equiv \sum_{j=1}^{n} h_j^{\gamma}, \tag{5.35}$$

where $|a|_1$ is a function of D. Label the symmetric branch with n spikes by s_n. Then, the following result was shown numerically in [50]:

Proposition 5.3 (see [50]) *An n-spike asymmetric solution branch with n_1 small spikes of type A provides the connection as D is varied between the symmetric branches s_n and s_{n-n_1}. All of the asymmetric branches with n spikes bifurcate from the symmetric branch s_n at the critical value $D = D_b$ given by*

$$D_b = \frac{\mu}{n^2 \left[\log\left(\sqrt{\hat{r}} + \sqrt{\hat{r}+1}\right)\right]^2}. \tag{5.36}$$

Here $\hat{r}$ is defined in (5.33b).

The stability properties of asymmetric spike patterns was studied in [50]. In the analysis of [50], there were two classes of eigenvalues that needed to be considered. The first class are the large $O(1)$ eigenvalues, resulting from global spike interactions, that correspond to strong instabilities of small perturbations of the equilibrium solution on an $O(1)$ time-scale. This instability property, referred to here as profile instabilities, is not contained in the system (5.27). The second class of eigenvalues are the small $O(\epsilon^2)$ eigenvalues that are associated with near translation invariance and slow dynamics near the equilibrium solutions. These small eigenvalues arise from the linearization of (5.27) about equilibrium values for $\boldsymbol{h}$ and $\boldsymbol{x}$. Thus, these eigenvalues are contained in the system (5.27). Critical ranges of D that ensure the stability of the equilibrium solution with respect to both classes of eigenvalues were derived in [50].

The main qualitative stability conclusions from the analyses of §4 for symmetric solutions and [50] for asymmetric solutions are as follows. For a certain nontrivial range of D near the bifurcation value D_b, each n-spike asymmetric solution branch that bifurcates from the symmetric branch s_n is stable with respect to the large $O(1)$ eigenvalues. However, based on numerical evidence, each of these bifurcating asymmetric branches is always unstable with respect to the small $O(\epsilon^2)$ eigenvalues. The symmetric branch is stable with respect to the large eigenvalues when $D < D_n$ and is stable with respect to the small eigenvalues when $D < D_b$. Here $D_b < D_n$, and D_n is given by

$$D_n = 4\mu n^{-2}\left[\ln\left(\beta + \sqrt{\beta^2 - 1}\right)\right]^{-2}, \qquad \beta \equiv 1 + (1 + \cos(\pi/k))\,\hat{r}\,, \tag{5.37}$$

for $n \geq 2$, where $\hat{r}$ is defined in (5.33b). This results predicts that D_1 is infinite, but as shown in §4, D_1 is exponentially large as $\epsilon \to 0$. In Fig. 5.2 we plot a bifurcation diagram of $|a|_1$ versus D, showing the asymmetric and symmetric branches with fewer than four spikes and their stability ranges with respect to the large $O(1)$ eigenvalues.

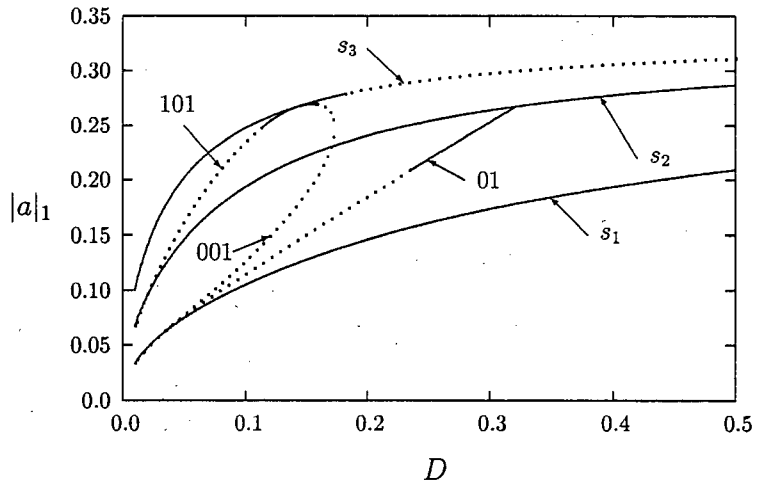

Figure 5.2: Plot of $|a|_1$ defined in (5.35) versus D for solutions with three or fewer spikes. Here $\mu = 1$ and $(p, q, r, s) = (2, 1, 2, 0)$. The symmetric branch with k spikes is labeled by s_k. The asymmetric patterns AB, BAB, and AAB are labeled by 01, 101, and 001, respectively. The portions of the branches that are solid (dotted) are stable (unstable) with respect to the large $O(1)$ eigenvalues.

The implication of these results is that there are many equilibria of the quasi-equilibrium

dynamics (5.27) with exactly n interior spikes. One of them corresponds to the symmetric spike pattern, and the rest correspond to asymmetric patterns. However, only the symmetric branches will be stable with respect to both the large and small eigenvalues when $D < D_b$. Hence, it is reasonable to expect that when $D < D_b$ the quasi-equilibrium dynamics (5.27) starting from some $\boldsymbol{x}(0)$, will tend to a symmetric equilibrium with n spikes. Based on the numerical evidence of §5.4, this scenario will only occur if the quasi-equilibrium solution is stable with respect to the large $O(1)$ eigenvalues *throughout* the slow dynamics. For symmetric equilibria, this stability threshold is given by D_n in (5.37). For the quasi-equilibrium solution, the stability threshold depends on the values of $\boldsymbol{h}$ and $\boldsymbol{x}$ at a given τ.

5.3 Stability of the Profile: The Large Eigenvalues

We now examine the stability, at a fixed value of τ, of the quasi-equilibrium profile constructed in §5.1. The quasi-equilibrium profile of §5.1 varies on a slow time-scale $\tau = \epsilon^2 t$. We would like to determine whether this profile can undergo an instability on a fast time-scale of $O(1)$. Hence, since there is a time-scale separation, in the eigenvalue analysis below we can treat τ as being a fixed parameter. To derive the eigenvalue problem, we substitute

$$a(x,t) = a_c + e^{\lambda t}\phi(x)\,, \qquad h(x,t) = h_c + e^{\lambda t}\eta(x)\,, \tag{5.38}$$

into (1.17) where a_c and h_c are defined in (5.20), and $\eta \ll 1$ and $\phi \ll 1$. This leads to

$$\epsilon^2\phi_{xx} - \phi + \frac{pa_c^{p-1}}{h_c^q}\phi - \frac{qa_c^p}{h_c^{q+1}}\eta = \lambda\phi\,, \qquad -1 < x < 1\,, \tag{5.39a}$$

$$D\eta_{xx} - \mu\eta = -\epsilon^{-1}r\frac{a_c^{r-1}}{h_c^s}\phi + \epsilon^{-1}s\frac{a_c^r}{h_c^{s+1}}\eta\,, \qquad -1 < x < 1\,, \tag{5.39b}$$

$$\phi_x(\pm 1) = \eta_x(\pm 1) = 0\,. \tag{5.39c}$$

The spectrum of (5.39) contains large eigenvalues that are $O(1)$ as $\epsilon \to 0$. In §5.4, we show that the quasi-equilibrium profile becomes unstable on an $O(1)$ time-scale when the $x_i(\tau)$, $h_i(\tau)$, for $i = 1, .., n$, are such that (5.39) has an eigenvalue with $\mathrm{Re}(\lambda) > 0$.

We look for an eigenfunction of (5.39) in the form

$$\phi(x) \sim \sum_{j=1}^{k} \phi_j \left[\epsilon^{-1}(x - x_j)\right] , \tag{5.40}$$

where $\phi_j(y) \to 0$ exponentially as $|y| \to \infty$. Then, the right-hand side of (5.39b) with $s = 0$ behaves like a sum of delta functions when $\epsilon \ll 1$. Substituting (5.20) and (5.40) into (5.39b), we get

$$D\eta_{xx} - \left[\mu + sb_r \sum_{j=1}^{n} h_j^{\gamma r-(s+1)} \delta(x - x_j)\right] \eta = -\sum_{j=1}^{n} \omega_j \delta(x - x_j) , \tag{5.41a}$$

$$\eta_x(\pm 1) = 0 , \tag{5.41b}$$

where

$$\omega_j \equiv r h_j^{\gamma(r-1)-s} \int_{-\infty}^{\infty} u_c^{r-1} \phi_j \, dy . \tag{5.41c}$$

This problem is equivalent to

$$D\eta_{xx} - \mu\eta = 0 , \qquad -1 < x < 1 ; \qquad \eta_x(\pm 1) = 0 , \tag{5.42a}$$

$$[\eta]_j = 0 , \qquad [D\eta_x]_j = -\omega_j + sb_r h_j^{\gamma r-(s+1)} \eta(x_j) , \tag{5.42b}$$

where $[v]_j \equiv v(x_{j+}) - v(x_{j-})$. By solving this system on each subinterval as in Appendix A, we can show that

$$\left(\mathcal{B} + \frac{sb_r}{\sqrt{\mu D}} \mathcal{H}^{\gamma r-(s+1)}\right) \boldsymbol{\eta} = \boldsymbol{\omega}/\sqrt{\mu D} , \qquad \boldsymbol{\eta} \equiv \begin{pmatrix} \eta(x_1) \\ \vdots \\ \eta(x_n) \end{pmatrix} , \qquad \boldsymbol{\omega} \equiv \begin{pmatrix} \omega_1 \\ \vdots \\ \omega_n \end{pmatrix} . \tag{5.43}$$

Here $\mathcal{H}$ and $\mathcal{B}$ are defined in (5.23a) and (5.25), respectively. Since $s > 0$ and $\mathcal{H}$ is a positive matrix, we can solve for $\boldsymbol{\eta}$ as

$$\boldsymbol{\eta} = \frac{rb_r}{\sqrt{\mu D}} \left(\mathcal{B} + \frac{sb_r}{\sqrt{\mu D}} \mathcal{H}^{\gamma r-(s+1)}\right)^{-1} \mathcal{H}^{\gamma(r-1)-s} \left(\frac{\int_{-\infty}^{\infty} u_c^{r-1} \boldsymbol{\phi} \, dy}{\int_{-\infty}^{\infty} u_c^r \, dy}\right) . \tag{5.44}$$

Next, we substitute (5.20) and (5.40) into (5.39a) to obtain for $j = 1, .., n$ that

$$\phi_j'' - \phi_j + p u_c^{p-1} \phi_j - q h_j^{\gamma-1} u_c^p \eta(x_j) = \lambda \phi_j , \qquad -\infty < y < \infty , \tag{5.45}$$

with $\phi_j(y) \to 0$ as $y \to \infty$. We can write (5.45) in matrix form as

$$\boldsymbol{\phi}'' - \boldsymbol{\phi} + p u_c^{p-1} \boldsymbol{\phi} - q u_c^p \mathcal{H}^{\gamma-1} \boldsymbol{\eta} = \lambda \boldsymbol{\phi}\,, \tag{5.46}$$

Substituting (5.44) into (5.46), we obtain the eigenvalue problem

$$\boldsymbol{\phi}'' - \boldsymbol{\phi} + p u_c^{p-1} \boldsymbol{\phi} - r q u_c^p \left(\frac{\int_{-\infty}^{\infty} u_c^{r-1} \mathcal{E} \boldsymbol{\phi}\, dy}{\int_{-\infty}^{\infty} u_c^r\, dy} \right) = \lambda \boldsymbol{\phi}\,, \qquad -\infty < y < \infty\,, \tag{5.47a}$$

$$\boldsymbol{\phi} \to 0\,, \quad \text{as} \quad |y| \to \infty\,, \tag{5.47b}$$

where the matrix $\mathcal{E}$ is defined by

$$\mathcal{E} \equiv \frac{b_r}{\sqrt{\mu D}} \mathcal{H}^{\gamma-1} \left(\mathcal{B} + \frac{s b_r}{\sqrt{\mu D}} \mathcal{H}^{\gamma r - (s+1)} \right)^{-1} \mathcal{H}^{\gamma r - (s+1)} \mathcal{H}^{1-\gamma}\,. \tag{5.48}$$

Since $\mathcal{G} = \mathcal{B}^{-1}/\sqrt{\mu D}$ is positive definite and $\mathcal{H}$ is a positive diagonal matrix, we conclude that $\mathcal{E}$ has real positive eigenvalues. We decompose $\mathcal{E}$ as

$$\mathcal{E} = \mathcal{S}^{-1} \Lambda_e \mathcal{S}\,, \tag{5.49}$$

for some nonsingular matrix $\mathcal{S}$. Then, upon defining $\boldsymbol{\psi} = \mathcal{S}\boldsymbol{\phi}$, we obtain from (5.47) that

$$\boldsymbol{\psi}'' - \boldsymbol{\psi} + p u_c^{p-1} \boldsymbol{\psi} - r q u_c^p \left(\frac{\int_{-\infty}^{\infty} u_c^{r-1} \Lambda_e \boldsymbol{\psi}\, dy}{\int_{-\infty}^{\infty} u_c^r\, dy} \right) = \lambda \boldsymbol{\psi}\,, \qquad -\infty < y < \infty\,, \tag{5.50a}$$

$$\boldsymbol{\psi} \to 0\,, \quad \text{as} \quad |y| \to \infty\,. \tag{5.50b}$$

Since Λ_e is a diagonal matrix we obtain n uncoupled problems from (5.50).

The next step is to determine the conditions for which $\mathrm{Re}(\lambda) < 0$ in (5.50). For this we use Theorem 2.1. By comparing (5.50) with (2.11), we obtain the following result on the spectrum of (5.50):

Proposition 5.4 *Let $\lambda_0 \neq 0$ be the eigenvalue of (5.50) with the largest real part and assume condition (2.13a) holds. Let α_1 be the minimum eigenvalue of the matrix $\mathcal{E}$ defined in (5.48). Then, $Re(\lambda_0) > 0$ when*

$$\alpha_1 < \frac{(p-1)}{qr}\,. \tag{5.51}$$

Also, $Re(\lambda_0) < 0$ when $\alpha_1 > (p-1)/qr$.

A more convenient criterion is obtained by writing $\mathcal{E}$ in (5.48) as $\mathcal{E} = \mathcal{H}^{\gamma-1}\left(\tilde{\mathcal{E}} + sI\right)^{-1}\mathcal{H}^{1-\gamma}$, where

$$\tilde{\mathcal{E}} \equiv \frac{\sqrt{\mu D}}{b_r}\mathcal{H}^{-\gamma r+(s+1)}\mathcal{B}. \tag{5.52}$$

The eigenvalues of $\mathcal{E}$ and $\left(\tilde{\mathcal{E}} + sI\right)^{-1}$ are identical. We can then rewrite Proposition 4.1 as the following simple criterion:

Corollary 5.2 *Let $\lambda_0 \neq 0$ be the eigenvalue of (5.50) with the largest real part and assume condition (2.13a) holds. Let e_m be the maximum eigenvalue of the tridiagonal matrix $\tilde{\mathcal{E}}$ defined in (5.52). Then, $Re(\lambda_0) > 0$ when*

$$e_m > \frac{qr}{(p-1)} - s. \tag{5.53}$$

Also, $Re(\lambda_0) < 0$ when $e_m < qr/(p-1) - s$.

The results of §4 and [50] for the stability of symmetric and asymmetric *equilibrium* spike patterns, respectively, with respect to the large $O(1)$ eigenvalues were obtained from a criterion such as Corollary 4.1. In our numerical examples in §5.4 of the evolution of the quasi-equilibrium solution, we track the maximum eigenvalue of $\tilde{\mathcal{E}}$ as a function of τ and determine the behavior of the solution if the threshold in (5.53) is exceeded.

5.4 Comparison of Asymptotic and Numerical Results

We now compare the asymptotic results for the spike motion with corresponding numerical results computed from (1.17). Unless otherwise stated, in the comparisons below we have taken the parameter values $\mu = 1$, the exponent set $(p, q, r, s) = (2, 1, 2, 0)$, and $\epsilon = 0.02$. The comparisons are made for various values of the inhibitor diffusivity D, of the number of spikes n, and of the initial spike locations $x_j(0)$, for $j = 1, .., n$. The time variable given in the plots below correspond to the slow time variable τ defined in (5.1) by $\tau = \epsilon^2 t$. With $\epsilon = .02$, we get $t = 2500\tau$.

To compute the full numerical results from (1.17), we use the NAG library code [39] with 2001 equidistant meshpoints. For given values of D, n, and $x_j(0)$ for $j = 1, .., n$, we take the quasi-equilibrium solution (5.20) to be the initial condition for a and h. To compute $a(x, 0)$ and $h(x, 0)$, we must determine the initial values $h_j(0)$, for $j = 1, .., n$, from the nonlinear algebraic system for h_j in (5.27). This is done using Newton's method. In the Newton iteration we require an initial guess for the h_j. This is quite a nontrivial task, and to do so we use one of two different methods. The first method is to perform a homotopy in the spike locations starting from the symmetric equilibrium solution. The second method is a homotopy in the value of D, starting from a large value of D where $h_j \approx h_\infty$, for some easily determined h_∞, and then to decrease D to the desired value. Sometimes one of these homotopy approaches failed. This is because the linearized system for the h_j is not invertible at certain specific parameter values, as we explain below. Once the nonlinear system for the h_j in (5.27) is solved, the initial condition for $a(x, 0)$ and $h(x, 0)$ is known from (5.20) and the NAG solver [39] is used to compute the solution to (1.17) at later times τ. The locations of the spikes from these numerical results were obtained by a local quadratic interpolation.

The asymptotic results were obtained by solving the differential-algebraic system (5.27) for $x_j(\tau)$ and $h_j(\tau)$ using the ODE solver [42] coupled together with Newton's method to determine the h_j. Another method, which we found to work equally well, is to use the differential-algebraic solver DDASSL [5] directly. The initial values for $h_j(0)$ were obtained using one of the homotopy methods described above. It is very important to calculate the maximum eigenvalue e_m of (5.52) as a function of τ. The curve $e_m = e_m(\tau)$ is computed at each step by using the eigenvalue solver [2]. The asymptotic theory predicts that if $e_m > 2$ at any value of τ, the quasi-equilibrium profile develops an instability on an $O(1)$ time scale. We would like to check this asymptotic prediction with the full numerical results.

In §5.4.1 and §5.4.2 we give asymptotic and numerical results for the case of $n = 2$ and $n = 3$, respectively. Other cases, and some general results, are discussed briefly in §5.4.3.

5.4.1 Two Spikes $n = 2$

When $n = 2$, the nonlinear system in (5.27) for h_j is

$$c_1 h_1 + d_1 h_2 = b_r h_1^{\gamma r - s}/\sqrt{\mu D}\,, \tag{5.54a}$$

$$d_1 h_1 + c_2 h_2 = b_r h_2^{\gamma r - s}/\sqrt{\mu D}\,, \tag{5.54b}$$

where c_j and d_j are defined in (5.25a). From (5.54) we readily obtain an equation for h_1/h_2. The differential equations for x_j in (5.27) depend only on the ratio h_1/h_2. In this way, we obtain the next result.

Corollary 5.3 *When $n = 2$, the differential-algebraic system (5.27) is equivalent to*

$$\dot{x}_1 = -\zeta\left(\tanh[\theta(1+x_1)] - \coth[\theta(x_2-x_1)] + csch[\theta(x_2-x_1)]/\xi\right)\,, \tag{5.55a}$$

$$\dot{x}_2 = -\zeta\left(-csch[\theta(x_2-x_1)]/\xi + \coth[\theta(x_2-x_1)] - \tanh[\theta(1-x_2)]\right)\,, \tag{5.55b}$$

where $\xi \equiv h_1/h_2$ satisfies

$$f(\xi) \equiv csch[\theta(x_2-x_1)]\left(\xi^{\gamma m - s + 1} - 1\right) + \coth[\theta(x_2-x_1)]\left(\xi - \xi^{\gamma m - s}\right)$$
$$+ \tanh[\theta(1+x_1)]\xi - \tanh[\theta(1-x_2)]\xi^{\gamma m - s} = 0\,. \tag{5.55c}$$

Here $\zeta = q\theta/(p-1)$, where $\theta = \sqrt{\mu/D}$.

The behavior of the spike dynamics depends on the value of D with respect to D_b, the initial position of the spikes, and the initial value of e_m at $\tau = 0$. Recall from §4 and (4.116a) that a two-spike symmetric equilibrium solution with spikes located at $x_1 = -x_2 = -1/2$ will be unstable if $D < D_b \approx 0.3218$.

In the special case of symmetric initial data where $x_1(0) = -x_2(0)$, we have that $\xi \equiv 1$ is a root to (5.55c). In this symmetric case, $\xi = 1$ and $x_1 = -x_2$ for all τ. Combining (5.55a) and (5.55b) we obtain the next result.

Corollary 5.4 *Let $n = 2$ and assume that the initial data is symmetric in the sense that*

$x_1(0) = -x_2(0)$. *Let* $y = x_2 - x_1$. *Then, (5.55) is equivalent to the single differential equation*

$$\dot{y} = 2\zeta \left(csch(\theta y) - \coth(\theta y) + \tanh\left[\theta\left(1 - y/2\right)\right]\right) , \tag{5.56}$$

where $\zeta = q\theta/(p-1)$ *and* $\theta = \sqrt{\mu/D}$.

We now gives some examples of the theory.

Example 1 (Symmetric Initial Data): We consider two different cases of symmetric initial data with $x_1(0) = -x_2(0)$. The parameter values are

$$\text{Example 1a:} \qquad x_1(0) = -0.4 = -x_2(0)\,, \qquad D = 0.4\,, \tag{5.57a}$$

$$\text{Example 1b:} \qquad x_1(0) = -0.2 = -x_2(0)\,, \qquad D = 0.1\,, \tag{5.57b}$$

For Examples 1a and 1b we compute numerically that $e_m(0) = 1.944$ and $e_m(0) = 1.793$, respectively. Thus, for both examples, the initial profile is stable with respect to the large $O(1)$ eigenvalues. In Example 1b, $D < D_b$ and in Example 1a, $D > D_b$. Thus, in Example 1a the symmetric equilibrium solution is unstable with respect to the small eigenvalues.

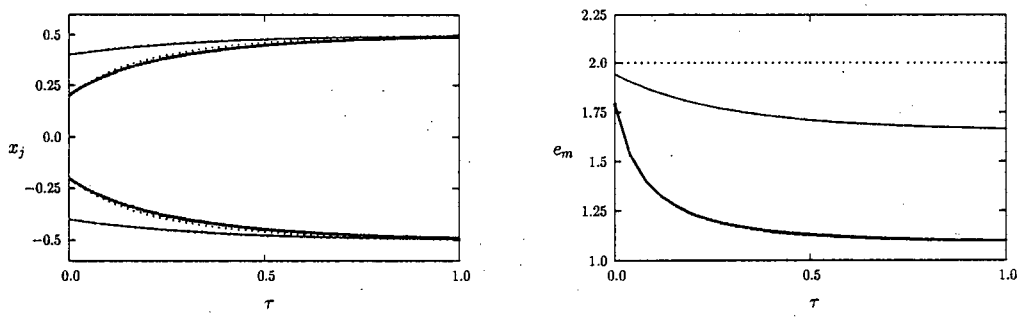

(a) x_j versus τ (b) e_m versus τ

Figure 5.3: In Fig. 5.3(a) we plot x_j versus τ for the two symmetric parameter sets in Example 1. The solid and heavy solid curves correspond to the full numerical results for Example 1a and Example 1b, respectively, given in (5.57). The asymptotic results computed from (5.56) correspond to the dotted curves. In Fig. 5.4(b) we plot the maximum eigenvalue e_m of (5.52) versus τ. The solid and heavy solid curves refer to Example 1a and Example 1b.

τ	x_1 (num)	x_2 (num)	x_1 (asy)	x_2 (asy)
0.06	-0.4163	0.4163	-0.4157	0.4157
0.09	-0.4238	0.4238	-0.4225	0.4225
0.18	-0.4419	0.4419	-0.4399	0.4399
0.27	-0.4557	0.4557	-0.4535	0.4535
0.36	-0.4662	0.4662	-0.4639	0.4639
0.45	-0.4742	0.4742	-0.4721	0.4721
0.54	-0.4803	0.4803	-0.4783	0.4783
0.63	-0.4850	0.4850	-0.4832	0.4832

Table 5.1: The numerical and asymptotic results for x_1 and x_2 versus τ for Example 1a.

The asymptotic result for these two examples is obtained by integrating (5.56). From (5.56) we observe that, for any initial data $y(0) > 0$ and *any value* of D, the solution satisfies $y \to 1$ as $\tau \to \infty$. Hence, for symmetric initial data, $x_1 \to -1/2$ and $x_2 \to 1/2$ as $\tau \to \infty$ for both Example 1a and Example 1b. To attempt to explain this paradox, we refer to Proposition 4.11 of §4 where it was shown that when $D > D_b$ there is exactly one positive and one negative small eigenvalue for the linearization of (1.17) about the two-spike symmetric equilibrium solution. The positive eigenvalue becomes negative when D crosses below D_b. Thus, when $D > D_b$, the symmetric equilibrium corresponds to a saddle point in phase-space with one only stable direction towards the equilibrium. Thus, we conjecture that by taking symmetric initial data we approach the equilibrium solution along the stable manifold. In Example 4 below we show that we do not tend to a symmetric equilibrium solution when we make a slight perturbation to symmetric initial data when $D > D_b$.

For Examples 1a and 1b, in Fig. 5.3(a) we compare the trajectories $x_j(\tau)$ for $j = 1, 2$ computed from the asymptotic result (5.56) with the full numerical results computed from (1.17). Selected values for x_j from the asymptotic and full numerical results are shown in Table 5.1 and Table 5.2 for Examples 1a and 1b, respectively. The agreement is found to be close. In Fig. 5.3(b) we plot $e_m = e_m(\tau)$ for both examples. The threshold for an $O(1)$ instability is given by the

τ	x_1 (num)	x_2 (num)	x_1 (asy)	x_2 (asy)
0.06	−0.2762	0.2762	−0.2670	0.2670
0.12	−0.3283	0.3283	−0.3146	0.3146
0.24	−0.3946	0.3946	−0.3779	0.3779
0.36	−0.4337	0.4337	−0.4177	0.4177
0.42	−0.4472	0.4472	−0.4321	0.4321
0.48	−0.4579	0.4579	−0.4439	0.4439
0.66	−0.4786	0.4786	−0.4681	0.4681
0.78	−0.4863	0.4863	−0.4781	0.4781

Table 5.2: The numerical and asymptotic results for x_1 and x_2 versus τ for Example 1b.

dotted line in Fig. 5.3(b). Notice that e_m decreases as τ increases, so that no $O(1)$ instability occurs at later times. In Fig. 5.4(a) and Fig. 5.4(b) we plot the numerical solution a versus x at different values of τ for Example 1a and Example 1b, respectively.

Example 2: (Generic Initial Data) We consider two sets of generic initial data. The parameter values are taken to be

$$\text{Example 2a:} \qquad x_1(0) = -0.2\,, \quad x_2(0) = 0.32\,, \qquad D = 0.1\,, \tag{5.58a}$$

$$\text{Example 2b:} \qquad x_1(0) = -0.8\,, \quad x_2(0) = 0.2\,, \qquad D = 0.2\,, \tag{5.58b}$$

For Examples 2a and 2b we compute numerically that $e_m(0) = 1.4846$ and $e_m(0) = 1.4106$, respectively. Thus, for both examples, the initial profile is stable with respect to the large $O(1)$ eigenvalues. For both examples $D < D_b$ so that the symmetric equilibrium solution is stable.

For Examples 2a and 2b, in Fig. 5.5(a) we compare the trajectories $x_j(\tau)$ for $j = 1, 2$ computed from the asymptotic result (5.55) with the full numerical results computed from (1.17). Selected values for x_j from the asymptotic and full numerical results are shown in Table 5.3 and Table 5.4 for Examples 2a and 2b, respectively. As seen in Fig. 5.5(b) the maximum eigenvalue once again decreases as τ increases and so no $O(1)$ instability is triggered. In Fig. 5.6(a) and

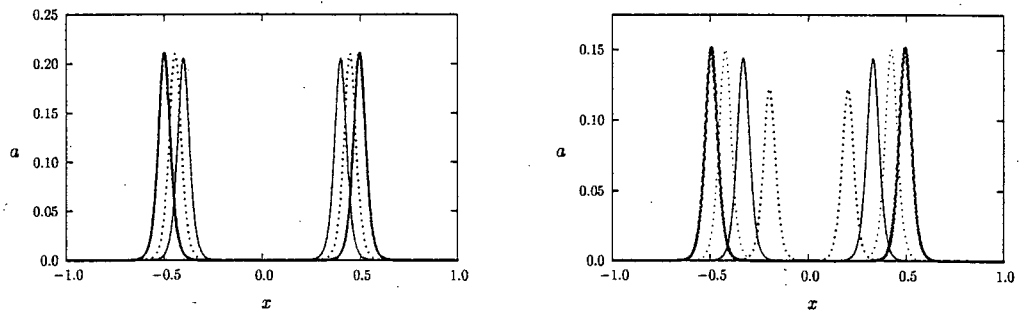

(a) a versus x at different τ (Example 1a) (b) a versus x at different τ (Example 1b)

Figure 5.4: The numerical results for a versus x at different values of τ are plotted in Fig. 5.4(a) for Example 1a and in Fig. 5.4(b) for Example 1b. In Fig. 5.4(a) the solid, dotted, and heavy solid curves correspond to $\tau = 0.0$, $\tau = .202$, and $\tau = 1.202$, respectively. In Fig. 5.4(b) the dotted, solid, light dotted, and heavy solid curves correspond to $\tau = 0.0$, $\tau = .123$, $\tau = .321$, and $\tau = 1.002$, respectively.

Fig. 5.6(b) we plot the numerical solution a versus x at different values of τ for Example 2a and Example 2b, respectively.

Example 3: (An Initial $O(1)$ Instability) We take the parameter values

$$x_1(0) = -0.2\,, \quad x_2(0) = 0.32\,, \qquad D = 0.25\,. \tag{5.59}$$

In this case, we compute numerically that $e_m(0) = 2.228$, so that the initial profile is unstable with respect to the large positive eigenvalues. Since $e_m(0) > 0$, the asymptotic result (5.55) does not apply.

In Fig. 5.7(a) we plot the numerically computed a versus x for $\tau = 0$ and for several very small values of τ. In terms of t, the plots in Fig. 5.7(a) are for $t < 20.0$. What we observe is that the smaller of the initial two spikes starts collapsing but that its locations remains quite fixed during the collapse. The other spike grows during the collapse of its neighbor. This type of collapse behavior is qualitatively very different than internal layer collapse behavior for phase transition models (see [47]). After one of the spikes has collapsed, the other one moves very slowly towards the symmetric one-spike equilibrium solution centered at the origin. This is

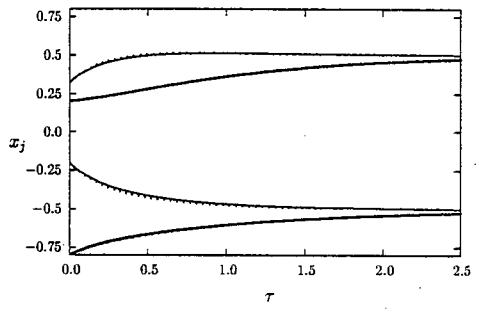

(a) x_j versus τ

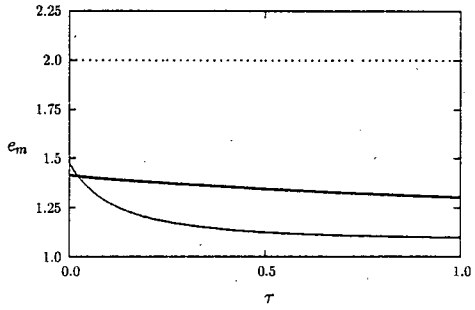

(b) e_m versus τ

Figure 5.5: In Fig. 5.5(a) we plot x_j versus τ for the two parameter sets in Example 2. The solid and heavy solid curves correspond to the full numerical results for Example 2a and Example 2b, respectively, given in (5.58). The asymptotic results computed from (5.55) correspond to the dotted curves. In Fig. 5.5(b) we plot the maximum eigenvalue e_m of (5.52) versus τ. The solid and heavy solid curves refer to Example 2a and Example 2b.

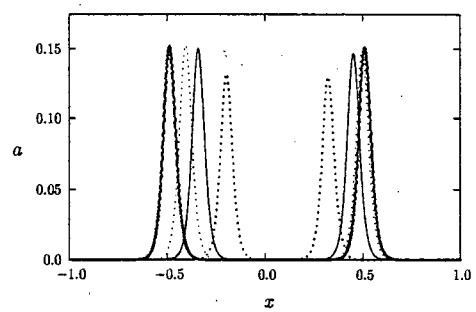

(a) a versus x at different τ (Example 2a)

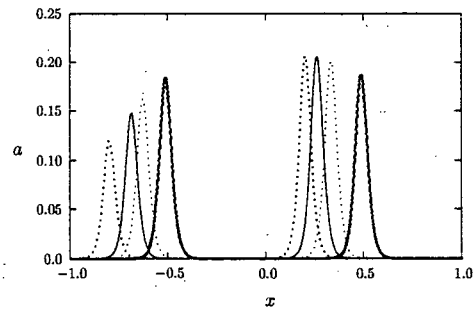

(b) a versus x at different τ (Example 2b)

Figure 5.6: The numerical results for a versus x at different values of τ are plotted in Fig. 5.6(a) for Example 2a and in Fig. 5.6(b) for Example 2b. In Fig. 5.6(a) the dotted, solid, light dotted, and heavy solid curves correspond to $\tau = 0.0$, $\tau = .202$, $\tau = .403$, and $\tau = 1.402$, respectively. In Fig. 5.6(b) the dotted, solid, light dotted, and heavy solid curves correspond to $\tau = 0.0$, $\tau = .404$, $\tau = .804$, and $\tau = 3.200$, respectively.

τ	x_1 (num)	x_2 (num)	x_1 (asy)	x_2 (asy)
0.032	−0.2329	0.3526	−0.2284	0.3480
0.08	−0.2724	0.3906	−0.2634	0.3817
0.30	−0.3782	0.4789	−0.3622	0.4667
0.40	−0.4051	0.4954	−0.3892	0.4853
0.48	−0.4218	0.5036	−0.4063	0.4953
0.60	−0.4410	0.5104	−0.4265	0.5048
0.80	−0.4619	0.5138	−0.4500	0.5118
1.28	−0.4856	0.5100	−0.4788	0.5117

Table 5.3: The numerical and asymptotic results for x_1 and x_2 versus τ for Example 2a.

shown in Fig. 5.7(b).

Example 4: (An O(1) Instability at a Later Time) We consider a case with near symmetric initial data, where we take

$$x_1(0) = -0.4\,, \qquad x_2(0) = .401\,, \qquad D = 0.4\,. \tag{5.60}$$

In this case, we compute that $e_m(0) = 1.941$, so that the initial profile is stable with respect to the large eigenvalues. However as time increases, the profile will become unstable with respect to the large eigenvalues before reaching equilibrium.

The results from these computations are plotted in Figures 5.8(a) and 5.8(b). Initially, the numerical results from the full system and the asymptotic system agree. However, at a later time these results start to diverge and one of the spikes from the numerical computation becomes unstable before the predicted asymptotic time. We speculate that the reason for this is that the nearly symmetric initial data is very close to the stable manifold and thus remains close to the stable manifold for some time. As the solution moves away from the stable manifold, errors in the simulation as well as differences between the asymptotic and full system begin to grow rapidly. We conjecture that it is this growth in errors that is responsible for the discrepancies between the simulation of the full system and that of the asymptotic differential equations.

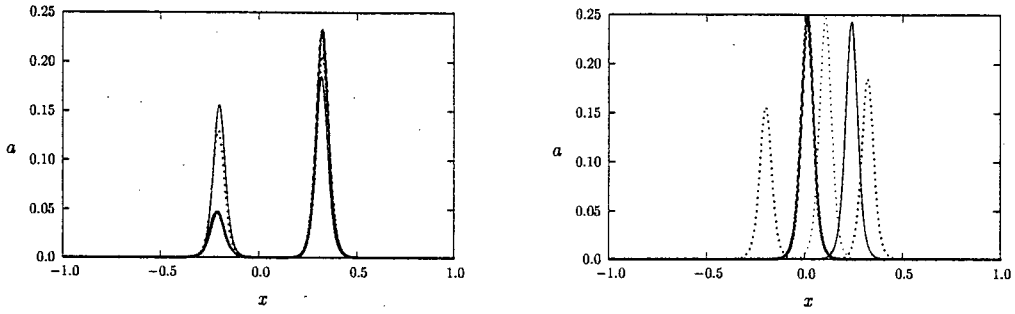

(a) a versus x (collapse event)

(b) a versus x (one-spike motion)

Figure 5.7: The numerical results for a versus x at different values of τ are plotted for Example 3. In Fig. 8a, where we show the collapse event, the solid, dotted, and heavy solid curves correspond to $\tau = 0.0$, $\tau = 0.00504$, and $\tau = 0.00704$, respectively. In Fig. 8b, where one spike drifts towards the origin, the solid, light dotted, and heavy solid curves correspond to $\tau = 0.4$, $\tau = 1.6$, and $\tau = 4.8$, respectively. The initial condition at $\tau = 0$ is the dotted curve.

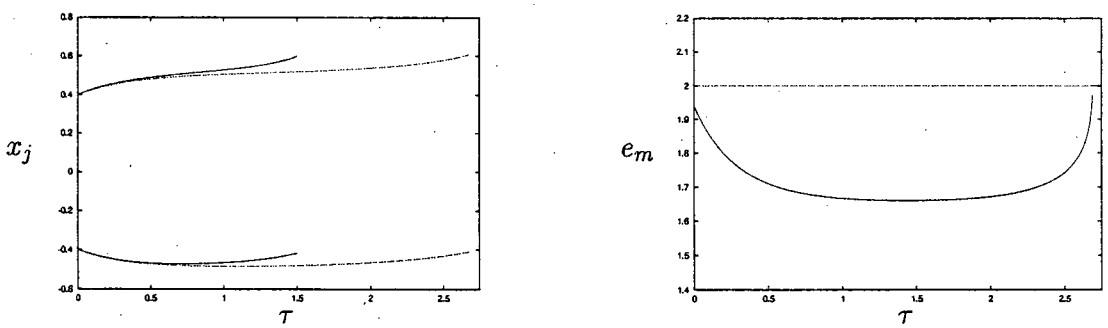

(a) x_j versus τ

(b) e_m versus τ

Figure 5.8: In Fig. 5.8(a) we plot x_j versus τ for Example 4. The solid curve corresponds to the full numerical results and the dotted curves corresponds to the asymptotic results. In Fig. 5.8(b), we plot the maximum eigenvalue e_m of (5.52) versus τ.

τ	x_1 (num)	x_2 (num)	x_1 (asy)	x_2 (asy)
0.06	−0.6556	0.2161	−0.6528	0.2157
0.66	−0.6171	0.3400	−0.6136	0.3383
0.84	−0.6003	0.3678	−0.5981	0.3657
1.00	−0.5866	0.3891	−0.5854	0.3868
1.40	−0.5585	0.4299	−0.5589	0.4273
1.60	−0.5476	0.4445	−0.5485	0.4420
1.90	−0.5347	0.4611	−0.5359	0.4588
2.50	−0.5180	0.4808	−0.5192	0.4793

Table 5.4: The numerical and asymptotic results for x_1 and x_2 versus τ for Example 2b.

5.4.2 Three Spikes $n = 3$

Example 5 (Symmetric Initial Data): We now consider the case of three spikes with symmetric initial data (i.e. $x_1(0) = -x_3(0)$ and $x_2(0) = 0$). In this case the two outer spikes will be of the same height, however the middle spike will generally be of a different height. Thus, unlike the case of two spikes with symmetric initial data, we can not reduce this differential algebraic system to a single ordinary differential equation. Another important difference between the case of two and three spikes with symmetric initial data is in the form of the stable and unstable manifolds with respect to the small eigenvalues. In the case of two spikes both the stable and unstable manifolds have one dimension. In the case of three spikes, we have a one dimensional stable manifold and a two dimensional unstable manifold. In this case, it appears that symmetric solutions are not confined to the stable manifold. To illustrate this, in this example we take the values

$$x_1(0) = -0.5\,, \quad x_2(0) = 0\,, \quad x_3(0) = 0.5\,, \quad D = 0.01\,. \tag{5.61}$$

The results of the simulations are given in Fig. 5.9.

τ	x_1 (num)	x_2 (num)	x_1 (asy)	x_2 (asy)
0.004	−0.40126	0.40226	−.40762	0.42297
0.032	−0.40894	0.41053	−.40618	0.42048
0.052	−0.41390	0.41614	−.40971	0.42662
0.08	−0.42032	0.42351	−.41423	0.43476
0.1	−0.42455	0.42844	−.41717	0.44026
0.3	−0.45404	0.46566	−.43574	0.48466
0.6	−0.47031	0.49756	−.43768	0.53190
0.988	−0.46514	0.52649	−.40640	0.59999

Table 5.5: The numerical and asymptotic results for x_1 and x_2 versus τ for Example 4.

Example 6 (Generic Initial data) We now compare simulations of (1.17) with (5.27) for the case of generic initial data. We use the parameters,

$$x_1(0) = -0.5\,, \qquad x_2(0) = 0.1\,, \qquad x_3(0) = 0.5\,, \qquad D = 0.04\,. \tag{5.62}$$

For these parameters, we calculate $e_m(0) = 1.6935$. As seen in Fig. 5.10(b) e_m once again decreases as τ increases, thus the profile is stable with respect to the large eigenvalues and no $O(1)$ instability is triggered. Asymptotic and numerical results for x_j are compared in Table 5.7.

5.4.3 Conclusions

In this section we give two results related to the dynamics of n-spike profiles which are not of sufficient importance to warrant a section of thier own. Firstly, we note that the simulation in Fig. 5.4.1 stops just as e_m approaches the critical value. The simulation stops here not only because the system is no longer valid, but at this value the nonlinear solver for the h system fails to converge. We will demonstrate that when e_m is at the critical value the system is no longer solvable. Finally we discuss the role of the $O(1)$ eigenvalues on the dynamics of the system.

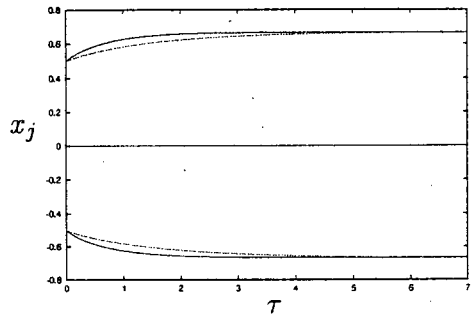

(a) x_j versus τ

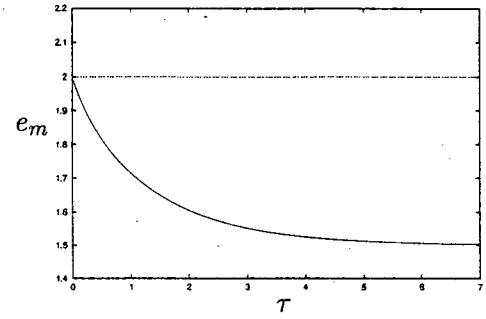

(b) e_m versus τ

Figure 5.9: In Fig. 5.9(a) we plot x_j versus τ for Example 5. The solid curve corresponds to the full numerical results and the dotted curves corresponds to the asymptotic results. In Fig. 5.9(b), we plot the maximum eigenvalue e_m of (5.52) versus τ.

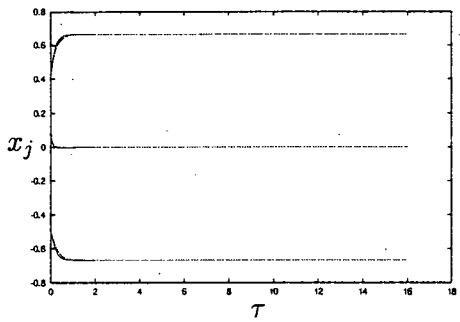

(a) x_j versus τ

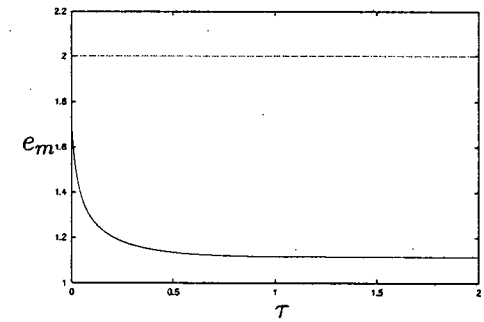

(b) e_m versus τ

Figure 5.10: In Fig. 5.10(a) we plot x_j versus τ for Example 6. The solid curve corresponds to the full numerical results and the dotted curves corresponds to the asymptotic results. In Fig. 5.10(b), we plot the maximum eigenvalue e_m of (5.52) versus τ.

τ	x_1 (num)	x_2 (num)	x_3 (num)	x_1 (asy)	x_2 (asy)	x_3 (asy)
0.004	−0.50134	0.0	0.50134	−0.50053	0.0	0.50053
0.1	−0.52484	0.0	0.52484	−0.51239	0.0	0.51239
0.2	−0.54443	0.0	0.54443	−0.52340	0.0	0.52340
0.3	−0.56064	0.0	0.56064	−0.53328	0.0	0.53328
0.4	−0.57434	0.0	0.57434	−0.54224	0.0	0.54224
0.5	−0.58615	0.0	0.58615	−0.55041	0.0	0.55041
0.6	−0.59638	0.0	0.59638	−0.55792	0.0	0.55792
0.7	−0.60535	0.0	0.60535	−0.56485	0.0	0.56485

Table 5.6: The numerical and asymptotic results for x_1, x_2 and x_3 versus τ for Example 5.

Solvability of (5.21) at critical values of e_m

We now demonstrate why the system (5.21a) is not solvable at the critical value of e_m. We begin by considering the system linearized about a solution. We begin by linearizing the system about

$$\boldsymbol{h} = \bar{\boldsymbol{h}} + \boldsymbol{\theta}\,, \tag{5.63}$$

where $\bar{\boldsymbol{h}}$ is a solution at the critical value of e_m and $\boldsymbol{\theta} \ll \bar{\boldsymbol{h}}$. Substituting into (5.21), we get

$$\left(\mathcal{B} - \frac{b_m(\gamma m - s)}{\sqrt{\mu D}}\mathcal{H}^{\gamma m - s - 1}\right)\boldsymbol{\theta} = 0\,. \tag{5.64}$$

From (5.52) and (5.53) we can see that this equation has a non-trivial solution at exactly the critical value of e_m. This implies that the Jacobian of (5.21a) is not invertible when $e = e_m$. Thus, this system does not have a unique solution at this point.

Role of the $O(1)$ Eigenvalues in the Dynamics

From the numerical experiments shown above, and further computations, we speculate that when we are above the threshold of $O(1)$ stability from (5.53) for an n-spike profile, at least one of the spikes collapse as the remaining spikes grow. At the end of this collapses time interval,

τ	x_1 (num)	x_2 (num)	x_3 (num)	x_1 (asy)	x_2 (asy)	x_3 (asy)
0.004	−0.50186	0.09228	0.40912	−0.50112	0.09354	0.40539
0.3	−0.62535	−0.00145	0.61632	−0.60449	0.00270	0.59417
0.6	−0.66074	−0.00230	0.65767	−0.65005	−0.00103	0.64704
0.9	−0.66631	−0.00143	0.66480	−0.66286	−0.00103	0.66150
1.2	−0.66692	−0.00818	0.66609	−0.66597	−0.00072	0.66520
1.5	−0.66688	−0.00046	0.66642	−0.66665	−0.00047	0.66617
1.8	−0.66680	−0.00026	0.66654	−0.66676	−0.00031	0.66645

Table 5.7: The numerical and asymptotic results for x_1, x_2 and x_3 versus τ for Example 6.

the profile again becomes stable, and the remaining spikes will then follow the dynamics of (5.21).

Chapter 6

Spike Pinning for the Gierer-Meinhardt Model

In this chapter we examine the effects of spatially varying coefficients in (1.18) and (1.17). The spatial variations can results from pre-existing polarities in the cells and can have dramatic effects on the dynamics and equilibrium positions of the cell. We now give a detailed outline of this chapter.

In §6.2 we examine the effect of a spatially variable inhibitor decay rate $\mu = \mu(x) > 0$ and a spatially variable activator decay rate $V(x)$ on the dynamics and equilibrium position of a one-spike solution to (1.17). In the biological context, these terms are examples of precursor gradients. The significance of precursor gradients from a biological viewpoint is discussed in [16]. From a mathematical viewpoint, we show that the effect of a spatially varying μ is to perturb the equilibrium location for a one-spike solution away from the midpoint of the interval. The exact equilibrium location now depends on certain global properties of $\mu(x)$ over the domain. The effect of a spatially varying activator decay rate also perturbs the equilibrium location, but the perturbation depends on local properties of $V(x)$.

In §6.1 we consider a related problem with a spatially inhomogeneous coefficient. Specifically, we now let μ be spatially uniform and we consider the shadow problem (1.18). A weak spatially inhomogeneous diffusivity for the activator equation is then introduced. This leads to the

perturbed shadow problem, defined by the scalar nonlocal problem

$$a_t = \frac{\epsilon^2}{\kappa}\left(\kappa a_x\right)_x - a + \frac{a^p}{h^q}, \qquad -1 < x < 1, \quad t > 0, \tag{6.1a}$$

$$h = \left(\frac{\epsilon^{-1}}{2\mu}\int_{-1}^{1} a^r\, dx\right)^{\frac{1}{s+1}}, \qquad a_x(\pm 1, t) = 0. \tag{6.1b}$$

The motivation for this form of κ is mentioned below in context with a related problem studied in [44] for the Ginzburg-Landau equation. When $\kappa \equiv 1$ in (6.1a) it was shown using formal asymptotic in §2, and then proved later in [7], that (6.1) admits a one-spike solution that drifts exponentially slowly towards the closest endpoint of the domain. In addition, the equilibrium one-spike solution, which is centered at $x = 0$, is unstable. The metastable behavior associated with (6.1) when $\kappa \equiv 1$ suggests that exponentially small changes in $\kappa - 1$ should influence the metastable dynamics greatly. Therefore, in §2 we study the dynamics of a one-spike solution for (6.1) as $\epsilon \to 0$ for a $\kappa(x;\epsilon)$ of the form

$$\kappa(x;\epsilon) = 1 + \epsilon^{\nu} g(x) e^{-\epsilon^{-1} d}. \tag{6.1c}$$

Here ν and $d > 0$ are constants and $g(x)$ is smooth. When $g''(x) < 0$ and $0 < d < d_c$, where d_c is some constant, we show in §2 that (6.1) can have a stable spatially inhomogeneous equilibrium one-spike solution where the spike is centered at a zero of $g'(x)$. Results for this problem are given in Propositions 6.1 and 6.2 below. This effect whereby a localized structure is stabilized by a weak but spatially inhomogeneous coefficient in the differential operator is called pinning.

The effect of weak spatially inhomogeneous terms has been examined in other contexts, including the pinning of vortices in superconductivity (cf. [6], [29]) and the pinning of an interface for the Ginzburg Landau equation posed in a thin cylinder of revolution, modeled by (cf. [44])

$$u_t = \frac{\epsilon^2}{A}\left(A u_x\right)_x + 2(u - u^3), \quad -1 < x < 1; \qquad u_x(\pm 1, t) = 0. \tag{6.2}$$

This equation was derived in the thin channel limit in [44]. In this context, x is the direction along the axis of the cylinder and $A = A(x;\epsilon)$ denotes the slowly varying cross-sectional area of the cylinder. For this problem, it was shown in [44] that an internal layer solution can be stabilized by an exponentially weak non-convex perturbation of a straight cylindrical domain

by taking $A(x;\epsilon)$ to have the form $A(x;\epsilon) = 1 + \epsilon^{\nu} e^{-d/\epsilon} g(x)$, where $g''(x) < 0$ and $d > 0$. A similar pinning result is obtained for spike solutions of the related problem (6.1).

6.1 One-Spike Dynamics: The Perturbed Shadow Problem

In this section we construct a one-spike solution to (6.1). When $\kappa \equiv 1$ in (6.1), the resulting unperturbed problem admits a quasi-equilibrium one-spike solution of the form (see §2)

$$a \sim a_e(x;x_0) \equiv h_e^{q/(p-1)} u_c\left[\epsilon^{-1}(x-x_0)\right], \tag{6.3a}$$

$$h \sim h_e \equiv \left(\frac{b_r}{2\mu}\right)^{\frac{p-1}{(s+1)(p-1)-qr}}, \qquad \text{where} \quad b_r \equiv \int_{-\infty}^{\infty} [u_c(y)]^r \, dy. \tag{6.3b}$$

Here $u_c(y)$ is the unique positive solution to

$$u_c'' - u_c + u_c^p = 0, \qquad -\infty < y < \infty, \tag{6.4a}$$

$$u_c'(0) = 0; \qquad u_c(y) \sim \alpha e^{-|y|}, \qquad \text{as} \quad y \to \pm\infty, \tag{6.4b}$$

for some $\alpha > 0$. The function a_e is called the quasi-equilibrium one-spike solution to (6.1) since a_e has exactly one localized maximum and it fails to satisfy the steady-state problem corresponding to (6.1) by only exponentially small terms as $\epsilon \to 0$ for any value of x_0 in $|x_0| < 1$.

For the time-dependent problem, our goal is to derive an asymptotic differential equation for the trajectory $x = x_0(t)$ of the localized maximum of a_e, which represents the center of the spike. Since $\kappa - 1$ is exponentially small, we begin by linearizing (6.1) in the form

$$a(x,t) = a_e\left[x; x_0(t)\right] + w(x,t), \tag{6.5}$$

where $w \ll a_e$. Substituting (6.5) into (6.1), we get the linearized problem for w

$$L_\epsilon w = \partial_t a_e + \partial_t w - \epsilon^2 \kappa_x \kappa^{-1} \partial_x a_e, \qquad -1 < x < 1, \quad t \geq 0, \tag{6.6a}$$

$$w_x(\pm 1, t) = -\partial_x a_e(\pm 1; x_0), \tag{6.6b}$$

where the nonlocal operator L_ϵ is defined by

$$L_\epsilon \phi \equiv \frac{\epsilon^2}{\kappa}(\kappa \phi_x)_x - \phi + p u_c^{p-1}\phi - \frac{rq\epsilon^{-1}u_c^p}{b_r(s+1)} \int_{-1}^{1} u_c^{r-1}\phi \, dx. \tag{6.6c}$$

Here b_r is defined in (6.3b). The coefficients in the operator L_ϵ are localized near $x = x_0$ since $u_c = u_c\left[\epsilon^{-1}(x - x_0)\right]$.

6.1.1 Exponentially Small Eigenvalue

Let $x_0 \in (-1, 1)$ be fixed and consider the eigenvalue problem

$$L_\epsilon \phi = \lambda \phi \qquad -1 < x < 1\,; \qquad \phi_x(\pm 1) = 0\,. \tag{6.7}$$

When $\kappa \equiv 1$, it was shown in §2 that, under the conditions on p and r given in (2.13a) below, the eigenvalue of (6.7) with the largest real part is exponentially small as $\epsilon \to 0$ and the corresponding eigenfunction is localized near $x = x_0$. We will estimate the change in this exponentially small eigenvalue as a result of the exponentially small perturbation $\kappa - 1$. To do so, we let $\kappa = 1$ and proceed as in §2 by introducing the localized eigenvalue problem for $\Phi = \Phi(y)$ given by

$$\mathcal{L}_0 \Phi = \sigma \Phi \quad -\infty < y < \infty\,; \qquad \Phi \to 0 \quad \text{exponentially} \quad \text{as} \quad y \to \pm\infty\,, \tag{6.8}$$

where $y = \epsilon^{-1}(x - x_0)$. Here $\mathcal{L}_0$ is defined by

$$\mathcal{L}_0 \Phi \equiv \Phi_{yy} - \Phi + p u_c^{p-1} \Phi - \frac{r q u_c^p}{b_r (s+1)} \int_{-\infty}^{\infty} u_c^{r-1} \Phi \, dy\,, \tag{6.9}$$

where $u_c = u_c(y)$. Results on the spectrum of (6.9) were given in Theorem 2.1 in §2.

The effects of the exponentially small perturbation $\kappa - 1$ and of the finite domain in (6.7) perturb this eigenvalue σ_0 by exponentially small terms as $\epsilon \to 0$. Let the perturbed eigenpair be denoted by λ_0 and ϕ_0. In order that ϕ_0 satisfy the boundary condition on $x = \pm 1$, we proceed as in §2 by constructing ϕ_0 in the boundary layer form

$$\phi_0 \sim u_c'\left[\epsilon^{-1}(x - x_0)\right] + \phi_{L0}\left[\epsilon^{-1}(1 + x)\right] + \phi_{R0}\left[\epsilon^{-1}(1 - x)\right], \tag{6.10a}$$

where

$$\phi_{L0}(\eta) = \alpha e^{-\epsilon^{-1}(1+x_0)} e^{-\eta}\,, \qquad \phi_{R0}(\eta) = -\alpha e^{-\epsilon^{-1}(1-x_0)} e^{-\eta}\,. \tag{6.10b}$$

To estimate λ_0 we first define the inner product $(u,v)_\kappa \equiv \int_{-1}^{1} uv\kappa\, dx$. Integrating by parts, we obtain for any two functions ϕ and ψ that

$$(L_\epsilon\phi,\psi)_\kappa = \epsilon^2\kappa\left(\phi_x\psi - \phi\psi_x\right)|_{-1}^{1} + (\phi, L_\epsilon^*\psi)\,, \tag{6.11}$$

where L_ϵ^* is the adjoint operator defined by

$$L_\epsilon^*\psi \equiv \frac{\epsilon^2}{\kappa}\left(\kappa\psi_x\right)_x - \psi + pu_c^{p-1}\psi - \frac{rq\epsilon^{-1}u_c^{r-1}}{b_r\kappa(s+1)}\int_{-1}^{1}\kappa u_c^p\psi\, dx\,. \tag{6.12}$$

Now let $\psi = u_c'$ and $\phi = \phi_0$. Then, since $\phi_{0x}(\pm 1) = 0$, we get from (6.11) that

$$\lambda_0\left(\phi_0, u_c'\right)_\kappa + \epsilon\kappa\phi_0 u_c''|_{-1}^{1} = \epsilon\left(\frac{\kappa_x u_c''}{\kappa}, \phi_0\right)_\kappa - \frac{rq\epsilon^{-1}}{b_r(s+1)}\left(\int_{-1}^{1}\phi_0 u_c^{r-1}\, dx\right)\left(\int_{-1}^{1}\kappa u_c^p u_c'\, dx\right)\,. \tag{6.13}$$

The two terms on the left side of (6.13) can be estimated as in §2 by using (6.10) for ϕ_0 and (6.4) for $u_c''(y)$ as $y \to \pm\infty$. The exponentially small perturbation $\kappa - 1$ does not affect the leading order asymptotic estimates for these quantities. Thus, for $\epsilon \to 0$, we get

$$\left(\phi_0, u_c'\right)_\kappa \sim \epsilon\beta_0\,, \qquad \beta_0 \equiv \int_{-\infty}^{\infty}\left[u_c'(y)\right]^2 dy\,, \tag{6.14a}$$

$$-\epsilon\kappa\phi_0 u_c''|_{-1}^{1} \sim 2\epsilon\alpha^2\left(e^{-2\epsilon^{-1}(1+x_0)} + e^{-2\epsilon^{-1}(1-x_0)}\right)\,. \tag{6.14b}$$

Next, we use (6.1c) to asymptotically estimate the first term on the right side of (6.13) as

$$\epsilon\left(\frac{\kappa_x u_c''}{\kappa}, \phi_0\right)_\kappa \sim \epsilon^{2+\nu}e^{-d/\epsilon}\int_{-\infty}^{\infty} g'(x_0+\epsilon y)u_c'(y)u_c''(y)\, dy\,. \tag{6.15}$$

Expanding g in a Taylor series, and using the fact that $u_c(y)$ is even, we integrate by parts to get

$$\epsilon\left(\frac{\kappa_x u_c''}{\kappa}, \phi_0\right)_\kappa \sim -\frac{\epsilon^{2+\nu}e^{-d/\epsilon}}{2}\sum_{j=0}^{\infty}\frac{\epsilon^{2j+1}}{(2j)!}g^{(2j+2)}(x_0)\beta_j\,, \qquad \beta_j \equiv \int_{-\infty}^{\infty} y^{2j}\left[u_c'(y)\right]^2 dy\,. \tag{6.16}$$

For the exponentially small perturbation $\kappa - 1$ to have a significant effect on the eigenvalue for at least some values of x_0 we must balance the exponential orders of (6.14b) and (6.16). Thus, for $\epsilon \to 0$ we take d to satisfy

$$0 < d \le 2 - c\epsilon\log\epsilon\,, \tag{6.17}$$

for some c independent of ϵ. With this restriction on d, the last term on the right side of (6.13) is estimated for $\epsilon \to 0$ as

$$\frac{rq\epsilon^{-1}}{b_r(s+1)}\left(\int_{-1}^{1}\phi_0 u_c^{r-1}\,dx\right)\left(\int_{-1}^{1}\kappa u_c^p u_c'\,dx\right) = O\left(\epsilon^q \max\left\{e^{-(r+d)\epsilon^{-1}(1+x_0)}, e^{-(r+d)\epsilon^{-1}(1-x_0)}\right\}\right), \tag{6.18}$$

for some q. Since $r > 0$, we conclude that the term in (6.18) is asymptotically smaller as $\epsilon \to 0$ than the inner product term in (6.16). Finally, substituting (6.14) and (6.16) into (6.13), and neglecting the last term on the right side of (6.13), we obtain the following main result for λ_0:

Proposition 6.1 (Exponentially Small Eigenvalue) *Let (2.13a) and (6.17) be satisfied. Then, for $\epsilon \to 0$ the eigenvalue λ_0 of (6.7) with the largest real part is exponentially small and it has the asymptotic estimate*

$$\lambda_0 = \lambda_0(x_0) \sim \frac{2\alpha^2}{\beta_0}\left(e^{-2\epsilon^{-1}(1+x_0)} + e^{-2\epsilon^{-1}(1-x_0)}\right) - \frac{\epsilon^{1+\nu}e^{-d/\epsilon}}{2\beta_0}\sum_{j=0}^{\infty}\frac{\epsilon^{2j+1}}{(2j)!}g^{(2j+2)}(x_0)\beta_j\,. \tag{6.19}$$

Here α is defined in (6.4) and β_j for $j \geq 0$ is defined in (6.16).

From the calculations above we observe that the nonlocal term in L_ϵ, which is not self-adjoint, does not influence the leading order asymptotic estimate for the exponentially small eigenvalue. Hence, the adjoint operator L_ϵ^* also has an exponentially small eigenvalue with the same estimate as that given in (6.19).

6.1.2 The Metastable Spike Motion

We now derive an ODE for $x_0(t)$ from (6.6). Assume that $w(x,0) = 0$ in (6.6) so that the initial condition for (6.1) is a spike-layer solution with spike center initially located at $x_0(0) = x_0^0 \in (-1,1)$. Since the principal eigenvalue of L_ϵ is exponentially small we can assume that the motion is quasi-steady by neglecting $\partial_t w$ in (6.6). To ensure that w is uniformly small over exponentially long time intervals, we must impose the condition that w is orthogonal to ϕ_0.

To derive an ODE for $x_0(t)$ we begin by using (6.11) with $\psi = \phi_0$ and $w = \phi$ to get

$$(L_\epsilon w, \phi_0)_\kappa = \epsilon^2\kappa\phi_0 w_x|_{-1}^{1} + (w, L_\epsilon^*\phi_0)_\kappa\,. \tag{6.20}$$

Using the remark following (6.19) above, we get $(w, L_\epsilon^* \phi_0) \sim \lambda_0 (w, \phi_0) = 0$ by our condition of orthogonality. From this condition, and by using (6.3a) and (6.6), (6.20) reduces to the following implicit differential equation for $x_0(t)$:

$$(\phi_0, \partial_t u_c)_\kappa + \epsilon \kappa \phi_0 u_c' |_{-1}^1 \sim \epsilon \left(\frac{\kappa_x u_c'}{\kappa}, \phi_0 \right)_\kappa . \tag{6.21}$$

The two terms on the left side of (6.21) can be estimated as in §2 by using (6.10) for ϕ_0 and (6.4) for $u_c''(y)$ as $y \to \pm\infty$. For $\epsilon \to 0$, we get

$$(\phi_0, \partial_t u_c)_\kappa \sim -x_0' \beta_0 , \tag{6.22a}$$

$$-\epsilon \kappa \phi_0 u_c' |_{-1}^1 \sim 2\epsilon \alpha^2 \left(e^{-2\epsilon^{-1}(1+x_0)} - e^{-2\epsilon^{-1}(1-x_0)} \right) . \tag{6.22b}$$

Next, for $\epsilon \to 0$, we calculate as in (6.15) that

$$\epsilon \left(\frac{\kappa_x u_c'}{\kappa}, \phi_0 \right)_\kappa \sim \epsilon^{2+\nu} e^{-d/\epsilon} \int_{-\infty}^{\infty} g'(x_0 + \epsilon y) \left[u_c'(y) \right]^2 dy \sim \epsilon^{2+\nu} e^{-d/\epsilon} \sum_{j=0}^{\infty} \frac{\epsilon^{2j}}{(2j)!} g^{(2j+1)}(x_0) \beta_j . \tag{6.23}$$

Finally, substituting (6.22) and (6.23) into (6.21), we obtain the following metastability result for $x_0(t)$:

Proposition 6.2 (Metastability) *Let (2.13a) and (6.17) be satisfied. Then, for $\epsilon \to 0$, the trajectory $x_0(t)$ of the center of the spike for a one-spike solution to (6.1) satisfies the asymptotic differential equation*

$$\frac{dx_0}{dt} \sim h(x_0) \equiv \frac{2\epsilon\alpha^2}{\beta_0} \left(e^{-2\epsilon^{-1}(1-x_0)} - e^{-2\epsilon^{-1}(1+x_0)} \right) - \frac{\epsilon^{2+\nu} e^{-d/\epsilon}}{\beta_0} \sum_{j=0}^{\infty} \frac{\epsilon^{2j}}{(2j)!} g^{(2j+1)}(x_0) \beta_j . \tag{6.24}$$

Here α is defined in (6.4) and β_j for $j \geq 0$ is defined in (6.16).

An important remark, as observed from (6.24), is that the behavior of $x_0(t)$ depends only on pointwise values of certain derivatives of the perturbation $\kappa - 1$. This will be different from the behavior that we will observe in §6.2.

6.1.3 An Example of the Theory

We now discuss the qualitative behavior associated with (6.19) and (6.24). From (6.24) we see that $h(-1) < 0$ and $h(1) > 0$ as $\epsilon \to 0$ when $d > 0$. Thus, there exists at least one equilibrium value x_0^e for $x_0(t)$. The existence of any other equilibria for x_0 depends on the constants d and ν and the function $g'(x)$. In particular, when $d > 0$ is sufficiently small, then (6.24) has an equilibrium point near each zero of $g'(x)$. As shown in the example below, we can have other equilibrium points in the interval $[-1, 1]$ when d is near some critical value.

The next result concerns the stability of the equilibria of (6.24). Let x_0^e satisfy $h(x_0^e)=0$. Then, by comparing (6.19) and (6.24), we find that $h'(x_0^e) = 2\lambda_0(x_0^e)$. This shows that the decay rate for the differential equation (6.24) associated with infinitesimal perturbations about x_0^e is $2\lambda_0(x_0^e)$. This leads to the next result.

Corollary 6.1 (Stability of Equilibrium) *Let x_0^e satisfy $h(x_0^e) = 0$. Then (6.1) has a one-spike equilibrium solution of the form given in (6.3) and this solution is stable (unstable) if $\lambda_0(x_0^e) < 0$ $(\lambda_0(x_0^e) > 0)$. Here $u_c(y)$, $\lambda_0(x_0)$ and $h(x_0)$ are given in (6.4), (6.19) and (6.24).*

Thus a one-spike equilibrium solution centered at x_0^e is unstable when $g''(x_0^e) < 0$. Since $g''(x) < 0$ corresponds to a weakly convex domain, this result predicts that there is no stable spike-layer solutions in such domains. However, when $g''(x_0^e) > 0$, then $\lambda_0(x_0^e)$ can be negative for certain choices of ν and d, resulting in a stable spike-layer solution centered at x_0^e. The key point to construct such a stable equilibrium solution is to guarantee that (6.24) has multiple equilibria corresponding to simple zeroes of $h(x_0)$. Then, we must have exactly one stable equilibrium of (6.24) between every two consecutive unstable equilibria.

To illustrate the result, let $p = 2$ for which $u_c(y) = (3/2)\,\mathrm{sech}^2\,(y/2)$. Then, we calculate from (6.4) and (6.14a) that $\beta_0 = 6/5$ and $\alpha = 6$. Thus, to leading order (6.19) becomes

$$\lambda_0 = \lambda_0(x_0) \sim 60\left(e^{-2\epsilon^{-1}(1+x_0)} + e^{-2\epsilon^{-1}(1-x_0)}\right) - \frac{\epsilon^{\nu+2}}{2} e^{-\epsilon^{-1}d} g''(x_0) + \cdots, \qquad (6.25)$$

and (6.24) reduces to

$$x_0' \sim h(x_0) = 60\epsilon\left(e^{-2\epsilon^{-1}(1-x_0)} - e^{-2\epsilon^{-1}(1+x_0)}\right) - \epsilon^{\nu+2}e^{-\epsilon^{-1}d}g'(x_0) + \cdots . \tag{6.26}$$

Choose $g(x) = x^2/2$, which corresponds to a non-convex domain. In this case, $x_0^e = 0$ is an equilibrium solution to (6.26) for any ν and d. This solution can be stable if d is small enough. From (6.25), we calculate $\lambda_0(0) = -\frac{\epsilon^{\nu+2}}{2}e^{-\epsilon^{-1}d} + 120e^{-2\epsilon^{-1}}$. Let d_c be the zero of $\lambda_0(0)$ as a function of d. Then, $d_c = 2 - \epsilon\log 240 + (\nu+2)\epsilon\log\epsilon$. From Corollary 6.1 it follows that the equilibrium $x_0^e = 0$ is stable (unstable) when $d < d_c$ ($d > d_c$). When $d < d_c$ there are two other equilibrium points for (6.26) on either side of $x = 0$ that are unstable. This example clearly shows the effect of pinning whereby the exponentially weak non-convex perturbation of the original domain leads to a stable one-spike equilibrium solution to the shadow problem (6.1) centered at the midpoint of the domain.

6.2 One-Spike Dynamics: The Perturbed Gierer-Meinhardt Model

We now analyze the effects of spatially varying terms on the full system (1.17). We first examine the effects of a spatially varying inhibitor decay rate $\mu = \mu(x)$. We consider two cases. If $D = O(1)$ we repeat the process used to derive the differential equation governing the motion of the spike from §5.1. The resulting differential equation depends on the global properties of $\mu(x)$ and clearly demonstrates the qualitative effects of the spatially varying coefficient. However, as demonstrated in §4.3, for n-spike solutions to be stable we require that D to be small. Thus we also examine the effect of a spatially varying inhibitor decay rate when D is small. In this case we must use WKB theory to solve the inhibitor equation. (more here). Finally we examine the effect of a spatially varying activator decay rate.

6.2.1 A Spatially Varying Inhibitor Decay Rate When $D = O(1)$

In this section we analyze the dynamics of a one-spike solution to (1.17). For finite inhibitor diffusivity D and for $\mu = \mu(x) > 0$, we derive a differential equation determining the location $x_0(t)$ of the maximum of the activator concentration for a one-spike solution to (1.17).

In the inner region near the spike we introduce the new variables

$$y = \epsilon^{-1}\left[x - x_0(\tau)\right], \qquad \tilde{h}(y) = h(x_0 + \epsilon y), \qquad \tilde{a}(y) = a(x_0 + \epsilon y), \qquad \tau = \epsilon^2 t. \tag{6.27a}$$

We then expand the inner solution as

$$\tilde{h}(y) = \tilde{h}_0(y) + \epsilon\tilde{h}_1(y) + \cdots, \qquad \tilde{a}(y) = \tilde{a}_0(y) + \epsilon\tilde{a}_1(y) + \cdots. \tag{6.27b}$$

The spike location is to satisfy $\tilde{a}_0'(0) = 0$. Substituting (6.27) into (1.17), and collecting terms that are $O(1)$ as $\epsilon \to 0$, we get the leading order problem for $\tilde{a}_0$ and $\tilde{h}_0$:

$$\tilde{a}_0'' - \tilde{a}_0 + \tilde{a}_0^p/\tilde{h}_0^q = 0, \qquad -\infty < y < \infty, \tag{6.28a}$$

$$\tilde{h}_0'' = 0, \tag{6.28b}$$

with $\tilde{a}_0'(0) = 0$. In order to match to the outer solution, to be constructed below, we require that $\tilde{h}_0$ is independent of y. Thus, we set $\tilde{h}_0 = H$, where $H = H(\tau)$ is a function to be determined. We then write the solution to (6.28a) as

$$\tilde{a}_0 = H^\gamma u_c, \qquad \text{where} \qquad \gamma \equiv q/(p-1), \tag{6.29}$$

where u_c satisfies (6.4).

Collecting the $O(\epsilon)$ terms in the inner region expansion, we obtain the problem for $\tilde{a}_1$ and $\tilde{h}_1$,

$$\tilde{a}_1'' - \tilde{a}_1 + \frac{p\tilde{a}_0^{p-1}}{\tilde{h}_0^q}\tilde{a}_1 = \frac{q\tilde{a}_0^p}{\tilde{h}_0^{q+1}}\tilde{h}_1 - x_0'\tilde{a}_{0y}, \qquad -\infty < y < \infty, \tag{6.30a}$$

$$D\tilde{h}_{1yy} = -\tilde{a}_0^r/\tilde{h}_0^s. \tag{6.30b}$$

Here $x_0' \equiv dx_0/d\tau$. Next, we write $\tilde{a}_1$ as

$$\tilde{a}_1 = H^\gamma u_1. \tag{6.31}$$

Using (6.29), (6.31), and $\tilde{h}_0 \equiv H$, (6.30) becomes

$$L(u_1) \equiv u_1'' - u_1 + pu_c^{p-1}u_1 = \frac{qu_c^p}{H}\tilde{h}_1 - x_0'u_c', \qquad -\infty < y < \infty, \tag{6.32a}$$

$$D\tilde{h}_{1yy} = -H^{\gamma r - s}u_c^r, \tag{6.32b}$$

where u_1 is to decay exponentially as $|y| \to \infty$. Since $Lu_c' = 0$ and $u_c' \to 0$ exponentially as $|y| \to \infty$, the right side of (6.32a) must satisfy the solvability condition that it is orthogonal to u_c'. From this condition we obtain the differential equation

$$x_0' = \frac{q}{H\int_{-\infty}^{\infty}[u_c'(y)]^2\,dy}\int_{-\infty}^{\infty} u_c^p u_c' \tilde{h}_1\,dy\,. \tag{6.33}$$

If we integrate (6.33) by parts twice, and use the facts that h_1'' and u_c are even functions, we get

$$x_0' = -\frac{q}{2H(p+1)}\left(\frac{\int_{-\infty}^{\infty}[u_c(y)]^{p+1}\,dy}{\int_{-\infty}^{\infty}[u_c'(y)]^2\,dy}\right)\left[\lim_{y\to+\infty}\tilde{h}_1' + \lim_{y\to-\infty}\tilde{h}_1'\right]. \tag{6.34}$$

In the outer region defined at an $O(1)$ distance away from the center of the spike, a is exponentially small and we expand h as $h = h_0(x) + o(1)$ as $\epsilon \to 0$. Then, from (1.17b), we obtain that h_0 satisfies

$$Dh_0'' - \mu h_0 = -H^{\gamma r - s} b_r \delta(x - x_0)\,, \qquad -1 < x < 1\,, \tag{6.35a}$$

$$h_0'(\pm 1) = 0\,. \tag{6.35b}$$

Here b_r is defined in (6.3b). Solving for h_0 we get

$$h_0(x) = H^{\gamma r - s} b_r G(x; x_0)\,, \tag{6.36}$$

where the Green's function $G(x; x_0)$ satisfies

$$DG_{xx} - \mu G = -\delta(x - x_0)\,, \qquad -1 < x < 1\,, \tag{6.37a}$$

$$G_x(\pm 1; x_0) = 0\,. \tag{6.37b}$$

To match with the inner solution we require that

$$h_0(x_0) = H\,, \qquad \lim_{y\to+\infty}\tilde{h}_1' + \lim_{y\to-\infty}\tilde{h}_1' = h_0'(x_{0+}) + h_0'(x_{0-})\,. \tag{6.38}$$

Substituting (6.36) into (6.38), we get

$$\lim_{y\to+\infty}\tilde{h}_1' + \lim_{y\to-\infty}\tilde{h}_1' = \frac{H}{G(x_0;x_0)}\left[G_x(x_{0+};x_0) + G_x(x_{0-};x_0)\right], \tag{6.39a}$$

$$H = \left[\frac{1}{b_r G(x_0;x_0)}\right]^{1/[\gamma r - (s+1)]}. \tag{6.39b}$$

Finally, substituting (6.39) into (6.29), (6.34) and (6.36) and letting $\tau = \epsilon^2 t$, we obtain the main result of this section:

Proposition 6.3 *For $\epsilon \ll 1$, the the dynamics of a one-spike solution to (1.17) is characterized by*

$$a(x,t) \sim H^{\gamma} u_c\left(\epsilon^{-1}[x - x_0(t)]\right) , \tag{6.40a}$$

$$h(x,t) \sim HG\left[x; x_0(t)\right] / G\left[x_0(t); x_0(t)\right] , \tag{6.40b}$$

where $H = H(t)$ is given in (6.39b). The spike location $x_0(t)$ satisfies the differential equation

$$\frac{dx_0}{dt} \sim -\epsilon^2 C \left(\frac{G_x(x_{0+}; x_0) + G_x(x_{0-}; x_0)}{G(x_0; x_0)} \right) , \tag{6.40c}$$

where $C > 0$ is defined by

$$C \equiv \frac{q}{2(p+1)} \left(\frac{\int_{-\infty}^{\infty} [u_c(y)]^{p+1}\, dy}{\int_{-\infty}^{\infty} [u_c'(y)]^2\, dy} \right) = \frac{q}{p-1} . \tag{6.40d}$$

In calculating the integral in (6.40d) we used (5.19)

6.2.2 Case 1: $\mu(x) > 0$ depends on x when D large

In general, when μ depends on x we must compute the Green's function satisfying (6.37) to determine the dynamics as described in (6.40c). However, to illustrate qualitatively the effect of a spatially varying $\mu(x)$, we now derive an approximate differential equation for x_0 in the limit $D \gg 1$ with D independent of ϵ.

In the limit $D \gg 1$, we expand G as

$$G(x; x_0) = G_0(x; x_0) + D^{-1} G_1(x; x_0) + O\left(D^{-2}\right) . \tag{6.41}$$

Substituting (6.41) into (6.37) and collecting powers of D^{-1}, we get

$$G_{0xx} = 0 ; \qquad G_{1xx} = \mu G_0 - \delta(x - x_0) , \tag{6.42}$$

with $G_{jxx} = 0$ at $x = \pm 1$ for $j = 0, 1$. The problem for G_1 does not have a solution unless G_0 satisfies a solvability condition. In this way, we calculate that

$$G_0 = (2\mu_a)^{-1}; \qquad G_{1x} = (2\mu_a)^{-1} \int_{-1}^{x} \mu(y)\, dy - \begin{cases} 0 & -1 < x < x_0\,, \\ 1 & x_0 < x < 1\,. \end{cases} \tag{6.43}$$

Here μ_a is the average of μ over the interval, defined by

$$\mu_a \equiv \frac{1}{2} \int_{-1}^{1} \mu(x)\, dx\,. \tag{6.44}$$

Substituting (6.43) into (6.40c) we obtain the following result:

Corollary 6.2 *For $\epsilon \ll 1$ and $D \gg 1$, with D independent of ϵ, the differential equation for the spike location (6.40c) reduces to*

$$\frac{dx_0}{dt} \sim -\frac{2\epsilon^2 C}{D} \left(\int_{-1}^{x_0} \mu(y)\, dy - \mu_a \right), \tag{6.45}$$

where C is defined in (6.40d).

From (6.45) we observe that the pinning effect induced by $\mu(x)$ depends on global properties of the spatial inhomogeneity $\mu(x)$, in contrast to the pointwise values as obtained in §6.1 for perturbations of the shadow problem. Since $\mu(x) > 0$, there is a unique equilibrium spike-layer location x_{0e} for (6.45) satisfying

$$\int_{-1}^{x_{0e}} \mu(y)\, dy = \mu_a\,. \tag{6.46}$$

This equilibrium is a stable fixed point for (6.45). Notice that if $\int_0^1 \mu\, dx < \int_{-1}^0 \mu\, dx$, then the equilibrium location satisfies $x_{0e} \in (-1, 0)$. Alternatively, if there is more mass of μ on the right side of $x = 0$, then $x_{0e} \in (0, 1)$.

As an example, let $\omega > 0$ and consider the profile

$$\mu(x) \equiv \frac{1}{2} \left(1 + \frac{\omega e^{-\omega x}}{\sinh \omega} \right). \tag{6.47}$$

It is easy to see that $\mu_a = 1$ for any $\omega > 0$. Also, as $\omega \to 0$ we have $\mu(x) \to 1$. As $\omega \to \infty$ we have $\mu(x) \to 1/2 + \omega e^{-\omega(x+1)}$, which has a boundary layer near $x = -1$. For any $\omega > 0$ there

is more mass of μ to the left of $x = 0$ than to the right of $x = 0$. From (6.46), x_{0e} satisfies the algebraic equation

$$x_{0e} - \frac{e^{-\omega x_{0e}}}{\sinh \omega} = 1 - \frac{e^{\omega}}{\sinh \omega}. \tag{6.48}$$

It is easily seen that $-1 < x_{0e} < 0$ when $\omega > 0$ and $x_{0e} \to -1$ as $\omega \to \infty$.

6.2.3 Case 2: $\mu(x) > 0$ depends on x when D is small

We now examine the effect of setting $\mu = \mu(x)$, in (1.17), to the dynamics of a one-spike solution when D is small. In the previous subsection we considered a spatially varying inhibitor decay rate in the limit $D \to \infty$. The motivation for considering the limit $D \to 0$ is that multi-spike solutions are only stable when D is sufficiently small. Although here we only consider the one-spike case when D is small, a similar analysis could be done for a multi-spike solution.

We now solve (6.40c) in the limit $D \to 0$ using the WKB method. Since D is small, we make the following ansatz as to the form of G,

$$G(x; x_0) = \exp\left(\frac{\theta_0(x)}{\sqrt{D}} + \theta_1(x) + \cdots\right). \tag{6.49}$$

Substituting (6.49) into (6.37) and collecting powers of D gives us the following set of equations,

$$\theta_0'^2 = \mu, \tag{6.50a}$$

$$\theta_0'' + 2\theta_0'\theta_1' = 0. \tag{6.50b}$$

This leads to the following leading order solution for G,

$$G(x; x_0) = \begin{cases} A\mu^{-1/4} \cosh\left(\frac{1}{\sqrt{D}} \int_{x_0}^{1} \mu^{1/2} dy\right) \cosh\left(\frac{1}{\sqrt{D}} \int_{-1}^{x} \mu^{1/2} dy\right), & -1 < x < x_0 \\ A\mu^{-1/4} \cosh\left(\frac{1}{\sqrt{D}} \int_{-1}^{x_0} \mu^{1/2} dy\right) \cosh\left(\frac{1}{\sqrt{D}} \int_{x}^{1} \mu^{1/2} dy\right) & x_0 < x < 1. \end{cases} \tag{6.51}$$

To solve for A we use the jump condition associated with (6.37),

$$G_x(x_0+; x_0) - G_x(x_0-; x_0) = -\frac{1}{D}. \tag{6.52}$$

Applying the condition above, results in the following value for A:

$$A = A(x_0) = \frac{1}{[\mu(x_0)]^{1/4}\sqrt{D}} \operatorname{csch}\left(\frac{2}{\sqrt{D}} \hat{\mu_a}\right), \tag{6.53}$$

where

$$\hat{\mu_a} \equiv \frac{1}{2}\int_{-1}^{1} [\mu(y)]^{1/2}\, dy\,. \tag{6.54}$$

Substituting (6.51), (6.53) and (6.54) into (6.40c gives us the following differential equation for x_0.

$$\frac{dx_0}{d\tau} = \frac{-\frac{1}{4}\mu^{-1}(x_0)\mu'(x_0)(\cosh(\frac{1}{\sqrt{d}}\mu^{\bar{1}/2}) + \cosh(\frac{1}{\sqrt{d}}\mu_{x_0}^{*\bar{1}/2})) + \frac{\mu^{3/4}}{\sqrt{D}}\sinh(\frac{1}{\sqrt{D}}\mu_{x_0}^{*1/2})}{\cosh(\frac{1}{\sqrt{D}}m\bar{u^{1/2}}) + \cosh(\frac{1}{\sqrt{D}}\mu_{x_0}^{*1/2})}\,, \tag{6.55}$$

where $\mu^{\bar{1}/2}$ is defined in (6.54 and $\mu_{x_0}^{*1/2}$ is given by,

$$\mu_{x_0}^{*1/2} = \int_{-1}^{x_0} \mu^{1/2}(y)\, dy - \int_{x_0}^{1} \mu^{1/2}(y)\, dy\,. \tag{6.56}$$

6.2.4 A variable activator decay rate

We now consider the case where the activator decay rate varies spatially and the inhibitor decay rate is a constant. The effect of adding spatial variation to the activator decay rate is to change both the equilibrium location of the spike and its dynamical behaviour.

The Gierer-Meinhardt system with a spatially varying activator decay rate is given by,

$$a_t = \epsilon^2 a_{xx} - V(x)a + \frac{a^p}{h^q}\,, \quad -1 < x < 1\,, \quad t > 0\,, \tag{6.57a}$$

$$0 = Dh_{xx} - \mu h + \frac{a^r}{h^s}\,, \quad -1 < x < 1\,, \quad t > 0 \tag{6.57b}$$

$$a_x(\pm 1) = h_x(\pm 1) = 0\,. \tag{6.57c}$$

We now extend the analysis given is §4.4.1 to derive an ordinary differential equation for the location of the spike for a one-spike solution. As we are examining a one spike solution, with the spike centered at $x = x_0$, we make the following change of variables,

$$y = (x - x_0)\epsilon^{-1}\,, \quad \tilde{a}(y) = a(x_0 + \epsilon y)\,, \quad \tilde{h}(y) = h(x_0 + \epsilon y)\,, \tag{6.58}$$

where $x_0 = x_0(\tau)$ with $\tau = \epsilon^2 t$. We then expand the inner solution as follows,

$$\tilde{h}(y) = \tilde{h}_0(y) + \epsilon\tilde{h}_1 + \ldots\,, \quad \tilde{a}(y) = \tilde{a}_0(y) + \epsilon\tilde{a}_1(y) + \ldots\,. \tag{6.59}$$

The spike location is to satisfy $\tilde{a}_0'(0) = 0$. Substituting (6.58) and (6.59) into (6.57), and collecting terms that are $O(1)$ as $\epsilon \to 0$, we get the leading order problem for $\tilde{a}_0$ and $\tilde{h}_0$:

$$\tilde{a}_0'' - V(x_0)\tilde{a}_0 + \tilde{a}_0^p/\tilde{h}_0^q = 0\,, \qquad -\infty < y < \infty\,, \tag{6.60a}$$

$$\tilde{h}_0'' = 0\,, \tag{6.60b}$$

with $\tilde{a}_0'(0) = 0$. In order to match to the outer solution, to be constructed below, we require that $\tilde{h}_0$ is independent of y. Thus, we set $\tilde{h}_0 = H$, where $H = H(\tau)$ is a function to be determined. We then write the solution to (6.60a) as

$$\tilde{a}_0 = H^\gamma [V(x_0)]^{1/(p-1)} u_c(\sqrt{V(x_0)}y)\,, \qquad \text{where} \qquad \gamma \equiv q/(p-1)\,, \tag{6.61}$$

where u_c satisfies (6.4).

Collecting the $O(\epsilon)$ terms in the inner region expansion, we obtain the problem for $\tilde{a}_1$ and $\tilde{h}_1$,

$$\tilde{a}_1'' - V(x_0)\tilde{a}_1 + \frac{p\tilde{a}_0^{p-1}}{\tilde{h}_0^q}\tilde{a}_1 = yV'(x_0)\tilde{a}_0 + \frac{q\tilde{a}_0^p}{\tilde{h}_0^{q+1}}\tilde{h}_1 - x_0'\tilde{a}_{0y}\,, \qquad -\infty < y < \infty\,, \tag{6.62a}$$

$$D\tilde{h}_{1yy} = -\tilde{a}_0^r/\tilde{h}_0^s\,. \tag{6.62b}$$

Here $x_0' \equiv dx_0/d\tau$. Next, we write $\tilde{a}_1$ as

$$\tilde{a}_1 = H^\gamma u_1\,. \tag{6.63}$$

Using (6.61), (6.63), and $\tilde{h}_0 \equiv H$, (6.62) becomes

$$L(u_1) = yV'(x_0)V(x_0)^{1/(p-1)}u_c(\sqrt{V(x_0)}y) + \frac{q[V(x_0)]^{p/(p-1)}u_c^p}{H}\tilde{h}_1$$
$$- x_0'[V(x_0)]^{(1+p)/2(p-1)}u_c'\,, \qquad -\infty < y < \infty\,, \tag{6.64a}$$

$$D\tilde{h}_{1yy} = -H^{\gamma r - s}u_c^r\,, \tag{6.64b}$$

where u_1 is to decay exponentially as $|y| \to \infty$ and

$$L(u_1) \equiv u_1'' - V(x_0)u_1 + pV(x_0)u_c^{p-1}u_1\,. \tag{6.65}$$

Since, $Lu_c'(\sqrt{V(x_0)}y) = 0$ and $u_c' \to 0$ exponentially as $|y| \to \infty$, the right side of (6.64a) must satisfy the solvability condition that it is orthogonal to $u_c'(\sqrt{V(x_0)}y)$. From this condition we

obtain the differential equation

$$x_0' = \frac{qV(x_0)}{H\int_{-\infty}^{\infty}[u_c'(y)]^2\,dy}\int_{-\infty}^{\infty} u_c^p(\sqrt{V(x_0)}y)u_c'(\sqrt{V(x_0)}y)\tilde{h}_1\,dy + \frac{V'(x_0)}{V(x_0)\int_{-\infty}^{\infty}[u_c'(y)]^2}\int_{-\infty}^{\infty} u_c(y)u_c'(y)y\,dy\,. \tag{6.66a}$$

If we repeat the process from §6.4.2, we then arrive at the following differential equation for x_0,

$$\frac{dx_0}{dt} \sim -\frac{\epsilon^2 q}{p-1}\left(\frac{G_x(x_{0+};x_0)+G_x(x_{0-};x_0)}{G(x_0;x_0)}\right) - \frac{\epsilon^2}{2}\left(\frac{p+3}{p-1}\right)\frac{V'(x_0)}{V(x_0)}\,. \tag{6.67}$$

If the second term on the right hand side of (6.67) were absent, the spike would tend towards $x_0 = 0$. If the first term on the right hand side of (6.67) were absent, the spike would tend towards a local minimum of V. The end result of the spatially inhomogeneous term is a competition between these two terms.

Chapter 7
Conclusions

In this chapter we give a brief review of the main results found in this thesis and an intuitive explanation of these results. The equations and details of these results will be omitted as these details are summarized in §1.4. We will also attempt to provide a framework to place these results in a useful context for those who use the Gierer-Meinhardt equations for modeling. Finally, we will discuss some possible extensions to the analysis as well as some possible connections to other systems. Before we proceed with the discussion, we must clear up some notation. In this chapter, when we refer to an n-spike profile, we are referring to a solution of the form (2.1) for the shadow system and a solution of the form (4.14) for the full system.

7.1 Overview of Results

We will begin by reviewing the results from §2 and §3. These chapters analyzed the reduced system (1.19) commonly referred to as the shadow system. By constructing spike-type solutions and linearizing about these solutions we find that any solution with a spike in the interior of the domain is unstable. Profiles with more than one spike are unstable with an $O(1)$ eigenvalue and one-spike profiles are unstable with an exponentially small eigenvalue. The presence of an exponentially small eigenvalue is used to construct an equation of motion for the spike which demonstrates that an internal spike will move towards the closest point on the boundary on an exponentially slow time scale. Once the spike begins to approach the boundary, the analysis becomes invalid. The spike is presumed to merge with the boundary. By linearizing about a spike confined to the boundary, we find that a spike confined to boundary will move in the direction of increasing boundary curvature in two dimensional domains and increasing

mean curvature in three dimensional domains. The analysis of the dynamics and stability of these spike profiles for (1.19), all rely on the interaction of the exponentially small tails of the spikes with the boundary. The results are thus very delicate. Inconsistencies with the shadow system and numerical calculations of the full system (1.17) suggest that this delicate structure is broken by finite values of inhibitor diffusivity. This limits the applicability of the results in these chapters to modeling of the full system. However, the methods used in this chapter may be of use in analyzing models other systems, specifically the microwave heating model presented in [4]. The results in this section are also interesting from a mathematical point of view. Specifically, the formal asymptotics in §2 have been verified vigorously in [7] using invariant manifold techniques.

In §3 and §4 we examine the stability and dynamics of spike profiles under the full system (1.17) with finite values of inhibitor diffusivity. The results from (1.19) do not coincide with numerical calculations of the full system (1.17) even for large values of inhibitor diffusivity. It is for this reason that we undertake the more difficult task of analyzing the full system. Again we construct an n-spike profile for the full system and linearize about this solution. Analyzing the spectrum of the operator resulting from a linearization about an n-spike profile results in a necessary and sufficient condition for the stability of any given profile. We find that there is a decreasing sequence of numbers D_i such that an n-spike solution is stable if the inhibitor diffusivity is less than D_n. The existence of an algebraically small eigenvalue is used to construct a solvability condition which results in a differential equation governing the motion of the spikes. This equation reveals that the shape of the inhibitor profile overrides the effects of the exponentially small tail in the activator profile and takes control of the dynamics. This is the main reason for discrepancies between the behavior of the numerical calculations of the full system and the shadow system. While these results are all in one spatial dimension, and most models are in two or three dimensions, we believe that similar qualitative behavior exist in higher dimension. Again these results are also interesting from a purely mathematical point of view and the formal asymptotics of §4 have been vigorously verified in [51].

In §6 we consider the effects of spatially varying coefficients. Three different scenarios are

considered, a spatially varying activator diffusivity for the shadow system, a spatially varying inhibitor decay rate and a spatially varying activator decay rate. In all three cases the effect of the spatially varying coefficient is to add an extra term to the solvability condition which provides the deferential equation governing the motion of the spike. This chapter may be of particular interest to those who use the Gierer-Meinhardt equation for modeling as many of the models use spatially varying coefficients to account for preexisting patterns.

7.2 Possible Extensions

There are still many open ares of research for the Gierer-Meinhardt model. The most obvious being the extension of the results in §4, §5 and §6 from one to higher dimensions. The main difficulty to be overcome for this extension is the complexity and domain reliance on the Green's function for the inhibitor equation. Another important extension is to include the effects of non-zero values of τ. Numerical computations suggest that for reasonable small values of τ, the simplification of setting τ to 0 presents no problems. However, for larger values of τ, many interesting phenomena, such as oscillatory behavior, are possible. For examples of such behavior see [31].

The methodology used in this thesis may also be extended to other systems. At present the analysis in §4 is being modified to analyse the Schnakenberg model, another reaction diffusion system used in developmental biology modeling. The analysis in §2 may also be of use in analyzing the microwave heating model presented in [4].

Appendix A
Proof of Theorem 2.1

In this appendix, we prove Theorem 2.1. Although this has been proved in by J. Wei in [52], we include a proof here for the convenience of the readers. We present a proof which works in the general case of $\mathbb{R}^N$. Let

$$r = 2, \quad 1 < p \leq 1 + \frac{4}{N}, \qquad \text{or} \qquad r = p + 1, \quad 1 < p < (\frac{N+2}{N-2})_+ ,$$

where $(\frac{N+2}{N-2})_+ = \frac{N+2}{N-2}$ if $N \geq 3$ and $= +\infty$ if $N = 1, 2$. Define $w(|\boldsymbol{y}|)$, with $\boldsymbol{y} = (y_1, .., y_N)^t$, to be the unique positive solution to

$$w'' + \frac{N-1}{\rho} w' - w + w^p = 0 , \qquad \rho > 0 ,$$
$$w'(0) > 0 , \qquad w(\rho) \sim \alpha \rho^{(1-N)/2} e^{-\rho} , \qquad \text{as} \quad \rho \to \infty .$$

When $N = 1$, then $w = u_c$, where u_c satisfies (3.6).

Suppose that (ϕ, λ_0), with $\lambda_0 \neq 0$, satisfies the following eigenvalue problem:

$$\Delta\phi - \phi + pw^{p-1}\phi - \gamma_0(p-1)\frac{\int_{\mathbb{R}^N} w^{r-1}\phi}{\int_{\mathbb{R}^N} w^r} w^p = \lambda_0 \phi , \qquad \phi \in H^2(R^1), \quad \gamma_0 > 1 . \tag{A.1}$$

When $N = 1$ this problem reduces to (3.39). Thus, the proof of (2.13) is complete once we show that

$$Re(\lambda_0) < 0 . \tag{A.2}$$

Let $\lambda_0 = \lambda_R + i\lambda_I, \phi = \phi_R + i\phi_I$.

We first introduce some notations and make some preparations. Set

$$L\phi := L_0\phi - \gamma_0(p-1)\frac{\int_{\mathbb{R}^N} w^{r-1}\phi}{\int_{R^1} w^r} w^p ; \qquad \phi \in H^2(R^1) ,$$

where $\gamma_0 > 1$ and $L_0 := \Delta - 1 + pw^{p-1}$. Note that L is not self-adjoint if $r \neq p + 1$.

It is well-known that L_0 admits the following set of eigenvalues:

$$\mu_1 > 0, \qquad \mu_2 = 0 , ... \mu_{N+1} = 0 , \qquad \mu_{N+2} < 0 , \tag{A.3}$$

where the eigenfunction corresponding to μ_1 is of constant sign (see Theorem 2.1 of [27]).

Let

$$X_0 := kernel(L_0) = span\{\frac{\partial w}{\partial y_j}, j = 1, ..., N\}.$$

Then

$$L_0 w = (p-1)w^p\,, \qquad L_0(\frac{1}{p-1}w + \frac{1}{2}x\nabla w) = w\,, \tag{A.4}$$

and

$$\int_{\mathbb{R}^N}(L_0^{-1}w)w = \int_{\mathbb{R}^N} w(\frac{1}{p-1}w + \frac{1}{2}x\nabla w) = (\frac{1}{p-1} - \frac{N}{4})\int_{\mathbb{R}^N} w^2, \tag{A.5}$$

$$\int_{\mathbb{R}^N}(L_0^{-1}w)w^p = \int_{\mathbb{R}^N} w^p(\frac{1}{p-1}w + \frac{1}{2}x\nabla w)$$

$$= \int_{\mathbb{R}^N}(L_0^{-1}w)\frac{1}{p-1}L_0 w = \frac{1}{p-1}\int_{\mathbb{R}^N} w^2. \tag{A.6}$$

We divide our proof into three cases:

Case 1: $r = 2, 1 < p < 1 + \frac{4}{N}$.

Since L is not self-adjoint, we introduce a new operator as follows:

$$L_1\phi := L_0\phi - (p-1)\frac{\int_{\mathbb{R}^N} w\phi}{\int_{\mathbb{R}^N} w^2}w^p - (p-1)\frac{\int_{\mathbb{R}^N} w^p\phi}{\int_{\mathbb{R}^N} w^2}w + (p-1)\frac{\int_{\mathbb{R}^N} w^{p+1}\int_{\mathbb{R}^N} w\phi}{(\int_{\mathbb{R}^N} w^2)^2}w. \tag{A.7}$$

We have the following important lemma:

Lemma A.1 *(1) L_1 is self-adjoint and the kernel of L_1 (denoted by X_1) = span $\{w, \frac{\partial w}{\partial y_j}, j = 1, ..., N\}$. (2) There exists a positive constant $a_1 > 0$ such that*

$$L_1(\phi, \phi)$$

$$:= \int_{\mathbb{R}^N}(|\nabla\phi|^2 + \phi^2 - pw^{p-1}\phi^2) + \frac{2(p-1)\int_{\mathbb{R}^N} w\phi\int_{\mathbb{R}^N} w^p\phi}{\int_{\mathbb{R}^N} w^2} - (p-1)\frac{\int_{\mathbb{R}^N} w^{p+1}}{(\int_{\mathbb{R}^N} w^2)^2}(\int_{\mathbb{R}^N} w\phi)^2$$

$$\geq a_1 d^2_{L^2(\mathbb{R}^N)}(\phi, X_1)\,,$$

for all $\phi \in H^1(\mathbb{R}^N)$, where $d_{L^2(\mathbb{R}^N)}$ denotes distance in the L^2-norm.

Proof: By (A.7), L_1 is self-adjoint. Next we compute the kernel of L_1. It is easy to see that $w, \frac{\partial w}{\partial y_j}, j = 1, ..., N, \in kernel(L_1)$. On the other hand, if $\phi \in kernel(L_1)$, then by (A.4)

$$L_0\phi = c_1(\phi)w + c_2(\phi)w^p = c_1(\phi)L_0(\frac{1}{p-1}w + \frac{1}{2}x\nabla w) + c_2(\phi)L_0(\frac{w}{p-1}),$$

where

$$c_1(\phi) = (p-1)\frac{\int_{\mathbb{R}^N} w^p\phi}{\int_{\mathbb{R}^N} w^2} - (p-1)\frac{\int_{\mathbb{R}^N} w^{p+1}\int_{\mathbb{R}^N} w\phi}{(\int_{\mathbb{R}^N} w^2)^2}, \qquad c_2(\phi) = (p-1)\frac{\int_{\mathbb{R}^N} w\phi}{\int_{\mathbb{R}^N} w^2}.$$

Hence

$$\phi - c_1(\phi)(\frac{1}{p-1}w + \frac{1}{2}x\nabla w) - c_2(\phi)\frac{1}{p-1}w \in kernel(L_0). \tag{A.8}$$

Note that

$$c_1(\phi) = (p-1)c_1(\phi)\frac{\int_{\mathbb{R}^N} w^p(\frac{1}{p-1}w + \frac{1}{2}x\nabla w)}{\int_{\mathbb{R}^N} w^2} - (p-1)c_1(\phi)\frac{\int_{\mathbb{R}^N} w^{p+1}\int_{\mathbb{R}^N} w(\frac{1}{p-1}w + \frac{1}{2}x\nabla w)}{(\int_{\mathbb{R}^N} w^2)^2}$$

$$= c_1(\phi) - c_1(\phi)(\frac{1}{p-1} - \frac{N}{4})\frac{\int_{\mathbb{R}^N} w^{p+1}}{\int_{\mathbb{R}^N} w^2}$$

by (A.5) and (A.6). This implies that $c_1(\phi) = 0$. By (A.8), this proves (1).

It remains to prove (2). Suppose (2) is not true, then by (1) there exists (α, ϕ) such that (i) α is real and positive, (ii) $\phi \perp w$, $\phi \perp \frac{\partial w}{\partial y_j}$, $j = 1, \ldots, N$, and (iii) $L_1\phi = \alpha\phi$.

We show that this is impossible. From (ii) and (iii), we have

$$(L_0 - \alpha)\phi = (p-1)\frac{\int_{\mathbb{R}^N} w^p\phi}{\int_{\mathbb{R}^N} w^2}w. \tag{A.9}$$

We first claim that $\int_{\mathbb{R}^N} w^p\phi \neq 0$. In fact if $\int_{\mathbb{R}^N} w^p\phi = 0$, then $\alpha > 0$ is an eigenvalue of L_0. But by (A.3), $\alpha = \mu_1$ and ϕ has constant sign. This contradicts with the fact that $\phi \perp w$. Therefore $\alpha \neq \mu_1, 0$, and hence $L_0 - \alpha$ is invertible in $X_0^\perp$. So (A.9) implies

$$\phi = (p-1)\frac{\int_{\mathbb{R}^N} w^p\phi}{\int_{\mathbb{R}^N} w^2}(L_0 - \alpha)^{-1}w.$$

Thus

$$\int_{\mathbb{R}^N} w^p\phi = (p-1)\frac{\int_{\mathbb{R}^N} w^p\phi}{\int_{\mathbb{R}^N} w^2}\int_{\mathbb{R}^N}((L_0 - \alpha)^{-1}w)w^p,$$

$$\int_{\mathbb{R}^N} w^2 = (p-1)\int_{\mathbb{R}^N}((L_0 - \alpha)^{-1}w)w^p,$$

$$\int_{\mathbb{R}^N} w^2 = \int_{\mathbb{R}^N} ((L_0-\alpha)^{-1}w)((L_0-\alpha)w+\alpha w),$$

$$0 = \int_{\mathbb{R}^N} ((L_0-\alpha)^{-1}w)w. \tag{A.10}$$

Let $h_1(\alpha) = \int_{\mathbb{R}^N}((L_0-\alpha)^{-1}w)w$. Then, $h_1(0) = \int_{\mathbb{R}^N}(L_0^{-1}w)w = \int_{\mathbb{R}^N}(\frac{1}{p-1}w + \frac{1}{2}x\cdot\nabla w)w = (\frac{1}{p-1}-\frac{N}{4})\int_{\mathbb{R}^N} w^2 > 0$ since $1 < p < 1+\frac{4}{N}$. Moreover $h_1'(\alpha) = \int_{\mathbb{R}^N}((L_0-\alpha)^{-2}w)w = \int_{\mathbb{R}^N}((L_0-\alpha)^{-1}w)^2 > 0$. This implies $h_1(\alpha) > 0$ for all $\alpha \in (0,\mu_1)$. Clearly, also $h_1(\alpha) < 0$ for $\alpha \in (\mu_1,\infty)$ (since $\lim_{\alpha\to+\infty} h_1(\alpha) = 0$). A contradiction to (A.10)! This completes this part of the proof.

We now finish the proof of (2.13) in Case 1. Since $\lambda_0 \neq 0$, we can choose $\phi \perp kernel(L_0)$. Then we obtain two equations

$$L_0\phi_R - (p-1)\gamma_0\frac{\int_{\mathbb{R}^N} w\phi_R}{\int_{\mathbb{R}^N} w^2}w^p = \lambda_R\phi_R - \lambda_I\phi_I, \tag{A.11}$$

$$L_0\phi_I - (p-1)\gamma_0\frac{\int_{\mathbb{R}^N} w\phi_I}{\int_{\mathbb{R}^N} w^2}w^p = \lambda_R\phi_I + \lambda_I\phi_R. \tag{A.12}$$

Multiplying (A.11) by ϕ_R and (A.12) by ϕ_I, and adding the resulting expressions together, we obtain

$$-\lambda_R\int_{\mathbb{R}^N}(\phi_R^2+\phi_I^2) = L_1(\phi_R,\phi_R) + L_1(\phi_I,\phi_I)$$

$$+(p-1)(\gamma_0-2)\frac{\int_{\mathbb{R}^N} w\phi_R\int_{\mathbb{R}^N} w^p\phi_R + \int_{\mathbb{R}^N} w\phi_I\int_{\mathbb{R}^N} w^p\phi_I}{\int_{\mathbb{R}^N} w^2}$$

$$+(p-1)\frac{\int_{\mathbb{R}^N} w^{p+1}}{(\int_{\mathbb{R}^N} w^2)^2}[(\int_{\mathbb{R}^N} w\phi_R)^2 + (\int_{\mathbb{R}^N} w\phi_I)^2].$$

Multiplying (A.11) by w and (A.12) by w we obtain

$$(p-1)\int_{\mathbb{R}^N} w^p\phi_R - \gamma_0(p-1)\frac{\int_{\mathbb{R}^N} w\phi_R}{\int_{\mathbb{R}^N} w^2}\int_{\mathbb{R}^N} w^{p+1} = \lambda_R\int_{\mathbb{R}^N} w\phi_R - \lambda_I\int_{\mathbb{R}^N} w\phi_I, \tag{A.13}$$

$$(p-1)\int_{\mathbb{R}^N} w^p\phi_I - \gamma_0(p-1)\frac{\int_{\mathbb{R}^N} w\phi_I}{\int_{\mathbb{R}^N} w^2}\int_{\mathbb{R}^N} w^{p+1} = \lambda_R\int_{\mathbb{R}^N} w\phi_I + \lambda_I\int_{\mathbb{R}^N} w\phi_R. \tag{A.14}$$

Multiplying (A.13) by $\int_{\mathbb{R}^N} w\phi_R$ and (A.14) by $\int_{\mathbb{R}^N} w\phi_I$, and adding them together, we obtain

$$(p-1)\int_{\mathbb{R}^N} w\phi_R\int_{\mathbb{R}^N} w^p\phi_R + (p-1)\int_{\mathbb{R}^N} w\phi_I\int_{\mathbb{R}^N} w^p\phi_I$$

$$= (\lambda_R + \gamma_0(p-1)\frac{\int_{\mathbb{R}^N} w^{p+1}}{\int_{\mathbb{R}^N} w^2})((\int_{\mathbb{R}^N} w\phi_R)^2 + (\int_{\mathbb{R}^N} w\phi_I)^2).$$

Therefore we have

$$-\lambda_R \int_{\mathbb{R}^N} (\phi_R^2 + \phi_I^2) = L_1(\phi_R, \phi_R) + L_1(\phi_I, \phi_I)$$

$$+(p-1)(\gamma_0 - 2)(\frac{1}{p-1}\lambda_R + \gamma_0 \frac{\int_{\mathbb{R}^N} w^{p+1}}{\int_{\mathbb{R}^N} w^2}) \frac{(\int_{\mathbb{R}^N} w\phi_R)^2 + (\int_{\mathbb{R}^N} w\phi_I)^2}{\int_{\mathbb{R}^N} w^2}$$

$$+(p-1)\frac{\int_{\mathbb{R}^N} w^{p+1}}{(\int_{\mathbb{R}^N} w^2)^2}[(\int_{\mathbb{R}^N} w\phi_R)^2 + (\int_{\mathbb{R}^N} w\phi_I)^2].$$

Set

$$\phi_R = c_R w + \phi_R^\perp, \quad \phi_R^\perp \perp X_1, \qquad \phi_I = c_I w + \phi_I^\perp, \quad \phi_I^\perp \perp X_1.$$

Then

$$\int_{\mathbb{R}^N} w\phi_R = c_R \int_{\mathbb{R}^N} w^2, \qquad \int_{\mathbb{R}^N} w\phi_I = c_I \int_{\mathbb{R}^N} w^2,$$

$$d^2_{L^2(\mathbb{R}^N)}(\phi_R, X_1) = \|\phi_R^\perp\|^2_{L^2}, \qquad d^2_{L^2(\mathbb{R}^N)}(\phi_I, X_1) = \|\phi_I^\perp\|^2_{L^2}.$$

By some simple computations we have

$$L_1(\phi_R, \phi_R) + L_1(\phi_I, \phi_I)$$

$$+(\gamma_0 - 1)\lambda_R(c_R^2 + c_I^2)\int_{\mathbb{R}^N} w^2 + (p-1)(\gamma_0 - 1)^2(c_R^2 + c_I^2)\int_{\mathbb{R}^N} w^{p+1} + \lambda_R(\|\phi_R^\perp\|^2_{L^2} + \|\phi_I^\perp\|^2_{L^2}) = 0.$$

By Lemma A.1 (2)

$$(\gamma_0 - 1)\lambda_R(c_R^2 + c_I^2)\int_{\mathbb{R}^N} w^2$$

$$+(p-1)(\gamma_0 - 1)^2(c_R^2 + c_I^2)\int_{\mathbb{R}^N} w^{p+1} + (\lambda_R + a_1)(\|\phi_R^\perp\|^2_{L^2} + \|\phi_I^\perp\|^2_{L^2}) \le 0.$$

Since $\gamma_0 > 1$, we must have $\lambda_R < 0$, which completes the proof of (2.13) in Case 1.

Case 2: $r = 2, p = 1 + \frac{4}{N}$.

In this case we have

$$\int_{\mathbb{R}^N}(L_0^{-1}w)w=\int_{\mathbb{R}^N}w(\frac{1}{p-1}w+\frac{1}{2}x\nabla w)=0. \tag{A.15}$$

Set

$$w_0=\frac{1}{p-1}w+\frac{1}{2}x\nabla w. \tag{A.16}$$

We will follow the proof in Case 1. We just need to take care of w_0. We first have the following lemma which is similar to Lemma A.1: The proof is omitted.

Lemma A.2 *(1) The kernel of L_1 is given by $X_1=span\ \{w,w_0,\frac{\partial w}{\partial y_j},j=1,...,N\}$. (2) There exists a positive constant $a_2>0$ such that*

$$L_1(\phi,\phi)=\int_{\mathbb{R}^N}(|\nabla\phi|^2+\phi^2-pw^{p-1}\phi^2)$$

$$+\frac{2(p-1)\int_{\mathbb{R}^N}w\phi\int_{\mathbb{R}^N}w^p\phi}{\int_{\mathbb{R}^N}w^2}-(p-1)\frac{\int_{\mathbb{R}^N}w^{p+1}}{(\int_{\mathbb{R}^N}w^2)^2}(\int_{\mathbb{R}^N}w\phi)^2$$

$$\geq a_2d^2_{L^2(\mathbb{R}^N)}(\phi,X_1),\quad \forall\phi\in H^1(\mathbb{R}^N).$$

Now we can finish the proof of (2.13) in Case 2. Similar to Case 1, we obtain two equations (A.11) and (A.12). We now decompose

$$\phi_R=c_Rw+b_Rw_0+\phi_R^\perp,\quad \phi_R^\perp\perp X_1,\qquad \phi_I=c_Iw+b_Iw_0+\phi_I^\perp,\quad \phi_I^\perp\perp X_1.$$

Similar to Case 1, we obtain

$$L_1(\phi_R,\phi_R)+L_1(\phi_I,\phi_I)$$

$$+(\gamma_0-1)\lambda_R(c_R^2+c_I^2)\int_{\mathbb{R}^N}w^2+(p-1)(\gamma_0-1)^2(c_R^2+c_I^2)\int_{\mathbb{R}^N}w^{p+1}$$

$$+\lambda_R(b_R^2(\int_{\mathbb{R}^N}w_0^2)^2+b_I^2(\int_{\mathbb{R}^N}w_0^2)^2+\|\phi_R^\perp\|^2_{L^2}+\|\phi_I^\perp\|^2_{L^2})\leq 0.$$

By Lemma A.2 (2)

$$(\gamma_0-1)\lambda_R(c_R^2+c_I^2)\int_{\mathbb{R}^N}w^2+(p-1)(\gamma_0-1)^2(c_R^2+c_I^2)\int_{\mathbb{R}^N}w^{p+1}$$

$$+\lambda_R(b_R^2(\int_{\mathbb{R}^N}w_0^2)^2+b_I^2(\int_{\mathbb{R}^N}w_0^2)^2)+(\lambda_R+a_2)(\|\phi_R^\perp\|^2_{L^2}+\|\phi_I^\perp\|^2_{L^2})\leq 0.$$

If $\lambda_R \geq 0$, then necessarily we have

$$c_R = c_I = 0, \qquad \phi_R^{\perp} = 0, \qquad \phi_I^{\perp} = 0\,.$$

Hence $\phi_R = b_R w_0, \phi_I = b_I w_0$. This implies that

$$b_R L_0 w_0 = (b_R - b_I) w_0\,, \qquad b_I L_0 w_0 = (b_R + b_I) w_0,$$

which is impossible unless $b_R = b_I = 0$. A contradiction! This completes this part of the proof.

Case 3: $r = p+1, 1 < p < (\frac{N+2}{N-2})_+$.

Let $r = p+1$. L becomes

$$L = L_0 - \frac{qr}{s+1} \frac{\int_{\mathbb{R}^N} w^p .}{\int_{\mathbb{R}^N} w^{p+1}} w^p.$$

We will follow the proof of Case 1. We need to define another operator.

$$L_3\phi := L_0\phi - (p-1)\frac{\int_{\mathbb{R}^N} w^p \phi}{\int_{\mathbb{R}^N} w^{p+1}} w^p. \tag{A.17}$$

We have the following lemma:

Lemma A.3 *(1) L_3 is self-adjoint and the kernel of L_3 (denoted by X_3) consists of $w, \frac{\partial w}{\partial y_j}, j = 1, ..., N$. (2) There exists a positive constant $a_3 > 0$ such that*

$$L_3(\phi,\phi) := \int_{\mathbb{R}^N} (|\nabla\phi|^2 + \phi^2 - pw^{p-1}\phi^2) + \frac{(p-1)(\int_{\mathbb{R}^N} w^p\phi)^2}{\int_{\mathbb{R}^N} w^{p+1}}$$

$$\geq a_3 d^2_{L^2(\mathbb{R}^N)}(\phi, X_3), \qquad \forall \phi \in H^1(\mathbb{R}^N).$$

Proof: The proof of (1) is similar to that of Lemma A.1. We omit the details. It remains to prove (2). Suppose (2) is not true, then by (1) there exists (λ, ϕ) such that (i) λ is real and positive, (ii) $\phi \perp w, \phi \perp \frac{\partial w}{\partial y_j}$, $j = 1, \ldots, N$, and (iii) $L_3\phi = \lambda\phi$.

We show that this is impossible. From (ii) and (iii), we have

$$(L_0 - \lambda)\phi = \frac{(p-1)\int_{\mathbb{R}^N} w^p\phi}{\int_{\mathbb{R}^N} w^{p+1}} w^p. \tag{A.18}$$

Similar to the proof of Lemma A.1, we have that $\int_{\mathbb{R}^N} w^p\phi \neq 0, \lambda \neq \mu_1, 0$, and hence $L_0 - \lambda$ is invertible in $X_0^{\perp}$. So (A.18) implies

$$\phi = \frac{(p-1)\int_{\mathbb{R}^N} w^p\phi}{\int_{\mathbb{R}^N} w^{p+1}} (L_0 - \lambda)^{-1} w^p.$$

Thus

$$\int_{\mathbb{R}^N} w^p \phi = (p-1)\frac{\int_{\mathbb{R}^N} w^p \phi}{\int_{\mathbb{R}^N} w^{p+1}} \int_{\mathbb{R}^N} ((L_0-\lambda)^{-1} w^p) w^p,$$

$$\int_{\mathbb{R}^N} w^{p+1} = (p-1)\int_{\mathbb{R}^N} ((L_0-\lambda)^{-1} w^p) w^p. \tag{A.19}$$

Let $h_3(\lambda) = (p-1)\int_{\mathbb{R}^N}((L_0-\lambda)^{-1}w^p)w^p - \int_{\mathbb{R}^N} w^{p+1}$, then $h_3(0) = (p-1)\int_{\mathbb{R}^N}(L_0^{-1}w^p)w^p - \int_{\mathbb{R}^N} w^{p+1} = 0$. Moreover $h_3'(\lambda) = (p-1)\int_{\mathbb{R}^N}((L_0-\lambda)^{-2}w^p)w^p = (p-1)\int_{\mathbb{R}^N}((L_0-\lambda)^{-1}w^p)^2 > 0$. This implies $h_3(\lambda) > 0$ for all $\lambda \in (0,\mu_1)$. Clearly, also $h_3(\lambda) < 0$ for $\lambda \in (\mu_1,\infty)$. A contradiction to (A.19)! This completes this part of the proof.

We now finish the proof of (2.13) in Case 3. Similar to case 1, we obtain two equations

$$L_0\phi_R - (p-1)\gamma_0 \frac{\int_{\mathbb{R}^N} w^p \phi_R}{\int_{\mathbb{R}^N} w^{p+1}} w^p = \lambda_R \phi_R - \lambda_I \phi_I, \tag{A.20}$$

$$L_0\phi_I - (p-1)\gamma_0 \frac{\int_{\mathbb{R}^N} w^p \phi_I}{\int_{\mathbb{R}^N} w^{p+1}} w^p = \lambda_R \phi_I + \lambda_I \phi_R. \tag{A.21}$$

Multiplying (A.20) by ϕ_R and (A.21) by ϕ_I and adding them together, we obtain

$$-\lambda_R \int_{\mathbb{R}^N} (\phi_R^2 + \phi_I^2) = L_3(\phi_R,\phi_R) + L_3(\phi_I,\phi_I)$$

$$+(p-1)(\gamma_0-1)\frac{(\int_{\mathbb{R}^N} w^p\phi_R)^2 + (\int_{\mathbb{R}^N} w^p\phi_I)^2}{\int_{\mathbb{R}^N} w^{p+1}}.$$

By Lemma A.3 (2)

$$\lambda_R \int_{\mathbb{R}^N} (\phi_R^2+\phi_I^2) + a_2 d_{L^2}^2(\phi, X_1) + (p-1)(\gamma_0-1)\frac{(\int_{\mathbb{R}^N} w^p\phi_R)^2 + (\int_{\mathbb{R}^N} w^p\phi_I)^2}{\int_{\mathbb{R}^N} w^{p+1}} \le 0,$$

which implies $\lambda_R < 0$ since $\gamma_0 > 1$. Thus, (2.13) in Case 3 is proved.

Appendix B

The Laplacian in the Boundary Layer Coordinate System

The derivation here is similar to that in [41]. We begin with a description of the boundary. Let $z = H(p_1, p_2)$ define the local height of the boundary at the point (p_1, p_2) on the boundary. For convenience here we will center the coordinate system around the point $p_1 = 0$ and $p_2 = 0$, where $z = 0$. In terms of these coordinates, H is given locally by

$$H(p_1, p_2) = \frac{1}{2}\kappa_1 p_1^2 + \frac{1}{2}\kappa_2 p_2^2 + O\left(p_1^2 + p_2^2\right) , \tag{B.1}$$

where κ_1 and κ_2 are the two principal curvatures at the center of the coordinate system. Our boundary layer coordinate system is (p_1, p_2, η), where $\eta > 0$ is the distance from $\boldsymbol{x} \in \Omega$ to $\partial\Omega$. Therefore, we define the following change of coordinates,

$$\mathbf{x}(p_1, p_2, \eta) = (p_1, p_2, H(s_1, s_2)) + \eta\, \mathbf{n}(p_1, p_2) , \tag{B.2}$$

where $\mathbf{n}(p_1, p_2)$ is the unit normal to the boundary defined by,

$$\mathbf{n}(p_1, p_2) = \frac{(-H_{p_1}, -H_{p_2}, 1)}{\sqrt{1 + H_{p_1}^2 + H_{p_2}^2}}. \tag{B.3}$$

In order to find the Laplacian in these new coordinate, we must calculate the scale factors,

$$\nu_{p_1} = \left|\frac{\partial \mathbf{x}}{\partial p_1}\right| , \quad \nu_{p_2} = \left|\frac{\partial \mathbf{x}}{\partial p_2}\right| , \quad \nu_\eta = \left|\frac{\partial \mathbf{x}}{\partial \eta}\right| . \tag{B.4}$$

To evaluate these expressions, we substitute (B.1) and (B.3) into (B.2) and differentiate to find,

$$\nu_{p_1} = 1 - \eta\kappa_1 + O(p_1^2 + p_2^2 + \eta^2) , \tag{B.5a}$$

$$\nu_{p_2} = 1 - \eta\kappa_2 + O(p_1^2 + p_2^2 + \eta^2) , \tag{B.5b}$$

$$\nu_\eta = 1 . \tag{B.5c}$$

In general curvilinear coordinates, the Laplacian is given by,

$$\Delta\phi = \frac{1}{\nu_{p_1}\nu_{p_2}\nu_\eta}\left[\frac{\partial}{\partial p_1}\left(\frac{\nu_{p_2}\nu_\eta}{\nu_{p_1}}\frac{\partial\phi}{\partial p_1}\right) + \frac{\partial}{\partial p_2}\left(\frac{\nu_{p_1}\nu_\eta}{\nu_{p_2}}\frac{\partial\phi}{\partial p_2}\right) + \frac{\partial}{\partial \eta}\left(\frac{\nu_{p_2}\nu_{p_1}}{\nu_\eta}\frac{\partial\phi}{\partial \eta}\right)\right] . \tag{B.6}$$

Thus, in these variables, the Laplacian is given to within quadratic terms by

$$\Delta\phi = \phi_{\eta\eta} - \left(\frac{\kappa_1}{1-\eta\kappa_1} + \frac{\kappa_2}{1-\eta\kappa_2}\right)\phi_\eta + \frac{1}{(1-\eta\kappa_1)(1-\eta\kappa_2)}\partial_{p_1}\left(\frac{1-\eta\kappa_2}{1-\eta\kappa_1}\phi_{p_1}\right) + \frac{1}{(1-\eta\kappa_1)(1-\eta\kappa_2)}\partial_{p_2}\left(\frac{1-\eta\kappa_1}{1-\eta\kappa_2}\phi_{p_2}\right) + O(p_1^2+p_2^2). \tag{B.7}$$

This coordinate change is then used in (3.1a) to obtain (3.26).

B.1 An Asymptotic Estimation of an Inner Product

Now we bound the term $(\mathcal{L}_\epsilon^*[\partial_x u_c], \phi_1)$ in (3.65), where $\mathcal{L}_\epsilon^*$ is defined in (3.56). Since $\partial_x u_c$ satisfies the local part of the operator in (3.56), we obtain

$$\mathcal{L}_\epsilon^*[\partial_x u_c] = -\frac{mq\epsilon^{-2}u_c^{m-1}}{\beta\pi(s+1)} \int_\Omega u_c^p \partial_x u_c \, d\mathbf{x}. \tag{B.8}$$

In §3.5 we assumed that the distance between $x = \xi$ and the curved part of the boundary $\partial\Omega_c$ is minimized at one of the two corner points. Let $r_m = \min(x_R - \xi, \xi - x_L)$ denote this minimum distance. Let B_r denote the semi-circle whose diameter is the interval $[\xi - r_m, \xi + r_m]$ along the x-axis. Then, by our assumption, B_r must be strictly contained within Ω. We then decompose the integral in (B.8) as

$$\int_\Omega u_c^p \partial_x u_c \, d\mathbf{x} = \int_{B_r} u_c^p \partial_x u_c \, d\mathbf{x} + \int_{\Omega\backslash B_r} u_c^p \partial_x u_c \, d\mathbf{x}. \tag{B.9}$$

Since the point $x = \xi$, $y = 0$ is the center of the semi-circle and the integrand is an odd function about the line $x = \xi$, the first integral on the right side of (B.9) is identically zero. Next, since u_c decays exponentially away from the point $x = \xi$, $y = 0$, the second integral on the right side of (B.9) is bounded by the maximum of the integrand on the boundary of $\Omega\backslash B_r$ multiplied by the area A_r of $\Omega\backslash B_r$. In this way, using the far-field behavior (3.14b), we get

$$\left| \int_{\Omega\backslash B_r} u_c^p \partial_x u_c \, d\mathbf{x} \right| \leq C\epsilon^q e^{-(p+1)r_m/\epsilon}. \tag{B.10}$$

Here q and C are constants independent of ϵ. Hence, in Ω, we have the estimate

$$|\mathcal{L}_\epsilon^*[\partial_x u_c]| \leq C\epsilon^{q-2} u_c^{m-1} e^{-(p+1)r_m/\epsilon}, \tag{B.11}$$

for some new constant C. Since $\phi_1 \sim \partial_x u_c$, we can then use the same reasoning as described above to estimate $(\mathcal{L}_\epsilon^*[\partial_x u_c], \phi_1)$, where $\mathcal{L}_\epsilon^*[\partial_x u_c]$ is given in (B.11). We find

$$|\,(\mathcal{L}_\epsilon^*[\partial_x u_c], \phi_1)\,| \leq C\epsilon^q e^{-(p+m+1)r_m/\epsilon}. \tag{B.12}$$

for some new constants q and C independent of ϵ.

Finally, we compare (B.12) with the asymptotic order of the boundary integral in (3.65). The boundary integral in (3.65) is clearly $O\left(\epsilon^q e^{-2r_m/\epsilon}\right)$. However, since $p > 1$ and $m > 0$, it follows that the inner product term in (B.12) is asymptotically exponentially smaller than the boundary integral term in (3.65). Hence, we were justified in asymptotically neglecting the inner product term in (3.65).

Appendix C
Calculation of $\mathcal{B}$ and $\mathcal{P}$

Consider the boundary value problem

$$Dy'' - \mu y = 0\,, \qquad y'(\pm 1) = 0\,, \tag{C.1a}$$

$$[Dy]_j = 0\,, \qquad \left[Dy'\right]_j = -\omega_j\,, \tag{C.1b}$$

for $j = 0, \ldots, n-1$, where $[v]_j \equiv v(x_{j+}) - v(x_{j-})$ and x_j satisfies (4.1). The solution is

$$y(x) = \sum_{k=0}^{n-1} G(x; x_k)\omega_k\,, \tag{C.2}$$

where G satisfies (4.10). Define the n-vectors $\boldsymbol{y}$ and $\langle \boldsymbol{y}' \rangle$ by

$$\boldsymbol{y}^t = (y_0, \ldots, y_{n-1})\,, \qquad \langle \boldsymbol{y}' \rangle^t = \left(\langle y' \rangle_0, \ldots, \langle y' \rangle_{n-1}\right)\,, \tag{C.3}$$

where $y_j \equiv y(x_j)$ and $\langle y' \rangle_j \equiv \left(y'(x_{j+}) + y'(x_{j-})\right)/2$. Then, we obtain from (C.2) that

$$\boldsymbol{y} = \mathcal{G}\boldsymbol{\omega}\,, \qquad \langle \boldsymbol{y}' \rangle = \mathcal{P}\boldsymbol{\omega}\,, \tag{C.4}$$

where $\boldsymbol{\omega}^t = (\omega_0, \ldots, \omega_{n-1})$. Here the matrices $\mathcal{G}$ and $\mathcal{P}$ are defined in (4.23) and (4.81), respectively. To determine these matrices explicitly we solve (C.1) analytically on each subinterval and impose the continuity of y to get

$$y(x) = \begin{cases} y_0 \frac{\cosh[\theta(1+x)]}{\cosh[\theta(1+x_0)]}\,, & -1 < x < x_0\,, \\ y_j \frac{\sinh[\theta(x_{j+1}-x)]}{\sinh[\theta(x_{j+1}-x_j)]} + y_{j+1} \frac{\sinh[\theta(x-x_j)]}{\sinh[\theta(x_{j+1}-x_j)]}\,, & x_j < x < x_{j+1}\,, \quad j = 0, \ldots, n-2\,, \\ y_{n-1} \frac{\cosh[\theta(1-x)]}{\cosh[\theta(1-x_{n-1})]}\,, & x_{n-1} < x < 1\,, \end{cases} \tag{C.5}$$

where $\theta = (\mu/D)^{1/2}$. To determine the relationship between $\boldsymbol{y}$ and $\boldsymbol{\omega}$, which yields $\mathcal{G}$, we use (C.5) and the jump condition $\left[Dy'\right]_j = -\omega_j$ in (C.1b) to get

$$\mathcal{B}\boldsymbol{y} = \frac{1}{D\theta}\boldsymbol{\omega}\,, \qquad \rightarrow \qquad \mathcal{G} = \frac{1}{D\theta}\mathcal{B}^{-1}\,, \tag{C.6}$$

where $\mathcal{B}$ is defined in (4.26b). Now using (C.5) we can calculate $\langle \boldsymbol{y}' \rangle$ in terms of $\boldsymbol{y}$ in the form

$$\langle \boldsymbol{y}' \rangle = -\frac{1}{2D} \operatorname{csch}\left(\frac{2\theta}{n}\right) \mathcal{C}^t \boldsymbol{y}\,, \tag{C.7}$$

where $\mathcal{C}$ is defined in (4.87b). Comparing (C.4) and (C.7), and using (C.6), we get the key relation

$$\mathcal{P} = -\frac{1}{2D} \operatorname{csch}\left(\frac{2\theta}{n}\right) \mathcal{C}^t \mathcal{B}^{-1}\,. \tag{C.8}$$

C.1 Calculation of Matrix Eigenvalues of $\mathcal{B}$

In this appendix we calculate the eigenvalues κ_j and eigenvectors $\boldsymbol{q}_j$ of the matrix problem

$$\mathcal{B}\boldsymbol{q} = \kappa\boldsymbol{q}\,, \tag{C.9}$$

where the tridiagonal matrix $\mathcal{B}$ is defined in (4.26) and $\boldsymbol{q}^t = (q_1, \ldots, q_n)$. The calculation below is similar to that given in [22].

From (4.26c) it follows that $d = e + f$. Therefore, we get the following recursion relation for the coefficients q_l of the eigenvector $\boldsymbol{q}$:

$$fq_{l-1} + (e-\kappa)q_l + fq_{l+1} = 0\,, \qquad l = 2, \ldots, n-1\,, \tag{C.10a}$$

$$fq_1 + (e-\kappa)q_1 + fq_2 = 0\,, \tag{C.10b}$$

$$fq_n + (e-\kappa)q_n + fq_{n-1} = 0\,. \tag{C.10c}$$

Hence, to solve for the q_l we can use the relation (C.10a) for $l = 1$ and $l = n$ and then impose the end conditions

$$q_0 = q_1\,, \qquad q_{n+1} = q_n\,. \tag{C.10d}$$

The solution to (C.10a) is

$$q_l = a\zeta_+^l + b\zeta_-^l\,, \qquad \zeta_\pm = \frac{1}{2f}\left(\kappa - e \pm \left[(\kappa-e)^2 - 4f^2\right]^{1/2}\right)\,. \tag{C.11}$$

The end conditions (C.10d) yield

$$a + b = a\zeta_+ + b\zeta_-\,, \tag{C.12a}$$

$$a\zeta_+^n + b\zeta_-^n = a\zeta_+^{n+1} + b\zeta_-^{n+1}\,. \tag{C.12b}$$

From (C.12) we get $\zeta_+ = \zeta_- = 1$ or $\zeta_+^n = \zeta_-^n$, which yields $\zeta_+ = \zeta_- \exp(2\pi ij/n)$, for $j = 1, \ldots, n-1$.

If $\zeta_+ = \zeta_- = 1$ we get $\kappa = e + 2f$ and $\boldsymbol{q}^t = (1, \ldots, 1)$. The other eigenvalues are calculated as in [22] to get $\kappa_j = e + 2f\cos(\pi(j-1)/n)$ for $j = 2, \ldots, n$ and $\zeta_\pm = \exp(\pm\pi i(j-1)/n)$. From (C.12b) we get $(1-\zeta_+)a + (1-\zeta_-)b = 0$. Substituting this relation into (C.11), and after rearranging the result, we obtain the unnormalized eigenvectors

$$q_{l,j} = \cos\left(\frac{\pi(j-1)}{n}(l-1/2)\right)\,, \quad j = 2, \ldots, n\,. \tag{C.13}$$

Here $q_{l,j}$ is the l^{th} component of the eigenvector $\boldsymbol{q}_j$. These eigenvectors can be normalized and the result is summarized in Proposition 4.2.

C.2 Calculation of $\mathcal{B}_g$ and $\mathcal{P}_g$

Consider the boundary value problem

$$Dy'' - \mu y = 0\,, \qquad y'(\pm 1) = 0\,, \tag{C.14a}$$

$$[Dy]_j = -\omega_j\,, \qquad \left[Dy'\right]_j = 0\,, \tag{C.14b}$$

for $j = 0, \ldots, n-1$, where $[v]_j \equiv v(x_{j+}) - v(x_{j-})$ and x_j satisfies (4.1). The solution is

$$y(x) = \sum_{k=0}^{n-1} g(x; x_k)\omega_k\,, \tag{C.15}$$

where g satisfies (4.76). In terms of the matrices $\mathcal{G}_g$ and $\mathcal{P}_g$, defined in (4.80) and (4.78), respectively, we have that

$$\boldsymbol{y}' = \mathcal{G}_g\boldsymbol{\omega}\,, \qquad \langle \boldsymbol{y} \rangle = \mathcal{P}_g\boldsymbol{\omega}\,, \tag{C.16}$$

where $\boldsymbol{\omega}^t = (\omega_0, \ldots, \omega_{n-1})$. Here $\boldsymbol{y}'$ and $\langle \boldsymbol{y} \rangle$ are defined by

$$\boldsymbol{y}'^t = \left(y_0', \ldots, y_{n-1}'\right)\,, \qquad \langle \boldsymbol{y} \rangle^t = \left(\langle y \rangle_0, \ldots, \langle y \rangle_{n-1}\right)\,, \tag{C.17}$$

where $y_j' \equiv y'(x_j)$ and $\langle y \rangle_j \equiv \left(y(x_{j+}) + y(x_{j-})\right)/2$. To determine $\mathcal{G}_g$ and $\mathcal{P}_g$ explicitly, we solve (C.14) analytically on each subinterval and impose the continuity of y' to get

$$y(x) = \begin{cases} \frac{y_0'}{\theta}\frac{\cosh[\theta(1+x)]}{\sinh[\theta(1+x_0)]}\,, & -1 < x < x_0\,, \\ \frac{y_{j+1}'}{\theta}\frac{\cosh[\theta(x-x_j)]}{\sinh[\theta(x_{j+1}-x_j)]} - \frac{y_j'}{\theta}\frac{\cosh[\theta(x_{j+1}-x)]}{\sinh[\theta(x_{j+1}-x_j)]}\,, & x_j < x < x_{j+1}\,, \quad j = 0, \ldots, n-2\,, \\ -\frac{y_{n-1}'}{\theta}\frac{\cosh[\theta(1-x)]}{\sinh[\theta(1-x_{n-1})]}\,, & x_{n-1} < x < 1\,, \end{cases} \tag{C.18}$$

where $\theta = (\mu/D)^{1/2}$. We then impose the jump condition $[Dy]_j = -\omega_j$ to obtain

$$\mathcal{B}_g\boldsymbol{y}' = \frac{\theta}{D}\boldsymbol{\omega}\,, \qquad \rightarrow \qquad \mathcal{G}_g = \frac{\theta}{D}\mathcal{B}_g^{-1}\,, \tag{C.19}$$

where $\mathcal{B}_g$ has the tridiagonal form given in (4.26b) with matrix entries defined in (4.85). Now we use (C.18) to calculate $\langle y \rangle_j$, and in this way we get

$$\langle \boldsymbol{y} \rangle = \frac{1}{2\theta}\mathrm{csch}\left(\frac{2\theta}{n}\right)\mathcal{C}\boldsymbol{y}'\,, \tag{C.20}$$

where $\mathcal{C}$ is defined in (4.87b). Substituting (C.19) into (C.20), and comparing with (C.16), we obtain the key result

$$\mathcal{P}_g = \frac{1}{2D}\mathrm{csch}\left(\frac{2\theta}{n}\right)\mathcal{C}\mathcal{B}_g^{-1}\,. \tag{C.21}$$

C.3 Calculation of Matrix Eigenvalues of $\mathcal{B}_g$

In this appendix we calculate the eigenvalues ξ_j and eigenvectors $\boldsymbol{v}_j$ of the matrix problem

$$\mathcal{B}_g \boldsymbol{v} = \xi \boldsymbol{v}\,, \tag{C.22}$$

where the tridiagonal matrix $\mathcal{B}_g$ has the form given in (4.26b) with the coefficients d, e and f satisfying (4.85).

From (4.85) it follows that $d = e - f$. Therefore, we get the following recursion relation for the coefficients v_l of the eigenvector $\boldsymbol{v}$:

$$f v_{l-1} + (e - \xi) v_l + f v_{l+1} = 0\,, \qquad l = 1, \ldots, n\,, \tag{C.23a}$$

$$v_0 = -v_1\,, \qquad v_n = -v_{n+1}\,. \tag{C.23b}$$

The solution to (C.23a) is

$$v_l = a\zeta_+^l + b\zeta_-^l\,, \qquad \zeta_\pm = \frac{1}{2f}\left(\xi - e \pm \left[(\xi - e)^2 - 4f^2\right]^{1/2}\right)\,. \tag{C.24}$$

The end conditions (C.23b) yield

$$a + b = -a\zeta_+ - b\zeta_-\,, \tag{C.25a}$$

$$a\zeta_+^n + b\zeta_-^n = -a\zeta_+^{n+1} - b\zeta_-^{n+1}\,. \tag{C.25b}$$

From (C.25) we get $\zeta_+ = \zeta_- = -1$ or $\zeta_+ = \zeta_- \exp(2\pi i j/n)$, for $j = 1, \ldots, n-1$. Substituting into (C.24) we get that the eigenvalues are

$$\xi_j = e + 2f\cos(\pi j/n)\,, \quad j = 1, \ldots, n\,, \tag{C.26}$$

which are ordered as $0 < \xi_1 < \ldots < \xi_n$ since $f < 0$. The corresponding unnormalized eigenvectors are found to be

$$v_{j,n} = \left(1, -1, 1, \ldots, (-1)^{n+1}\right)\,; \qquad v_{l,j} = \sin\left(\frac{\pi j}{n}\,(l - 1/2)\right)\,, \qquad j = 1, \ldots, n-1\,. \tag{C.27}$$

Here $v_{l,j}$ is the l^{th} component of the eigenvector $\boldsymbol{v}_j$. These eigenvectors can be normalized and the result is summarized in Proposition 4.9.

Bibliography

[1] N. Alikakos, X. Chen, G. Fusco, *Motion of a Drop by Surface Tension Along the Boundary*, (1998), preprint.

[2] E. Anderson et al. *Lapack User's Guide: Third Edition*, SIAM Publications (1999).

[3] U. Ascher, R. Christiansen, R. Russell, *Collocation Software for Boundary value ODE's*, Math. Comp., **33**, (1979), pp. 659-679.

[4] A. Bose, G. Kriegsmann, *Stability of Localized Structures in Non-Local Reaction-Diffusion Equations*, Methods Appl. Anal., **5**, (1998), no. 4, pp. 351–366

[5] K. Brenan, S. Campbell, L. Petzold, *Numerical Solution of Initial-Value Problems in Differential Algebraic Equations*, (1989), North Holland.

[6] S.J. Chapman, G. Richardson, *Vortex Pinning by Inhomogeneities in Type-2 Superconductors*, Physica D, **108**, (1997), pp. 397-407.

[7] X. Chen, M. Kowalczyk, *Slow Dynamics of Interior Spikes in the Shadow Gierer-Meinhardt System*, Center for Nonlinear Analysis report No. 99-CNA-002, (1999), preprint.

[8] M. Del Pino, P. Felmer, M. Kowalczyk, *Boundary Spikes in the Gierer-Meinhardt System*, Center for Nonlinear Analysis report No. 99-CNA-003, (1999), preprint.

[9] A. Doelman, R. Gardner, T. Kasso, *Stability analysis of singular patterns in the 1D Gray-Scott model: a matched asymptotics approach*, Phys. D, **122**,(1998), no. 1-4, pp. 1–36.

[10] A. Doelman, *private communication.*

[11] P. Freitas, *A Nonlocal Sturm-Liouville Eigenvalue Problem*, Proc. Roy. Soc. Edinburgh, **12A**, (1994), pp. 169-188,

[12] A. Gierer, H. Meinhardt, *A Theory of Biological Pattern Formation*, Kybernetik, **12**, (1972), pp. 30–39.

[13] C. Gui, *Multi-peaked Solutions to a Semilinear Neumann Problem*, Duke Math. J., **84**, No.3, (1996), pp. 739-769.

[14] C. Gui, J. Wei, *Multiple Interior Peak Solutions for some Singularly Perturbed Neumann Problems*, J. Diff. Eq., **158**, No. 1, (1999), pp. 1-27.

[15] C. Gui, J. Wei, *Multiple Mixed Boundary and Interior Peak Solutions for some Singularly Perturbed Neumann Problem*, Submitted JDE

[16] L. Harrison, D. Holloway, *Order and Localization in Reaction-Diffusion Pattern*, Physica A, **222**, (1995) pp. 210-33.

[17] C. Hsiung, *A First Course in Differential Geometry*, Wiley Interscience Series in Pure and Applied Mathematics, Wiley, New York, (1981).

[18] D. Iron, M. J. Ward, *A Metastable Spike Solution for a Non-Local Reaction-Diffusion Model*, SIAM J. Appl. Math., **60**, No. 3, (2000), pp. 778-802.

[19] D. Iron, *Metastability of the Gierer-Meinhardt Equations*, M. Sc. thesis in the Institute for Applied Mathematics, University of British Columbia, (1997).

[20] D. Iron, M. J. Ward, *The Dynamics of Boundary Spikes for a Nonlocal Reaction-Diffusion Model*, European J. of Appl. Math., **11**, N0. 5, (2000), pp. 491-514.

[21] D. Iron, M. J. Ward, J. Wei, *The Stability of Spike Solutions to the One-Dimensional Gierer-Meinhardt Model*, to appear, Physica D, Jan. 2000.

[22] A. Iserles, *A First Course in the Numerical Analysis of Differential Equations*, Cambridge Texts in Appl. Math. 15, (1996), Cambridge University Press, pp. 197-199.

[23] J. Keener, *Activators and Inhibitors in Pattern Formation*, Stud. Appl. Math., **59**, (1978), pp. 1-23.

[24] M. Kowalczyk, *Multiple Spike Layers in the Shadow Gierer-Meinhardt System: Existence of Equilibria and Approximate Invariant Manifold*, Duke M. Journal, **98**, No. 1, (1999), pp. 59-111.

[25] M. Kowalczyk, *Exponentially Slow Dynamics and Interfaces Intersecting the Boundary*, J. Diff. Eq. **138**, No. 1, (1997), pp. 55-85.

[26] G. L. Lamb, *Elements of Soliton Theory*, Wiley Interscience, (1980).

[27] C.-S. Lin, W.-M. Ni, *On the Diffusion Coefficient of a Semilinear Neumann Problem* in *Calculus of Variations and Partial Differential Equations (Trento, 1986)* pp. 160–174, Lecture Notes in Math., **1340**, Springer, Berlin-New York, 1988.

[28] T. C. Lacalli, L. G. Harrison, *Turing's Condition and the Analysis of Morphogenic Models*, J. Theo. Biol., **76**, (1979), pp. 419-436.

[29] F. H. Lin, Q. Du, *Ginzburg-Landau Vortices: Dynamics, Pinning and Hysteresis*, SIAM J. Math. Anal. **28**, (1997), pp. 1265-1293.

[30] D. McInerney, M. J. Ward, *The Dynamics and Pinning of a Spike for a Reaction-Diffusion Model*, (2000), preprint

[31] W. Ni, *Diffusion, Cross-Diffusion, and their Spike-Layer Steady-States*, Notices of the AMS, Vol. **45**, No. 1, (1998), pp. 9-18.

[32] H. Meinhardt, *Models of Biological Pattern Formation*, Academic Press, London, (1982)

[33] H. Meinhardt, *The algorithmic beauty of sea shells*, Springer Verlag, Berlin, (1995).

[34] W. Ni, *Diffusion, Cross-Diffusion, and their Spike-Layer Steady-States*, Notices of the AMS, Vol **45**, No 1, (1998), pp. 9-18.

[35] W. Ni, I. Takagi, *On the Shape of Least-Energy Solutions to a Semilinear Neumann Problem*, Comm. Pure Appl. Math, Vol. XLIV, (1991), pp. 819-851.

[36] W. Ni, I. Takagi, *Point-Condensation Generated by a Reaction-Diffusion system in Axially Symmetric Domains*, Japan J. Indust. Appl. Math., Vol. **12**, No. 2, (1995), pp. 327-365.

[37] W. Ni, I. Takagi, E. Yanagida, preprint, submitted to Tohoku Math J., (1999).

[38] Y. Nishiura, *Coexistence of Infinitely Many Stable Solutions to Reaction-Diffusion Equations in the Singular Limit*, in Dynamics Reported: Expositions in Dynamical Systems Volume 3 (editors: C. K. R. T. Jones, U. Kirchgraber), Springer-Verlag, New York, (1995).

[39] NAG Fortran library Mark 17, routine D03PCF, Numerical Algorithms Group Ltd. Oxford, United Kingdom (1995).

[40] I. Prigogine, R. Lefever, *Symmetry-Breaking Instabilities in Dissipative Systems*, J. Chem. Phys., **48** (1968), pp. 1695-1700.

[41] D. Sarocka, A. Bernoff, *An Intrinsic Equation of Interfacial Motion for the Solidification of a Pure Hypercooled Melt*, Physica D, **85**, (1995), pp. 348-374.

[42] L. Shampine, M. Gordon, *Computer Solution of Ordinary Differential Equations, the Initial Value Problem*, W. H. Freeman publishers, San Fransisco (1975).

[43] D. Stafford, M. J. Ward, B. Wetton, *The Dynamics of Drops and Attached Interfaces for the Constrained Allen-Cahn Equation*, submitted, Europ. J. Appl. Math.

[44] X. Sun, M. J. Ward, *Metastability for a Gereralized Burgers Equation with Applications to Propagating Flame Fronts*, Europ. J. Appl. Math., **10**, (1999), pp. 27-53.

[45] I. Takagi, *Point-Condensation for a Reaction-Diffusion System*, J. Diff. Eq., **61**, (1986), pp. 208-249.

[46] A. Turing, *The Chemical Basis of Morphogenesis*, Phil. Trans. Roy. Soc. B, **327**, (1952), pp. 37-72.

[47] M. J. Ward, *Exponential Asymptotics and Convection-Diffusion-Reaction Models*, book chapter in "Analyzing Multiscale Phenomena Using Singular Perturbation Methods", Proceedings of Symposia in Applied Mathematics, Vol. 56, AMS Short Course (1998). pp. 151-184

[48] M. J. Ward, *An Asymptotic Analysis of Localized Solutions for Some Reaction-Diffusion Models in Multi-Dimensional Domains*, Stud. Appl. Math., **97**, No. 2, (1996), pp. 103-126.

[49] M. J. Ward, *Metastable bubble solutions for the Allen-Cahn equation with mass conservation*, SIAM J. Appl. Math., **5**, (1996), pp. 1247-1279.

[50] M. J. Ward, J. Wei, *Asymmetric Spike Patterns for the One-Dimensional Gierer-Meinhardt Model: Equilibria and Stability*, submitted, Europ. J. Appl. Math., July 2000.

[51] J. Wei, *On the Interior Spike Layer Solutions to a Singularly Perturbed Neumann Problem*, Tohoku Math. J., **50**, (1998), pp. 159-178.

[52] J. Wei, *On Single Interior Spike Solutions for the Gierer-Meinhardt System: Uniqueness and Stability Estimates*, Europ. J. Appl. Math., **10**, No. 4, (1999), pp. 353-378.

[53] J. Wei, *Uniqueness and Eigenvalue Estimates of Boundary Spike Solutions*, (1998), preprint.

[54] E. Yanagida, *Stability of Stationary Solutions of the Gierer-Meinhardt System*, in China-Japan Symposium on Reaction-Diffusion Equations and their Applications and Computational Aspects (Shanghai 1994), World Sci. Publishing, River Edge, NJ (1997), pp. 191-198.